

**Investigations on an Innovative Antibiotic Approach –
Structure-Function-Analysis of Essential Enzymes Routing
the Vitamin B₁ *de novo* Biosynthesis and Vitamin B₆ Salvage
Pathway of *Staphylococcus aureus***

Dissertation

zur Erlangung des Doktorgrades der Naturwissenschaften (*Dr. rer. nat.*)

an der Fakultät für Mathematik, Informatik und Naturwissenschaften

der Universität Hamburg

Fachbereich Chemie

vorgelegt von

Madeleine Künz

Hamburg, Juni 2015

Die vorliegende Arbeit wurde im Zeitraum von Oktober 2011 bis Mai 2015 in der Arbeitsgruppe von Prof. Ch. Betzel im Laboratorium für Strukturbiologie von Infektion und Entzündung am Institut für Biochemie und Molekularbiologie, des Fachbereichs Chemie der Universität Hamburg, durchgeführt.

1. Gutachter: Prof. C. Betzel
2. Gutachter: JProf. H. Tidow

Tag der Disputation 24.07.2015

Für meine Familie.

Table of contents

List of abbreviations	i
I Introduction	1
1 Bacterial resistance - Onset of a post-antibiotic era?.....	1
2 The evolution of MRSA - Methicillin resistant <i>Staphylococcus aureus</i>	3
3 Treatments of bacterial and particularly MRSA infections.....	6
3.1 Antibiotics in extensive clinical use against MRSA.....	6
3.2 Antibiotic classes and the opposed resistance mechanisms in <i>S. aureus</i>	9
3.3 Current spread and costs of antibiotic resistances	11
3.4 Drawbacks in antibiotic therapy	12
3.5 Initiatives and strategies for the development of novel antibiotics	12
4 Bacterial vitamin metabolisms	14
4.1 Vitamin B ₁ - Thiamine.....	14
4.2 Vitamin B ₆ - Pyridoxine derivatives function, production and regulation	18
4.3 Bifunctional enzymes - ThiD and PdxK.....	20
4.4 Vitamin B ₁ <i>de novo</i> and vitamin B ₆ salvage pathway as potential drug targets.....	21
5 Advanced drug design - Shaping substrate analogs to suicide drugs	22
II Aims of this Work.....	24
III Methods	25
1 X-ray sources.....	25
2 Instrumentation.....	25
3 Buffers, solutions and consumables	27
4 Molecular biology and biochemical methods.....	31
4.1 PCR –Polymerase chain reaction.....	31
4.2 Control PCR - Colony PCR and bacmid PCR	32
4.3 Agarose gel electrophoresis	32
4.4 Restriction digest, template removal and dephosphorylation	32
4.5 Site directed mutagenesis	33
4.6 Ligation.....	33
4.7 DNA purification, concentration determination and sequencing.....	33
4.8 Preparation of chemically competent cells.....	34
4.9 Transformation of chemically competent bacteria.....	34
4.10 <i>E. coli</i> glycerol stock preparation	34
4.11 SDS-PAGE and native PAGE.....	34

4.12	Western Blot (WB)	35
4.13	Bacterial cell culture for recombinant protein production	35
4.13.1	Bacterial plasmids and oligonucleotides	36
4.13.2	Microbial growth media and selection antibiotics used for <i>E. coli</i> cultivation	39
4.14	Insect cell culture	39
4.14.1	Insect cell plasmids and oligonucleotides	39
4.14.2	Material, medium, buffer, solutions and cell lines for insect cell culture	41
4.14.3	Sequencing and control oligonucleotides	42
4.14.4	Transformation of DH10Bac for recombinant bacmid generation	42
4.14.5	Bacmid purification	42
4.14.6	<i>Sf9</i> cell culture	43
4.14.7	Transfection and virus stock production	44
4.14.8	<i>Sf9</i> cell lysate preparation and Bradford assay	44
4.15	Protein purification	45
4.15.1	Preparation of cleared lysates	45
4.15.2	Affinity chromatography and size exclusion chromatography	46
4.15.3	Strep-tactin and Ni-NTA matrix regeneration	46
4.16	Protein quantification	47
4.17	TEV protease expression, purification and standard TEV protease digest	47
4.18	Dynamic light scattering (DLS)	48
4.19	Circular dichroism (CD)	48
4.20	Mass spectrometry (MS)	49
4.21	Saturation transfer difference - nuclear magnetic resonance (STD-NMR)	49
4.22	Molecular docking	50
5	X-ray crystallography	50
5.1	Sample preparation and initial crystallization screening	50
5.2	Analysis of crystallization success and optimization of initial crystallization hits	51
5.3	Soaking	52
5.4	Automated nano-crystallization – XtalController 900	52
5.5	Diffraction data collection	52
5.6	Data processing and model building	53
5.7	Model evaluation	53
6	Small angle X-ray scattering (SAXS)	53
7	PdxK activity assay and binding affinity quantification	54
7.1	PdxK activity assay	54

7.2	Microscale thermophoresis (MST) for binding affinity quantification.....	54
IV	Results	55
1	<i>Staphylococcus aureus</i> ThiM.....	55
1.1	<i>S. aureus</i> ThiM: Optimization of purification and crystallization.....	56
1.2	<i>S. aureus</i> ThiM: Diffraction data collection, processing and model building.....	58
1.3	Structure analysis - <i>S. aureus</i> ThiM with bound substrate analogs	61
1.4	Effects of cpd12 on <i>S. aureus</i> ThiM.....	67
1.5	Investigations on <i>S. aureus</i> ThiM NPE-caged ATP complex formation and nano-crystallization	70
2	<i>Staphylococcus aureus</i> TPK.....	74
2.1	Recombinant expression, purification and characterization	74
2.2	Crystallization of <i>S. aureus</i> TPK in complex with thiamine	75
2.3	<i>S. aureus</i> TPK: Diffraction data collection, processing and model building.....	76
2.4	<i>S. aureus</i> TPK: Structure analysis	79
2.5	Evaluation of potential thiamine analogs - analyzing the activation via <i>S. aureus</i> TPK.	83
2.6	Comparison and differentiation of <i>S. aureus</i> TPK to eukaryotic TPK.....	85
2.7	Growth and evaluation of <i>S. aureus</i> TPK micro crystals	87
3	<i>Staphylococcus aureus</i> PdxK.....	88
3.1	<i>S. aureus</i> PdxK: Recombinant expression, purification and characterization.....	88
3.2	<i>S. aureus</i> PdxK SAXS structure	90
3.3	<i>S. aureus</i> PdxK: Crystallization	91
3.1	<i>S. aureus</i> PdxK: Diffraction data collection, processing and model building I	92
3.2	<i>S. aureus</i> PdxK: Diffraction data collection, processing and model building II	94
3.3	<i>S. aureus</i> PdxK: Structure analysis and comparison of the two models	96
3.4	Results of docking and analysis of peptidomimetics targeting <i>S. aureus</i> PdxK	103
3.5	Activity and analysis of substrate specificity of <i>S. aureus</i> PdxK.....	105
4	<i>Trypanosoma cruzi</i> PdxK.....	107
4.1	Recombinant expression, purification and characterization	107
4.2	Crystallization of <i>T. cruzi</i> PdxK.....	107
4.3	<i>T. cruzi</i> PdxK: Diffraction data collection, processing and model building	108
4.4	<i>T. cruzi</i> PdxK: Structure analysis.....	111
5	Insect cell expression and <i>in vivo</i> crystallization trials	116
V	Discussion	118
1	First steps to <i>in vivo</i> produced thiamine analogs in <i>S. aureus</i>	118
2	Cpd12 - a halogenated compound specifically unfolds <i>S. aureus</i> ThiM	120

3	Towards dynamics - <i>S. aureus</i> ThiM nano crystallization and NPE-caged ATP complex formation	121
4	Analysis of <i>S. aureus</i> TPK in complex with thiamine.....	122
5	Structure analysis of <i>S. aureus</i> PdxK - Peptidomimetics targeting <i>S. aureus</i> PdxK.....	123
6	Analyzing substrate promiscuity of <i>S. aureus</i> PdxK and ThiD.....	125
7	Structure analysis of <i>T. cruzi</i> PdxK - Analyzing the evolution and conservation of Vitamin B ₆ activating enzymes	126
8	Outlook: Mining the bacterial vitamin B ₁ metabolism and B ₆ salvage for advanced structural based drug developments.....	127
VI	Summary	129
VII	Zusammenfassung.....	130
VIII	References	132
IX	Acknowledgements	153
X	Curriculum vitae	154
XI	Appendix	155
XII	Risk and Safety Statements.....	160
1	Chemicals used (GHS classification).....	160
2	Commercial Protein Screens and Kits	162
3	GHS pictograms.....	163
4	GHS Hazard Statements.....	163
5	GHS Precautionary Statements	164
XIII	Eidesstattliche Erklärung	165

List of abbreviations

AA	Amino acids
ADP	Adenosine diphosphate
AMP	Adenosine monophosphate
AMP-PCP	5'-O-(Hydroxy{[hydroxy(phosphonomethyl)phosphoryl]oxy} phosphoryl)adenosine
AMP-PNP	5'-O-(Hydroxy{[hydroxy(phosphonoamino)phosphoryl]oxy} phosphoryl)adenosine
AP	Alkaline phosphatase
APS	Ammonium peroxydisulfate
ASU	Asymmetric unit
ATP	Adenosine triphosphate
<i>B. subtilis</i>	<i>Bacillus subtilis</i>
BCIP	5-bromo-4-chloro-3'-indolylphosphate
BLAST	Basic Local Alignment Search Tool
BSA	Bovine serum albumin
CA-MRSA	Community associated MRSA
CCD	Charge-coupled device
CD	Circular dichroism
CDC	Centers for Disease Control and Prevention
Cpd	Compound
<i>cfr</i>	<i>Chloramphenicol-florfenicol resistance gene</i>
CHIPS	Chemotaxis inhibitory protein
CV	Column volumes
DESY	Deutsches Elektronen Synchrotron
DLS	Dynamic Light Scattering
DMF	N,N-Di-methyl-formamide
DMSO	Dimethyl sulfoxide
DNA	Desoxyribonucleic acid
dNTPs	Desoxynucleotide triphosphates
DOC	Sodium deoxycholate
DTT	(2S,3S)-1,4-Disulfanyl-2,3-butanediol
DXP	Deoxyxylulose 5-phosphate
<i>E. coli</i>	<i>Escherichia coli</i>
<i>E. faecalis</i>	<i>Enterococcus faecalis</i>
ECDC	European Centre for Disease Prevention and Control
ECL	Enhanced chemiluminescence
EDTA	2,2',2'',2'''-(1,2-Ethanediyldinitrilo)tetraacetic acid
EGTA	3,12-Bis(carboxymethyl)-6,9-dioxa-3,12-diazatetradecane-1,14-dioic acid
EMA	European Medicines Agency
EMBL	European Molecular Biology Laboratory
<i>P. horikoshii</i>	<i>Pyrococcus horikoshii</i>
ESI	Electrospray ionization
EtOH	Ethanol
EU	European Union
FDA	U.S. Food and Drug Administration
FDASIA	US Food and Drug Administration Safety and Innovation Act
FPLC	Fast protein liquid chromatography
GCB	Granada crystallization boxes
GDP	Gross domestic product

GTP	Guanosine triphosphate
GTPase	Hydrolase that can bind and hydrolyze GTP
HABA	2-[4'-hydroxy-benzeneazo]benzoic acid
HA-MRSA	Healthcare associated MRSA
HEPES	4-(2-hydroxyethyl)-1-piperazineethanesulfonic acid
HIV	Human Immunodeficiency Virus
HMP	4-amino-5-hydroxymethylpyrimidine
HMP-P	HMP-phosphate
HMP-PP	HMP-pyrophosphate
HRP	Horseradish peroxidase
IDSA	Infection Disease Society of America
IPTG	Isopropyl-1-thio- β -D-galactopyranosid
ITC	Isothermal titration calorimetry
IUPAC	International Union of Pure and Applied Chemistry
kDa	Dalton $\cdot 10^3$
KISS	German hospital infection surveillance system
K_m	Michaelis constant
LA-MRSA	Livestock associated MRSA
LB	Luria Bertani
MBP	Maltose binding protein
MME	Monomethyl ether
MoA	Mode of action
MRE	Mean residue ellipticity
MRW	Mean residue weight
MRSA	Methicillin resistant <i>Staphylococcus aureus</i>
MSSA	Methicillin susceptible <i>Staphylococcus aureus</i>
MST	Microscale thermophoresis
MW	Molecular weight
NBT	Nitro-blue tetrazolium
ND4BB	"New drugs 4 bad bugs" (antibiotic program in 2011)
Ni-NTA	Nitrilotriacetic acid
NMR	Nuclear magnetic resonance
NPE-caged ATP	5'-O-(Hydroxy{[hydroxy{[hydroxy[1-(2-nitrophenyl)ethoxy]phosphoryl}oxy]phosphoryl}oxy]phosphoryl)adenosine
NTZ	Nitazoxanide (2-acetolyloxy-N-(5-nitro 2-thiazolyl)
O/N	Over night
OD ₆₀₀	Optical density at 600 nm
PAGE	Polyacrylamide gel electrophoresis
PBP2a	Penicillin binding protein 2a
PBS	Phosphate buffered saline
PCR	Polymerase chain reaction
PD	Pharmacodynamics
PDC	Pyruvate decarboxylase
PDH	Pyruvate dehydrogenase
PdxK	ATP-dependent pyridoxal kinase
PEG	Polyethylene glycol
PFOR	Pyruvate-ferredoxin oxidoreductase
<i>Pfu</i>	<i>Pyrococcus furiosus</i>
PK	Pharmacokinetics
PL	Pyridoxal
PLP	Pyridoxal-5'-phosphate
PM	Pyridoxamine
PMSF	Phenylmethanesulfonyl fluoride

PN	Pyridoxine
PNP	Pyridoxine-5'-phosphate
PNPOx	Pyridoxine 5'-phosphate oxidase
PVL	Panton-Valentine leukocidine
Q/D	Quinupristin-dalfopristin
R&D	Research and development
R5P	D-ribose 5-phosphate
R _H	Hydrodynamic radius
RIPA	Radioimmunoprecipitation assay buffer
ROS	Reactive oxygen species
RMSD	Root-mean-square deviation
RNA	Ribonucleic acid
rRNA	ribosomal RNA
RT	Room temperature
<i>S. aureus</i>	<i>Staphylococcus aureus</i>
SAXS	Small-angle X-ray scattering
SCCmec	Staphylococcal cassette chromosome mec
SCIN	Staphylococcal complement inhibitor
SDS	Sodium dodecyl sulfate
SMILES (string)	Simplified molecular-input line-entry system
Ssss	Staphylococcus saprophyticus subsp. saprophyticus
STD -NMR	Saturation transfer difference-NMR
<i>T. brucei</i>	<i>Trypanosoma brucei</i>
<i>T. cruzi</i>	<i>Trypanosoma cruzi</i>
TAE buffer	Tris-acetate-EDTA buffer
Taq	Thermus aquaticus
TBS	Tris buffered saline
TDP	Thiamine diphosphate
TEMED	Tetramethylethylenediamine
TenA	Thiaminase type II
TEV	Tobacco etch virus
ThiD	4-amino-5-hydroxymethyl-2-methylpyrimidine (HMP) kinase
ThiE	Thiamine phosphate synthase
ThiM	THZ- kinase
THZ	2-(4-methyl-1,3-thiazol-5-yl)ethanol
TIZ	Tizaxonide
T _m	Melting temperature
TMP	Thiamine monophosphate
TPK	Thiamine pyrophosphokinase
TTP	Thiamine triphosphate
UV	Ultraviolet
v/v	Volume per volume
VISA	Vancomycin intermediate MRSA
VRSA	Vancomycin resistant MRSA
w/v	Weight per volume
WB	Western blot
WHA	World Health Assembly
WHO	World Health Organization

On letter code	Three letter code	Amino acid
A	Ala	Alanine
C	Cys	Cysteine
D	Asp	Aspartate
E	Glu	Glutamate
F	Phe	Phenylalanine
G	Gly	Glycine
H	His	Histidine
I	Ile	Isoleucine
K	Lys	Lysine
L	Leu	Leucine
M	Met	Methionine
N	Asn	Asparagine
P	Pro	Proline
Q	Gln	Glutamine
R	Arg	Arginine
S	Ser	Serine
T	Thr	Threonine
V	Val	Valine
W	Trp	Tryptophan
Y	Tyr	Tyrosine

Abbreviation	base
A	Adenine
C	Cytosine
G	Guanine
T	Thymine

I Introduction

1 Bacterial resistance - Onset of a post-antibiotic era?

Since the very first broad-spectrum antibiotic - penicillin - entered the market in 1943 [1] an increasing number of bacterial infectious diseases became routinely controllable. Humans benefit from wealth and the economic vitality accompanied with this fundamental therapeutic progress. But as Alexander Fleming already predicted in his Nobel Lecture `it is not difficult to make microbes resistant to penicillin` [2], resistances to almost any given class of subsequent developed antibiotics, not only penicillin, evolved and spread.

Regardless which target class or which chemical entity of any ordinary acting antibiotic resistance is intrinsically present [3], it will be evolved by genetic variance, evolutionarily selected and inherited in consequence [4]. Additional to the transmission of the genetic adaption to an antibiotic environment between organisms through reproduction, resistance is further transmitted between organisms and even species via horizontal gen transfer of plasmids, prophages, pathogenicity islands and transposons [5, 6]. The prokaryotes' extremely high genetic plasticity allows them to expeditiously adapt to tremendous environmental changes [7].

But not only the intrinsic dynamic of resistance and natural selection - survival of the fittest individual - is giving rise to antibiotic resistance development, in particular the incorrect and thriftless use of antibiotics by humans is a major driving force for the spread of resistance [8, 9]. This includes the empirical prescription [10] and missing diagnostic coverage of antibiotic use [11–15] as well as the misuse of antibiotics as animal growth promoter¹ [16] and the preventive feeding to lower infection rates in livestock [17].

For all antibiotic classes recently released on the market at least one resistance mechanism is present in a distinct bacterial strain and these mechanisms are further emerging [3]. The rapid development of resistance, indicated by the first detection of resistance for the main classes of antibiotics is illustrated in Figure 1.

¹ Entire prohibition in EU since 01/01/2006 (Regulation 1831/2003/EC on additives for use in animal

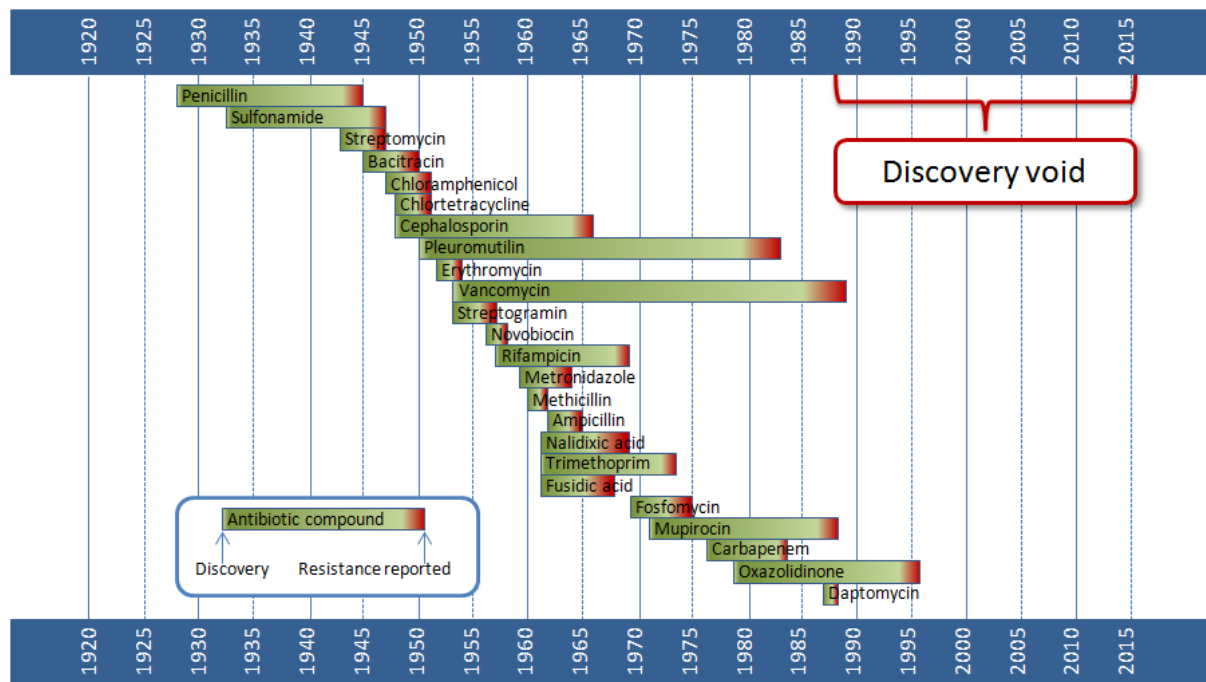


Figure 1: Illustration of the time course of antibacterial resistance development.

The illustration includes the discovery date of discrete classes and compounds of antibiotics adapted from Silver [18] and is extended by the first documented resistance of any bacteria - clinical isolates and *in vitro* studies - against them. The references for the earliest resistance detection can be found in the appendix (Table 36).

The figure clearly highlights that after 1987 an exceptional “discovery void” is present - no new antibiotic class has been developed since [18]. This lack in scientific discovery, abuse and the ignorance of bacterial versatility opened the prospect to eventuate a “postantibiotic era” [19]. Thereby, antibiotic treatment of infections and the performance of medical and surgical procedures under the antibiotic prevention will be problematic and this exceptional precious medicine might completely lose its potency. In particular strains from *Staphylococcus aureus*, *Escherichia coli*, *Klebsiella pneumoniae*, *Streptococcus pneumoniae*, species of *Salmonella* and *Shigella*, *Neisseria gonorrhoeae*, *Mycobacterium tuberculosis* [19] as well *Acinetobacter baumannii*, and *Pseudomonas aeruginosa* [20, 21] are resistant to virtually all antibiotics and thus of major concern.

The global economic burden was primarily evaluated by the “Review on Antimicrobial Resistance” commissioned by the UK Prime Minister - for the very first time it issues an estimation of the global consequences, if antimicrobial resistance is not tackled. Taking only statistics for *Staphylococcus aureus*, *Escherichia coli*, *Klebsiella pneumoniae*, *Mycobacterium tuberculosis* but also *Plasmodium falciparum* and Human Immunodeficiency Virus (HIV) into account, the study estimates that 10 million people *per annum* will die in the next 35 years in consequence of recent and further resistance development; the global Gross Domestic Product (GDP) will be reduced by 2.0 % to 3.5 % [22]. This factual prediction on the available data calculates up to US\$ 100 trillion extra costs only due to the reduced economic output of the world’s population [22].

A hypothetical calculation on an obvious medical example from Smith and Coast clearly quantifies the consequences of imminent antimicrobial limitation: Without prophylactic antimicrobial treatment the number of postoperative infections after an ordinary hip replacement will increase to 50 % and consequently fatality will rise up to 30 % [23].

In order to react to this global problem the World Health Assembly (WHA) assigned the WHO for the elaboration of an initial world action plan in March 2014, which was discussed in the very last WHA in May 2015. Resolution 67.39 on Antimicrobial Resistance of the WHA out of 2014 already exhorts all member states to develop national strategies to combat resistance [24] and the global action plan adopted in course of the WHA in May 2015 now scheduled national action plans for all member states consistent with the global action plan by May 2017 [25]. Further already existing national action plans and realized strategies are listed in detail in chapter I 3.5.

Consequent development of new antibacterial treatments and antibiotic strategies is strongly needed and will result in association with improved infection control practice, more frequent surveillance, better hygiene and decontamination, improved diagnostic and less empirical treatment of patients as well as improved inspection of treatment success and clearance to better disease management.

2 The evolution of MRSA - Methicillin resistant *Staphylococcus aureus*

Staphylococcus aureus (*S. aureus*) is a gram-positive, facultative anaerobic, coccal bacterium which was reported first by Sir Alexander Ogston in the 1880s [26]. It is ordinarily found as commensal part of the regular skin flora and nasal passages as a normal part of the human microbiota. Up to 30 % of individuals are persistent carriers and 60 % of the population carries various strains intermittently [27–29]. In contrast, it was as well identified as the causative agent for minor skin infections, post-operative wound infections up to necrotizing fasciitis and also pneumonia, endocarditis and osteomyelitis particularly under nosocomial settings [30–32]. Hence, asymptomatic carriage represents an extra risk factor to health-care associated infections, as it may invade surgical sites and promotes spreading between individuals [33–36].

With the invention of penicillin the first option to treat *S. aureus* arose [37, 38]. But already less than 10 years after optimization of mass production of penicillin [1] more than 40-50 % of *S. aureus* strains were reported to be resistant in the end of the 1940s [39, 40]. The resistance is mediated through a narrow activity spectrum β -lactamase which is located on a plasmid.

Subsequently, *S. aureus* again became a pandemic infection in the community. This was counteracted by the introduction of the first semisynthetic penicillinase resistant β -lactam, Methicillin, in 1959. But already shortly after the introduction, in 1961, resistance against Methicillin

was observed [41, 42]. The resistance is mediated through the low affinity penicillin binding protein 2a (PBP2a) [43], which is genetically located on a mobile element, the staphylococcal cassette chromosome mec (SCCmec), identified in 2000 [44]. The origin of the corresponding *mecA* cassette is suspected to be a result of horizontal gen transfer between Methicillin susceptible *S. aureus* strain (MSSA) and coagulase negative strains [45]. Moreover, the resistance via *mecA* or PBP2a respectively confers also resistance to onwards developed antibiotics like penicillins, cephalosporins and carbapenems [44]. On its genetic element it could be in association with additional resistances against kanamycin, lincosamides, macrolides, bleomycin, tobramycin, tetracycline and streptogramin [45]. The increasing burden of **Methicillin resistant *Staphylococcus aureus***-MRSA was soon represented by the rising number of nosocomial infections in worldwide dissemination and MRSA became rapidly the leading cause of hospital-acquired (HA) infections [46].

Successively, the treatment mainly focused on the last unfailing “drug of last resort”, the glycopeptid vancomycin [47]. But its increased use came along with a rigorous selection and yielded to first treatment failures owing to decrease in vancomycin susceptibility in 1997 [48]. Later on it could be elucidated that prolonged exposure to vancomycin leads to a selection of vancomycin intermediate MRSA (VISA) strains with thickened extra-cellular peptidoglycan material [49, 50]. These altered peptidoglycans are showing a lower level of cross-linking and are exposing more D-Ala-D-Ala dipeptides, which confiscate the antibiotic vancomycin as well as the later developed related antibiotic teicoplanin and hence reduces susceptibility [51–54]. In 2002, the first entirely vancomycin resistant *S. aureus* (VRSA) strain was isolated, and VISA as well as VRSA are nowadays globally disseminated [55–58].

In 2002, the vancomycin resistance was determined to be mediated through a plasmid from *Enterococcus faecalis* harboring the *vanA* operon. A low vancomycin concentration allows the bacteria to specifically modify the terminal cell wall peptide from D-alanyl-D-alanine to D-alanyl-D-lactate. This results in reduced vancomycin affinity and consequently diminishes effectivity [59, 60]. This precise regulation of the cell wall alteration by vancomycin itself saves biosynthetic energy and results in an ecological extraordinary fitness and supports the global spread [61]. Additionally, it should be noted that Avoparcin, a glycopeptid chemically related to vancomycin, has been utilized as growth promoter for livestock in Europe since the 1970s and perhaps can therefore be linked to the resistance development and spread [62, 63].

Since the 1990s, an alarming trend of increasing numbers of community associated (CA)-MRSA severe infections was detected [31, 64]. Community association is reflected in patients, who are habitual healthy, immunocompetent and young individuals, had no history of previous hospitalization, dialysis or surgery procedures and hence actually no risk for colonization.

An increasing number of these CA-MRSA shows – besides their good susceptibility to non- β -lactam antibiotics – an enhanced virulence, infection and disease manifestation [64, 65]. The leading cause for this frequent fatal outcome is still not clearly identified, but an association to the leukocyte destructive and tissue necrotizing exotoxin Panton-Valentine leukocidine (PVL) [66] is suspected at least for the epidemic strain USA300 in the United States [65, 67] and still under debate [68, 69]. As additional virulence determinants of CA-MRSA Wang and colleagues identified secreted peptides, which can recruit, activate and subsequently lyse human neutrophils and thus modulate the cellular defense [70]. Moreover, superantigens like bacterial proteins which activate a massive T-cell response [71], advanced modulators of the innate immune system like SCIN (staphylococcal complement inhibitor), staphylokinase and CHIPS (chemotaxis inhibitory protein) [72] as well as enterotoxins were identified [30]. Currently these extra virulent MRSA strains started to emerge back to hospitals and replace or join healthcare associated (HA)-MRSA strains [73]. CA-MRSA strains display an important reservoir which is very difficult to control, and serves as a recurrent source of importation into hospitals.

In the 2000s livestock, the third reservoir for massive MRSA infection, genetic selection and exchange, moved into focus and revision of the infection control [74–76]. In 2006, CA-MRSA could be clearly genetically linked to livestock associated (LA)-MRSA [77, 78]. Although only low zoonotic transmission rates are detected so far, this reservoir serves as an additional exchange portal for distinct MRSA strains and as a probable source for different virulence features due to specific host adaption mechanisms [79–82].

The WHO stated in the Global Report on Surveillance for Antimicrobial Resistance 2014, based on summary of national data, that the MRSA proportion resistant to regularly used antibacterial drugs exceeded 50 % in many settings [19]. In addition, the ECDC (European Centre for Disease Prevention and Control) and EMA (European Medicines Agency) confirmed that MRSA is the most frequent causative multidrug-resistant germ in the EU and of major public health concern [83]. Routine surgical procedures, chemotherapies and treatments of immune deficient patients in a clinical environment could be as difficult as in the pre-antibiotic era without effective antimicrobials.

In summary, this brief overview about the MRSA evolution already greatly exemplifies its efficient genetic plasticity and extreme versatility. Most recent treatment options and the accompanied ongoing resistance development are illustrated in chapter I 3.2 and will further highlight the germs adaptability. A constant accumulation of resistance genes and adaption to different environmental settings are to be expected in future and will possibly generate a phenotypical superbug that could consistently conquer antibiotic treatment efforts.

3 Treatments of bacterial and particularly MRSA infections

Currently, various approaches are used in MRSA prevention, treatment, resistance control and management. These include national and global collaborating surveillance systems, especially in terms of continuously developing resistances. In hospital and under healthcare settings, where the risk of an infection disease is superior, more consequent sanitation precaution and surveillance for prior asymptomatic bacterial colonization going along with patient's isolation is greatly required. Furthermore, standardization of diagnostics and therapies clearly monitoring and defining cure as well as restricted access and appropriate and conservative prescription of antibiotics is desirable. Additionally, the education and inclusion of community and patients needs particular attention, as the constant transmission of infection diseases as well the selection and spread of resistances will be accelerated by the societies behavior [84].

Preventive immunization, which is globally used to restrict many infection disease spreads, is not applicable to MRSA and several trials failed until now or are still under preclinical or clinical investigation [85–88]. Local MRSA skin infections can be occasionally treated by local drainage [89], but in most cases, especially with systematic impairment, a well selected antimicrobial therapy and consequent monitoring of the vital parameters and infrequently surgical excision is needed.

Presently eleven antimicrobial drugs are in clinical use for the treatment of systematic and local MRSA/VISA/VRSA infections and will be specified in chapter I 3.1. Nevertheless, the need for new classes of antibiotics as a gold standard of treatment, facing the ongoing resistance development by advanced drug research and discovery, is indispensable. The following chapters will describe the antimicrobial treatment options and difficulties arising from the growing number of multi resistant MRSA strains.

3.1 Antibiotics in extensive clinical use against MRSA

The general mechanism of antibiotics is either bactericidal, thus killing bacteria, or bacteriostatic, impede the growth of bacteria, and can be used for a rough classification [90]. More precisely, antibiotic classes could be assigned to the chemical entity of the active ingredient, mode of action (MoA), which is based on the target structure as well, or by the differentiation of the component in natural or semi- and full-synthetic chemical entities.

Even if *S. aureus* is practically susceptible to every developed antibiotic [91], there are presently eleven drugs (summarized in Table 1) in extensive clinical use against MRSA, VRSA and multidrug-resistant *S. aureus*: In supremacy vancomycin, but also linezolid, tigecycline, telavancin, quinupristin-dalfopristin, ceftaroline, ceftobiprole, daptomycin and most recently, since 2014, dalbavancin, oritavancin and tedizolid [92–96].

Table 1: Overview of the antibiotics in current extensive use to treat MRSA, VRSA and multidrug-resistant *S. aureus*.

Glycopeptids and lipoglycopeptids are colored in yellow, cyclic lipopeptides in orange, oxazolidinones in green, cephalosporins in rose, streptogramins in grey and tetracycline derivatives (glycylcyclines) in blue. Resistance discovery under clinical or laboratory settings was summarized from [96–103] : ✓ = resistance was discovered, - = no resistance discovered so far, x = no data included.

Antibiotic compound	Target	Innovative Mode of action	Resistance discovered in <i>S. aureus</i>	other bacteria
vancomycin	cell wall synthesis	-	✓	✓
oritavancin	cell wall synthesis	-	-	-
telavancin	cell wall synthesis	-	✓	✓
dalbavancin	cell wall synthesis	-	-	-
daptomycin	cytoplasmic membrane	Yes	✓	✓
linezolid	protein biosynthesis	-	✓	✓
tedizolid	protein biosynthesis	-	-	-
ceftobiprole	cell wall synthesis	-	✓	x
ceftaroline	cell wall synthesis	-	✓	x
quinupristin-dalfopristin	protein biosynthesis	-	✓	✓
tigecycline	protein biosynthesis	-	-	✓

Currently, the natural glycopeptide vancomycin is still the main treatment for MRSA infections and a kind of “gold standard”, although it entails high nephrotoxicity, has a poor lung tissue penetration and needs monitored dosing for appropriate pharmacokinetics (PK) and -dynamics (PD) [92, 96].

Additionally, three semisynthetic lipoglycopeptides derived from the vancomycin scaffold are on the market: Telavancin, oritavancin and dalbavancin. Like vancomycin, they all show a complex and extended half-life time and complex PK. So far only single data are available, because they entered the market very recently: Telavancin in 2011 and oritavancin as well as dalbavancin in 2014 [96]. Moreover, telavancin has still an FDA (U.S. Food and Drug Administration) black box warning due to purification issues and observed QT prolongations in the heart’s electrical cycle and demonstrates possible cross resistance due to *vanA* [99, 104]. To the current knowledge the semisynthetic derivative of the glycopeptide antibiotic chloroeremomycin oritavancin seems to evade the *vanA* mechanism due to additional molecular target interactions yielding in tighter target binding [105]. Since no resistance to dalbavancin could be identified so far, the only disadvantage is the missing oral formulation of dalbavancin [106].

Daptomycin is vended as a member of the very new class of the cyclic lipopeptides on the market since 2003. But in fact daptomycin belongs to the original class of acidic lipopeptides and has already been described in 1986 [107, 108]. Its MoA is not completely elucidated so far, but a calcium dependent binding to the bacterial membrane yielding in fast polarization and permeabilization is

assumed [109]. So again an old target, the cell wall, is under attack. But even though it displays a new MoA, unfortunately cross resistance to vancomycin and additional resistance through cell membrane modification and cell wall thickening have been demonstrated already [109, 110].

Linezolid is administered in MRSA pneumonia more frequently [111], even though it is 10- to 20-fold more expensive than vancomycin [92]. Linezolid, the first member of the oxazolidinone on the market, has been expected to be relatively insensitive to resistance, because it is a completely synthetic drug and no natural preexisting resistance genes are expected. It inhibits the protein biosynthesis via binding to the 23S ribosomal RNA (rRNA) of the 50S subunit of bacterial ribosomes [112]. Nevertheless, *S. aureus* already shows resistance due to a point mutation (usually G2576T), however this spontaneous event occurs in low frequency only [113]. The detection of acquisition of the natural resistance gene *cfr* (chloramphenicol-florfenicol resistance gene) by horizontal gene transfer, which led to the first linezolid resistant *S. aureus* outbreak in 2008 [97, 114] and the presence of oxazolidinone multi-resistant LA-MRSA strains is much more worrisome [115]. A further oxazolidinone, tedizolid appears to be at least 4-fold more potent than linezolid, has less side effects and no cross resistance with linezolid could be detected in MRSA so far [98, 116, 117].

Ceftobiprole and ceftaroline are 3rd generation descendants of cephalosporins, belonging to the sophisticated β -lactam antibiotics and showing similar or even improved outcomes compared to vancomycin and linezolid [118, 119]. Ceftobiprole has limited approval compared to ceftaroline and resistance has already been detected in endemic MRSA strains in Australia [120]. Under laboratory conditions resistance development can be shown for both [103].

Quinupristin-dalfopristin (Q/D) is a streptogramin cocktail comprised of quinupristin a derivative of pristinamycin IA (a group B streptogramin), and dalfopristin, which is a derivative of pristinamycin IIA (a group A streptogramin) [121]. It acts via binding to the 50S ribosome, inhibits protein biosynthesis and thus synergistically kills the bacteria [122]. Management of MRSA infections with Q/D seems still promising [123], but resistance in *S. aureus* is known since 1975. It is mediated through multiple mechanisms (acetyltransferases, lyases, efflux pumps, L22 ribosomal protein mutation and other) and needs to be further elucidated [121, 124]. But the first LA-MRSA associated emerge of Q/D resistance, which was reported in 2014, is even more disturbing and clearly highlights the further spread of Q/D resistance [100].

Tigecycline is a 3rd generation tetracycline derivate, acting by blocking of the acceptor site in the 30S ribosomal subunit, thus inhibiting the incorporation of transfer RNA and blocking the protein biosynthesis [125]. In MRSA so far no lowered susceptibility due to regular tetracycline pumps has been observed, but in *Acinetobacter baumannii* efflux pumps confer to resistance [101]. Currently,

tigecycline carries a black box warning in the US due to FDA warning of increased mortality [126, 127] and also has significant side effects, like nausea and vomiting [128].

All highlighted antibiotics - with the exception of daptomycin, which targets the cytoplasmic membrane directly - are addressing two already previously focused bacterial targets, namely cell wall synthesis and protein biosynthesis. Moreover, the use of some therapeutic entities is restricted due to their limited capability to penetrate tissues, like lung tissue in case of vancomycin [111]. Presently also combination therapies are used and maybe show some synergetic effects, but also a risk for complex unforeseen toxicity [20].

Furthermore, all listed antibiotics are based on already known chemical scaffolds and no new entity has been developed since 1988 [18]. Even if synthetic tailoring on known scaffolds is a valid and resource efficient way of improving existing antibiotics - expanding its spectrum or improving its safety and PK - it is very likely that currently preexisting resistances will further evolve. Therefore, novel scaffolds and (multi-)targets are essential for combating the rising resistance.

Besides the absence of clear innovation regarding the target class and the chemical scaffold, the treatment is supplementary complicated, because of the restricted approval of some of the highlighted antibiotics to specific illnesses. For example ceftobiprole is approved for community- and hospital, but not for ventilation-acquired pneumonia [96]. Another example is linezolid, which is approved for hospital-acquired pneumonia and complicated skin infections by the FDA, but not for catheter-related bloodstream infections or catheter-site infections [129].

3.2 Antibiotic classes and the opposed resistance mechanisms in *S. aureus*

Bacteria combat various antibiotics with numerous mechanisms, these include: Target variation, inactivation by modification of the antibiotic substance (acetylation etc.), destruction of antibiotics e.g. by hydrolysis or prevention of accumulation of the antibiotics through efflux pumps.

Table 2 shows the categorization of antibiotics into six different classes according to their target mechanism and summarizes the counteracting resistance mechanisms in *S. aureus*.

Table 2: Outline of the six antibiotic classes according to target mechanism with counteracting resistance in *S. aureus*.

Representative members of subclasses and several counteracting resistance mechanisms were summarized according to Dale *et al.*, 1997; Lim *et al.*, 2014; Sanfilippo *et al.*, 2012; Stryjewski and Corey, 2014; Vimberg *et al.*, 2015; Walsh *et al.*, 2011 [130–135].

Target mechanism	Antibiotic subclass	Resistance mechanism in <i>S. aureus</i>
Inhibition of cell wall synthesis	• β -lactam derivatives (penicillin, carbapenems, monobactams, cephalosporins)	⇒ target affinity changed PBP2a, carbapenem hydrolysis by New Delhi metallo- β -lactamase
	• glycopeptide derivatives (vancomycin, oritavancin)	⇒ trapping of vancomycin and target modification
Inhibition of protein synthesis	• oxazolidinone (linezolid)	⇒ target modification (acetylation)
	• tetracyclins (doxycycline)	⇒ efflux pumps
	• macrolides (erythromycin)	⇒ efflux pumps
	• streptogramins (Q/D)	⇒ target modification (acetylation)
	• ketolids (telithromycin)	⇒ efflux pumps
Inhibition of DNA replication and repair	• fluoroquinolons	⇒ target modification
Inhibition of RNA synthesis	• rifamycin (rifampicin)	⇒ target modification
Membrane reassembling	• cyclic lipopeptides (daptomycin)	⇒ target modification (cell wall thickening)
Competitive inhibition of folic acid synthesis	• sulfonamids (sulfamethoxazole/trimethoprim)	⇒ target modification

All representative subclasses included in Table 2 are at least opposed by a single or even multiple resistance mechanisms. Although resistance to the very recently discovered novel entities like dalbavancin or tedizolid has not been detected yet (Table 1, Table 2), an ongoing development and selection for resistance is expected.

For entirely synthetic antibiotic substances the chance of a preexisting, naturally occurring resistance caused by common antibiotic-producing (soil) bacteria or organisms in an environmental niche is somewhat smaller [3, 113]. Nevertheless, the completely synthetic antibiotics ciprofloxacin and linezolid are good examples for disproving this paradigm as MRSA harbors resistance mechanisms against both [5, 136, 137].

3.3 Current spread and costs of antibiotic resistances

The expenses for treatment and social costs in the EU on antibiotic-resistant infections in 2007 are estimated to be EUR 1.5 billion, coming along with some 25.000 patients deaths as a direct outcome of these infections [83]. 2.5 million extra hospital days, resulting in more than EUR 900 million in-hospital costs, could be calculated for 2007 [83].

In 2013, the CDC (Centers for Disease Control and Prevention) stated that at least 2 million people in the US were infected with antibiotic-resistant bacteria in 2012 and at least 23,000 individuals died in consequence. This is very similar to the number of people dying in Europe, estimated by the European Centre for Disease Prevention and Control. Current estimations assume the yearly economic impact of antibiotic resistance in the US to rise up to US\$ 20 billion due to additional direct healthcare costs and additional costs of US\$ 35 billion for lost productivity [138].

In the EU the population weighted average MRSA dissemination remains at a high level of 18 % (up to 25-50 %, country specific); it still represents one of the big health burdens in Europe. Visualization of the surveillance period between 2010 and 2013 is showing a decreasing trend of MRSA isolates (Figure 2), but this decrease is significantly smaller than that of the previous four-year period [139].

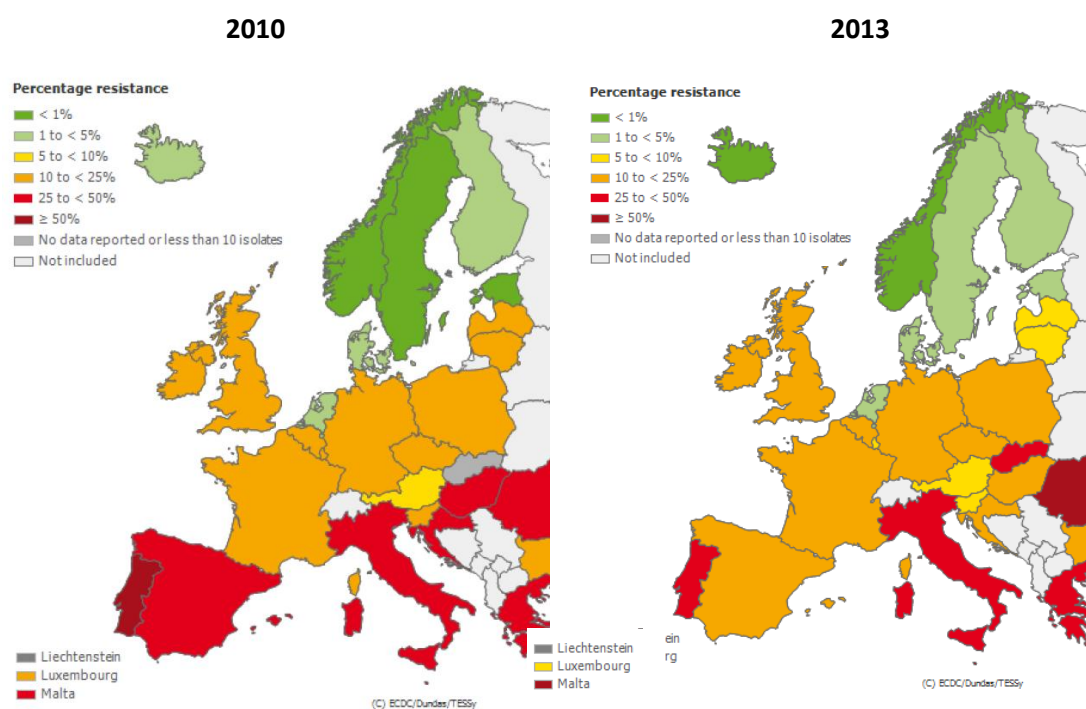


Figure 2: Spread of invasive methicillin resistant *S. aureus* isolates in 2010 and 2013 in the EU/EEA.

Data were obtained from the European Surveillance System – TESSy [140].

Invasive MRSA infections caused 80,461 medical cases and 11,285 associated fatalities in the US in 2011 [138]. Furthermore, the number of less severe infections in community and in healthcare

setting is expected to be much higher and, although a downtrend for HA-MRSA is monitored already, the same does actually not apply for or is not predictable for the more virulent CA-MRSA [138].

The German Hospital Infection Surveillance System (Krankenhaus-Infektions-Surveillance-System, KISS) detected a drop from 33 % to 27 % MRSA infections between 2007 and 2012. For primary sepsis the percentage of infections due to MRSA dropped from 36 % to 31 % and from 36 % to 30 % for lower respiratory tract infections [74]. CA-MRSA as well as LA-MRSA are not covered by this surveillance system and their future occurrence needs specific examination.

3.4 Drawbacks in antibiotic therapy

Beside the resistance limitations mentioned above antibiotic treatment always entails consequences for the host's microbiome. Especially broad band antibiotics are always killing also the natural and beneficial bacterial flora, which developed in co-evolution, and the microbial intestinal homeostasis in patients is greatly affected due to antibiotic therapy [141, 142]. On the one hand this can lead to secondary and opportunistic infections, often superficial [143], and on the other hand shifts the balance to a more resistant microbiome which henceforth loses its acquired resistance only very slowly again [4, 144].

Kohanski and colleagues could elucidate a general mechanism ordinarily arising while under bactericidal antibiotic treatment [145]. They could demonstrate the production of reactive oxygen species (ROS) in the antibiotic mediated bacterial death [145]. Under sub-lethal antibiotic concentration this production of ROS results in a higher level of genetic recombination and lesion tolerant error-prone DNA synthesis. This is facilitated via specialized polymerases with an activated SOS DNA damage response pathway and can thereby produce resistance by mutation [146, 147]. In other words the administration of a bactericidal antibiotic alone or in a therapeutic cocktail may indirectly lead to resistance due to increased DNA damage and genetic maladjustment. Or to put differently: The antibiotic substance itself triggers the bacteria to become resistant against precisely this treatment.

3.5 Initiatives and strategies for the development of novel antibiotics

Taking the current global resistance distribution into consideration, it can be assumed that sooner or later also resistance mechanisms against the "drugs of last resort" will exist and spread. Exploring novel strategies to overcome antibiotic resistance in microorganisms is therefore of global interest and the gap in innovation desperately needs to be filled.

Virtually the summation of all resistances in one particular strain, which shows a superior virulence pattern, is not inconceivable at all. It's in bacteria's nature to combat and evolutionary fight the circumstances it is exposed to. Chapter I 3.1 illustrates the current treatment options for MRSA

and obviously there is no really new discovery of an antibiotic chemical class. Only daptomycin objects a mode of action targeting the cell membrane, but it belongs to the previously invented chemical class of acid lipopeptids and thus does not present a clear innovation prospective. All eleven treatments, currently in the center of attention, are members of the antibiotic classes already developed up to 1988.

In 2013, Bassetti and colleagues listed new antibiotics under development. Even though five of the 30 listed new antibiotics are already FDA approved, all these antibiotics – possibly fighting MRSA – belong to the well established, but already often faced, target classes and no true innovation of the mode of action can be observed so far [18, 93].

The loss of innovation could have miscellaneous reasons, but it is assumed that big pharmaceutical companies withdraw from antibiotic development, because the revenues for the treatment of this short term diseases is likely not to cover the costs for drug development; profits are rather small compared with the profits of chronic diseases, because of the considerable shorter time of ingestion. [18].

In 2005, an increased attentiveness through global resistance rising led the EU Commission, in cooperation with the first international network ReAct (Action on Antibiotic Resistance) from the WHO and the Swedish Ministry of Health and Social Affairs and Uppsala University, to a release of a five-years action plan including the antibiotic program “New drugs 4 bad bugs - ND4BB” in 2011. ND4BB’s vision is to create an innovative collaborative public-private partnership based approach that will revive antibiotic research and discovery (R&D) [148–150].

In the US the first “National Strategy for Combating Antibiotic Resistant Bacteria” was adopted in September 2014 [151]. Current governmental motivations developed and guided by special FDA task forces, include regulatory and economic incentives like the 5 years additional patent protection and priority review as well as fast track designation stated in the GAIN Act (Generating Antibiotics Incentives Now Act of the US Food and Drug Administration Safety and Innovation Act (FDASIA)) in 2012 [152]. Their intention is the stimulation of research and discovery in industry and the encouraging of effective collaborations in academics to feed pharmaceutical pipelines for clinical development [152].

The Infection Disease Society of America (IDSA) started the global collaboration initiative 10x'20 primary by the recognition of the empty drug pipeline fighting the “ESKAPE” pathogens (*Enterococcus faecium*, *Staphylococcus aureus*, *Klebsiella pneumoniae*, *Acinetobacter baumannii*, *Pseudomonas aeruginosa* and *Enterobacter* species), already in 2010. It aims to create a sustainable global antibacterial drug R&D enterprise to create 10 new systemic antibiotics by the year 2020 to fight growing patient morbidity and mortality due to multidrug-resistant pathogens [153].

The cooperation of these initiatives and guidance of the WHO, which clearly requests for further national action plans in 2015, will hopefully lead to innovative research and strategies [24, 154]. Pioneering strategies and regulation after the World Health Day of “Antimicrobial resistance: No action today, no cure tomorrow” in 2011, as well as the global action plan will be needed to achieve this goal.

In the course of these initiatives for example oritavancin, dalbavancin, and tedizolid phosphate were approved most recently by the FDA, but the innovation potential is still missing [155]. The examples of the antimicrobial peptide brilacidin or the lipid II binding antibiotic teixobactin directed against MRSA are quite more innovative [156, 157]. The innovative mining of the former inculturable soil bacteria *in situ* on a chip, resulted in the discovery of teixobactin [157]. Yet again this chemical entity focuses the cell wall synthesis, but the molecular target is a highly conserved motif of lipid II (peptidoglycan precursor) and lipid III (teichoic acid precursor) [157]. In serial dilution no resistant mutants of *S. aureus* or *Mycobacterium tuberculosis* could be selected. Nevertheless, acquiring resistance through horizontal gene transfer would be an additional option [157]. Teixobactin is still in a preclinical state, its applicability needs to be proven and resistance development should be under particular revision, as the soil resistome is present and only needs genetical contact to *S. aureus* and an appropriate selection mechanism [3, 158].

4 Bacterial vitamin metabolisms

4.1 Vitamin B₁ - Thiamine

Vitamin B₁ (thiamine) consists of a thiazole- and a pyrimidine moiety, covalently linked by a methylene bridge. Humans – in contrast to bacteria, yeast and plants – have to rely on dietary ingestion of this essential cofactor, because they are not capable of *de novo*-synthesis [159]. Vitamin B₁ hypovitaminosis results in beriberi and sometimes polyneuritis via inhibition of pyruvate decarboxylase (PDC). Additionally, a deficiency can cause Wernick-Korsakoff syndrome and is further linked to depressive syndromes as well as neurodegenerative diseases [160–163].

S. aureus's thiamine biosynthetic pathway, genetical encoded on two operons - *tenA-thiM-thiD-thiE* and *gtpase-epi-tpk* - was characterized by Müller *et al.* The general overview of the metabolism is given in Figure 3 [164].

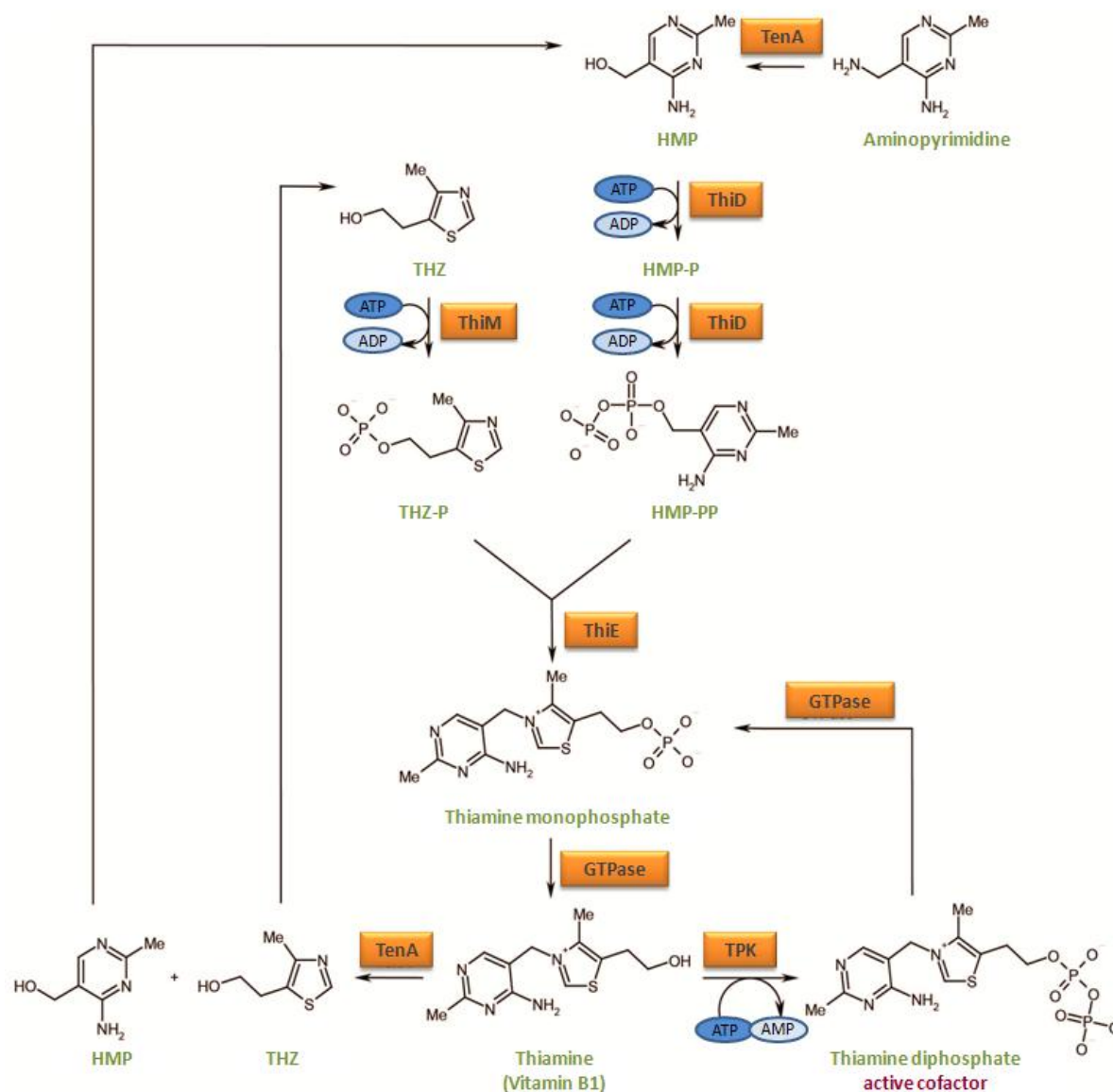


Figure 3: Vitamin B₁ *de novo* biosynthesis in *S. aureus*.

Bacterial enzymes are shown in orange boxes; chemical entities are given in green. In the bacterial cytoplasm the aminopyrimidine moiety is deaminated by TenA to HMP. HMP becomes phosphorylated by ThiD twice to HMP-PP. ThiM phosphorylates THZ to THZ-P which is then condensed with HMP-PP to thiamine monophosphate by ThiE. A GTPase dephosphorylates thiamine monophosphate to thiamine, which is afterwards either pyrophosphorylated by TPK or cleaved to HMP and THZ by TenA ([164], modified).

TenA (thiaminase type II, EC 3.5.99.2) deaminates aminopyrimidine and is thereby creating the pyrimidine moiety 4-amino-5-hydroxymethylpyrimidine (HMP). HMP is further pyrophosphorylated in a two step mechanism by ThiD (4-amino-5-hydroxymethylpyrimidine (HMP) kinase EC 2.7.1.49) to HMP-PP (HMP-pyrophosphate). In parallel the thiazole moiety is monophosphorylated by ThiM 2-(4-methyl-1,3-thiazol-5-yl)ethanol (THZ) kinase EC 2.7.1.50). In the subsequent step, ThiE (thiamine phosphate synthase, EC 2.5.1.3) fuses the HMP and THZ moieties to thiamine monophosphate (TMP). At this point the enzymes encoded in the second operon are producing thiamine diphosphate (TDP) in two steps. First an unspecific GTPase dephosphorylates TMP again, followed by the activation of

thiamine by pyrophosphorylation conducted via TPK (thiamine pyrophosphokinase, EC 2.7.6.2) [164]. No enzyme which is able to phosphorylate TMP directly is known in *S. aureus*. Recycling is conducted via TenA, which is also able to hydrolyze thiamine. However the hydrolysis reaction is 100 times slower than the initial deamination of aminopyrimidine [165]. Additionally, TDP can be dephosphorylated by the GTPase, which can regulate the active cofactor quantity on a translational level [164]. For numerous bacteria the regulation of thiamine biosynthesis is mediated through riboswitches, which bind TDP in a receptor-like manner and down-regulate the gene expression [166]. The substrate mediated regulation of the protein biosynthesis has been shown for the *tenA-thiM-thiD-thiE* operon as 28 % of TDP bind to the 5'-UTR of this gene cluster, but not for the *gtpase-epi-tpk* operon [164].

Hitherto there is no evidence that *S. aureus* can import thiamine through its cell membrane. An import of thiamine and TDP is known only for *Salmonella typhimurium* by ATP (adenosine triphosphate)-binding cassette transporters [167], for *E. coli* via the thiamine binding protein [168] and for yeast via YKoC, YkoD and YkoE [169].

TDP is essential in central metabolisms like glycolysis, citric acid cycle and pentose phosphate pathway [170–172]. It operates as an electrophilic covalent catalyst in the decarboxylation of 2-oxo acids, in carboligations of aldehydes and lyase-type reactions [173]. The catalytic cycle - where TDP acts as an electron sink - is initiated by an initial proton transfer, which enables the central ylid formation and was already elucidated by Breslow in 1958 [174]. For the initial tautomerization (Figure 4) the V-position of TDP (planar conformation of the thiazole and pyrimidine) as well as a highly conserved glutamate (Glu) residue in the TDP dependent enzymes are essential [172, 173, 175].

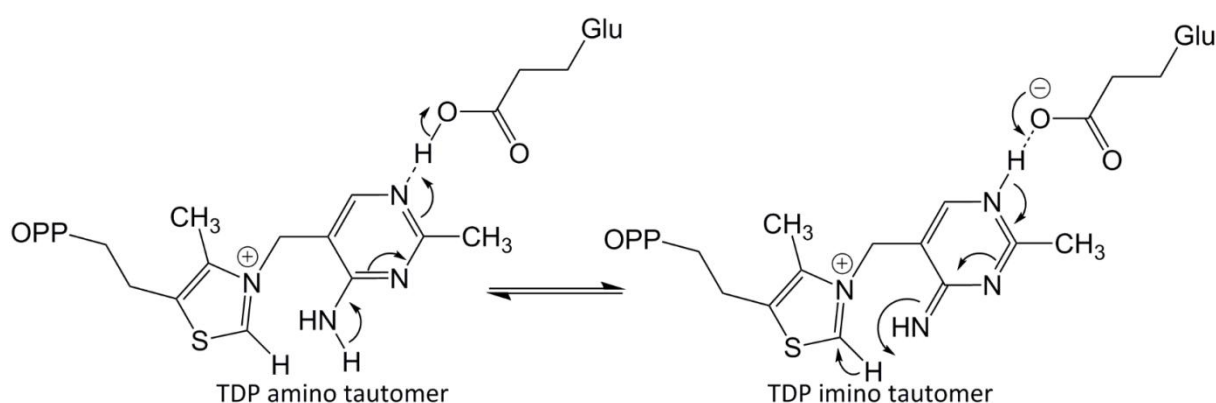


Figure 4: Tautomerization of thiamine diphosphate in thiamine dependent enzymes.

Thiamine diphosphate tautomerization is the basis for the ylid formation which is induced by the high energy V-conformation of thiamine and a conserved Glu residue of the thiamine dependent enzyme. Figure was created with ChemDraw (PerkinElmer Inc.) following Leeper and Agyei-Owusu & Leeper [175, 176].

The next steps of the general reaction mechanism are illustrated by the PDC (Figure 5). The resulting ylid creates a nucleophilic attack on the keto group of the substrate pyruvate leading to an

acetaldehyde intermediate which after decarboxylation forms the enamine intermediate. The enamine represents an α -carbanion which is an excellent nucleophil. By PDC the enamine gets protonated and acetaldehyde is released to regenerate the ylid.

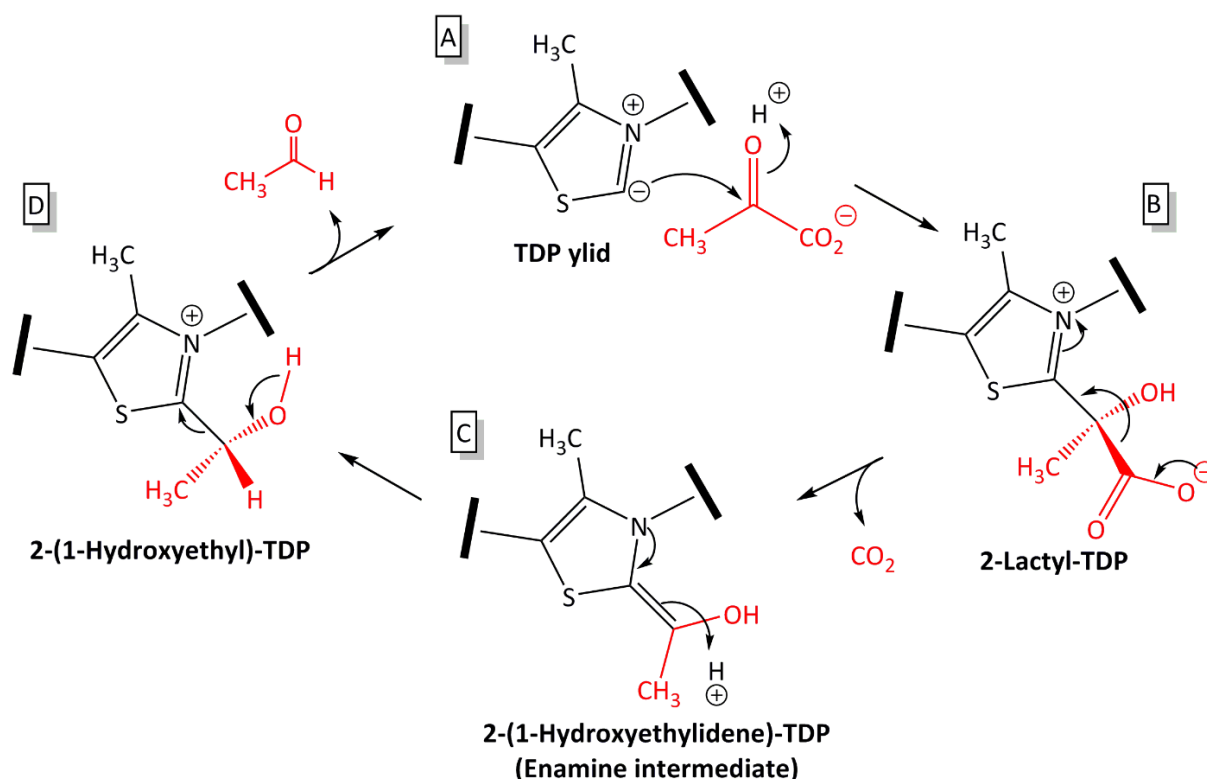


Figure 5: TDP enamine formation in the decarboxylation of pyruvate by PDC.

Carbanion (enamine intermediate) formation (C) as a result of the nucleophilic attack (A) on the keto group and the subsequent decarboxylation (B), as well as the recycling of the ylid (D) is shown. Figure was created with ChemDraw (PerkinElmer Inc.) following Leeper and Agyei-Owusu & Leeper [175, 176].

Analogues of thiamine containing an oxazolium or imidazole ring instead of the thiazole moiety show less reactivity due to the missing 3d orbitals and the absent stabilization of the carbanion [177, 178]. Furthermore, methylation of the C2 atom in the THZ moiety leads to inactivation of pyruvate decarboxylase [179]. The same enzyme is inhibited if the hydrogen at the C2 atom is replaced by oxygen, probably due to additional hydrogen bonds formed between the cofactor and the enzyme [180]. The transketolase of yeast can be inhibited by C2-tetrahydro-TDP [181]. If the nitrogen in the thiazol moiety is exchanged to a carbon atom resulting in a neutral thiophene ring, 3-deaza-TDP is formed. This analogue, which cannot form an ylid anymore, is used to study thiamine dependent enzymes and shows an exceptional irreversible inhibition of *Zymomonas mobilis* PDC [182]. Mimicking the overall neutral zwitterionic ylid, a tighter binding than TDP is possibly mediated through increased hydrophobic interaction [176].

Besides the role of TDP as prosthetic group, thiamine triphosphate (TTP) is suspected to signal the metabolic state, like nutrition starvation in *E. coli* [183, 184]. Furthermore, adenylated derivatives, adenosine thiamine triphosphate and TTP, were detected in humans and are suspected

to be important in neurochemical and metabolic sensing or cell differentiation, but their exact role is still unclear [165, 185–187].

4.2 Vitamin B₆ - Pyridoxine derivatives function, production and regulation

Vitamin B₆ occurs in three chemical entities in nature: pyridoxal (PL), pyridoxine (PN) and pyridoxamine (PM). Pyridoxal-5'-phosphate (PLP), the activated vitamin, is an essential cofactor for a variety of biochemical reactions, including decarboxylation, transamination, racemization, elimination and replacement of electrophilic groups at the β - or γ - carbons, mainly on amino compounds in prokaryotes as well as eukaryotes [188]. Its versatile participation in 140 discrete catalytic functions – accounting for 4 % of all classified reactions – denotes its remarkable role in divergent evolution as a covalently linked electrophilic catalyst, stabilizing carbanionic reaction intermediates [189–192]. In Figure 6 the underlying chemical mechanism is shown.

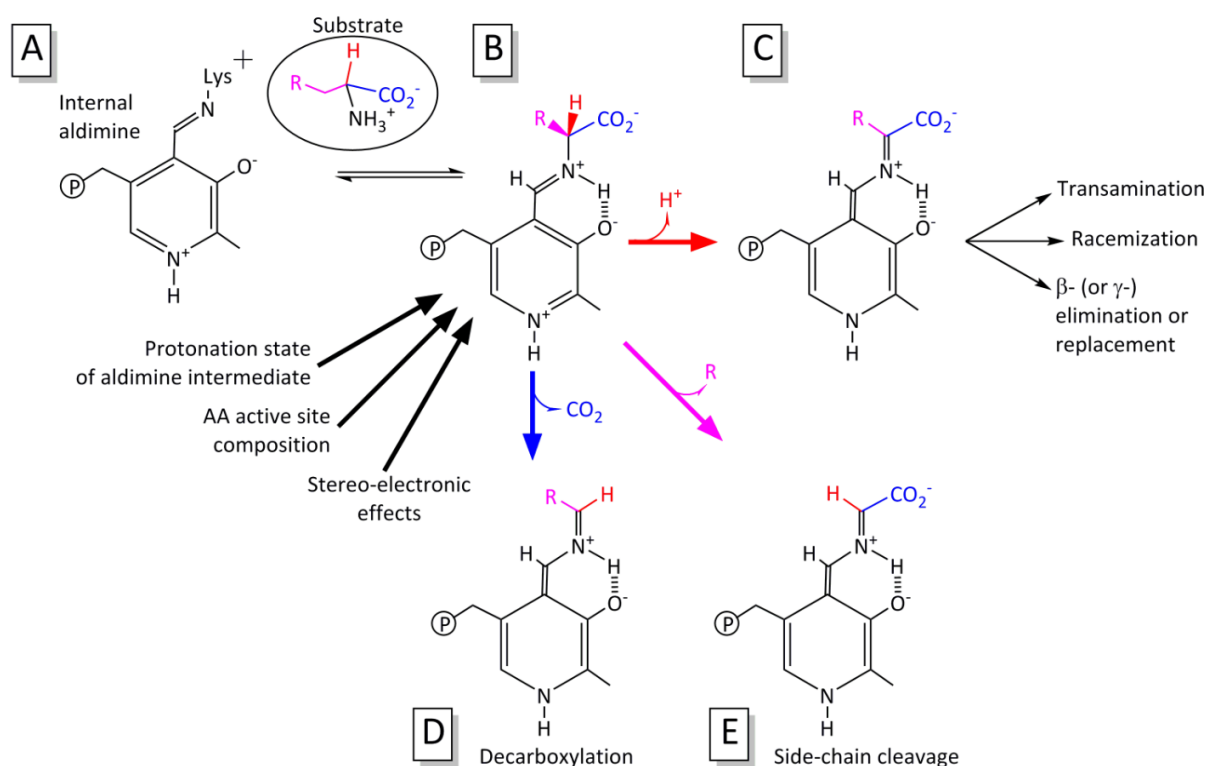


Figure 6: Internal and external aldimine formation of protonated PLP resulting in the diverse reaction type catalysis.

A: Internal aldimine formation with lysine in active side. B: External aldimine formation upon substrate binding. The protonated PLP, acting as a molecular sink, stabilizes the negative charge at C α (carbanion). C: Proton abstraction leads to a quinonoid intermediate which is acting in transamination, racemisations and β/γ -eliminations and replacements. D: Carboxylate removal results in an amine formation. E: C α –C β bond cleavage such as occurring in retro-aldol condensation. Figure was created with ChemDraw (PerkinElmer Inc.) following Percudani & Peracchi and Toney [189, 193].

PLP is covalently linked via the aldehyde group to the ϵ -nitrogen of a catalytic lysine side chain of the apoenzyme forming a secondary aldimine (Schiff base) also termed internal aldimine (Figure 6 A). Once the substrate amino group exchanges the lysine residue in a transamination reaction, the external aldimine is formed (Figure 6 B). Depending on the protonation state of aldimine

intermediates, interaction of specific stabilizing amino acids (AA) in the active site and on stereoelectronic effects the reaction selectivity is determined. This results in either a proton abstraction, removal of a carboxylate group, or a side chain cleavage at the C_α in the external aldimine giving the carbanionic intermediate (Figure 6 C,D,E) [191–194].

Besides the pyridine ring acting as an electron sink which stabilizes negative charges, vitamin B₆ was identified to operate in haem [195], niacin [196] and serotonin [197] synthesis. It is further presumed to act regulatively on transporters [198] as well as on transcription factors [199] and hormonal balance [200]. Furthermore, vitamin B₆ is implicated in tumor development and progression [201, 202] and is known as a very potent antioxidant trapping superoxide radicals and singlet oxygens [203, 204]. Moreover, it could be shown that some PLP-dependent enzymes necessitate the cofactor for refolding and dimerization processes, suggesting an extra function as a chaperone like molecule. This is the case for *Bacillus subtilis* serine hydroxymethyltransferase, tryptophan synthase β₂ subunit and aspartate aminotransferase from *E. coli*, cystalysin from *Treponema denticola* and dopa decarboxylase out of humans [205–208].

Humans, in contrast to bacteria, fungi and plants, have to rely on dietary uptake and trapping in the salvage pathway of this precious cofactor [209, 210]. In bacteria generally two different biosynthetic pathways for *de novo* synthesis are known: Firstly the deoxyxylulose 5-phosphate (DXP) dependent pathway resulting in pyridoxine-5'-phosphate (PNP), very well characterized for *E. coli* and restricted to eubacteria and secondly the D-ribose 5-phosphate (R5P) pathway also named DXP-independent pathway resulting in pyridoxal-5'-phosphate, extensively studied e.g. in *B. subtilis* [211, 212]. Figure 7 shows an overview of the distribution of the *de novo* and salvage pathways. The *de novo* pathways are only present in bacteria and plants. The salvage pathway, which is responsible for the recycling of the vitamin B₆ from protein turnover, can be found in bacteria and humans. For a more detailed analysis of the two *de novo* pathways please find details in Fitzpatrick *et al.*, 2007 and Mukherjee *et al.*, 2011 [213, 214].

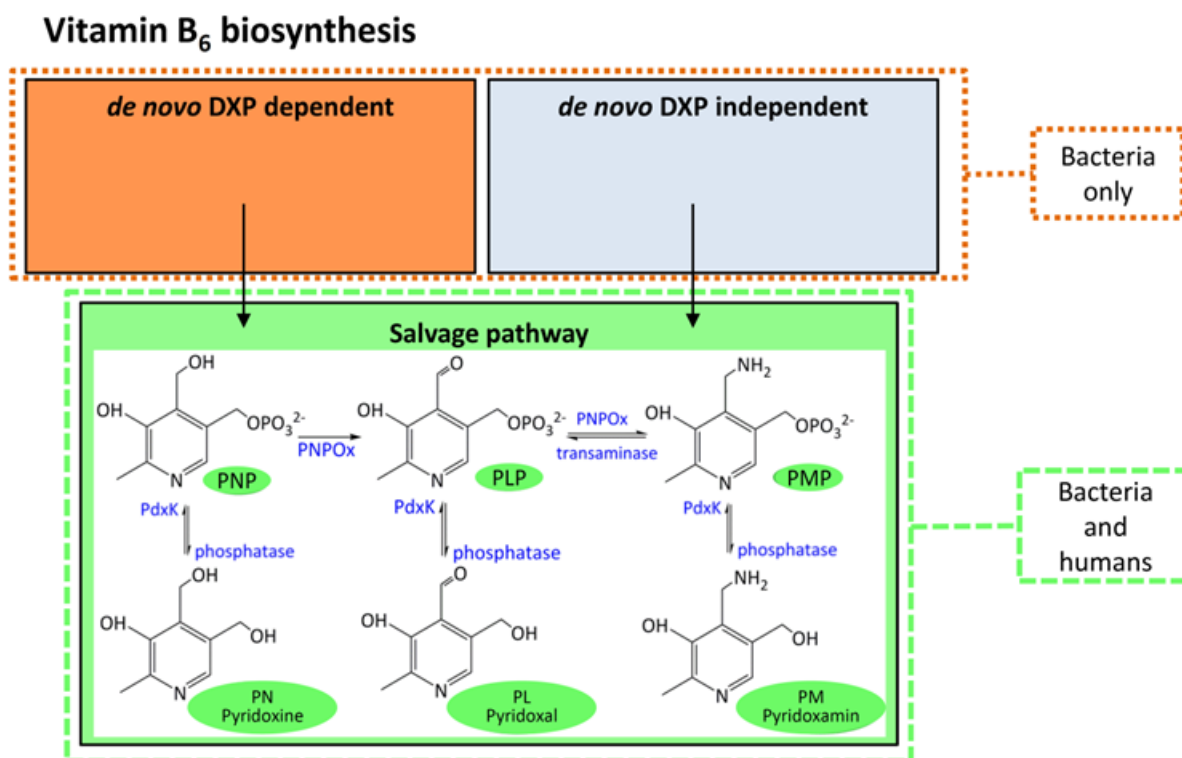


Figure 7: Overview of the vitamin B₆ biosynthesis and salvage pathway in bacteria and humans.

The feeding of the DXP dependent and independent *de novo* vitamin B₆ biosynthesis and the vitamin B₆ salvage pathway is given. Figure was created with ChemDraw (PerkinElmer Inc.) following Fritzpatrick *et al.* [213] and Tanaka *et al.* [210].

In cause of the omnipresent salvage pathways PNP as well as PMP both are convertible to PLP via pyridoxine 5'-phosphate oxidase (PNPOx). Counteracting, PdxK, an ATP-dependent pyridoxal kinase, can phosphorylate the alcohol group of PL, PN and PM and hence trap the vitamers.

The level of free PLP, an extremely reactive aldehyde, and thus the vitamin B₆ homeostasis is believed to be regulated via substrate inhibition of PdxK and PNPOx in the presence of Mg²⁺ and ATP [215–217]. Malfunction or deregulation of the PLP level, possible by influencing the regulatory enzymes PdxK and PNPOx due to drug ingestion or directly by mutations, may result in neurological disorders like seizures, depressions or anemia [218–220].

In *S. aureus*, a *de novo* pathway is present which is homologue to the *B. subtilis* pathway and naturally the salvage pathway for trapping and regulating the vitamin B₆ homeostasis [221, 222].

4.3 Bifunctional enzymes - ThiD and PdxK

In yeast it has been shown that the precursor of the HMP majority of thiamine metabolism can be PLP as well [223–225]. This linkage between both metabolisms was already suspected by Schultz and colleagues in 1940 and probably can provide information about the evolution of these both essential pathways [226].

S. aureus ThiD (gi: 14247866) is clustered on the thiamine operon *tenA-thiM-thiD-thiE*, whereas *S. aureus* PdxK (gi: 14246348) is identified as PL salvage enzyme [164, 222]. But PdxK is a member of ThiD thiamine monophosphate (TMP) synthase family and also has affinity to HMP, which is the substrate of ThiD from vitamin B₁ pathway [222]. The acceptance of the three discrete B₆ vitamin substrates and HMP is also known for *Plasmodium falciparum* PdxK [227], *E. coli* PdxK [228, 229], *Trypanosoma brucei* PdxK [230] and the *thid* gene product from *B. subtilis* [231].

This expanded substrate specificity, or in other words substrate promiscuity, additionally will be attractive for clarifying the evolution and interplay of the pathways. Subsequently this information can be used to distinguish and predict side effects occurring by poisoning one of these pathways.

4.4 Vitamin B₁ *de novo* and vitamin B₆ salvage pathway as potential drug targets

The example of nitazoxanide (2-acetyloxy-N-(5-nitro 2-thiazolyl) benzamide; NTZ) gives clear evidences on the rewards of targeting a cofactor as a potential antibiotic target. Since 2004, NTZ is an FDA approved drug against protozoan parasites (genus *Cryptosporidium*, most commonly *Cryptosporidium hominis* and *C. parvum*) causing cryptosporidiosis [232]. It shows chemical similarity with the already well known compound metronidazole, which is a 5-nitroimidazole drug widely used for microaerobic bacteria like *Helicobacter pylori* [233]. In contrast to metronidazole the nitro group of NTZ (Figure 8) does not have to be activated by reduction and no DNA impairment could be elucidated as MoA. Although it presents an entity of the pro-drug class and for its activity NTZ has to be deacetylated to tizaxonide (TIZ) as could be seen in Figure 8 [234].

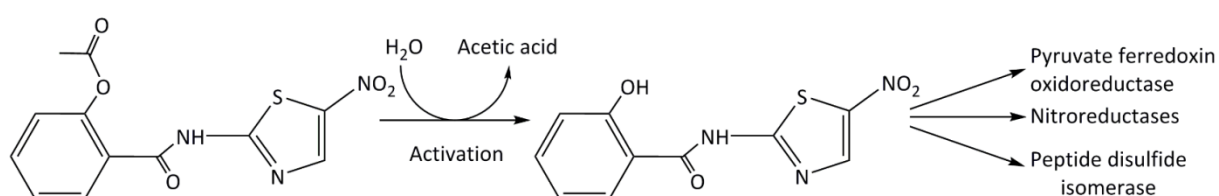


Figure 8: Activation of nitazoxanide (NTZ) to tizaxonide (TIZ).

The figure shows the formation of the active metabolite of the prodrug nitazoxanide by deacetylation and its possible targets ferredoxin oxidoreductase, nitroreductase and peptide disulfide isomerase on protozoans and bacteria [235].

Subsequently, it was discovered that the anionic form of NTZ specifically inhibits pyruvate-ferredoxin oxidoreductase (PFOR) by abstracting a proton from the activated cofactor thiamine diphosphate, leading to a dissociation of the complex [236]. Thus targeting the activated cofactor TDP could be elucidated as MoA. In addition, NTZ showed activity against *Mycobacterium tuberculosis*, *Clostridium difficile* and further gastrointestinal infections causing parasites [235, 237]. It principally seems to evade resistance, because it was neither possible to generate NTZ resistance in laboratory nor has resistance been observed after more than ten years of clinical use [238].

Summarizing this variety of target germs by NTZ and the so far elucidated MoA, the first exceptionally potential antibacterial and antiparasitical compound targeting the essential cofactor dependent enzymes demonstrates the drugability and advantages of TDP targeting.

Equivalent to the enzymatic equipment of *B. subtilis* also for *S. aureus* a vitamin B₆ salvage pathway was identified and discriminated from the thiamine biosynthetic pathway [164, 222, 231]. Because of this extraordinary eclectic role, PLP was already evaluated as potential drug target for *Plasmodium falciparum*, the causative agent for malaria tropica [162, 239–242], and also in particular for *Trypanosoma brucei* [243].

Very recently, primaquine, a quinoline commonly used for the treatment of malaria and trypanosomiasis, was identified to inhibit human *Trypanosoma cruzi*, *Plasmodium vivax* and human PdxK *in vitro* [244]. For the human pyridoxal kinase a competitive mechanism with a K_i of $5.72 \pm 7.3 \mu\text{M}$ could be observed *in vitro* [244]. This is comparable low to the primaquine serum concentration of $0.59 \mu\text{M}$, but maybe the drugs success is related to an accumulation inside the parasite [244].

These two fundamental examples, illustrating the targeting of the vitamin B₁ and the B₆ metabolism respectively, clearly suggest the possible drugability of B₁ and B₆ in *S. aureus* and the potential advantages of a cofactor mediated multi-target approach. Targeting this vital bacterial and parasitic niche directly, represents a novel development and possibly leads to a complete new broad spectrum antibiotic with low resistance potential.

5 Advanced drug design - Shaping substrate analogs to suicide drugs

As highlighted in chapter I 4.1 and I 4.2, an extraordinary dependence of bacteria on the cofactor synthesis, availability and function, especially for vitamin B₁ und B₆, is evident. If one of these versatile cofactors is inactive or only limited accessible, this will lead to multiple downstream effects, like the impairment of glycolysis, pentose phosphate pathway or carboanhydrate metabolism. Infiltrating unique bacterial vitamin biosynthesis pathways with compounds, termed suicide drugs, further processed by bacterial metabolism *in vivo* to inactive cofactors, will have two remarkable advantages:

Fundamentally, an inactive cofactor will block multiple downstream enzymes and an uncoupling of compounds entrance and site of action is achieved. In consequence such compounds will act like a pro-drug, but in an advanced way. Several metabolism steps prior the production of the blocking and inactive compound will lower the probability of a bacterium to evade the selective pressure by a single mutation. Furthermore, due to the high conservation of the metabolism in bacteria, the approach will be prokaryote-specific and applicable to a multitude of bacteria [245].

As mentioned in chapter I 4.4 no mutation development could be observed for NTZ, which targets the active cofactor TDP, so far. This clearly illustrates the advantages of targeting vitamin B₁, with the extension that the approach of producing an inactive cofactor *in vivo* would be bacteria specific, as humans lack this particular pathway.

In consequence, impairment of bacterial homeostasis by cofactor obstruction will lead to direct germs death or a slowdown of growth, which will give the immune system or the beneficial natural flora a chance to fight and overgrow the bug. Further, a boost of the hosts immune system in combination with the suicide drug would be a vital possibility to eradicate the germ completely [246].

In turn to the manifold downstream effects by targeting an essential cofactor, distinguishing features have to be characterized for the metabolic pathways and possible downstream targets. Structural biology, consistent with biophysical and biochemical characterization, will be particularly important to discover and reveal candidate enzymes and compounds of advanced target oriented medical chemistry approaches.

II Aims of this Work

Today, *Staphylococcus aureus* represents yet again one of the most devastating, health threatening human pathogens. In Europe it is still a dominant cause for nosocomial infections coming along with some 25,000 patients' deaths and EUR 1.5 billion healthcare costs in 2007 [83]. Up to now no antibiotic targeting any innovative bacterial structure is available, which is not opposed to an already existing bacterial resistance mechanism. This and the additional increasing number of community acquired severe infections alarmingly demonstrate the urgent need for the development of new antibiotics. In this work a structure based pro-drug investigation targeting the essential vitamin B₁ metabolism of *S. aureus*, which is absent in humans, via specific metabolizable compounds is focused. Pro-drug like compounds which will be converted inside this unique bacterial pathway into toxic cofactor derivatives referred to as suicide drugs, will be investigated. This approach will avoid the selective pressure on single antibacterial drug targets and will result in multiple downstream effects on key enzymes of the carbohydrate and amino acid metabolism.

The first core aspect in this work is the structural characterization of two selected substrate analogs of ThiM in comparison to the natural substrate THZ via X-ray crystallography. The analysis of these previously identified compounds would provide the opportunity to further optimize the compounds and present a vital basis for advanced rational substrate analog development. Further focus will be placed on the analysis of the activation of the fully functional natural cofactor B₁ via the enzyme TPK. This kinase in complex with its natural substrate thiamine is expected to provide insights about how the approach with the substrate analogs for ThiM is applicable and to define possible influences on human vitamin metabolism by comparative structural analysis of the enzyme. Second core aspect of this study is the elucidation of the interplay of the highly conserved vitamin B₁ *de novo* synthesis in *S. aureus* and the B₆ salvage pathway, which is present in bacteria, but also protozoan and higher eukaryotes. In terms of this relationship a delimitation of the structural configuration of enzymes of the vitamin B₆ pathway needs to be defined. For this purpose the structure of essential vitamin B₆ kinase PdxK from *S. aureus* as well as the protozoan PdxK from *Trypanosoma cruzi* are planned to be studied by X-ray crystallography. An analysis of the evolutionary traces conserved in protein structure also in comparison to human homologues for a rational understanding of the selectivity shall be conducted. Additional emphasis is placed on the preparation and analysis of potential dynamic studies of the analyzed enzymes. For this purpose crystallization experiments with caged ATP are planned and it is intended to find parameters and conditions to produce micro and nano crystals of target proteins. Moreover, opportunities of *in vivo* crystallization within insect cells as well as extension of the protein production in this complementary expression system of all pathway proteins are to be considered.

III Methods

1 X-ray sources

The following beamlines were used to generate high resolution structural data, the rotation anode X-ray generator was used to test and score crystallization trials.

P14	EMBL (European Molecular Biology Laboratory, DESY, Hamburg, Germany) Source: PETRAIII storage ring Focal spot: 4 x 9 μm^2 up to 300 x 300 μm^2 Wavelength: 0.976262 / 0.976300 Å Detector: Pilatus 6M
SAXS (X33)	EMBL, Hasylab, DESY, Hamburg, Germany Source: DORIS bending magnet Focal spot: 2 mm x 0.6 mm Wavelength: 1.5 Å Detector: Photon counting Pilatus 1M-W pixel detector; Photon counting Pilatus 300K-W pixel detector; Mar345 image plate (345 mm ²)
Rotating anode	University Hamburg Source: Rigaku RU 200 X-ray generator Wavelength: Cu K α = 1.5418 Å Detector: MAR300 image plate

2 Instrumentation

Table 3: Instrumentation (alphabetically listed).

Instrumentation	Manufacturer
Agarose gel electrophoresis:	
Gel caster	PerfectBlue™ Mini S (Peqlab, Germany)
Power supply	PowerPac 200 (Bio-Rad, Germany)
Electrophoresis unit	PerfectBlue™ Mini S (Peqlab, Germany)
UV transilluminator	Gel iX Imager (INTAS Science Imaging Instruments, Germany)
Balance	TE3102S (Sartorius, Germany)
CD spectrometer	J-815 (Jasco, UK)
Centrifuges	5415R/5415C/5424/5804R/5810R MinispinPlus (Eppendorf, Germany) Multifuge X3R (Thermo Fisher Scientific, Germany)

Clean bench	Hera Safe, Thermo Electron corporation (Thermo Fisher Scientific, Germany)
Crystal imaging	Digital Sight DS-L3 (Nikon, Japan) CrystalScore (Diversified Scientific Inc., US) Microscope SZX12 (Olympus, Japan)
DLS instrumentation	SpectroSize 300 (XtalConcepts, Germany) Spectro Light 500 (XtalConcepts, Germany)
FPLC (Fast protein liquid chromatography)	ÄKTA Purifier P-901 (GE Healthcare, UK) ÄKTA Prime (GE Healthcare, UK)
Freezer:	
-20 °C	Liebherr premium (Liebherr, Germany)
-80 °C	B35-85 (FRYKA-Kältetechnik, Germany)
Incubator 37 °C	Heraeus B6120 (Heraeus, Germany)
Incubator 27 °C	Heraeus B-5060 (Heraeus, Germany)
Crystal plate incubator 4 °C and 20 °C	RUMED 3001 incubator (Rubarth, Germany)
Microbalance	CP224S-OCE (Sartorius, Germany)
Microscopes	Stereo microscope SZX12 (Olympus, Japan) Axiovert 25 (Zeiss, Germany)
Micropipette	Micropipette ResearchPlus (Eppendorf, Germany)
Multichannel pipette	Multichannel pipette ResearchPlus (Eppendorf, Germany)
Microwave	NN-e202W (Panasonic, Japan)
Pipetting robots	Honeybee 961 (Genomic Solutions, US) Lissy (Zinsser, Germany) Oryx4 (Douglas Instruments Ltd, UK)
pH-meter	SevenEasy (Mettler Toledo, US)
Roller mixer	Stuart Roller Mixer SRT9 (Stuart, UK)
SDS-PAGE:	
Gel caster	Four Gel Caster (SE275)
Power supply	EV 231 (Peqlab, Germany)
Electrophoresis unit	SE260 Mighty Small II Deluxe Mini electrophoresis unit (Hoefer, US)
Sonifier ultrasonic cell disruptor	Sonifier S-250A analog ultrasonic processor 200 W (Emerson Electric Co, US)
Spectrophotometer	GeneQuant 1300 (GE Healthcare, UK) Nanodrop 2000c and NanoDrop Lite (Thermo Fisher Scientific, Germany) UVICON 933 (BIO-TEK Kontron Instruments, US)
Stirrer	VMS-A (VWR, US) MR 3001 (Heidolph, Germany)
Thermocycler	Mastercycler gradient (Eppendorf, Germany) Mastercycler personal (Eppendorf, Germany) MyCycler Thermal Cycler™ (Bio-Rad, US) Primus 25 Advanced (Peqlab, Germany)

Thermomixer	Thermomixer comfort (Eppendorf, Germany)
UV-light source	CrystalLIGHT 100 (Nabitec, Germany)
Western blot transfer unit	V20-SDB Semi-Dry Blotter Unit (SCIE-PLAS Ltd., UK)

3 Buffers, solutions and consumables

All standard buffers and solutions were produced in deionised H₂O and listed in Table 4 unless stated otherwise. Plastic consumables were obtained from Sarstedt or Eppendorf.

Table 4: Comprehensive list of all standard buffers and solutions arranged according to their application.

Buffer or solution	Composition / Supplier
Agarose-Gelelectrophoresis:	
TAE-buffer (50x)	2 M Tris, 950 mM Acetic acid, 50 mM EDTA
Loading dye (5x)	0.05 % (w/v) bromophenol blue, 0.35 % (w/v) Xylene cyanol, 1 mM EDTA, 60 % (w/v) glycerol
DNA Marker	FastRuler (SM1123, SM1103, SM1113) High Range DNA Ladder (10 kbp-500 bp) Medium Range DNA Ladder (5000-100 bp) Low Range DNA Ladder (1500-50 bp) (Thermo Fisher Scientific, Germany)
Ethidium bromide staining solution	0.5 µg mL ⁻¹ in H ₂ O #E1510 (Sigma, Germany)
Enzymes and buffers:	
dNTPs mix	#R0181 (Thermo Fisher Scientific, Germany) Preparation of 2 mM dATP, dCTP, dGTP, dTTP each
<i>Pfu</i> polymerase and buffer	#EP0501 (Thermo Fisher Scientific, Germany)
<i>Taq</i> polymerase and buffer	#EP0401 (Thermo Fisher Scientific, Germany)
T4 ligase and buffer	#EL0014 (Thermo Fisher Scientific, Germany)
Fast XbaI	#0684 (Thermo Fisher Scientific, Germany)
BamHI	#ER0051 (Thermo Fisher Scientific, Germany)
BsaI	#R0535S (New England BioLabs, US)
EcoRI	#ER0271 (Thermo Fisher Scientific, Germany)
HindIII	#ER0501 (Thermo Fisher Scientific, Germany)
CaCl₂-Buffer	100 mM CaCl ₂ , 10 % (v/v) glycerol
Protein buffers (Protein buffers were supplemented with 0-400 mM imidazole for His₆-tag based purification, details are specified in the results IV)	
T/N-buffer	50 mM Tris, 150 mM NaCl, pH 8.0
T/N300-buffer	50 mM Tris, 300 mM NaCl, pH 8.0
T/M-buffer	50 mM Tris, 300 mM MgCl ₂ , pH 8.0
P/N-buffer	50 mM K - phosphate, 150 mM NaCl, pH 8.0

Buffer or solution	Composition / Supplier
TEV1-buffer	T/N300 buffer supplemented with 5 mM DTT ((2S,3S)-1,4-Disulfanyl-2,3-butanediol) and 2 % (v/v) glycerol and 20 mM imidazole
TEV2-buffer	TEV1-buffer with 50 mM imidazole
TEV3-buffer	TEV1-buffer with 300 mM imidazole
IPTG solution	100 mM IPTG (Isopropyl-1-thio- β -D-galactopyranosid)
Anhydrotetracyclin	2 mg mL ⁻¹ in DMF (N,N-Di-methyl-formamide)
Strep-tactin elution buffer (10x)	1 M Tris-HCl, pH 8.0 1.5 M NaCl 10 mM EDTA 25 mM desthiobiotin (IBA, Germany)
Ni-Nitrilotriacetic acid agarose regeneration:	
Regeneration buffer	6 M Guanidine hydrochloride, 0.1 M acetic acid
SDS solution	2 % (w/v) Sodium dodecyl sulfate
Ethanol solutions	20, 50, 75, 100 % (v/v) ethanol (MEK-den.)
EDTA solution	100 mM EDTA, pH 8.0
NiSO₄ solution	100 mM NiSO ₄
Strep-tactin sepharose regeneration:	
Strep-tactin regeneration buffer (10x)	10 mM HABA (IBA, Germany) (2-[4'-hydroxy-benzeneazo]benzoic acid) in buffer T/N
SDS-PAGE:	
Stacking gel buffer	0.5 M Tris-HCl, pH 6.8
Separating gel buffer	1.5 M Tris-HCl, pH 8.8
APS solution	10 % (w/v) Ammonium peroxydisulfate
TEMED (Tetramethylethylenediamine)	~99 % (Sigma Aldrich, Germany)
SDS solution	10 % (w/v) sodium dodecyl sulfate
SDS-PAGE electrode buffer	25 mM Tris 0.192 mM glycine 0.1 % (w/v) SDS
SDS-PAGE sample buffer (5x)	95 mM Tris-HCl pH 6.8 40 % (v/v) Glycerol 3 % (w/v) SDS 0.17 % (w/v) Bromophenol blue 0.5 % (w/v) DTT
SDS-PAGE Marker	Unstained Protein Molecular Weight Marker #26610, Size range 14.4-114 kDa (Thermo Fisher Scientific, Germany)
Coomassie staining solution	25 % (v/v) 2-Propanol 10 % (v/v) Acetic acid

Buffer or solution	Composition / Supplier
Coomassie destaining solution	0.25 % (w/v) Coomassie brilliant blue G-250
Native PAGE	20 % (v/v) Acetic acid SERVAGE™ N Native Starter Kit (Serva, Germany)
Western Blot (WB):	
Transfer buffer	25 mM Tris, 192 mM Glycin, 20 % (v/v) Isopropanol, pH 8.3
Marker	PageRuler Plus Prestained Protein Ladder #26619, 10-250 kDa (Thermo Fisher Scientific, Germany) PageRuler Unstained Protein Ladder (Fermentas, Germany)
Nitrocellulose membrane	Roti®-NC, 0.2 µm (Carl Roth, Germany)
Ponceau staining solution	0.2 % (w/v) Ponceau-S 2 % (v/v) Acetic acid
PBS (Phosphate buffered saline)	140 mM NaCl 25 mM KCl 0.5 mM MgCl ₂ 1 mM CaCl ₂ 10 mM Na ₂ HPO ₄ (pH 7.5)
TBS (Tris buffered saline)	1 M Tris/HCl, 750 mM NaCl, pH 7.5,
PBS-T/TBS-T	1x PBS/ 1x TBS 0.05 % (v/v) Tween 20
Blocking solution	4 % (w/v) BSA (Bovine serum albumin) in PBS or TBS buffer
Antibodies and WB detection:	
1st antibodies	Murine Anti-Strep-tag II antibody, IgG1; #2-1507-001, 0.2 mg mL ⁻¹ in PBS (IBA, Germany) final dilution: 1:2000 Murine Anti-His-tag antibody, IgG1; #65250, 0.5 mg mL ⁻¹ in PBS, 0.09 % (w/v) NaN ₃ (BioLegend, US) final dilution: 1:10000
2nd antibodies	Goat anti-mouse IgG-HRP (horseradish peroxidase) conjugated, #SC-2005 (Santa Cruz Biotechnology, US) final dilution: 1:3000 Goat anti-mouse IgG-AP conjugated, #A3562 (Sigma, Germany) final dilution: 1:30000
AP reaction buffer	100 mM Tris/HCl, 4 mM MgCl ₂ , pH 9.5

Buffer or solution	Composition / Supplier
BCIP solution	20 mg mL ⁻¹ (w/v) BCIP (5-bromo-4-chloro-3'-indolylphosphate) in DMF
NBT solution	50 mg mL ⁻¹ NBT (nitro-blue tetrazolium) in 70 % DMF
ECL (enhanced chemiluminescence) detection	Amersham ECL Western Blotting Detection Reagents
Crystallization screens and chemicals:	
PCT™ Pre-Crystallization Test	Hampton Research, US
AmSO ₄ -Suite	Qiagen, Germany
Classics Suite	Qiagen, Germany
Cryos Suite	Qiagen, Germany
JCSG-plus	Molecular Dimensions, UK
Morpheus	Molecular Dimensions, UK
PACT premier	Molecular Dimensions, UK
Stura Footprint Screen & MacroSol	Molecular Dimensions, UK
NPE-caged ATP	#02017 (releases of the parent compound from its cage after irradiation with pulses of $\lambda = 360$ nm, (Sigma, Germany))
(Adenosine 5'-triphosphate P3-[1-(2-nitrophenyl)ethyl ester] disodium salt)	
ATP	#A1852 (Sigma, Germany)
THZ	#W320404 (Sigma, Germany)
(2-(4-methyl-1,3-thiazol-5-yl)ethanol)	
Thiamine	T4625 (Sigma, Germany)
Pyridoxal	#0960,0025 (AppliChem, Germany)
Pyridoxine	#T914.1 (Carl Roth, Germany)
AMP-PNP	#A2647 (Sigma, Germany)
AMP-PCP	#M7510 (Sigma, Germany)
Cpd1	#4016593 (ChemBridge, US)
(2-(1,3,5-trimethyl-1H-pyrazole-4-yl)ethanol)	
Cpd2	#4027195, (ChemBridge, US)
(2-(2-methyl-1H-imidazole-1-yl)ethanol)	
Cpd12	#069532 (Matrix Scientific, Egypt)
(2-(3-brom-1,2-oxazol-5-yl)ethanol)	
NMR protein buffer	50 mM Tris- <i>d</i> 11-D ₂ O, 150 mM NaCl, pH 8 (pH adjusted with DCl)

4 Molecular biology and biochemical methods

4.1 PCR - Polymerase chain reaction

Exponential DNA fragment amplification to clone a gene of interest into an expression vector was carried out using a PCR [247]. Ordinary PCR reactions using either *Taq* or *Pfu* polymerase derived from the thermophilic bacterium *Thermus aquaticus* [248] and *Pyrococcus furiosus* [249] contained the following components shown in Table 5. MgCl_2 was only added to *Taq* polymerase based reactions as the buffer for *Pfu* polymerase is already supplemented with 2 mM MgSO_4 .

Table 5: Typical standard polymerase chain reaction components.

Component	Final concentration
Polymerase buffer (10x)	1x
dNTPs	0.2 mM
Primer fwd	0.1 μM
Primer rev	0.1 μM
MgCl_2	1-3 mM (<i>Taq</i> only)
Template DNA	10 pg- 1 μg
Polymerase	1-1.25 U

DNA sequences below 1000 nt as well as control PCRs were performed using *Taq* polymerase. Mutagenesis of fragments in the range of 1000 nt was performed using *Pfu* polymerase. A mixture of dNTPS containing 2 mM dATP, dCTP, dGTP, dTTP was used in all PCR reactions. PCR was carried out in any PCR cycler listed in Table 3. A program was run with parameters as listed in Table 6. Primer melting temperatures (T_m) were calculated omitting the non binding part of the oligonucleotides used as primers using calculations and parameters from Breslauer *et al.* and Sugimoto *et al.* [250, 251].

Table 6: Standard PCR parameters for *Taq* and *Pfu* polymerase based reactions.

Step	Temperature [°C]	Time	Number of cycles
Initial denaturation	95	1-3 min	1x
Denaturation	95	30 s	25-35x
Primer annealing	T_m-5	30 s	
Extension	72	1min/kb (<i>Taq</i>) 2 min/kb (<i>Pfu</i>)	
Final extension	72	5-15 min	1x
Storage	4-6	∞	hold

4.2 Control PCR - Colony PCR and bacmid PCR

Additionally, PCR was used to verify successful cloning or bacmid generation.

A standard colony PCR reaction contained *Taq* polymerase (0.2 U/reaction) and the reaction template was added by dipping the colony of interest shortly into 20 µL of prepared PCR reaction solution with the appropriate primers before amplification and was conducted under appropriate conditions according to III 4.1.

A bacmid control PCR was performed with *Taq* polymerase (0.2 U/reaction), total reaction size was 20 µL with the addition of 0.1-1 µg bacmid and the pUC/M13 fwd and rev oligonucleotides as primer (listed in Table 19) according to the parameter selection in Table 7.

Table 7: Parameters of a standard bacmid control PCR.

Step	Temperature [°C]	Time	Number of cycles
Initial denaturation	95	5 min	1x
Denaturation	95	45 s	} 25x
Primer annealing	53	45 s	
Extension	72	1 min/kb	
Final extension	72	7 min	1x
Storage	4-6	∞	hold

4.3 Agarose gel electrophoresis

Agarose gel electrophoresis was used to verify and purify amplified or digested DNA fragments and vectors. Negatively charged DNA migrates, depending on the agarose concentration or rather pore size of immobile phase, size and conformation, in an electric field to the anode. Depending on the desired separation range 0.8-2 % (w/v) agarose gels in TAE-buffer were produced. Chambers and gel casts from Peqlab and a power supply from Bio-Rad were used. The sample buffer was prepared according to Table 4. A gel run was performed applying a voltage of 70-100 V corresponding to approx. 5-7 V per cm electrode distance. Visualization was performed using ethidium bromide solution soaking and an ultraviolet (UV) transilluminator.

4.4 Restriction digest, template removal and dephosphorylation

All restriction digests were performed according to manufacturer's protocols. BsaI restriction digests were performed in CutSmart buffer. XbaI digest using Fast XbaI enzyme was performed in FastDigest buffer. Double digest reactions of BamHI and EcoRI were performed in 2x Tango buffer. Double digest reactions of BamHI and HindIII were performed in BamHI buffer with BamHI and HindIII in a ratio of 1 : 2.

FastAP - alkaline phosphatase catalyzing the hydrolysis of 5' phosphate groups of cut vectors was utilized to prevent recircularization and religation of linearized cloning vectors. Routinely the reaction was performed after restriction digests of vectors in the corresponding buffers for 15 min at 37 °C.

4.5 Site directed mutagenesis

Site directed mutagenesis was either performed by overlap-extension PCR (two-fragment PCR) [252, 253] or by whole plasmid PCR [254] [255]. In these reactions in general *Pfu* polymerase was used. To enhance the efficient DNA denaturation in whole plasmid reactions 2-4 % (v/v) DMSO (Dimethyl sulfoxide) was added to the PCR.

4.6 Ligation

Amplified or mutated DNA fragments were ligated to target vectors, cut with the appropriate restriction enzymes, using T4-ligase. A standard reaction contained 1x ligase buffer, 1 U of T4-ligase, 10-20 ng of cut vector DNA and the three- to fivefold molecular quantity of insert DNA in 10 µL total volume. The reaction was incubated either for 1 h at RT or at 14 °C overnight. Subsequent to ligation the complete reaction was transformed to XL10Gold or DH5α cells to amplify the plasmid DNA.

4.7 DNA purification, concentration determination and sequencing

Bacterial plasmid DNA was purified using GeneJET Plasmid Miniprep Kit (Thermo Fisher Scientific, Germany) from 5-10 mL bacterial culture. Gen fragments and digested vectors separated in agarose gels were purified using GeneJET Gel Extraction Kits (Thermo Fisher Scientific, Germany). This kit was also used for PCR clean up or processing DNA after restriction digests. All reactions were carried out according to the manufacturer's protocols.

DNA concentration was determined by measuring corrected sample absorption at 260 nm in Nanodrop 2000c or NanoDrop Lite and applying Lambert-Beer Equation 1 assuming an extinction coefficient of 0.02 µg mL⁻¹cm⁻¹ for double stranded DNA:

$$A_{260} = \varepsilon \cdot b \cdot c$$

Equation 1: Lambert-Beer equation; A_{260} = Absorption at 260 nm, ε = molecular extinction coefficient [M⁻¹cm⁻¹], b = layer thickness, c = concentration.

Sequencing reactions with purified DNA plasmids were performed by GATC Biotech AG using the Sanger sequencing in Phred20 quality which has a 99 % base call accuracy. Oligonucleotide sequences used for sequencing are listed in Table 13.

4.8 Preparation of chemically competent cells

According to Hanahan and Inoue [256, 257] *E. coli* bacteria were treated to confer chemical competence. In the standard procedure 100 mL LB (Luria Bertani, Lennox) media supplemented with the *E. coli* specific selection antibiotics were inoculated and grown until an OD₆₀₀ von 0.6 – 0.8 was reached and subsequently incubated for 10 min on ice. After a centrifugation at 800 x g, 4 °C for 15 min the pellet of 50 mL culture was resuspended in 10 mL CaCl₂-buffer and further incubated on ice for 30-60 min. Finally the cells were pelletized again and resuspended in 2 mL CaCl₂-buffer supplemented with 10 % (v/v) glycerol, separated into 50 µL aliquots, flash-frozen in liquid nitrogen and stored at -80 °C.

4.9 Transformation of chemically competent bacteria

Chemically competent cells were thawed on ice, 1-100 ng DNA was added and incubated on ice for additional 20-30 min. This was followed by a heat shock at 42 °C for 45 s and a further incubation of the mixture on ice for 2 min. Addition of 500 µL LB-medium and an incubation at 37 °C at 400 rpm for 45 min started cell growth and developed inherited resistance. Finally cells were sedimented for 2 min at 3000x g and the bulk of the supernatant was discarded. This was followed by resuspending and streaking of the cells on LB-agar containing corresponding antibiotics as selection marker.

4.10 *E. coli* glycerol stock preparation

Transformed single clones were grown to high log-phase and preserved by the addition of 20 % (v/v) glycerol to the culture and stored at -80 °C.

4.11 SDS-PAGE and native PAGE

To analyze protein samples in the range of 10-200 kDa SDS-PAGE gels containing 4 % polyacrylamide in stacking gel and 12 % polyacrylamide in separating gel (components listed in Table 8) were prepared and gel electrophoresis was performed according to Laemmli [258].

Table 8: Components for preparation of SDS-PAGE gels.

Component	Stacking gel (4 %)	Separating gel (12 %)
Acrylamid/Bisacrylamid Ratio 37,5 : 1	4 %	12 %
Separating gel buffer	-	0.37 M
Stacking gel buffer	0.125 M	-
SDS	0.1 % (w/v)	0.1 % (w/v)
TEMED	0.1 % (v/v)	0.1 % (v/v)
APS	0.05 % (w/v)	0.05 % (w/v)

Generally, protein samples complemented with 5x sample buffer were denaturated at 96 °C for 10 minutes, applied on gels, mounted in SE260 Mighty Small II Deluxe Mini electrophoresis unit and run applying 120 V in the stacking gel part and continued applying 220 V to the separating gel. Standard molecular weight (MW) markers listed in Table 4 were used for size assessment. An unspecific protein staining was performed via incubation of the gel in Coomassie staining solution for >3 h and subsequent destaining in destain solution for adequate contrast.

For clear native PAGE analysis precasted SERVAGel™ N 4-16 (4 - 16 %) and SERVAGel™ N 3-12 (3 - 12 %) with the SERVA Native Marker, Liquid Mix for BN/CN with a resolution range of 720 to 21 kDa were used. The gels were mounted in SE260 Mighty Small II Deluxe Mini electrophoresis unit, run according to the manufacturer's description and stained via the procedure mentioned above.

4.12 Western Blot (WB)

Western blot (WB) was used to identify the protein of interest in *E. coli* and *Sf9* based expression studies. Semi-dry transfer in V20-SDB Semi-Dry Blotter Unit (SCIE-PLAS Ltd., UK) was done at RT with transfer buffer (Table 4). The transfer was achieved at 80-200 mA for 30-40 min and verified using a short unspecific protein staining in Ponceau staining solution. Blocking to exclude unspecific binding of the antibody was accomplished through incubation of the membrane in PBS-Tween, complemented with 3-5 % (w/v) BSA, for 30 min at RT. For specific detection the membrane was incubated with the primary antibody in PBS-Tween supplemented with 3 % (w/v) BSA, overnight at 4 °C. After three consecutive washing steps for 5 min with PBS-Tween the blot was incubated with the secondary antibody in PBS-T supplemented with 1 % (w/v) BSA for 1 h at 4 °C for AP (alkaline phosphatase) or HRP (horseradish peroxidase) mediated specific detection. After a second identical washing procedure the blot was either transferred to WB reaction buffer and developed with NBT and BCIP or, for HRP coupled secondary antibodies, developed with the ECL detection solution.

4.13 Bacterial cell culture for recombinant protein production

Plasmid propagation, recombinant gene expression and bacmid generation were performed in bacteria using *E. coli* strains listed in Table 9.

Table 9: Bacterial strains used for cloning, recombinant gene expression and bacmid generation.

<i>E.coli</i> strain	Supplier	Genotype
BLR (DE3)	Novagen (Merck), US	F ⁻ <i>ompT hsdS_B(r_B⁻ m_B⁻) gal dcm</i> (DE3) Δ(<i>srl-recA</i>)306::Tn10 (Tet ^R)
BL21 Star (DE3)	Life Technologies, Germany	F ⁻ <i>ompT hsdS_B(r_B⁻ m_B⁻) gal dcm rne 131</i> (DE3)
BL21 (DE3)pLysS	Promega, US	F ⁻ <i>ompT hsdS_B(r_B⁻ m_B-m) dc, gal, λ</i> (DE3) pLysS Cm ^r
DH5α	Life Technologies,	F ⁻ Φ80/ <i>lacZ</i> ΔM15 Δ(<i>lacZYA-argF</i>) U169 <i>recA1 endA1</i>

<i>E. coli</i> strain	Supplier	Genotype
XL10-Gold	Germany	<i>hsdR17 (rk⁻, mk⁺) phoA supE44 λ⁻thi⁻1 gyrA96 relA1</i>
	Agilent	Tet ^r delta- (<i>mcrA</i>)183 delta- (<i>mcrCB-hsdSMR-mrr</i>)173
	Technologies, US	<i>endA1 supE44 thi-1 recA1 gyrA96 relA1 lac Hte [F' proAB lacI^qZDM15 Tn10 (Tet^r) Amy Cam^r]</i>
BL21	Agilent	B F ⁻ <i>ompT hsdS(r_B-m_B-) dcm⁺ Tet^r gal λ(DE3) endA Hte</i>
CodonPlus(DE3)-RIL	Technologies, US	[<i>argU ileY leuW C am^r</i>]
DH10Bac™	Life Technologies, Germany	F ⁻ <i>mcrA Δ(mrr-hsdRMS-mcrBC) φ80lacZΔM15 ΔlacX74 recA1 endA1 araD139 Δ(ara, leu)7697 galU galK λ⁻ rpsL nupG/bMON14272/pMON7124</i>

4.13.1 Bacterial plasmids and oligonucleotides

Most plasmids used in this work for recombinant gene expression in *E. coli* were constructed with the plasmid pASK-IBA 3plus and thus under the control of tet-promotor [259]. The promotor is induced by a non inhibitory concentration (200 ng mL⁻¹) of anhydrotetracycline (AHT). Additionally, the plasmid pMal-C2x containing a P_{tac}-promotor was used [260, 261]. Gene expression is induced by the addition of 0.1-1 mM IPTG.

All plasmids used in this study, the corresponding vector, supplier and person who provided the expression construct and the genetic features are listed in Table 10.

Table 10: Compilation of all bacterial plasmids and their features used in this study.

Plasmid	Vector backbone, supplier (provided by)	Genetic features
pASK-IBA 3plus	IBA, Germany	c-term Strep-tag tet-promotor f1 origin ampicillin resistance
pMAL-c2X	New England BioLabs, United States	N-terminal <i>MalE</i> sequence (for Maltose binding protein-MBP), without signal sequence P _{tac} -promotor f1 origin pBR322 origin ampicillin resistance
pThiM-TEVHis₆	pASK-IBA 3plus IBA, Germany (J. Drebes)	insert of <i>S. aureus</i> ThiM fused to TEV (tabacco etch virus) protease recognition site and His ₆ -tag (C-terminal), discontinued before Strep-tag
PTPK-TEVHis₆	pASK-IBA 3plus	insert of <i>S. aureus</i> TPK fused to TEV protease

Plasmid	Vector backbone, supplier (provided by)	Genetic features
	IBA, Germany (<i>J. Drebes</i>)	recognition site and His ₆ -tag, (C-terminal), discontinued before Strep-tag
pPdxK-TEVHis₆	pASK-IBA 3plus IBA, Germany (<i>J. Drebes</i>)	insert of <i>S. aureus</i> PdxK fused to TEV protease recognition site and His ₆ -tag, (C- terminal), discontinued before Strep-tag
pPdxK-Strep	pASK-IBA 3plus IBA, Germany (<i>C. Wrenger</i>)	insert of <i>S. aureus</i> PdxK
pTcPdxK-His₆	pASK-IBA 3plus IBA, Germany (<i>T. Kronenberger</i>)	insert of <i>T. cruzi</i> PdxK fused to a His ₆ -tag (C- terminal), discontinued before Strep-tag
pThiD-Strep	pASK-IBA 3plus IBA, Germany (<i>Müller et al.</i> , [164])	insert of <i>S. aureus</i> ThiD
pThiD-TEVHis₆	pASK-IBA 3plus IBA, Germany (<i>J. Drebes</i>)	insert of <i>S. aureus</i> ThiD fused to TEV protease recognition site and His ₆ -tag, (C- terminal), discontinued before Strep-tag
pThiD-nAAAHis₆	pASK-IBA 3plus IBA, Germany	insert of <i>S. aureus</i> ThiD fused to a triple alanine linker and His ₆ -tag (N-terminal), discontinued before Strep-tag
pMBP-TEV-ThiD-TEVHis₆	pMal-C2x New England BioLabs, United States	insert of <i>S. aureus</i> ThiD fused to TEV protease recognition site (N-and C-terminal) and a His ₆ -tag (C-terminal), discontinued before Strep-tag
pThiE-nTEVHis₆	pASK-IBA 3plus IBA, Germany (<i>J. Drebes</i>)	insert of <i>S. aureus</i> ThiE fused to TEV protease recognition site and His ₆ -tag, (N- terminal), discontinued before Strep-tag
pGTPase-Strep	pASK-IBA 3plus IBA, Germany (<i>Müller et al.</i> [164])	insert of <i>S. aureus</i> GTPase
pRK793 [262, 263]	pMal-C2 New England BioLabs, United states (<i>Lab: D. Waugh</i>)	Vector backbone pMal-C2 with TEV protease, S219V mutant insert, N-terminal MBP and His ₆ -tag on insert) and C-terminal polyarginine-tag P _{tac} -promotor f1 origin pBR322 origin

Table 11 summarizes the oligonucleotides used for the production of the vector (pMBP-TEV-ThiD-TEVHis₆) for producing the fusion protein MBP-ThiD of *S. aureus*.

Table 11: Oligonucleotides used for ThiD MPB fusion in plasmid pMBP-TEVThiD-TEVHis₆.

Bases for restriction enzyme cutting efficiency are in lower case, the restriction enzyme recognition site underlined.

Name	Sequence 5'-3'
pMBP-TEVThiD-TEVHis₆ fwd	aaGGATCCGGCGAGAACCTCTACTTTCAGGGCGGTGGCA TTAAACCTAAAATAGCA
pMBP-TEVThiD-TEVHis₆ rev	ggtAAGCTTTTAATGATGATGATGATGATGGCCCTGAAAATACAGGTTCTC GCCTTTAGATAATTCATCGTC

In Table 12 the oligonucleotides used for site directed mutagenesis of *S. aureus* PdxK are listed. All 14 plasmids generated on the basis of the plasmids pPdxK-Strep and pPdxK-TEVHis₆ harbor the features listed in Table 10 and are named according to the basal plasmid (pPdxK-Strep and pPdxK-TEVHis₆) with the addition of the site specific mutation.

Table 12: Oligonucleotides used for *S. aureus* PdxK mutagenesis.

Name	Sequence 5'-3'
SaPdxK-S12A-fwd	GCCGGTGCGGACACAAGTGC
SaPdxK-S12A-rev	GCCGGTGCGGACACAAGTGC
SaPdxK-H51Q-fwd	CATGGTCACAGGATGTTACAC
SaPdxK-H51Q-rev	GTGTAACATCCTGTGACCATG
SaPdxK-M80A-fwd	TAAAACAGGTGCGTTAGGTAC
SaPdxK-M80A-rev	GTACCTAACGCACCTGTTTAA
SaPdxK-A212T-fwd	ACCATGGTACCGGTTGTACAT
SaPdxK-A212T-rev	ATGTACAACCGGTACCATGGT
SaPdxK-C214D-fwd	GGTGCTGGTGATACATTTGCTG
SaPdxK-C214D-rev	CAGCAAATGTATCACCAGCACC
SaPdxK-C214A-fwd	GGTGCTGGTGCGACATTTGCTG
SaPdxK-C214A-rev	CAGCAAATGTGCGACCAGCACC
SaPdxK-N252G-fwd	GGAAAATGGGTGATTTTGTTG
SaPdxK-N252G-rev	CAACAAAATCACCCATTTTCC

In Table 13 the oligonucleotides used for Sanger sequencing reactions according to chapter III 4.7 are listed.

Table 13: Oligonucleotides used for Sanger sequencing reactions.

Name	Sequence 5'-3'
IBA fwd	GAGTTATTTTACCACTCCCT
IBA rev	CGCAGTAGCGGTAAACG
malE	TCAGACTGTCGATGAAGC

4.13.2 Microbial growth media and selection antibiotics used for *E. coli* cultivation

The following tables (Table 14 and Table 15) list the growth media and supplements used for the cultivation of *E. coli* cells.

Table 14: Microbial growth media for *E. coli* cultivation.

Medium	Composition
LB (Luria Bertani, Lennox) [264]	10 g L ⁻¹ tryptone, 5 g L ⁻¹ NaCl, 5 g L ⁻¹ yeast extract
LB-Agar	1.5 % (w/v) agar in LB
2YT	16 g L ⁻¹ , tryptone, 5 g L ⁻¹ NaCl, 10 g L ⁻¹ yeast extract
TB (Terrific Broth)	12 g L ⁻¹ , tryptone, 4 mL L ⁻¹ glycerol, 24 g L ⁻¹ yeast extract, 72 mM K ₂ HPO ₄ , 17 mM KH ₂ PO ₄

Table 15: Preparation and working concentration of antibiotics and media supplements used in this study.

Antibiotic	Preparation	Working concentration
Ampicillin	100 mg mL ⁻¹ in 50 % EtOH (v/v)	100 µg mL ⁻¹
Chloramphenicol	34 mg mL ⁻¹ in EtOH	34 µg mL ⁻¹
Kanamycin	10 mg mL ⁻¹ in 50 % EtOH (v/v)	100 µg mL ⁻¹
Tetracyclin	17 mg mL ⁻¹ in EtOH	17 µg mL ⁻¹
Betaine	2.5 M in H ₂ O	2.5 mM

4.14 Insect cell culture

On the basis of the Bac-to-Bac Baculovirus Expression System from Life Technologies, Germany recombinant baculoviruses for insect cells transfection were generated [265]. The system makes use of a site specific transposition of an expression cassette into a baculovirus shuttle vector proliferated in *E. coli*.

4.14.1 Insect cell plasmids and oligonucleotides

All proteins were cloned into pFastBac1 to generate a tag-free protein variant in insect cells to study potential *in vivo* crystallization with and without the carboxy-terminal peroxisomal targeting

signal 1 (PTS1). Furthermore, a construct in pFastBacHTb was cloned to provide a possibility to detect a successful recombinant production via western blot and to purify the proteins from this expression system. The donor plasmid supplier and genetic features are listed in Table 16 and the oligonucleotides used for DNA amplification and cloning are listed in Table 17.

Table 16: Vectors for donor plasmid preparation for recombinant bacmid production used in this study.

Plasmid	Supplier	Genetic features (size in bp)
pFastBac1	Life Technologies (Thermo Fisher Scientific, Germany)	AcMNPV (<i>Autographa californica</i> multiple nuclear polyhedrosis virus) polyhedrin (P_H) promoter (4776 bp)
pFastBacHTb	Life Technologies (Thermo Fisher Scientific, Germany)	AcMNPV polyhedrin (P_H) promoter N-terminal His ₆ -tag TEV protease recognition site between tag and multiple cloning site (4856 bp)

Table 17: Oligonucleotides for insect cell vector construction and consecutive bacmid generation.

Bases for restriction enzyme cutting efficiency are in lower case, bases coding for the carboxy-terminal peroxisomal targeting signal 1 (PTS1) are colored in green, restriction enzyme recognition site is underlined.

Name	Sequence 5'-3'
TPK fwd	gagaGGATCCATGCATATAAAATTTATTATGTTCTGATCGA
TPK rev	gagaGAATTCTTAATTTAAATCTGTACTTCTAATTGCAA
ThiM fwd	gagaGGATCCATGAATTATCTAAATAACATACGTATTGAAAAC
ThiM rev	gagaGAATTCTTATTCCACCTCTTGAATGCG
ThiE fwd	gccgGGATCCATGTTTAACCAATCGTATCTAAATGTGT
ThiE rev	attaGAATTCCTAATTATTAATAAAAAATCTTTGAATCGATTAAACAG
ThiD fwd	gagaGGATCCATGATTAAACCTAAAATAGCATTAAACCATT
ThiD rev	cgaaGAATTCTTATTTAGATAATTCATCGTCTAATCCCTC
GTPase fwd	tattGGATCCatgAAGACAGGTCGAATAGTGAAATCAA
GTPase rev	tttaGAATTCCTTAATATCTAACCTTTCTATTGAAATTTTC
TenA fwd	gagaGGATCCATGGAATTTTCACAAAAATTGTACC
TenA rev	tataGAATTCCTTAATCATTTACTTTTCCTCCAAATTC
PdxK fwd	gcgcGGATCCATGGCTTTAAAGAAAGTTTAAACAATT
PdxK rev	atatGAATTCCTTAACCTCTGTACTTCAACATCGA
TPK SKL rev	gagaGAATTCCTTACAGCTTGGAATTTAAATCTGTACTTCTAATTGCAA
ThiM SKL rev	gagaGAATTCCTTACAGCTTGGAATTCACCTCTTGAATGCG
ThiE SKL rev	attaGAATTCCTTACAGCTTGGAATTATTAATAAAAAATCTTTGAATCGATTAAACAG

Name	Sequence 5'-3'
ThiD SKL rev	cgaagGAATTCTTACAGCTTGGATTTAGATAATTCATCGTCTAATCCCTC
GTPase SKL rev	atatGAATTCTTACAGCTTGGAAATATCTAACCTTTCTATTTGAAATTTTC
TenA SKL rev	tataGAATTCTTACAGCTTGGAAATCATTACTTTTCTCCAAATTC
PdxK SKL rev	atatGAATTCTTACAGCTTGGAAACCTCTGTTACTTCAACATCGA

4.14.2 Material, medium, buffer, solutions and cell lines for insect cell culture

The entire material, solutions and selection antibiotics used for insect cell culture are listed in Table 18. The used cell line was *Sf9* from fall army worm, *Spodoptera frugiperda* parental cell line IPLBSF-21 (Life Technologies (Thermo Fisher Scientific, Germany)).

Table 18: Material, solutions and selection antibiotics used for *Sf9* cell cultivation and recombinant bacmid production.

Media, solutions and antibiotics	Product supplier
EX-CELL 420 Serum-Free Medium for Insect Cells, with L-glutamine	#14420C (Sigma, Germany)
100x Penicillin-Streptomycin solution (10,000 U mL ⁻¹ penicillin and 10 mg mL ⁻¹)	#P0781 (Sigma, Germany)
Gentamicin (10 mg mL ⁻¹)	#G1272 (Sigma, Germany)
Bluo-Gal	#B2904 (Sigma, Germany)
T25/T75/T175 cell culture flasks	#20003527, 20003528, 20003529 (Sarstedt, Germany)
6 well plates	#83.3920 (Sarstedt, Germany)
24 well plates	#83.3922 (Sarstedt, Germany)
DMSO cell culture grade	#D2438 (Sigma, Germany)
Trypan blue	#T6146 (Sigma, Germany)
Transfection reagent Escort IV	#L3287 (Sigma, Germany)
Sodium-Butyrate	#B5887 (Sigma, Germany)
RNaseA	#R6513 (Sigma, Germany)
PBS	#10010-015, Life Technologies (Thermo Fisher Scientific, Germany)

4.14.3 Sequencing and control oligonucleotides

Oligonucleotides pFastBac fwd and pFastBac rev were used in the normal sequencing service to validate correct construct design in pFastBac1 and pFastBacHTb vectors (Table 19). Oligonucleotides pUC/M13 fwd and pUC/M13 rev were used for qualitative analysis of efficient recombination after bacmid production and purification (chapter III 4.14.5) via Bacmid PCR (chapter 0).

Table 19: Sequencing and control oligonucleotides for bacmid construction.

Name	Sequence 5'-3'
pFastBac fwd	TATTCGGATTATTCATACC
pFastBac rev	TTCAGGTTTCAGGGGAGGTG
pUC/M13 fwd	CCCAGTCACGACGTTGTAAAACG
pUC/M13 rev	AGCGGATAACAATTCACACAGG

4.14.4 Transformation of DH10Bac for recombinant bacmid generation

Competent DH10Bac cells were thawed on ice and supplemented with 1 ng of vector construct. After 30 min of incubation on ice a heat shock was performed for 45 s at 42 °C. After subsequent chilling on ice for 2 min, 900 µL LB medium was added and the tubes incubated at 37 °C at 400 rpm for 4 h. After a preparation of a 10- and 100-fold dilution of the grown cells with LB media, 100 µL of each dilution were streaked on LB agar plates containing 50 µg mL⁻¹ kanamycin, 7 µg mL⁻¹ gentamicin, 10 µg mL⁻¹ tetracycline, 100 µg mL⁻¹ Bluo-Gal, and 40 µg mL⁻¹ IPTG to select for DH10Bac transformants. The plates were incubated for 48 hours at 37 °C. Consequently, a single white colony was picked for growth in 3-5 mL of LB supplemented with 50 µg mL⁻¹ kanamycin, 7 µg mL⁻¹ gentamicin and 10 µg mL⁻¹ tetracycline for further bacmid amplification.

4.14.5 Bacmid purification

Cells were harvested (14000x g, 2 min, RT) and the pellet was resuspended in 250 µL P1 solution (solutions for bacmid purification listed in Table 20). Subsequently 250 µL P2 were added and the reaction tubes were inverted for gentle mixing. Successively 350 µL P3 were added and the mixture gently mixed by inverting. The lysed cells were centrifuged for 10 min at 14000 x g at RT to separate cellular debris and the supernatant was transferred to a fresh tube. To precipitate the bacmid DNA 700 µL precooled isopropanol was added and the reaction, 10-60 min incubated at 4 °C and subsequently centrifuged for 15 min at 14000x g at RT. The supernatant was discarded and the pellet resuspended in 700 µL precooled Ethanol (70 %, v/v). After a subsequent centrifugation (15 min at 14000 x g at RT) the pellets were dried in a clean bench and resuspended in 30 µL sterile deionized water. Long term storage was performed in aliquots at 4 °C or at -20 °C.

Table 20: Composition of solutions used for bacmid purification.

Solution	Components
P1	50 mM Tris (pH 8.0) 10 mM EDTA 100 µg mL ⁻¹ RNaseA
P2	200 mM NaOH 1 % (w/v) SDS
N3	4.2 M guanidinium-HCl 0.9 M potassium acetate (pH 4.0)

In Table 21 the estimated gene product size of cloning, corresponding bacmid cassette size as well as the expected protein size after recombinant gene expression in *Sf9* cells are summarized. The bacmid size corresponds to a cassette made up from ~2300 bp and the DNA of interest.

Table 21: Summary of the bacmid DNA size and corresponding protein molecular weight.

Size of the amplified gene, expected bacmid cassette for the control bacmid PCR and size of the His₆-tagged proteins from *S. aureus* are listed.

Protein	Gene [bp]	Bacmid cassette	MW [kDa]
		[~bp]	His ₆ -tag variant
ThiD	831	3131	33.3
TenA	690	2990	29.9
ThiE	642	2942	26.5
ThiM	792	3092	31.1
TPK	642	2942	27.0
GTPase	876	3176	37.0
PdxK	831	3131	33.0

4.14.6 *Sf9* cell culture

In general *Sf9* cells, a cell line derived from the pupal ovarian tissue of the fall army worm *Spodoptera frugiperda*, were cultured in EX-CELL 420 Serum-Free medium after serum free adaption according to manufacturer's description. To initiate cell culture a cell aliquot (2 x 10⁷ cells) was removed from -80 °C and thawed in a 37 °C water bath by gently agitating. After transfer of the cells to a sterile 50 mL tube, slowly 15 mL pre-warmed media were added. Cells were seeded in a T75 flask directly and incubated for 20-30 min at 27 °C. After a media exchange cells were incubated for 2-3 d in a humidified incubator at 27 °C.

Cells were adherently cultured in T75 with 12 mL and in T175 with 25 mL media, supplemented with 1x Penicillin-Streptomycin solution. Standard densities before passaging the cells were 1.2×10^7 in T75 flasks or 2.4×10^7 in T175 flasks, corresponding to 85-95 % confluency. For normal maintenance cells were dislodged via tapping and rinsing and an aliquot was taken for viability determination and cell counting. 200 μ L cell suspension were mixed with the same amount of trypan blue solution (0.08 % (w/v) in PBS) and a Neubauer improved hemacytometer was loaded with cells. Subsequent $1-3 \times 10^5$ cells mL^{-1} were seeded for further cultivation depending on the application and cultivation time.

Cell preservation was prepared in mid log growth ($3-4 \times 10^6$ mL^{-1}) and a viability >95 %. Cells were harvested and centrifuged at 600x g for 8 min and resuspended to a final concentration of 1×10^7 mL^{-1} in 7.5 % (v/v) DMSO, 46.25 % conditioned and 46.25 % fresh medium. Aliquots were immediately frozen in an isopropanol filled Mr. Frosty freezing container (Thermo Fisher Scientific, Germany) and stored at -80 °C.

4.14.7 Transfection and virus stock production

Sf9 cells in log-phase with a viability of >95 % were seeded to a 6-well plate (9×10^5 cells/well in 1 mL) in antibiotic free medium. For transfection 1 μ g bacmid DNA (1-2 μ L) was prepared in 98 μ L medium in one tube and in a second tube 2 μ L Escort IV transfection reagent were mixed with 98 μ L medium. These two premixes were combined and incubated for 15-30 min at RT. As a control a MOCK transfection, without addition of any bacmid DNA, was performed in parallel. This mixture was added dropwise to the cells and incubated for 5-6 h at 27 °C before medium was exchanged for further cultivation. Virus stocks were harvested in the late infection stages 48-72 h post transfection/infection, harvested supernatant was cleared from cells debris via centrifugation for 5 min at 500 x g; virus stocks were stored protected from light at 4 °C. P2 was generated to higher viral titer of the stocks by adding 300 μ L virus stock to a well containing 1×10^6 cells. Preliminary expression experiments were performed until P3 using 200 μ L to 300 μ L recombinant virus stock and the infected cells were harvested for expression analysis.

4.14.8 *Sf9* cell lysate preparation and Bradford assay

Two days post (P3) infection cells of a 6-well plate were harvested via rinsing in 1 mL PBS, centrifuged at 500x g at 4 °C and the supernatant was discarded. The cells pellets were stored at -20 °C and resuspended in RIPA buffer (composition in Table 22) for later analysis.

Table 22: Composition of RIPA buffer.

Concentration	Component
50 mM	Tris HCl, pH 7.5
150 mM	NaCl
1 % (v/v)	NP-40 (4-Nonylphenyl-polyethylene glycol)
0.5 % (w/v)	DOC (sodium deoxycholate)
0.1 % (w/v)	SDS
2 mM	β -Glycerolphosphate
1 mM	Na_3VO_4
0.4 mM	PMSF (Phenylmethanesulfonyl fluoride)
1 mM	EGTA
1 mM	NaF
1 tablet 50 mL ⁻¹	Protease-Inhibitor (Roche, Germany)

Cells were disrupted via mechanically sheering through a needle and syringe, cracked cells were further incubated for 30 min on ice. Cell debris was separated via centrifugation (20,000 x g, 15 min at 4 °C). The protein amount in the supernatant was assayed via Bradford [266] and 20 µg total protein content was applied to a 12 % SDS-PAGE for further western blot analysis.

For Bradford analysis Bio-Rad Protein Assay solution was diluted 1:5 in dH₂O (Bradford reagent). For calibration curve preparation 0, 1, 5, 10 and 25 µg BSA were added to 1 mL Bradford reagent and incubated for 5 min at RT; subsequently, the absorption at 595 nm was determined. A linear regression curve was calculated, 5 µL of protein solution of interest measured and the protein concentration determined via the calibration curve line function.

4.15 Protein purification

4.15.1 Preparation of cleared lysates

E. coli cell pellets stored at -20 °C were resuspended in lysis buffer (approx. 3-5 g wet weight per 25 mL buffer); if not stated otherwise this buffer was T/N supplemented with 0.1 mM PMSF and a spatula tip of lysozyme. In case of His₆-tagged proteins generally 5-10 mM imidazole was included to prevent unspecific binding in the subsequent affinity chromatography. Cell disruption was carried out by four times sonication for 4 min pulsed at 40 kHz on ice with 3 min pauses in between to convey produced heat energy. The lysate was centrifuged at 14,100 x g, 4 °C for 40-60 min. For further analysis on SDS-PAGE a small amount of the cell debris pellet was resuspended in 50 µL 5x SDS-PAGE

sample buffer and 20 µL of the supernatant containing all soluble proteins was supplemented with 5 µL sample buffer.

4.15.2 Affinity chromatography and size exclusion chromatography

All affinity chromatography runs were usually performed as gravity flow. For Strep-tagged proteins the supernatant was applied to the pre-equilibrated Strep-Tactin Matrix after the preparation of the cleared lysate, the column was washed twice with lysis buffer (50 mL). Subsequently the bound protein was eluted with 2.5 mM desthiobiotin containing T/N300 elution buffer.

For His-tagged proteins, the cleared lysate was applied to the pre-equilibrated Ni-NTA (nitrilotriacetic acid) matrix and incubated for 30-60 min at 4 °C. Flow through was collected and the column was washed twice with lysis buffer (50 mL) and subsequently twice with 10 mL of wash buffer. This wash buffer was supplemented with 20-60 mM of imidazole to remove unspecific bound protein. Subsequently the bound protein was eluted with 250-300 mM imidazole containing elution buffer. Occasionally, the elution fractions were applied again to the matrix to increase the concentration of the protein in solution.

All size exclusion chromatography runs were performed using ÄKTA FPLC purification system (ÄKTA Purifier P-901; GE Healthcare, UK) maintained at 4 °C, if not stated otherwise. Hi Load 16/60 Superdex 75, Hi Load 16/60 Superdex 200 and XK Sephadex G-25 Fine columns from GE Healthcare were used. For evaluation, absorbance at 280 nm and 230 nm and conductivity were monitored. Calculations for molecular weights from retention volume were done by applying calibration curve using the following proteins: lysozyme (14 kDa), thaumatin (*Thaumatococcus daniellii*; 22 kDa; Sigma), ovalbumin (44 kDa), conalbumin (75 kDa), aldolase (158 kDa), ferritin (440 kDa), thyroglobulin (669 kDa) and Blue Dextran 2000 (all GE Healthcare, calibration kit).

4.15.3 Strep-tactin and Ni-NTA matrix regeneration

After elution of the target protein Strep matrix was washed three times with five CV (column volumes) 1x Strep-tactin regeneration buffer and stored in 1x Strep-tactin regeneration buffer. For subsequent purification matrix was rinsed with buffer W until the matrix was white again and thereafter equilibrated with the corresponding lysis buffer.

Ni-NTA matrix was washed with two CV of regeneration buffer and rinsed twice with five CV H₂O. After rinsing with three CV 2 % SDS solution an ethanol gradient starting with 25 % (v/v), followed by 50 % (v/v) and 75 % (v/v), 1 CV each, was applied. After a wash step of five CV 100 % ethanol the gradient was applied in reverse order. To unload the coordinated Ni²⁺ ions the matrix was washed with 1 CV water followed by 5 CV of EDTA solution. To freshly load the matrix after rinsing with 2 CV

H₂O, two CV NiSO₄ were applied and then the matrix was rinsed with 2 CV H₂O again. Finally, the column was either stored in 25 % (v/v) ethanol at 4 °C or equilibrated with buffer.

4.16 Protein quantification

Protein concentrations were determined by measuring specific absorbance at a wavelength of 280 nm according to the law of Lambert-Beer-equation:

$$A_{280} = \varepsilon \cdot b \cdot c$$

Equation 2: Lambert-Beer equation; A_{260} = Absorption at 260 nm, ε = molecular extinction coefficient [$M^{-1}cm^{-1}$], b = layer thickness, c = concentration.

Physicochemical parameters of protein sequences listed in Table 23 and were extracted from ProtParam of the SIB (Swiss Institute of Bioinformatics) ExPASy Bioinformatics Resources Portal [267].

Table 23: Physicochemical parameters of proteins produced and purified in this study.

Extinction coefficient - ε_{280} , molecular weight - MW and theoretical isoelectric point - pI are given.

Protein	ε_{280} [$M^{-1} cm^{-1}$]	MW [kDa]	Theoretical pI
<i>S. aureus</i> ThiM-TEV-His ₆	13410	29.8	4.86
<i>S. aureus</i> TPK-TEV-His ₆	21430	25.6	6.03
<i>S. aureus</i> TPK-TEV-cut	21430	24.7	5.58
<i>S. aureus</i> PdxK-TEV-His ₆	28880	31.6	5.23
<i>S. aureus</i> PdxK-TEV-cut	28880	30.7	4.80
<i>S. aureus</i> PdxK-Strep	32890	31.1	4.94
TEV protease	32290	28.6	9.53
<i>T. cruzi</i> PdxK- His ₆	23380	34.2	6.23

4.17 TEV protease expression, purification and standard TEV protease digest

E. coli BL21 CodonPlus(DE3)-RIL transformed with pRK793 were used to produce the catalytic domain (S219V mutant) of tobacco etch virus (TEV) protease as an MBP fusion protein with a C-terminal poly-arginine and an N-terminal His₆-tag [262, 268, 269].

Overnight culture grown in LB supplemented with ampicillin and chloramphenicol at 37 °C were diluted to an OD₆₀₀ 0.05. After further growth to an OD₆₀₀ of 0.5, gene expression was induced with 1 mM IPTG. After preparing a regular cleared lysate in TEV1-buffer, 6 mL Ni-NTA slurry were combined with the supernatant in a falcon tube. After 30 min incubation at 4 °C, the matrix was settled via 2 min centrifugation (900x g, 6 °C) and the supernatant was discarded. Subsequently the matrix was washed by the same procedure three times with 45 mL TEV2-buffer and in the last step transferred to a gravity flow column. Elution was performed with 5 mL TEV3-buffer four times and the protein was transferred to a TEV1-buffer containing 0.5 mM DTT by dialysis and subsequently

supplemented with 20 % (v/v) glycerol and finally flash frozen in aliquots in liquid nitrogen and stored at -80 °C.

A standard TEV digest, targeting the amino acid recognition site (ENLYFQS/G) [269] inserted between protein of interest and His₆-tag, was performed in buffer W supplemented with 3 mM glutathione reduced and 0.3 mM glutathione oxidized and a volume ratio of 1:100 of the total protein content. To optimize reaction time, temperature and ratio of protein to protease small batches were analyzed comparatively. To eliminate uncut protein as well as the protease in the purified target protein solutions the digest preparation was incubated on a pre-equilibrated Ni-NTA column and the flow through was collected.

4.18 Dynamic light scattering (DLS)

In order to specify dispersity as well as the hydrodynamic radius (R_H) of proteins in solution dynamic light scattering was applied. Before each measurement samples were centrifuged at 16,100× g for 15-30 min. Within this work different devices were used: For standard measurements the SpectroSize 300, which applying 9 µL sample in a quartz cuvette was used; for long term measurements the SpectroLight 600 was utilized, as it gives the possibility to observe the development of dispersity over a long period with minor sample usage (1-2 µl) and without evaporation because the sample is covered with paraffin oil. All devices are utilizing a red light laser (λ = 690 nm and power 10-50 mW) which applies insignificant energies to the sample. In all devices the sample temperature is continuously monitored and stabilized.

4.19 Circular dichroism (CD)

CD spectroscopy was routinely utilized to examine general secondary structure elements and to analyze thermal stability and folding properties upon compound addition or buffer exchange of proteins. The intrinsic signal of unequal absorption of right- and left-handed circular polarized light of proteins arises in a quantitative dependence from the amides in the protein backbone (far UV) and aromatic groups (near UV). The recorded ellipticity is reflected in Equation 3.

$$\theta = \frac{180 \cdot \ln 10}{4\pi} (A_L - A_R)$$

Equation 3: θ is the observed ellipticity [degrees]; the absorbance of right- and left-handed circular polarized light is reflected in A_L and A_R .

Proteins with a high α -helical content show characteristic minima at 208 and 222 nm and a maximum positive ellipticity at 192 nm. Increasing β -folds are reflected through a more distinct minimum around 218 nm. Standard curves as published in 1986 from Yang *et al.* [270] served as qualitative comparison.

Standard measurements were performed with the CD spectrometer J-815 (Jasco, UK) using a peltier element for thermal stabilization or ramping in the experiments. Protein samples were diluted resulting in a low salt (NaCl) concentration with a low buffering capacity of 5-15 mM Tris and habitually measured in a 1 mm quartz cuvette scanning the near UV wavelength 190-260 nm. To reach high accuracy general scanning speed was set to 10 nm min⁻¹ and the spectral bandwidth was fixed to 1 nm. Recorded ellipticity was directly converted to mean residue ellipticity according to Equation 4 and plotted against the wavelength.

$$MRE = \frac{MRW \cdot \theta}{c \cdot d \cdot 10}$$

Equation 4: θ is the observed ellipticity [degrees], MRW (mean residue weight)= molecular mass of the polypeptide chain in Dalton divided by the peptide bonds in the protein [Da], c protein concentration [g mL⁻¹] and d path length [cm] [271].

4.20 Mass spectrometry (MS)

Mass spectrometry data collection and analysis was performed in cooperation with the research group of *Prof. H. Schlüter (UKE, Hamburg)*. Coomassie-stained protein samples from an SDS-PAGE gel were excised and subsequently destained. In the core facility reduction of disulfide bonds and digestion by trypsin was conducted. Peptides were extracted by adding acetonitrile and trifluoroacetic acid desalted by reversed phase chromatography. An electrospray ionization (ESI) ion trap instrument (LC/MSD Trap XCT Ultra II) was used to detect peptides and results were analyzed using the mascot search engine (Matrix Science).

4.21 Saturation transfer difference - nuclear magnetic resonance (STD-NMR)

Saturation transfer difference - nuclear magnetic resonance (STD-NMR) spectroscopy was performed in cooperation with *J. Klare* in the research group of *Dr. T. Hackl (University of Hamburg)*. This method was used to characterize the binding of NPE-caged-ATP in presence of THZ to *S. aureus* ThiM. For STD-NMR measurements *S. aureus* ThiM was transferred into 50 mM tris-*d*11, pH 8.0 containing 150 mM sodium chloride and 1 mM magnesium chloride; THZ and NPE-caged-ATP were diluted in the same deuterated buffer. Samples containing 5 μ M ThiM, 50 μ M THZ and 200 μ M ATP-NPE and 100 μ M THZ and 150 μ M AMP-PCP respectively were measured at 300 K with a Bruker Avance III 600 MHz NMR spectrometer. STD-NMR spectra were acquired applying a Bruker standard sequence (stdiffesgp.3) incorporating a spin-lock filter of 10 ms duration to suppress residual protein resonance. On resonance irradiation was applied at 600 Hz and off resonance irradiation at 40000 Hz. Saturation was achieved by a cascade of 40 90° Gaussian pulses with duration of 50 ms to give a total saturation time of 2 s. Reference spectra and STD spectra were acquired with a spectral width of 8403 Hz applying 65,536 data points 2 transients. FIDs were multiplied with an exponential

function (line broadening 1.0 Hz) before Fourier transform. Ligands were assigned by means of ^1H -NMR. Data were processed with TopSpin 3.2 (Bruker, US).

Resonances in the STD spectrum were integrated with respect to the reference spectrum to verify the size of STD effects. For relative epitope mapping, all STD effects of one ligand were normalized to the resonance of the largest STD effect in the molecule, which equals 100 %.

4.22 Molecular docking

To analyze preferred orientations and binding properties of selected peptides into the active site of *S. aureus* PdxK molecular docking, using FlexiDock implemented in SYBYL-X 1.3 computational suite (Tripos International, US) was performed in cooperation with Dr. D. Rehders (University of Hamburg). The refined model of *S. aureus* PdxK was used for modelling studies. Before docking all water molecules as well as the malonic acid molecule were removed from the crystal structure. Subsequently, B-factors were replaced by charges using the Gasteiger-Huckel-algorithm. Additionally an energetic minimization of the structure was performed. On this basis di- and tripeptides were manually prepositioned into the active site of *S. aureus* PdxK and docked for 190000 iterations. Preeminent results were analyzed by comparing FlexiDock binding energies and manual verification of precise orientation within the binding pocket.

5 X-ray crystallography

5.1 Sample preparation and initial crystallization screening

In the first step all target proteins were purified using gravity flow affinity chromatography by the use of Strep- or His₆-tag. *S. aureus* ThiM and *T. cruzi* PdxK were subsequently applied to a size exclusion chromatography using the Hi Load 16/60 Superdex 200. *S. aureus* TPK and *S. aureus* PdxK purified via Ni-NTA affinity chromatography were subsequently relieved from His₆-tag and thus of artificial amino acids and consequently flexible regions via TEV protease digest.

Protein concentrations were increased stepwise and the dispersity monitored by DLS. To estimate a sensible crystallization concentration the Pre-Crystallization test (Hampton Research, UK) was applied, according to the manufacturer's protocol. For ligand incorporations intended for co-crystallization preincubation of protein and ligand was performed for at least 2 h on ice.

In initial trials, the commercially available screens JCSG-plus, PACT premier, Classics Suite and Cryos Suite were used routinely. Applying the pipetting robot Honeybee 961 (Genomic solutions, UK) MRC 96-well sitting drop crystallization plate (Molecular Dimensions, UK), containing 192 optical wells were set up for vapor diffusion screening in sitting drop format. Habitually, the first well contained 400 nL of protein solution and 400 nL of the respective precipitant solution. The second

well was set up with 400 nL protein solution and 700 nL precipitant solution to double the screening array. The reservoir was filled with 55 μ L of precipitant solution; plates were sealed and stored at 20 °C or 4 °C.

If no initial condition could be obtained or in order to further optimize crystallization, Morpheus, Stura FootPrint & MacroSol and AmSO₄ Suite were used. The plates were monitored every second day in the first week and then weekly to identify crystallization hits.

5.2 Analysis of crystallization success and optimization of initial crystallization hits

If crystal hits were observed and the protein contained aromatic amino acids analysis for intrinsic fluorescence was performed applying the CrystalScore. Further, if sufficient crystal quantity was present, they were resuspended in SDS-sample buffer and analyzed on an SDS-PAGE. Additionally, before synchrotron experiments crystals and cryo conditions were analyzed on the rotating anode generator (Rigaku RU 200 X-ray generator).

As the initial screening was a sitting drop vapor diffusion setup in general the first choice of optimization was a setup in MRC MAXI 48-well optimization plate (Molecular Dimensions, UK). Typical drop size was 3 μ L with varying precipitant amount and 220 μ L precipitant solution placed in the reservoir. Complementary setups of hanging drop vapor diffusion experiments in Linbro plates (Jena Bioscience) were performed. Typical drop size was 3 μ L with varying precipitant amount on a siliconized cover slip and 400 μ L precipitant solution in the reservoir. In general a comparison to the initial crystallization hits was done with the Hofmeister series and identification of chemical tendencies was attempted. Additionally, micro batch setups using Terazaki plates (Nunc, Denmark) under paraffin oil or mixtures of paraffin and silicon oil [272] were used. Furthermore, counter diffusion approaches were used to complementarily test crystallization conditions [273]. In general Granada Crystallization Boxes (GCB) Domino (Triana Science & Technology S.L., Spain) were filled with precipitant solution and sealed with 1.5 % (w/v) low melting agarose. Capillaries with an inner diameter of 0.1-0.4 mm were filled with protein solution, sealed with clay and stuck into the precipitant solution through the agarose (up to six simultaneous experiments).

In particular for crystal growth of *S. aureus* TPK seeding as well as cross seeding were tested [274–276]. For seeding procedures a seed stock from single or multiple conditions was produced with Beads-for-Seeds (Jena Bioscience, Germany) according to manufacturer's description. After preparing a dilution series up to 10^{-3} in precipitant solution fresh droplets were seeded via streaking with horse tail hair.

5.3 Soaking

In addition to co-crystallization experiments, ready grown *S. aureus* ThiM crystals were soaked in a 3-50 fold molecular excess of compound. Several approaches were tested: Dissolving compounds in the appropriate precipitant solution and adding them to crystallization drops 24-48 h before measurement or soaking crystals in cryo-protectant solutions supplemented with compounds of interest directly before the diffraction data collection. If these approaches were not efficacious, dissolving compounds in DMSO precipitant mixtures (0.5-5 % (v/v)) was tested. Additionally, dissolving compounds in 100 % DMSO and after almost complete evaporation adding precipitant or protein was examined.

5.4 Automated nano-crystallization - XtalController 900

For investigating automated nano-crystallization the XtalController 900 (XtalConcepts, Germany) in cooperation with *R. Schubert (University of Hamburg)* was used. The XtalController allows charting a course across the phase diagram to produce crystalline samples of various sizes, optimized for diffraction experiments, by controlling evaporation and precipitant addition through piezo pumps. The device has been developed in cooperation with the University of Lübeck and a detailed description of the experimental setup was published previously [277].

For XtalController experiments the relative humidity in the process chamber was raised above 98 %. A siliconized glass cover slip was placed on the microbalance inside the process chamber. A drop of ThiM protein solution ($1.0\ \mu\text{L}$ of $15\ \text{mg mL}^{-1}$) was applied on the cover slip and the hydrodynamic radius of the protein was determined by DLS. Evaporation of water was monitored by the microbalance and counteracted by injecting 70 pL water droplets with a piezo pump. Precipitant solution (0.1 M HEPES sodium salt pH 7.5, 1.5 M lithium sulfate) was injected to the protein droplet by using an additional piezo pump in a predefined time-step program. Initial nucleation during injection has been monitored and detected by DLS to find optimal conditions for nano-crystal formation.

5.5 Diffraction data collection

For diffraction data collection beamlines P14 (EMBL, Hamburg) at the PETRAIII synchrotron radiation source and the rotating anode generator (Rigaku RU 200 X-ray generator, University of Hamburg) were used. All measurements were conducted under cryogenic conditions at 100 K in a liquid nitrogen stream. For cryo-protection crystals were embedded in precipitant conditions containing glycerol, PEG (polyethylene glycol) 400, malonic acid or isopropanol. Generally, the crystal mounting was carried out using polymer loops (Dual-Thickness MicroMounts from Mitegen, US) or

nylon loops (Mounted CryoLoop, Hampton Research, US); if crystal separation was necessary microtools (Mitegen, US) were used.

P14 beamline was operated with the user interface mxCuBE v2 (Hamburg version). Always fine sliced data sets with oscillation range 0.1° per frame were recorded. For optimized data collection at the rotating anode generator the oscillation range ($\Delta\phi/\text{frame}$) was selected after estimation of the mosaicity in IDXREF job out of a first XDS run.

5.6 Data processing and model building

Routinely data reduction from single crystal diffraction experiments was conducted with the program package XDS [278]. For scaling either XSCALE out of the XDS package or SCALA [279] was applied. Ancillary, iMOSFLM [280] was used to verify solutions from XDS. Generally, for retrieving best solutions in XDS a lead run was conducted: Optimized values of correct space group, unit cell parameters, refined experimental geometry as well as beam divergence were included in a second XDS run. All data were selected and cut monitoring R_{merge} , $I/\sigma(I)$, CC1/2 and completeness in the following steps. Molecular replacement was performed with MOLREP [281] and Phaser [282] implemented in the CCP4 software suite [283]. Models were manually revised using Coot [284] and refined by refmac5 [285]. Coordinate file of ligands with optimized geometry and library description with molecular restraints was produced with elbow out of the Phenix software suite [286].

5.7 Model evaluation

The following online tools, listed in Table 24, were routinely used for structure model evaluation.

Table 24: Online tools for model evaluation.

Tool	Application	Citation
ClustalW	Primary sequence comparison	[287]
Blast	Sequence homology analysis	[288]
PDBePISA	Exploration of macromolecular interfaces	[289]
eFold	Comparison and 3D alignment of protein structures (C α -alignments)	[290]
PDBsum	Pictorial database of the content of each 3D structure	[291]

6 Small angle X-ray scattering (SAXS)

For SAXS measurements of *S. aureus* PdxK four different protein concentrations of 1.6, 2.2, 4.8 and 8.2 mg mL⁻¹ in buffer T/N300 were prepared and centrifuged at 100,000x g for 50 min at 4 °C. DLS measurements were performed to monitor the dispersity of the solution. SAXS measurements were conducted at P33 beamline (HASYLAB/EMBL, Germany) at a wavelength of 1.5 Å with a detector

distance of 2.7 m at 10 °C. The momentum transfer of $0.01 < s < 0.6 \text{ \AA}^{-1}$ was covered ($s = 4\pi \sin\theta/\lambda$, where 2θ is the scattering angle). Data were normalized to the intensity of the transmitted beam, radially averaged, the scattering of the buffer was subtracted and the difference curves were scaled according to the protein concentration and finally extrapolated to infinite dilution to yield the final composite scattering curves (PRIMUS from the *Atsas* suite [292]). The Guinier approximation was used to evaluate the forward scattering $I(0)$ and the radius of gyration (R_g), assuming that at very small angles ($s < 1.3 \cdot R_g^{-1}$) the intensity is represented as $I(s) = I(0) \exp(-(sR_g)^2 \cdot 3^{-1})$. R_g was computed using the indirect transform package GNOM [293] from the entire scattering pattern, the pairwise distribution function $p(r)$ and the size of the particle D_{\max} . *Ab initio* modelling was performed using the program DAMMIF [294] from the *Atsas* online server applying P2 symmetry in the slow mode. The resulting single models were further averaged with DAMAVER [295] and refined with DAMMIN [296] to a final *ab initio* model. Bovine serum albumin (66 kDa; in 50 mM HEPES, pH 7.5) was measured as a molecular weight reference.

7 PdxK activity assay and binding affinity quantification

7.1 PdxK activity assay

The kinase activity of *S. aureus* PdxK was measured according to Kwok and Churchich [297]. In a double beam spectrophotometer UVICON 933 (BIO-TEK Kontron) the formation of pyridoxal 5'-phosphate catalyzed by purified *S. aureus* C-terminally TEV His₆-tagged PdxK was followed by monitoring the change in absorbance at its absorption maximum at 388 nm (extinction coefficient of $4900 \text{ M}^{-1}\text{cm}^{-1}$). The kinetic enzymatic assay was performed in a total volume of 1 ml at 30 °C in 70 mM potassium phosphate buffer, pH 6.5 containing 50 µg enzyme, 0-1000 µM pyridoxal, 3 mM ATP, and 10 mM MgCl₂. The results were analyzed using GraphPad PRISM 5 (GraphPad, GraphPad Software, Inc.).

7.2 Microscale thermophoresis (MST) for binding affinity quantification

For analysis of *S. aureus* PdxK binding affinity the Monolith NT.115, channel combination Nano-blue/red, was used. Strep-tagged *S. aureus* PdxK was labeled with NT-647-NHS fluorescent dye (fluorescence excitation and emission maxima of approximately 650 and 670 nm, respectively) from Monolith Protein Labeling Kit NT 647 V012 via NHS-ester chemistry, which reacts with primary amines. The assay was performed with 30 nM PdxK in 25-50 mM Tris, 50-150 mM NaCl and 1-10 mM MgCl₂ supplemented with 0.05 % (v/v) Tween 20 at 25 °C at an LED power of 80 % and Laser power of 20, 40 and 60 % in standard capillaries.

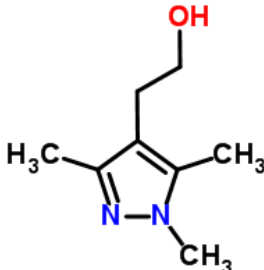
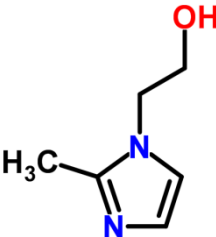
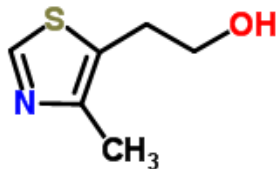
IV Results

All genes recombinantly expressed were verified beforehand via Sanger sequencing. Recombinant protein entity was verified by western blot analysis and mass spectrometry (chapter III 4.12 and III 4.20) from purified samples. For general protein quality assessment the folding was analyzed from different batches and in different buffers via CD spectroscopy and the dispersity was monitored by dynamic light scattering.

1 *Staphylococcus aureus* ThiM

The native structure of *S. aureus* ThiM as well a complex of ThiM with its natural ligand THZ has already been solved by Dr. J. Drebes (University of Hamburg) [298]. In her study promising substrate analogs were selected on the basis of the high resolution structure via docking experiments (Dr. B. Windshügel, European Screening Port, Fraunhofer IME Hamburg) and could be evaluated for successful metabolization [298]. Nevertheless, co-crystallization attempts were not successful and the high resolution structures of ThiM in complex with these promising lead compounds were absent. For detailed complex analysis this co-crystallization of ThiM with two selected compounds (referred to as cpd1 and cpd2) listed in Table 25 was the aim of this part of this project.

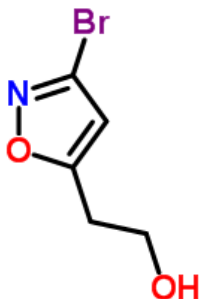
Table 25: Summary of the compounds and THZ used for co-crystallization into *S. aureus* ThiM and soaking experiments. The IUPAC (International Union of Pure and Applied Chemistry) conform chemical name, SMILES (simplified molecular-input line-entry system) string, molecular weight (MW), chemical structure (ChemDraw; PerkinElmer Inc.) as well as the kinetical parameters determined in an *in vitro* assay are summarized [164, 298].

Compound	cpd1	cpd2	THZ
IUPAC name	2-(1,3,5-trimethyl-1H-pyrazole-4-yl)ethanol	2-(2-methyl-1H-imidazole-1-yl)ethanol	2-(4-methyl-1,3-thiazol-5-yl)ethanol
SMILES string	<chem>Cc1c(c(n1)C)CCO</chem>	<chem>Cc1nccn1CCO</chem>	<chem>Cc1c(scn1)CCO</chem>
MW [g mol ⁻¹]	154.1	126.1	143.0
Structure			
Specific Activity [nmol min ⁻¹ mg ⁻¹]	7297 ± 267	7418 ± 91	4880 ± 488
K _M [μM]	834 ± 147	831 ± 169	44 ± 5
k _{cat} [min ⁻¹]	215 ± 8	218 ± 3	137 ± 13

Furthermore, a compound which was selected in the study of *J. Drebes* as well, 2-(3-Brom-1,2-oxazol-5-yl)ethanol referred to as cpd12, that showed an inhibitory effect on ThiM's kinase activity, was studied (Table 26).

Table 26: Summary of the compound 12.

The IUPAC conform chemical name, SMILES string, molecular weight, chemical structure (ChemDraw; PerkinElmer Inc.) as well as the kinetical parameters determined in an *in vitro* assay [298] are summarized.

Compound	cpd12
IUPAC name	2-(3-brom-1,2-oxazol-5-yl)ethanol
SMILES string	C1=C(ON=C1Br)CCO
MW [g mol ⁻¹]	191.0
Structure	
K _i [μM]	17 ± 4
Inhibition type	mixed

1.1 *S. aureus* ThiM: Optimization of purification and crystallization

S. aureus ThiM linked through a TEV protease recognition site to a His₆-tag was recombinantly expressed in *E. coli* BLR(DE3) cells. Gene expression was conducted for 3.5 h at 37 °C starting at an OD₆₀₀ of 0.5-0.6. The protein was purified from the cleared cell lysates, obtained from the standard procedure described in III 4.15.1, via affinity chromatography using two washing step of 20 mM imidazole in buffer T/N and was finally eluted in buffer T/N supplemented with 250 mM imidazole. Subsequently, the eluate was applied to a HiLoad 16/60 Superdex 200 column operated at 4 °C (chapter III 4.15.2). ThiM was thereby transferred to an imidazole free T/N buffer. Applying a calibration curve function revealed a calculated molecular weight of the eluted *S. aureus* ThiM of approx. 88 kDa. Figure 9 A shows the DLS pattern of ThiM protein solution with a concentration of 6 mg mL⁻¹ before an additional size exclusion chromatography, representing a polydispers hydrodynamic radius (R_h). After the size exclusion chromatography the protein shows a highly monodispers radius of 3.4 ± 0.0 nm and a calculated molecular weight for an ideal sphere of 55.5 kDa. The DLS pattern shown in Figure 9 B was recorded at a concentration of 15.5 mg mL⁻¹ but it remains constant up to a protein concentration up to 20 mg mL⁻¹.

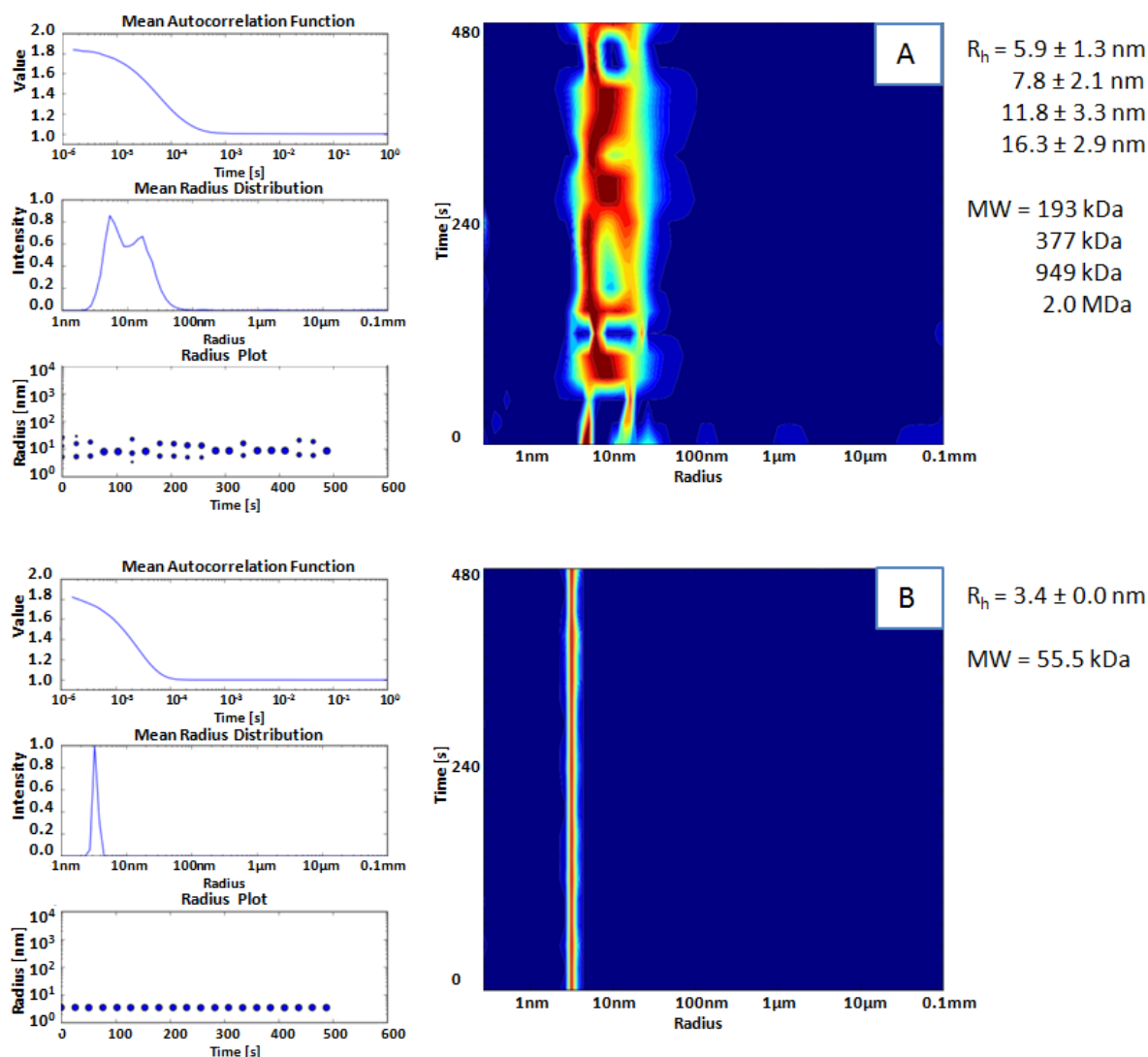


Figure 9: ThiM DLS pattern after affinity chromatography (A) and subsequent size exclusion chromatography (B).

DLS pattern, mean autocorrelation function of the recorded DLS signal, mean radius distribution: plotting radius against intensity, radius plot: plotting time against radius the hydrodynamic radius (R_h) as well as the calculated molecular weight (MW) are given.

A crystallization condition (15-22 % (w/v) PEG 3350, 0.2 M magnesium formate, 5 % (v/v) isopropanol) already optimized from *Dr. J. Drebes* that yielded in well diffracting crystals for native as well as THZ containing ThiM, were tested for co-crystallization. All co-crystallization and soaking attempts of *S. aureus* ThiM and cpd1 and cpd2 according to chapter III 5.2 and III 5.3 in this condition were not successful. Thus, a new initial crystallization screen was performed with 13.5 mg mL⁻¹ protein concentration using PACT premier, JCSG-plus, Classics and Cryos Suite crystallization screens in the setup described in chapter III 5.1 in order to find crystallization conditions for compound binding. Automated screening in a sitting drop, vapor diffusion setup at RT resulted in slightly intergrown crystals in the size of approx. 0.2 x 0.1 x 0.05 m³ in the crystallization condition 0.1 M Tris pH 8, 20 % (w/v) PEG 6000 and 0.2 M MgCl₂ after approx. two weeks. Optimization was performed in sitting drop, vapor diffusion setup in MRC MAXI 48-well optimization plate (Molecular Dimensions,

UK) with a ratio of protein to precipitant of 1:1. The PEG 6000 concentration (18 % - 22 % (w/v)) and the MgCl_2 concentration (0.17-0.26 mM) were varied against each other. An increase in the PEG concentration yielded in smaller crystals. The combination of the highest salt and PEG concentration resulted in needle shaped crystals (Figure 10).

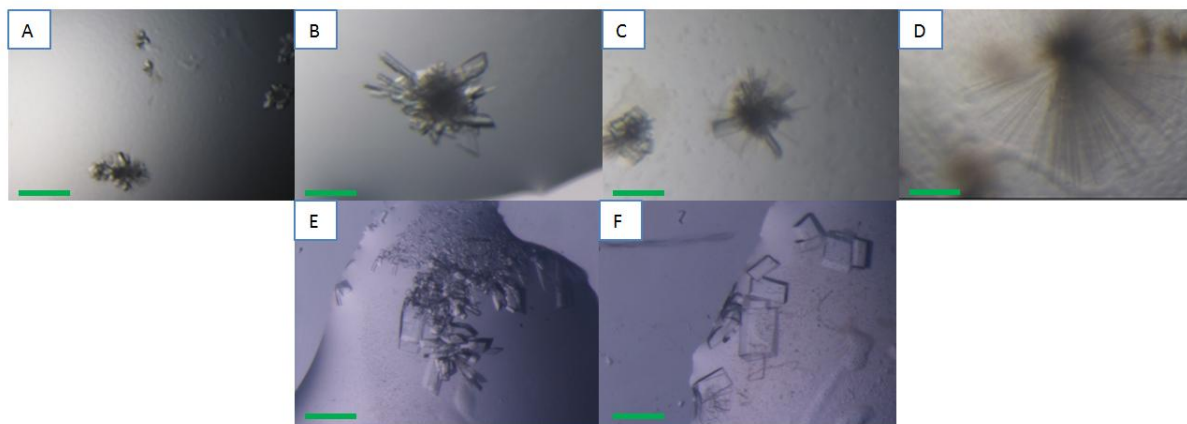


Figure 10: Crystals of *S. aureus* ThiM.

Initial condition: 0.1 M Tris pH 8.0, 20 % (w/v) PEG 6000 with 0.2 M MgCl_2 , A, B, C, D are showing a variation of the PEG 6000 concentration over 18 %, 19.6 %, 20.4 % to 21.2 % (w/v) with 0.1 M Tris pH 8.0 and 0.17 M MgCl_2 ; E and F are crystals grown with the addition of 0.1 M Tris pH 8.0, 20 % (w/v) PEG 6000 with 0.2 M and 0.26 M MgCl_2 respectively; scale bar equals to 100 μm .

In conclusion, crystals grown in condition 0.1 M Tris pH 8.0, 20 % (w/v) PEG 6000 with 0.26 M MgCl_2 were successfully soaked with cpd1 and crystals grown condition 0.1 M Tris pH 8, 20 % (w/v) PEG 6000 with 0.2 M MgCl_2 were successfully soaked with cpd2.

1.2 *S. aureus* ThiM: Diffraction data collection, processing and model building

A diffraction data set of *S. aureus* ThiM in complex with cpd1 and cpd2 was collected at 100 K at P14 EMBL beamline at DESY campus. The crystals had dimensions of approx. $0.1 \times 0.2 \times 0.1 \text{ mm}^3$. For cryoprotection the crystals were soaked with precipitant solution supplemented with 20 % (v/v) glycerol and 25 mM and 20 mM cpd1 and cpd2, respectively. Diffraction data were collected using the oscillation method (0.1 degree) and subsequently indexed, integrated and scaled with XDS. Data were cut to 1.87 Å (cpd1) and 1.62 Å (cpd2) monitoring R_{merge} , I/σ and CC1/2. Both crystals were found to belong to the triclinic space group P1 with unit cell dimensions of 62.0 Å, 62.4 Å, 108.3 Å and α , β , γ angles of 92.6°, 91.4°, 101.3° for ThiM-cpd1 and unit cell dimensions of 62.4 Å, 62.5 Å, 109.2 Å and α , β , γ angles of 92.6°, 92.1°, 101.5° for ThiM-cpd2. The Matthews coefficient was calculated for both cpd-complexes to $2.3 \text{ Å}^3 \text{ Dalton}^{-1}$ which corresponded to a solvent content of 47 % with six ThiM monomers in the asymmetric unit.

The structure was determined by the molecular replacement technique using MOLREP [281]. One trimer of *S. aureus* ThiM (structure determined by Dr. J. Drebes with a resolution of 2.09 Å, with

molecular replacement on basis of *B. subtilis* ThiK – pdb code: 1C3Q) crystallized in a monoclinic space group $P2_1$ was used as a search model. Calculation of rotation and translation functions using full resolution revealed a solution for two trimers in the asymmetric unit with an R-factor of 42.3 % and 41.1 % for the complex data sets ThiM-cpd1 and ThiM-cpd2 respectively. The contrast value (the ratio of the top score to the mean score) for the solution was 2.74 (ThiM-cpd1) and 1.87 (ThiM-cpd2). A contrast value >2.5 indicates a definite solution, a contrast <1.5 is probably no solution [299]. 5 % of reflections were used for the calculation of R_{free} to monitor the progress of refinement. Subsequently, the model was completed and further modified using Coot [284] and refined using refmac5 [285] (Restrained refinement with isotropic B factors). After the first round of refinement clear density for cpd1 and cpd2 was visible in the active centers of ThiM. The ligands were integrated in the model and included in the further refinement process. In the models the loop regions - amino acids 128-140 - as well as the last residues of the TEV cleavage site and the His₆-tag showed only limited diffraction. In a few monomers the loop region is stabilized through symmetry contacts, but commonly no electron density could be observed and thus the loop was excluded from the model. Furthermore, four Mg²⁺ ions were identified in the ThiM-cpd1 and five Mg²⁺ ions in the ThiM-cpd2 complex structure. Additionally, six TLS groups were defined; the TLS contribution is finally included in the pdb file. The final model of ThiM-cpd1 has an R-factor of 16.86 % and an R_{free} -factor of 19.90 %. The final model of ThiM-cpd2 has an R-factor of 18.24 % and an R_{free} -factor of 20.28 %. Both models demonstrate excellent geometry and no Ramachandran outliers. Data collection, processing and refinement statistics are summarized in Table 27. The parameters of *S. aureus* ThiM in complex with THZ structure (data from Dr. J. Drebes) were included in Table 27 as well, because the results of the cpd complex structures will be discussed by comparing it with the structure of ThiM with its natural ligand THZ.

Table 27: Data collection and refinement statistics for ThiM in complex with cpd1, cpd2 and THZ.

Data collection statistics^a			
	ThiM-cpd1	ThiM-cpd2	ThiM-THZ ²
Beamline	P14	P14	DORIS X13 (HASYLAB, DESY)
Wavelength [Å]	0.976262	0.976300	0.81
Space group	P1	P1	P1
Unit cell parameters: a, b, c [Å] α, β, γ [°]	62.0, 62.4, 108.3 92.6, 91.4, 101.3	62.4, 62.5, 109.2 92.6, 92.1, 101.5	62.6, 62.7, 108.5 92.2, 91.4, 101.3
Resolution [Å]	30.0 - 1.87	30 - 1.62	20.0 - 1.90
Temperature [K]	100	100	100
R _{merge} ^b	6.9 (54.9)	6.9 (51.3)	2.7 (21.1)
Measured reflections	447227	687175	236935
Unique reflections	125936	191461	119565
Average I/σ(I)	12.7 (2.5)	10.7 (2.5)	21.8 (4.0)
Mn(I) half-set correlation CC(1/2)	99.8 (79.8)	99.7 (84.0)	99.9 (68.3)
Completeness [%]	95.8 (94.7)	93.4 (90.5)	94.7 (92.9)
Redundancy	3.6 (3.5)	3.6 (3.6)	2 (1.9)
Refinement statistics			
Resolution range [Å]	30.0 - 1.87	30 - 1.62	20.0 - 1.90
R/ R _{free} [%]	16.86/19.90	18.24/20.28	18.61/20.93
Protein atoms	11228	11453	11149
Water molecules	486	511	371
Ligand atoms	66	54	54
Ions	4 Mg ²⁺	5 Mg ²⁺	4 Mg ²⁺
Rms deviation			
Bond-length [Å]	0.019	0.017	0.017
Bond angle [°]	1.738	1.699	1.597
B factor [Å ²]			
Protein	37.5	30.5	41.1
Water	38.1	24.9	26.2
Ligands	44.8	43.6	43.2
Ions	33.8	26.1	41.3
Ramachandran plot analysis:			
Most favored regions [%]	99.1	99.2	99.0
Allowed regions [%]	0.9	0.8	1.0
Generously allowed regions [%]	0	0	0

^aValues in parentheses are for the highest resolution shell. ^bR_{merge}: $\sum_{hkl} \sum_i |I_i(hkl) - \langle I(hkl) \rangle| / \sum_{hkl} \sum_i I_i(hkl)$, where $I(hkl)$ is the mean intensity of the reflections hkl, \sum_{hkl} is the sum over all reflections and \sum_i is the sum over i measurements of reflection hkl.

² Data were collected and initially processed by Dr. J. Drebes

1.3 Structure analysis - *S. aureus* ThiM with bound substrate analogs

S. aureus ThiM monomer belongs to the Rossmann-like fold group of kinases and is further classified to the ribokinase-like kinases belonging to the ribokinase superfamily, and to EC: 2.7.1.50 hydroxyethylthiazole kinases [300]. In ribokinases a general fold of a central eight stranded β -sheet in the order 2-1-3-4-5-6-7-8, where β_7 is antiparallel, flanked by two α -helical domains is characteristic [301]. In ThiM the central eight stranded β -sheet in the order 2-1-3-4-5-6-7-8 with the addition of one extra antiparallel β -strand at the C-terminus, which is flanked by five α -helices and two 3_{10} -helices on one site and six α -helices and one 3_{10} -helix on the other site, is present (Figure 11).

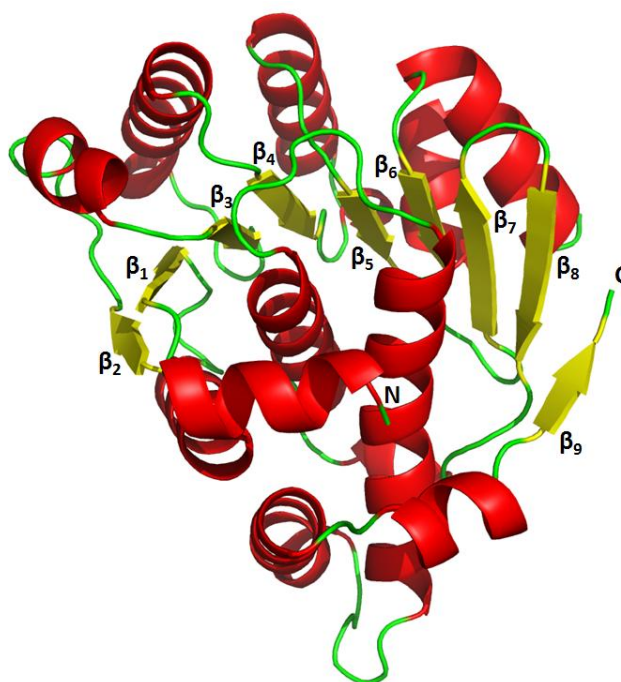


Figure 11: Secondary structure and overall fold of a *S. aureus* ThiM monomer.

S. aureus ThiM monomer in secondary structure representing cartoon illustration is shown; yellow is used for β -sheets, red for α -helix and green for turns and loops; labels of the N- and C-terminus as well as the central β -strands are shown. Figure was created with The PyMOL Molecular Graphics System, Version 1.7.4 Schrödinger, LLC.

Each monomer has a surface area of approx. 11500 \AA^2 . In the trimeric assembly 1950 \AA^2 of each monomer is buried and the mean surface area is 28500 \AA^2 . The active sites are built in the interface region of two monomers in the quaternary structure of a homo-trimer, resulting in three active sites per trimer as shown in Figure 12 A and B.

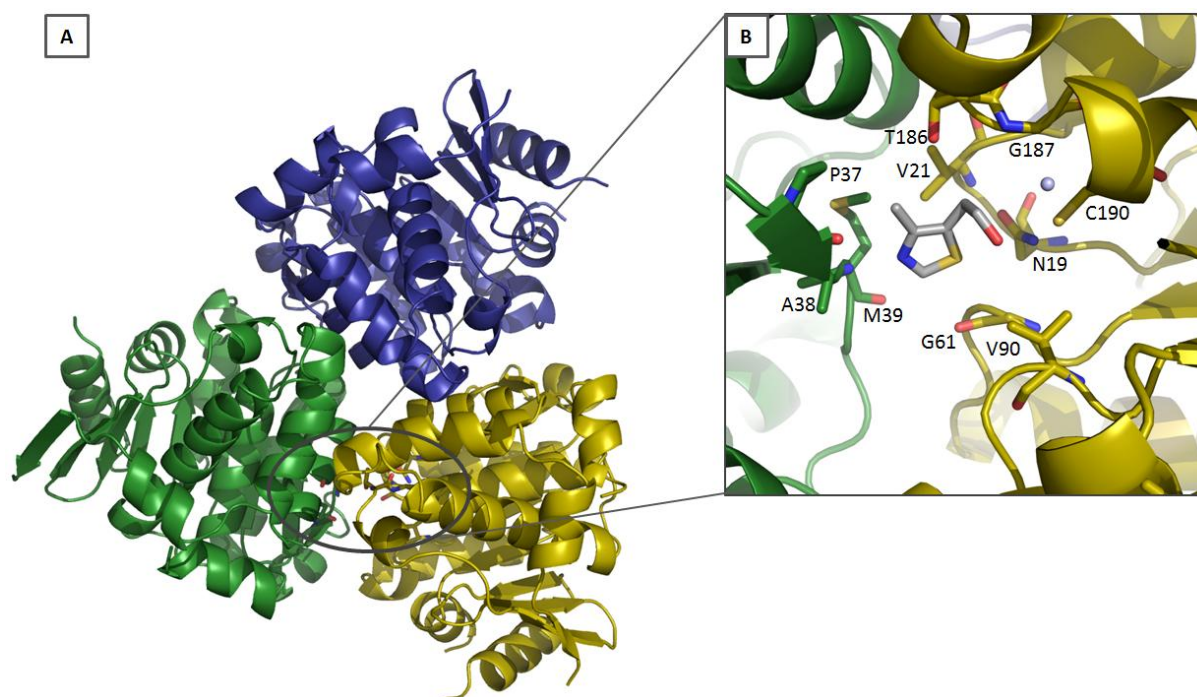


Figure 12: Quaternary structure of a *S. aureus* ThiM trimer (A) and active site architecture in complex with THZ (B).

A: The trimeric assembly of *S. aureus* ThiM is shown in cartoon representation, each color represents a monomer. B: In the enlarged representation of the active site in the interface of two monomers (green and yellow) in stick representation with the natural ligand THZ is shown; amino acids are labeled and atoms N, O, S are colored in blue, red and yellow in the stick representation respectively, a water atom is shown as a light blue sphere. Figure was created with The PyMOL Molecular Graphics System, Version 1.7.4 Schrödinger, LLC.

The binding of THZ, the natural ligand, is mediated by interactions of amino acids N19, V21, G61, V90, T186, G187 and C190 of one monomer and P37, A38 and M39 of the corresponding monomer, all located in the interface region as shown in Figure 12 B. The binding of the natural substrate is essentially stabilized by a hydrogen bond formed between the nitrogen of the thiazole ring and M39 as well as a water-mediated hydrogen bond between the flexible hydroxyl group of THZ and C190 although the orientation of the hydroxyl group is more flexible.

In both solved ThiM-cpd complex structures analyzed, all six active sites in the asymmetric unit were occupied with cpd1 and cpd2 respectively. In Figure 13 *S. aureus* ThiM active site in complex with cpd1 (Figure 13 A) and cpd2 (Figure 13 B) among a $F(o)-F(c)$ map for the compounds contoured at 3σ is depicted.

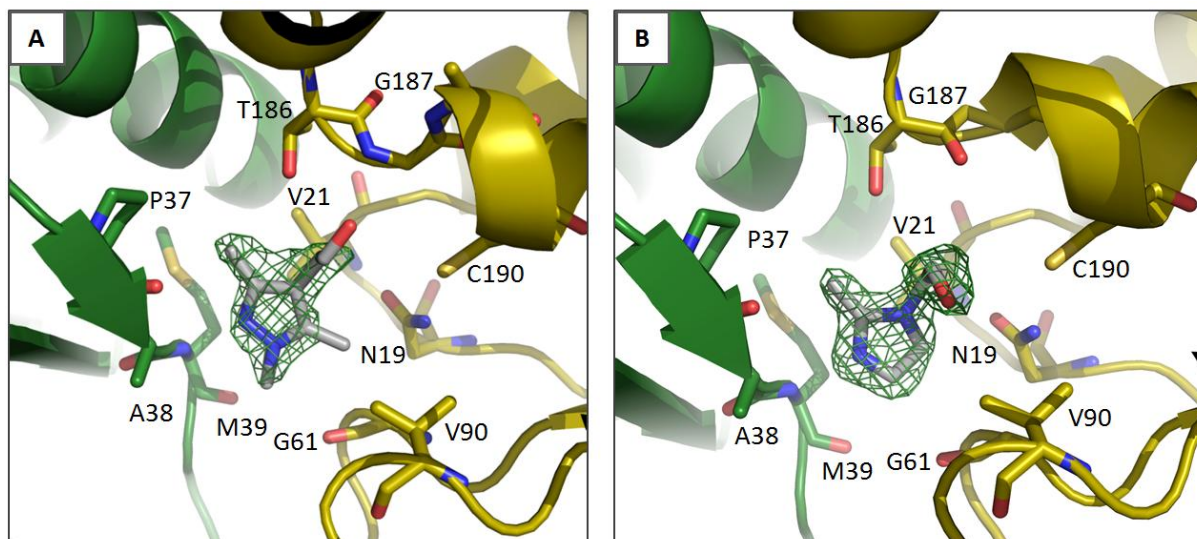


Figure 13: *S. aureus* ThiM active site in complex with cpd1 (A) and cpd2 (B).

The active site residues in the interface region are shown in stick representation embedded in cartoon representation. Cpd1 and cpd2 are given in grey stick representation; in the stick representation all atoms N, O, S are colored in blue, red and yellow respectively. A $F_o - F_c$ map for the compounds is contoured at 3σ and depicted as a green mesh. Figure was created with The PyMOL Molecular Graphics System, Version 1.7.4 Schrödinger, LLC.

The general positioning of THZ and the two compounds in a direct comparison are shown in Figure 14 A, B and C. To further compare the three ligands a chemical consensus nomenclature of THZ and cpd1 and cpd2 is introduced in Figure 14 D, E and F. In both analogs sulfur in position 5 in the heterocycle of THZ is changed to carbon. Furthermore, the carbon in position 4 of THZ was exchanged to nitrogen in cpd2, resulting in an imidazole heterocycle. Beyond that cpd1 has an additional nitrogen atom in position 6 yielding in a pyrazole heterocycle and moreover two additional methyl groups at position 5 and 6 are introduced (Figure 14 D, E and F, respectively).

Both compounds could form, like THZ, a hydrogen-bond to the main chain nitrogen of M39 and show a similar orientation of their hydroxyethyl groups in the direction of the catalytic C190. In all three ligands the hydroxyl group can adopt different orientations, reflected in the high standard deviations of contact distances summarized in Table 28 which were calculated out of six active site contacts. This flexibility of the hydroxyl group is also reflected in relative high B-factors ranging up to 60 \AA^2 .

Distances that span the location of the compounds in the area of the active site are comparatively listed in Table 28. They clearly illustrate that the overall location of the analog compounds 1 and 2 in the active sites of ThiM is remarkably comparable to the position of natural substrate THZ (Figure 14 G). Only the additional methyl group at cpd1 shifts the binding sparsely.

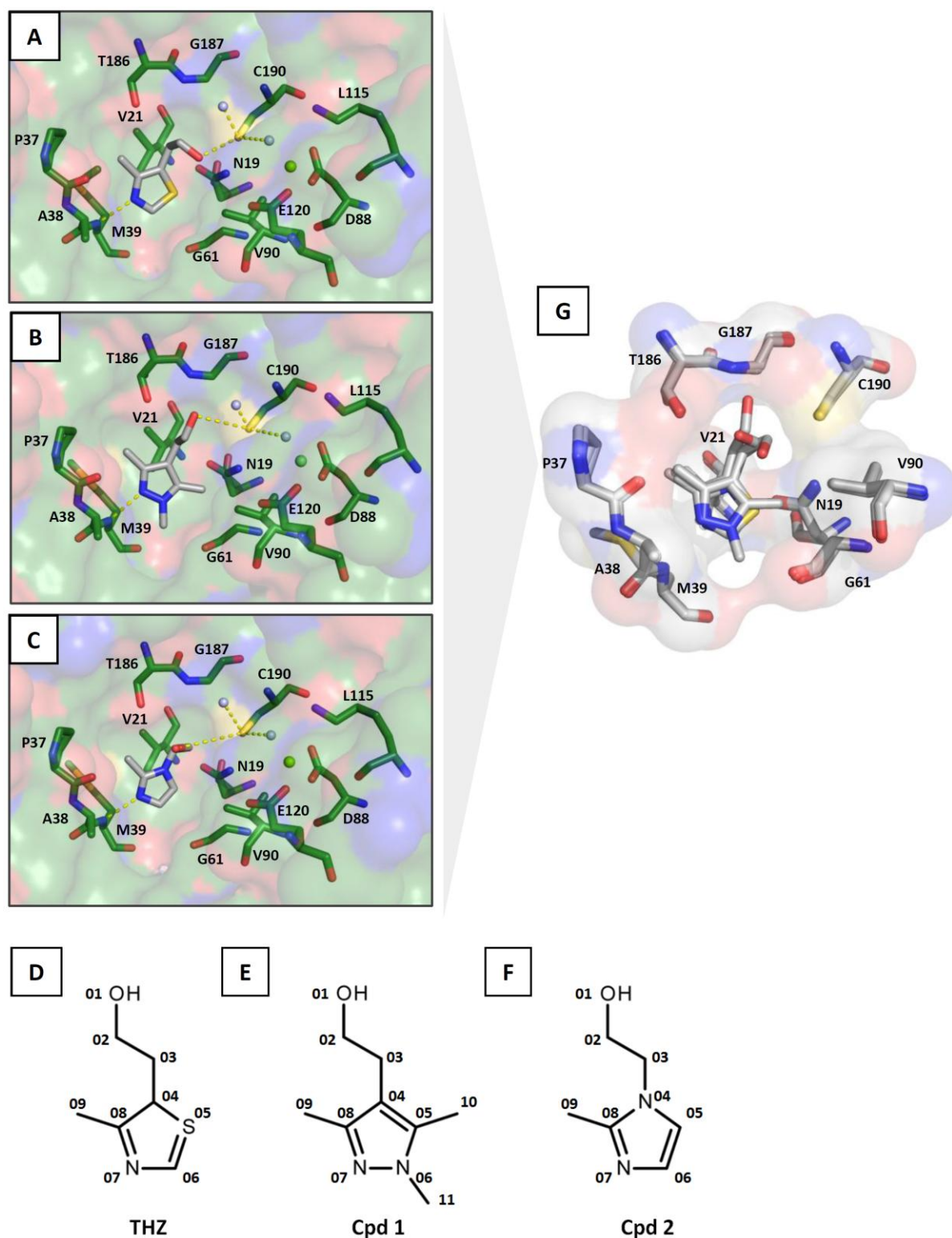


Figure 14: A comprehensive overview of THZ cpd1 and cpd2 in the active site of *S. aureus* ThiM.

In A, B, C the interacting and Mg^{2+} coordinating residues are shown in green stick representation, THZ and cpds are colored in grey, atoms N, O and S are colored in blue, red and yellow respectively, water molecules are represented as light blue spheres, Mg^{2+} ions as green spheres, surface is shown. In D, E, F the chemical formula and the consensus nomenclature of THZ and compounds are depicted. G shows a superimposition of THZ and the compounds in the active site; atoms C, N, O and S are colored in light grey, blue, red and yellow respectively. Figure was created with ChemDraw (PerkinElmer Inc.) and The PyMOL Molecular Graphics System, Version 1.7.4 Schrödinger, LLC.

Table 28: Comparative array of the positioning of THZ, cpd1 and cpd2 in *S. aureus* ThiM.

Selected mean distances with standard deviations between amino acids and THZ or cpd atoms respectively, calculated from six active sites, numbered according to the consensus nomenclature stated in Figure 14, are listed to define the overall positioning of THZ and cpds in the active site.

ThiM	THZ/cpd	THZ		cpd1		cpd2	
amino acid and atom	consensus nomenclature	mean distance	standard deviation	mean distance	standard deviation	mean distance	standard deviation
		[Å]	[Å]	[Å]	[Å]	[Å]	[Å]
N19 ND2	05	3.80	0.08	4.51	0.27	4.01	0.06
N19 ND2	10	-	-	3.42	0.37	-	-
V21 CG2	08	4.17	0.15	4.23	0.24	3.93	0.08
G61 O	06	3.43	0.12	4.21	0.34	3.49	0.09
P37 O	09	3.32	0.09	3.37	0.05	3.48	0.09
A38 CA	07	3.66	0.09	3.54	0.05	3.73	0.06
M39 N	07	2.95	0.14	2.86	0.10	2.91	0.05
T186 OG1	03	3.59	0.28	3.27	0.09	3.58	0.12
C190 SG	01	3.25	0.85	3.97	0.25	4.60	0.45

Residues D88, K115 and E120 coordinate a magnesium ion, including one solvent water molecule (Figure 14 A, B, C). In the ThiM-THZ complex, just as in ThiM-cpd1 complex, four Mg^{2+} ions were indentified which are essential for the phosphate group transfer reaction. In the ThiM-cpd2 complex five Mg^{2+} ions were identified, four in the formerly coordination and one in the potential nucleotide binding region.

A probable mode of action can be predicted with structural information obtained from ThiM complex structures, the understanding about the conserved phosphoryl transfer within Rossmann-like folded kinases [302] and data published for the homologue enzyme ThiK from *B. subtilis* [303] with bound ATP and THZ (pdb code: 1ESQ).

An enhanced nucleophilicity of the THZ or compound hydroxyl group by a proton-relay system can be assumed, build up by a water molecule coordinated by the magnesium ion and its interaction with C190. After binding of ATP to the enzyme and following protonation of the ATP's C8, a transfer of H^+ to the α - PO_4 via T160 in ThiM could occur (push mechanism). Onwards the proton is transferred to the β - PO_4 via R121 and the K115 in coordination with Mg^{2+} and the μ - PO_4 and thereby could subsequently ensure the formation of the pentavalent intermediate after the nucleophilic attack of THZ.

In Figure 15 the sequence alignment of *S. aureus* ThiM with homolog structures from *Enterococcus faecalis* ThiM (PDB code: 3DZV), *B. subtilis* ThiK (PDB code: 1C3Q) and *Pyrococcus horikoshii* ThiM (PDB code: 3HPD) is given. They share 32 %, 38 % and 39 % sequence identity, respectively. The corresponding C α RMSD values are 1.6, 1.3, and 1.2 Å and maximum displacements

were calculated to 4.6, 4.5 and 4.2 Å, determined by protein structure comparison service PDBeFold [290]. The substrate binding, probable ATP binding and the Mg^{2+} ion coordinating residues are highlighted. Further the conserved ribokinase anion hole motif for the phosphate transfer [216, 301] is boxed in green.

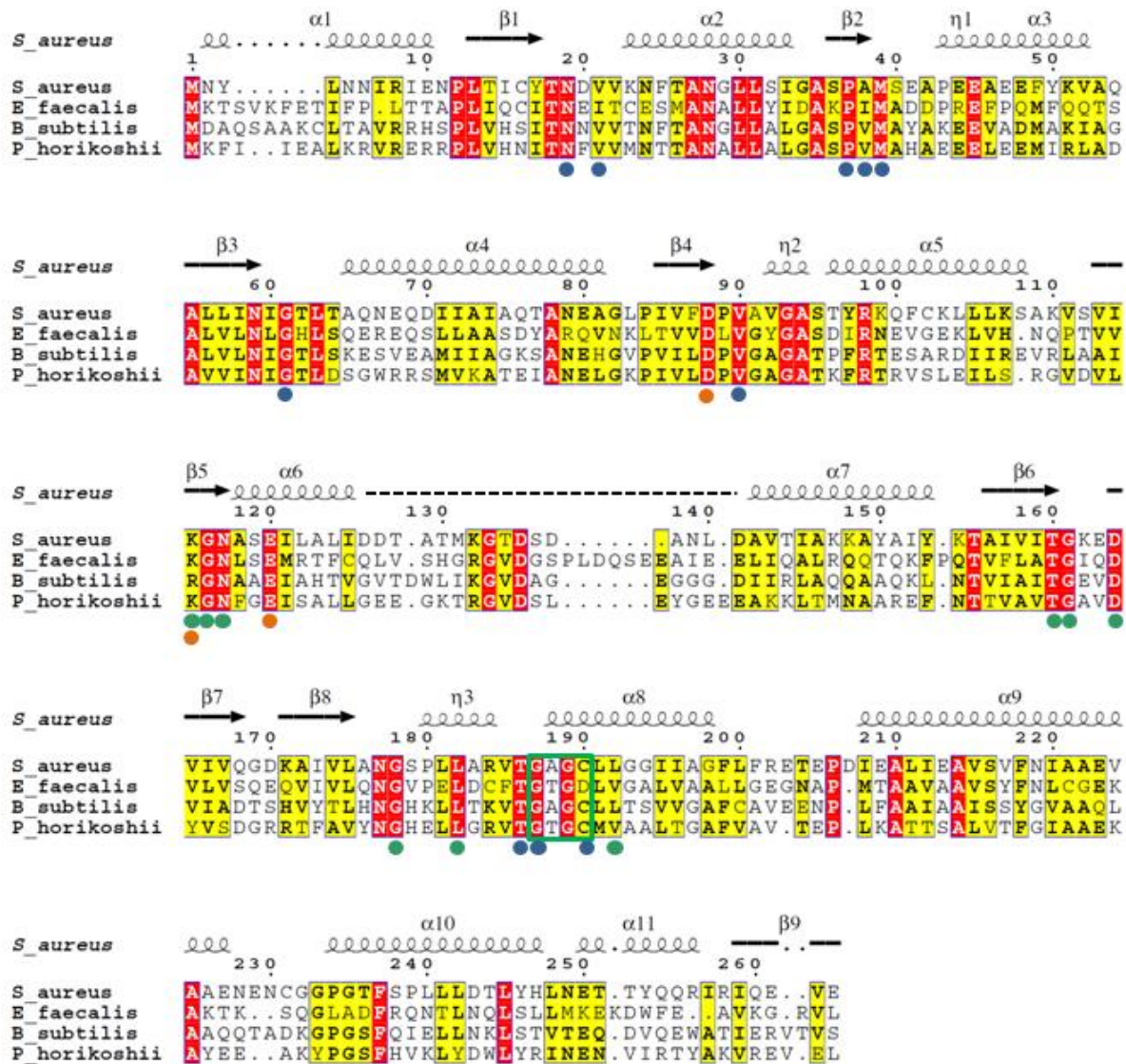


Figure 15: Sequence alignment of *S. aureus*, *E. faecalis*, *B. subtilis* and *P. horikoshii* ThiM.

Multiple sequence alignment was performed using ClustalW2, representation was generated with ESPrit. Identical residues are highlighted in red boxes, similar residues in yellow boxes. The secondary structure of *S. aureus* ThiM is annotated on the top, spirals represent α -helices, arrows represent β -strands, T stands for turns, μ do represent 3_{10} helices. The dashed line indicates a disordered region. Blue circles below the sequence indicate THZ, cpd1 and cpd2 binding residues. Green dots indicate the probable ATP-binding site as found for the homologous structure ThiK of *B. subtilis* and orange dots indicate residues coordinating Mg^{2+} . The anion hole is boxed in green.

1.4 Effects of cpd12 on *S. aureus* ThiM

The brominated cpd12, showing an unexpected inhibitory effect on ThiM, was in focus for extensive co-crystallization attempts and soaking experiments in both known crystallization conditions but no co-crystallization or soaking was feasible. The crystals either did not grow or were not stable after the addition of cpd12. Thus the effect of cpd12 on ThiM was studied by DLS, native PAGE and CD spectroscopy. In long term DLS measurements a promoted aggregation of the protein upon cpd12 addition could be observed. ThiM habitually shows a slight tendency to aggregate at RT over time. However, if cpd12 was added in molar ratios 1 : 40, 1 : 80 and 1 : 120 to a protein solution of 6.4 mg mL⁻¹ the tendency for aggregation is increased as can be seen from Figure 16. The calculated hydrodynamic radius (R_h) and the relative occurrence (A) of the particles in the analyzed protein solution from a Contin analysis embedded in the DLS software are given. A relative decrease of the smaller particles (~4.5 nm) and a relative increase of bigger, aggregated particles (~16-23 nm) could be detected over time in a cpd12 concentration dependent manner.

Nevertheless, in native PAGE analysis no specific higher oligomeric intermediate could be detected (PAGE not shown). Thus for a folding analysis via CD spectroscopy cpd12 was added to purified *S. aureus* ThiM (0.089 mg mL⁻¹ in a buffer containing 10 mM Tris pH 8.0, 0.5 mM NaCl) in molar ratios of 1 : 0, 1 : 50 and 1 : 100 (Figure 17 A, B and C respectively). The CD spectra clearly demonstrated that ThiM was time- as well concentration-dependent partially unfolded upon cpd12 addition. As a control experiment BSA standard solution (2 mg mL⁻¹, PierceTM, Life Technologies, Germany) was supplemented with the same molar ratio of the compound. The effect of a promoted unfolding and aggregation subsequent cpd12 addition could neither be demonstrated in CD spectroscopy nor in DLS measurements with the BSA standard (results not shown).

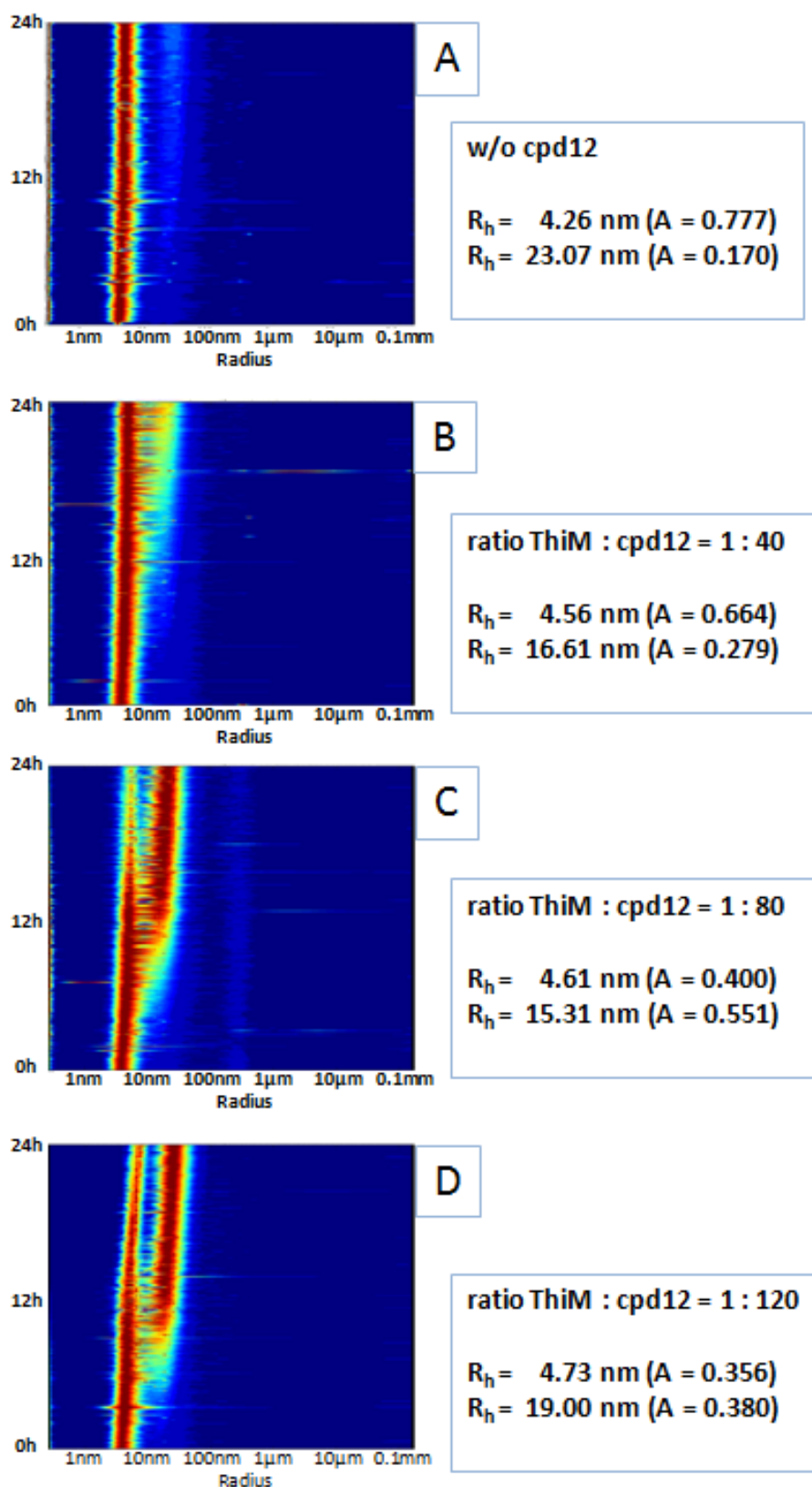


Figure 16: Long term (24 h) DLS measurements of *S. aureus* ThiM.

A: Control measurement of *S. aureus* ThiM without (w/o) the addition of cpd12. B, C, D: Cpd12 was added in molar ratios 1 : 40, 1 : 80 and 1 : 120 to a protein solution of 6.4 mg mL^{-1} respectively. The particle size was plotted against the time of the measurements and the calculated hydrodynamic radius (R_h) and the relative occurrence (A) of the particles in the analyzed protein solutions are given.

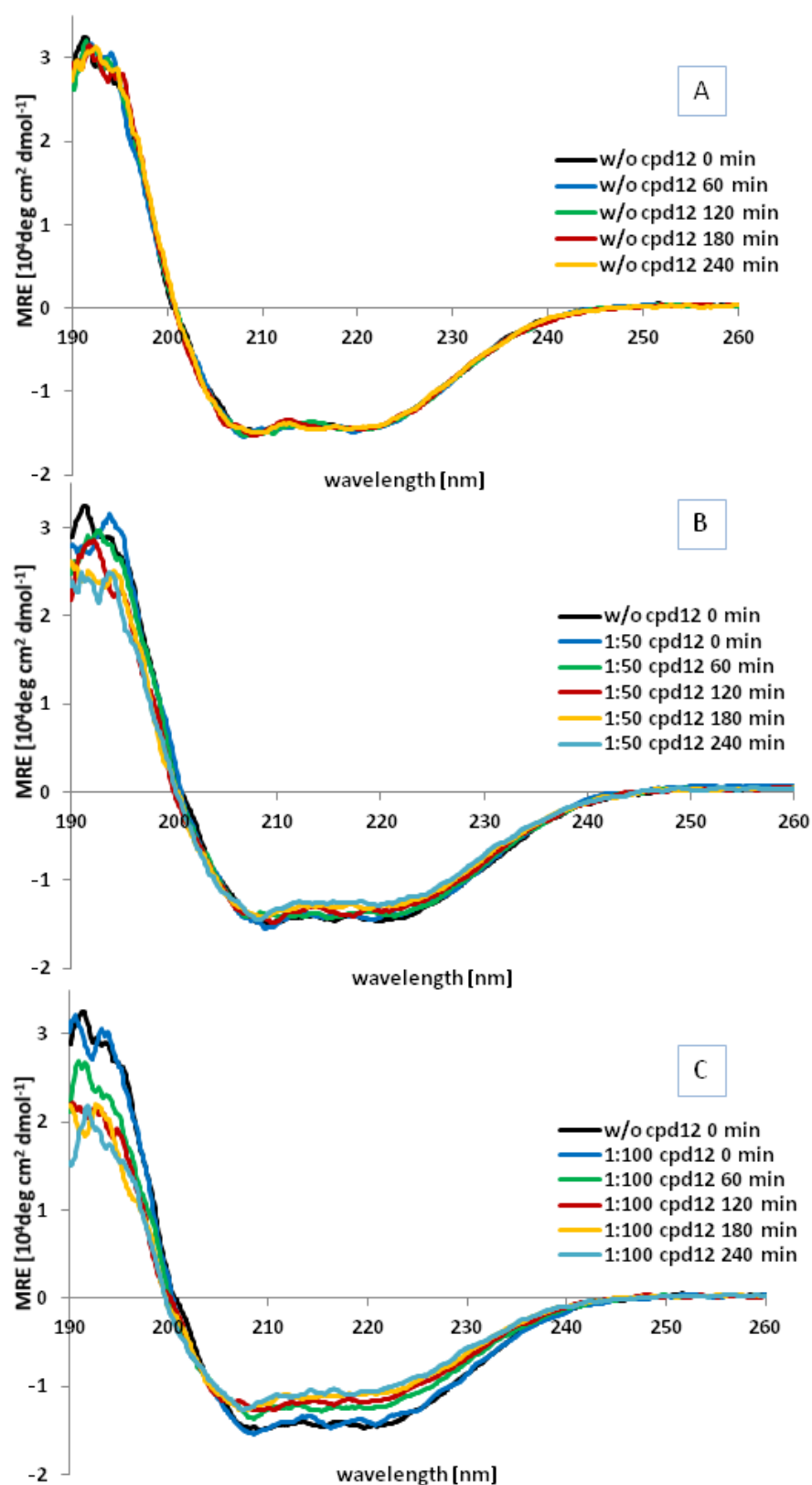


Figure 17: CD spectra of a time course experiment adding cpd12 to *S. aureus* ThiM.

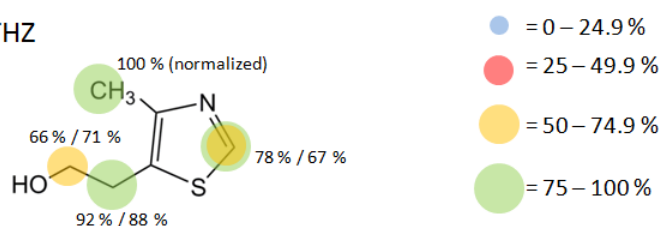
The folding state of *S. aureus* ThiM was monitored in far UV spectra (190-260 nm) at 20 °C for up to 4 h. A depicts the folding of *S. aureus* ThiM without (w/o) the addition of cpd12; B and C show the CD spectra after the addition 1 : 50 and 1 : 100 molar ratio of cpd12 respectively; 10 measurements were accumulated. Figure was created with GraphPad Prism 5 version 5.01 for Windows (GraphPad Software, Inc.).

1.5 Investigations on *S. aureus* ThiM NPE-caged ATP complex formation and nano-crystallization

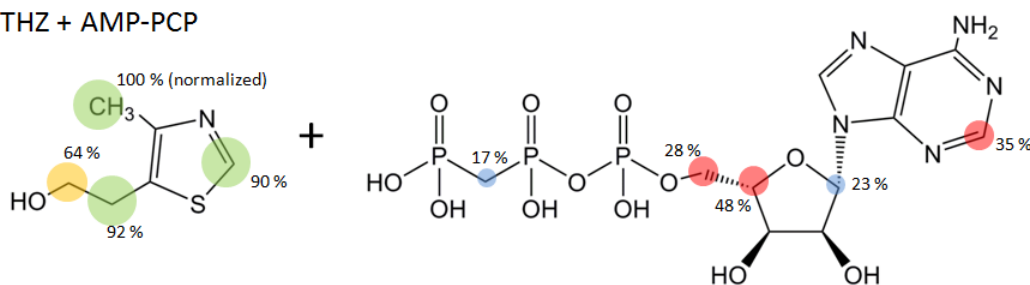
To further elucidate the reaction mechanism of the kinase in time resolved serial X-ray pump probe experiments, *S. aureus* ThiM was tested for co-crystallization with NPE-caged-ATP and THZ. Co-crystallization, in the condition successfully used for elucidating ThiM in complex with the compounds as well as the earlier optimized condition of *Dr. J. Drebes*, yielded in gel-like none crystalline material. Also no complex with the caged compound could be obtained after soaking experiments in this condition. Thus to verify the ability of ThiM to bind NPE-caged-ATP in the presence of THZ, STD-NMR experiments according to III 4.21 were conducted in cooperation with *J. Klare* in the research group of *Dr. T. Hackl (University of Hamburg)*.

For the epitop mapping of NPE-caged ATP in presence of THZ first spectra of ThiM in the presence of THZ and AMP-PNP were recorded to assign the proton chemical shifts. The absolute STD effects were calculated from off-resonance and STD-resonance signal intensities. The normalized STD-effects are depicted in Figure 18 and clarify the distances of the respective protons in the protein-ligand complex. The spectra with the assignment and the overall numerical STD-effects are summarized in Figure 51, Figure 52 and Table 37 - 40 in the appendix.

A: ThiM + THZ



B: ThiM + THZ + AMP-PCP



C: ThiM + THZ + NPE-caged ATP

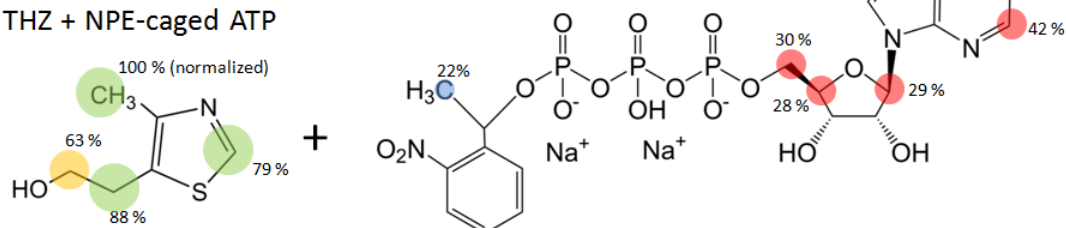


Figure 18: Mapping of the binding epitopes of THZ (A), AMP-PCP (B) and NPE-caged ATP (C) in the presence of THZ.

The color code depicts the relative STD effect. Figure was created with ChemDraw (PerkinElmer Inc.)

For THZ a strong binding at the methyl moiety (100 %), the hydroxyethyl (66-88 %) and the thiazole ring (C2) (67/78 %) could be identified. The first number depicted in the epitop mapping corresponds to the measurement of *S. aureus* ThiM with the addition of 100 μ M THZ and the second to the measurement with the addition of 50 μ M THZ. Two measurements with the addition of 50 and 100 μ M THZ respectively were performed to generate a suitable comparative for analysis of ThiM and THZ in the presence of the nucleotides AMP-PCP and NPE-caged ATP, which were measured in the presence of 100 and 50 μ M THZ respectively. From the high resolution structure it is already known, that THZ forms a hydrogen bond to M39 which could not be identified as it is lacking hydrogen, needed for the STD detection. In the presence of the non hydrolyzable ATP analog AMP-PCP the prepositioning of THZ is exceptionally similar as could be seen from the same relative epitop mapping in the STD effect. AMP-PCP shows the highest STD effect at the ribose (48 %) and the adenine base (35 %). In presence of the NPE-caged ATP analog the prepositioning of THZ is exceptionally similar as well, but for the hydrogen at the C2 of the adenine base and the hydrogens at C1 and C4 of the ribose a relatively stronger STD effect compared to the AMP-PCP could be detected. In conclusion the binding of the NPE-caged ATP analog in presence of THZ could be confirmed with a reasonable prepositioning of THZ.

On the basis of the confirmed binding of NPE-caged ATP to ThiM at least in the protein buffer a further crystallization screen was performed and resulted in a successful new crystallization condition. Plate like 2D-crystals of ThiM (16 mg mL⁻¹) supplemented with 5 mM NPE-caged ATP (molar ratio protein over NPE-caged ATP 1 : 8.3) were obtained in the presence of 0.2 M ammonium sulfate, 0.1 M MES pH 6.5, 30 % PEG (w/v) 5000 MME in a 1:1 ratio of protein over precipitant. This condition only resulted in crystals if the NPE-caged ATP was added. Diffraction up to 2.4 Å could be recorded; however it was not possible to collect a full diffraction data set as the signal faded out after rotating less than 8 degrees.

Defined nano crystallization of *S. aureus* ThiM was tested with *R. Schubert* (University of Hamburg) applying the XtalController 900. A previously detected crystallization condition (0.1 M HEPES sodium salt pH 7.5, 1.5 M lithium sulfate) forming plate-like crystals of ThiM in vapor diffusion sitting drop format at a protein concentration of 15 mg mL⁻¹ was used.

In Figure 19 the evolution of the hydrodynamic radius distribution of ThiM, determined by DLS, after adding precipitant to a final concentration of 0.5 M lithium sulfate over a time period of 30 minute can be seen.

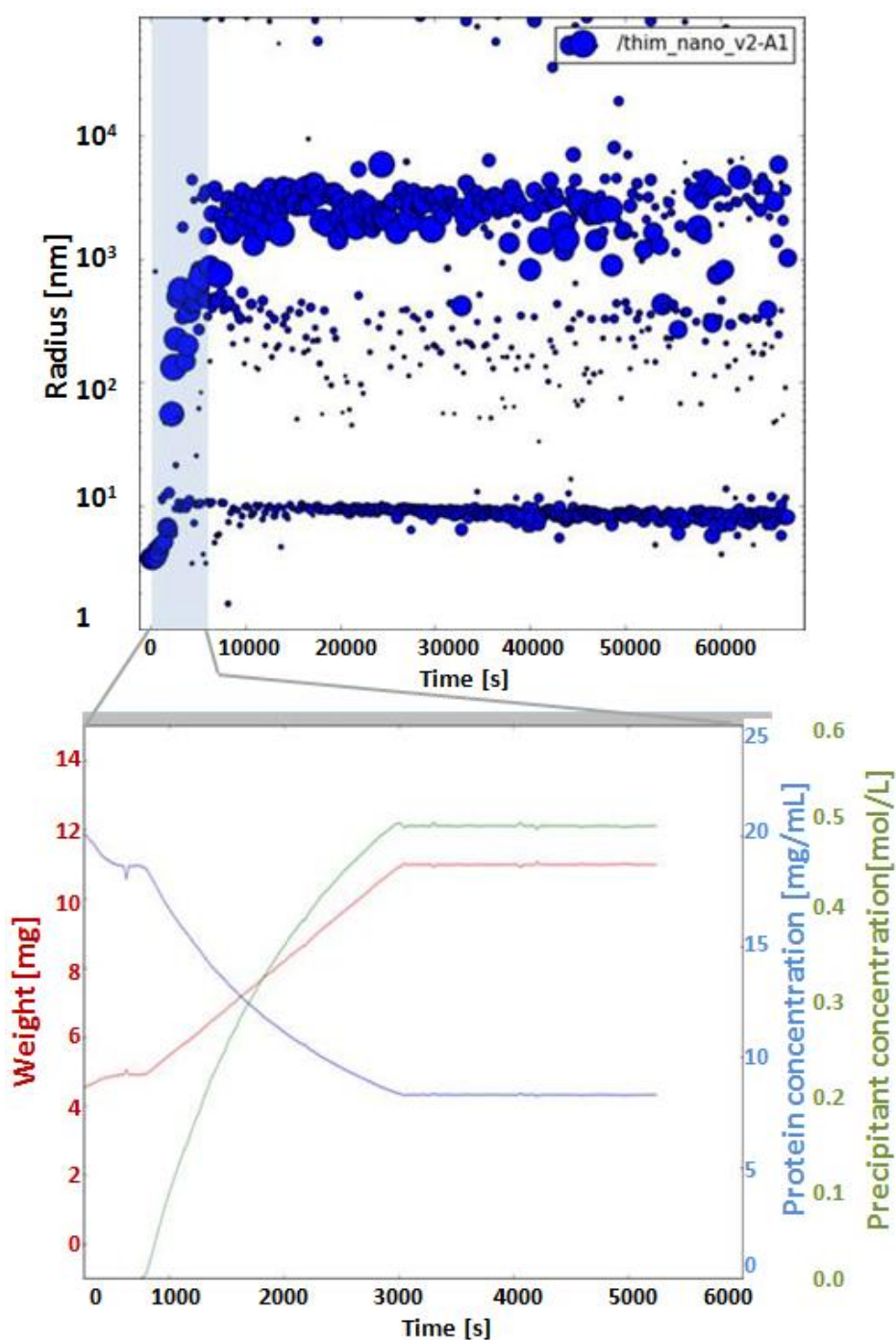


Figure 19: Hydrodynamic radius distribution determined by DLS using the XtalController 900.

The radius distribution against the time is plotted in the upper graph. For the initial 10 minutes of the experiment the change of the sample weight (red curve), protein and precipitant concentration (blue and green curve) are shown in the graph below.

The upper graph in Figure 19 shows the radius distribution of ThiM during the crystallization experiment. During successive addition of precipitant a complex radius distribution pattern was detected, reporting the successful formation of protein nano crystals. For the initial 10 minutes of the experiment the monitored sample weight is depicted in the graph beneath (red curve). In the graph the protein (blue curve) as well as the precipitant (green curve) concentration can be followed during the experiment online.

The initial hydrodynamic radius of ThiM was 3.8 ± 0.4 nm before precipitant injection, representing the trimeric protein complex in solution. Upon precipitant injection the radius of the trimer fraction increases due to viscosity changes of the solution, which is not taken into consideration. In addition, a second radius fraction occurred, which was separating into two radius fractions during the experiments. Initial investigations with other proteins indicate, that this characteristic radius distribution pattern reports the successful formation of protein nano crystals. These results need further verification by imaging techniques like electron microscopy and will be continued by *R. Schubert*.

2 *Staphylococcus aureus* TPK

2.1 Recombinant expression, purification and characterization

TPK linked through a TEV site (ENLYFQG/S) to a His₆-tag was recombinantly expressed in *E. coli* BLR cells. Gene expression was conducted for 3.5 h at 37 °C starting at an OD₆₀₀ of 0.5 - 0.6, the expression profile is given in Figure 20A.

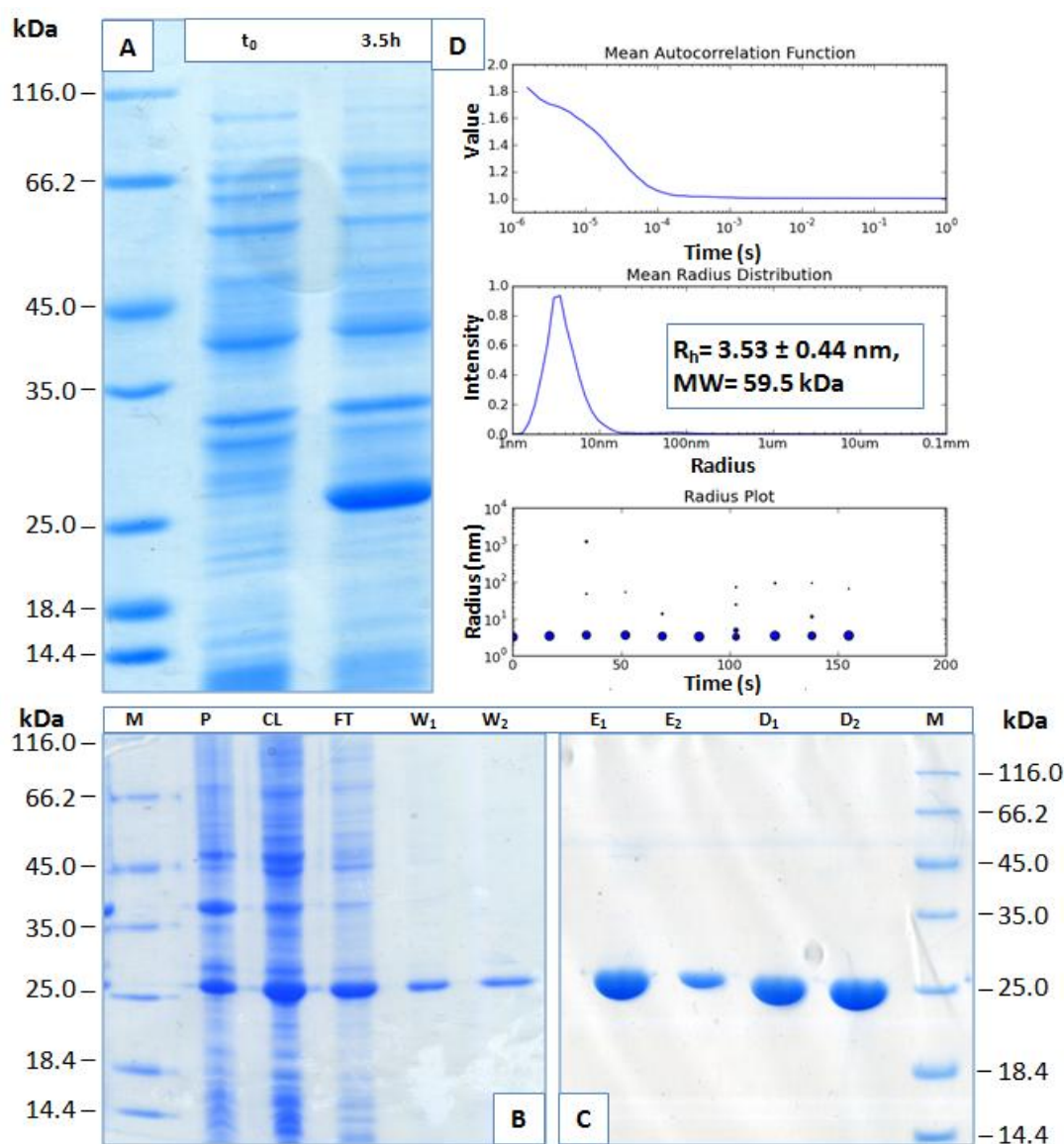


Figure 20: Summary of recombinant gene expression, purification and DLS characterization of *S. aureus* TPK.

A: Expression profile of *S. aureus* TPK at t_0 and 3.5h [5 μ L], respectively; B: Purification and digest of recombinant TPK, M- protein molecular weight marker [8 μ L], P- pellet [1 μ L], CL- crude extract [2 μ L], FT- flow trough [2 μ L], W₁- wash step1 [2 μ L], W₂- wash step2 [5 μ L]; C: E₁- elution step1 [2 μ L], E₂- elution step2 [5 μ L], D₁-TEV digest before 2nd affinity chromatography [5 μ L], D₂-TEV digest after 2nd affinity chromatography [5 μ L], M- protein molecular weight marker [8 μ L]; D top down: DLS pattern, mean autocorrelation function of the DLS signal; Mean radius distribution: plotting radius against intensity; Radius plot: plotting time against radius; the hydrodynamic radius is given as well as the calculated molecular weight (MW).

The protein was purified from the cleared cell lysate, obtained from the standard procedure described in chapter III 4.15.1 via affinity chromatography (chapter III 4.15.2) using two washing steps of 20 mM imidazole in buffer T/N and a final elution in buffer T/N supplemented with 250 mM imidazole (Figure 20 B and C). After a buffer exchange applying the eluted protein to a Sephadex G-25 Fine, XK 50/30 column operated with the ÄKTA prime system, a TEV digest under standard conditions (chapter III 4.17) and successively a second affinity chromatography were performed. All chromatography experiments were conducted at 4 °C. The cut protein was dialysed O/N into a T/M buffer and successively concentrated to 5.0, 9.7 and 16.7 mg mL⁻¹. The dispersity of the protein solution was monitored via DLS. Figure 20 D shows the DLS pattern of the protein solution at a concentration of 5 mg mL⁻¹ representing a hydrodynamic radius of 3.53 ± 0.44 nm and a calculated molecular weight for an ideal sphere of 59.5 kDa.

2.2 Crystallization of *S. aureus* TPK in complex with thiamine

Crystallization screens were performed with a solution containing 5.0 mg mL⁻¹, 9.7 mg mL⁻¹ and, close to the solubility limit, 16.7 mg mL⁻¹ of protein. The protein solution was supplemented with a final concentration of 3 mM thiamine, yielding in a molecular ratio of thiamine over protein of 15.4, 7.9 and 9.6 respectively. Automated screening in a sitting drop, vapor diffusion setup at 4 °C yielded in diverse needle shaped crystals after approx. two weeks. Tendencies for the preference of kosmotropic chemicals (NH₄⁺, K⁺, Na⁺, Li⁺) at buffers systems ranging from pH 4.0 - 8.0 with no systematic in PEG and salt precipitants could be identified. Optimization was performed in sitting drop, vapor diffusion (plates) oil sealed batch methods (Terazaki plates (Nunc, Denmark) and immuno stripwell (Corning) as well as counter diffusion setups.

Solitarly optimization of a crystallization condition containing 2.2 - 2.8 M sodium malonate pH 7.0 with 8.4 mg mL⁻¹ protein in a 1.1 ratio grown at 18 °C resulted in broader and less intergrown needle shaped crystals shown in Figure 21 A, B, C when the batch method under oil was applied. However, from these crystals no sufficient diffraction pattern was observed. After more than four weeks, an optimization of the initial condition (85 mM HEPES pH 7.5, 8.5 % (w/v) PEG 8000, 15 % (v/v) glycerol) to 85 mM HEPES pH 7.5, 9.5 % (w/v) PEG 8000, 15 % (v/v) glycerol with a protein concentration of 5 mg mL⁻¹ at a ratio of protein over precipitant 1 : 1.5 lead to the slightly intergrown crystals shown in Figure 21 D. Crystals grown in the slightly changed original condition were finally used for diffraction data collection (shown in Figure 21 E).

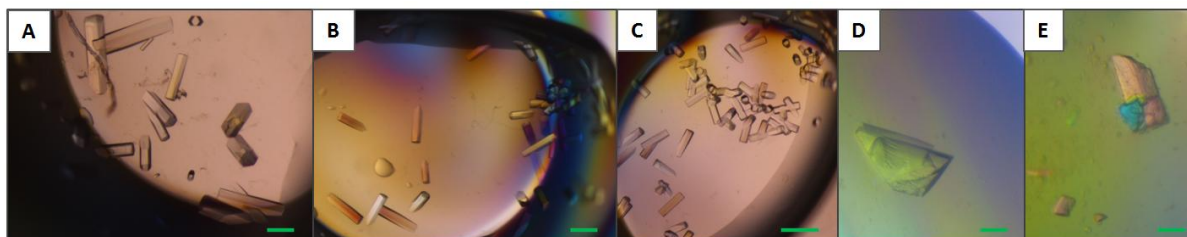


Figure 21: Crystals from *S. aureus* TPK.

A, B, C: TPK crystals grown at 18 °C in batch method under oil after addition of 2.2, 2.4, 2.8 M sodium malonate pH 7.0 respectively (8.4 mg mL^{-1} protein). D, E: Crystals of the optimization of a condition containing 85 mM HEPES pH 7.5, 8.5 % (w/v) PEG 8000, 15 % (v/v) glycerol; D: ratio protein over precipitant 1 : 1.8, protein concentration: 5 mg mL^{-1} ; E: PEG 8000 changed to 9.5 % (w/v), ratio protein over precipitant 1 : 1; protein concentration: 5 mg mL^{-1} ; scale bar equals to 100 μm .

2.3 *S. aureus* TPK: Diffraction data collection, processing and model building

A data set of the native TPK in complex with thiamine was collected at 100 K at P14 EMBL beamline at DESY campus. The crystal had dimensions of approx. $0.1 \times 0.2 \times 0.1 \text{ mm}^3$. No additional cryo protection was necessary due to the 15 % (v/v) glycerol in the precipitant solution. Diffraction data were collected to 1.4 Å resolution using the oscillation method (0.1 degree) and subsequently indexed, integrated and scaled with XDS. Data were cut to 1.4 Å monitoring R_{merge} , I/σ and CC1/2. The crystal was found to belong to the monoclinic space group $P2_1$ with unit cell dimensions of $a = 46.6$, $b = 85.3$ and $c = 52.5 \text{ Å}$ and a β angle of 110.6° . The Matthews coefficient was calculated $2.0 \text{ Å}^3 \text{ Dalton}^{-1}$, which corresponded to a solvent content of 38 % with two molecules in the asymmetric unit.

Sequence identity was analyzed using Basic Local Alignment Search Tool (BLAST) applying the protein-protein BLAST algorithm. Highest sequence identity was 50 % identified to thiamine pyrophosphokinase from *Staphylococcus saprophyticus subsp. saprophyticus* (Ssss) (pdb code: 3L8M). Second most identical protein is the thiamine pyrophosphokinase from *B. subtilis* with an identity of 46 %, deposited in pdb as 3LM8. The human thiamine pyrophosphokinase shares 25 % sequence identity with *S. aureus* TPK and is deposited under pdb code 3S4Y. The following Figure 22 shows a sequence alignment of *S. aureus*, Ssss and *B. subtilis* TPK. The secondary structure of *S. aureus* TPK is annotated on the top.

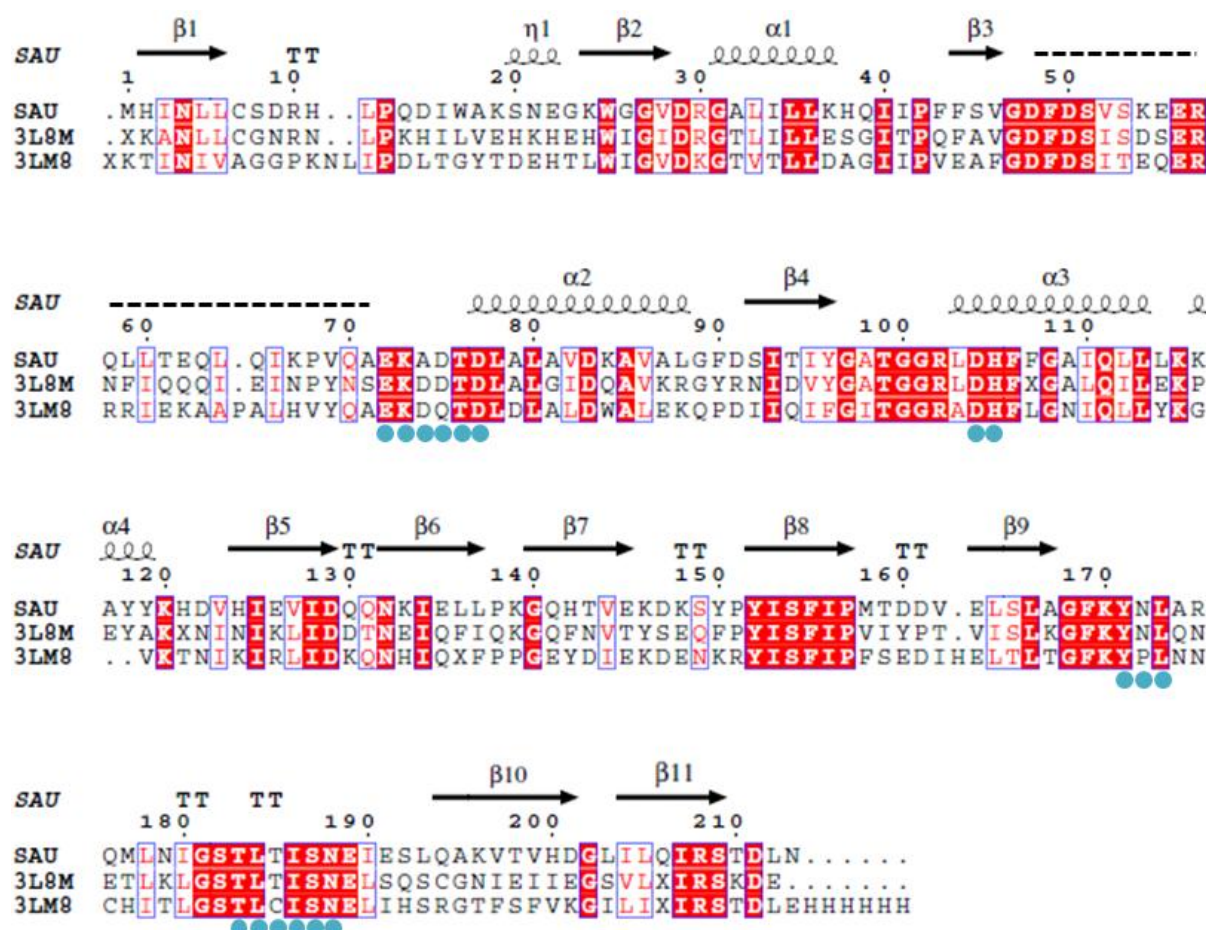


Figure 22: Sequence alignment of *S. aureus* (SAU), *Ssss* (3L8M) and *B. subtilis* (3LM8) TPK.

Multiple sequence alignment was performed using ClustalW2, representation was generated with ESPrit. Identical residues are highlighted in red boxes, similar residues in white boxes. The secondary structure of *S. aureus* TPK is annotated on the top, spirals represent α -helices, arrows represent β -strands, T stands for turns and μ represents 3_{10} helices. A dashed line indicates a disordered region. The teal circles below the sequence indicate the residues stabilizing the substrate thiamine.

The RMSD could be determined to 1.1 Å for *Ssss* TPK (pdb code: 3L8M), 1.5 Å for *B. subtilis* (pdb code: 3LM8) determined by protein structure comparison service PDBFold [290]. Molecular replacement using *S. aureus* monomeric TPK (structure determined by Dr. J. Drebes at a resolution of 3.06 Å, with molecular replacement on basis of *Ssss* TPK – pdb code: 3L8M) was performed with MOLREP [281]. Search for two monomers resulted in a solution with an R-factor of 54.0 % and a correlation coefficient of 55.4 %. The contrast value for the solution was 17.24. Subsequently, the model was completed and further modified using Coot [284] and refined using refmac5 [285] (Restrained refinement with isotropic B-factors). Two TLS groups were defined; the TLS contribution is finally included in the pdb file. The final model has an R-factor of 16.46 % and an R_{free} -factor of 19.05 %. The model shows excellent geometry and no Ramachandran outliers. Data collection, processing and refinement statistics are summarized in Table 29.

Table 29: Data collection and refinement statistics for *S. aureus* TPK in complex with thiamine.

Data collection statistics^a	
Beamline	P14 EMBL
Wavelength [Å]	0.976300
Space group	P2 ₁
Unit cell parameters: a, b, c [Å]	46.6, 85.3, 52.5
β [°]	110.6
Resolution [Å]	30.0 - 1.40
Temperature [K]	100
R _{merge} ^b	5.1 (51.9)
Measured reflections	499979
Unique reflections	74602
Average I/σ(I)	21.4 (4.3)
Mn(I) half-set correlation CC(1/2)	99.9 (89.5)
Completeness [%]	99.0 (98.1)
Redundancy	6.7 (6.8)
Refinement statistics	
Resolution range [Å]	30.0 - 1.40
R/ R _{free} [%]	16.46/19.05
Protein atoms	2977
Water molecules	263
Ligand atoms (thiamine)	36
Rms deviation	
Bond-length [Å]	0.02
Bond angle [°]	1.900
B factor [Å ²]	
Protein	19.30
Ligand (thiamine)	13.58
Water	25.62
Ramachandran plot analysis:	
Most favored regions [%]	99.7
Allowed regions [%]	1.3
Generously allowed regions [%]	0

^aValues in parentheses are for the highest resolution shell. ^b $R_{merge} = \frac{\sum_{hkl} \sum_i |I_i(hkl) - \langle I(hkl) \rangle|}{\sum_{hkl} \sum_i I_i(hkl)}$, where $I(hkl)$ is the mean intensity of the reflections hkl, \sum_{hkl} is the sum over all reflections and \sum_i is the sum over i measurements of reflection hkl.

2.4 *S. aureus* TPK: Structure analysis

The structure shows a homodimeric assembly arranged out of two inverse oriented monomers in the asymmetric unit. Amino acids 49-71 as well as the last amino acid N213, are disordered in both monomers and no electron density could be observed. The overall diameter is approx. 48 Å.

Each monomer comprises of two domains: first a $\alpha\beta$ -domain, which has a twisted β -sheet created from five parallel β -strands linked through α -helices on both sides. This domain shows a non-classical Rossmann-fold; topology diagram is shown in Figure 23. Rossmann-fold can be regularly found in nucleotide binding proteins [304]. Secondly a β -sandwich domain with a jelly-roll fold composed of three two stranded antiparallel β -sheet could be identified (Figure 23). Together the parallel β -sheet of the first domain and the one antiparallel β -sheet of the second domain assemble in an approx. 90° twisted, eight strand mixed β -sheet.

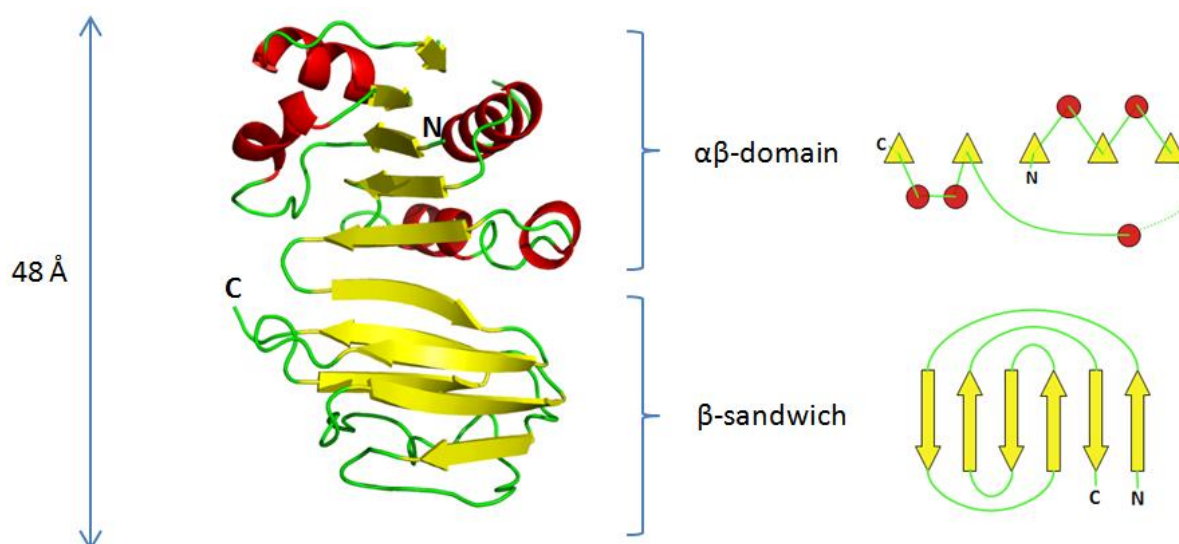


Figure 23: TPK monomer along with domain and topology details.

A TPK monomer with an approx. diameter of 48 Å in secondary structure representing cartoon illustration is shown; yellow is used for β -strands, red for α -helix and green for turns and loops; labels of the N- and C-terminus are shown. The respective domains are annotated and the topology plot of the non classical Rossmann-fold of the $\alpha\beta$ -domain and the jelly roll fold of the β -sandwich domain are given next to it using the same colors. The not resolved region 49-71 is depicted in green dots. Figure was created with The PyMOL Molecular Graphics System, Version 1.7.4 Schrödinger, LLC.

The dimer interface area could be determined to 1578 Å² using PDBePISA [289]. This compromises about 15 % of the total solvent accessible area, which is 10393 Å² and 10293 Å² for the monomers respectively. A CONTACT analysis out of CCP4 software suite [283] shows 15 hydrogen bond and 176 non bonded contacts of 36/37 residues in the interface area.

Immediately after the first round of refinement electron density for thiamine was visible in the $F(o) - F(c)$ and $(2F(o) - F(c))$ maps in the two active sides formed by both monomers in the asymmetric crystal units.

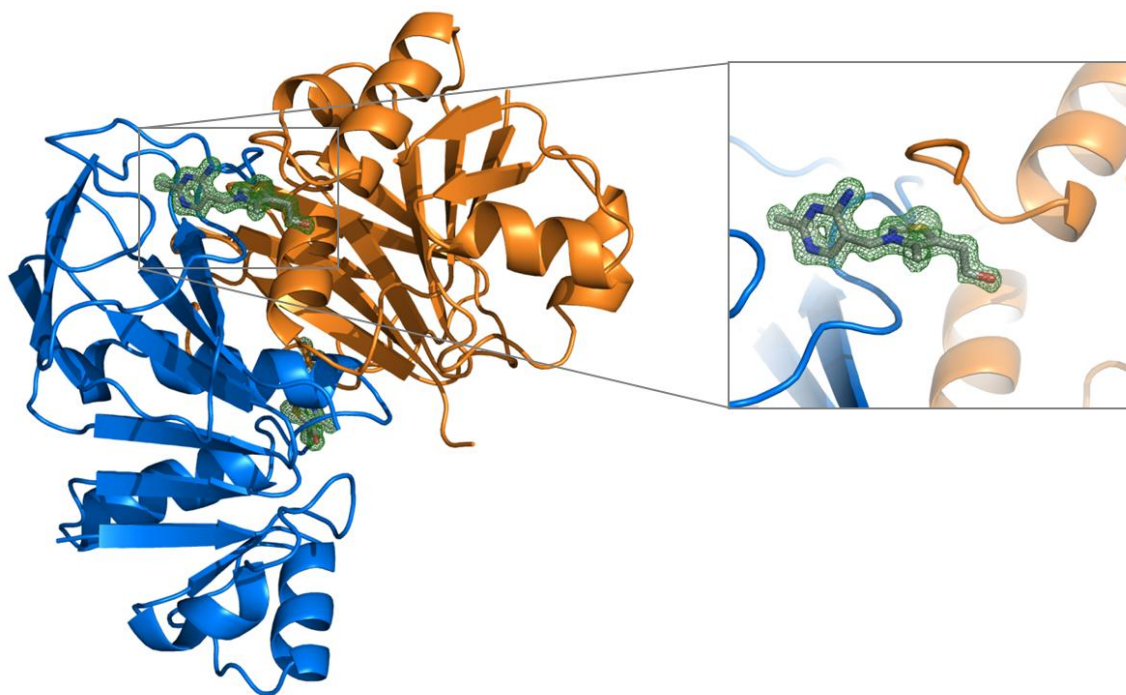


Figure 24: Dimeric *S. aureus* TPK in complex with thiamine depicted with an omit map.

The biological dimer of TPK (AB) is shown in orange and blue in secondary structure representing cartoon illustration. Thiamine is given in grey stick representation; atoms N, O, S are colored in blue, red and yellow respectively. The enlargement shows thiamine with a $F(o)$ - $F(c)$ map contoured at 3σ in a green mesh. Figure was created with The PyMOL Molecular Graphics System, Version 1.7.4 Schrödinger, LLC.

Figure 24 shows the homodimer of TPK occupying the asymmetric unit (ASU) with the ligand thiamine in each active site in stick representation as well as a $F(o)$ - $F(c)$ omit map contoured at 3σ . The binding of thiamine could be observed in a groove formed by the interface of both monomers. The approximate size is $16 \times 6 \text{ \AA}^2$ yet it is relatively solvent accessible.

Thiamine is known to adopt three distinct conformations in nature although the methylene bridge between the thiazole and pyrimidine moiety is not further restrained. They are defined via the torsion angles between $C5'-C7'-N3-C2$ (ϕ_T) and $N3-C7'-C5'-C4'$ (ϕ_P) (Figure 25).

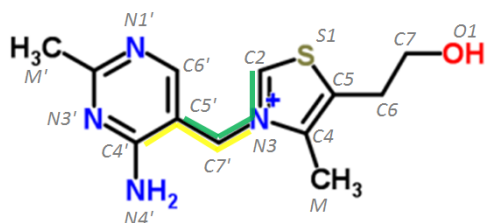


Figure 25: Structural formula of thiamine with torsion angles definitions ϕ_T and ϕ_P .

The structural formula of thiamine with atom identifiers is given. The torsion angles ϕ_T and ϕ_P are defined and depicted in the formula in green and yellow respectively. Figure was created with ChemDraw (PerkinElmer Inc.).

Torsion angle definitions:

$$\phi_T = C5'-C7'-N3-C2$$

$$\phi_P = N3-C7'-C5'-C4'$$

In the low energy F-conformation the torsion angle ϕ_T is defined to be $\sim 0^\circ$ and ϕ_P is defined to approx. $\pm 90^\circ$, while in the high energy V-conformation, found in TDP dependent enzymes, both torsion angles, ϕ_T and ϕ_P , are defined to $\sim \pm 90^\circ$ [305]. In the high energy conformation the C2 is in proximity to the amino group of the pyrimidine moiety and thus facilitates the carbanion formation. In the structure of TPK with its natural ligand thiamine ϕ_T adopts 1.85° and -8.95° and ϕ_P 90.34° and 81.06° in the first and second active centre respectively (numbering corresponding to label of thiamine in chain C in the pdb file). Both torsion angles are suiting well to the low energy F-conformation.

The groove with thiamine is partially closed due to the interaction of E72B and Y171A. The binding is stabilized by the positive charged N3 of the thiazolium ring forming a hydrogen bond to the main chain carbonyl group of I186A (2.8 Å) or with the main chain carbonyl group of K73B (2.9 Å). The hydroxyl group could form a water mediated contact with the nitrogen of D77B and a hydrogen bond to NE2 of H105B supported by D104B. Hydrophobic interactions between thiamine and T76B, S187A, D75B, A74B, T183A and T185A additionally stabilize the binding.

The aminopyrimidine ring could stabilize the thiamine binding through a slightly shifted π -stacking to Y171A at a distance of 3.3 Å. Additionally, the N1' and the carbonyl group of L184A as well as the N4' and E72B could form hydrogen bonds (3.2 Å, 2.9 Å respectively). Further, hydrophobic contacts between the methyl group M' and L173A, Y171A, and N188A mediate stabilization. The following Figure 26 is representing the binding of thiamine in the active site. In Figure 26 A, the binding is depicted with the labeled corresponding amino acids and a stereo view of the binding is given in Figure 26 B.

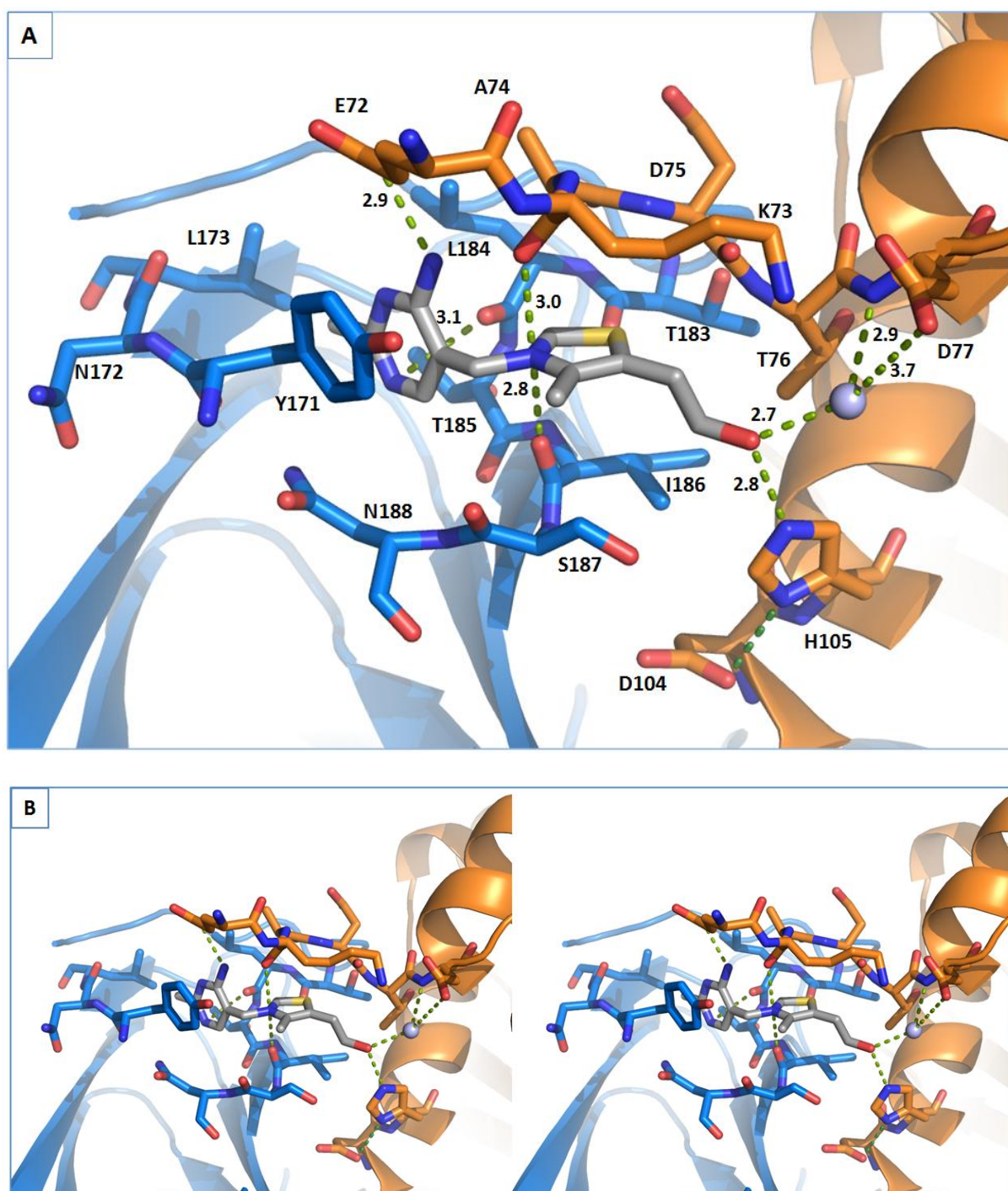


Figure 26: Thiamine binding site in *S. aureus* TPK.

A: The active site of dimeric TPK is shown in orange and blue; the stick illustration shows the active site residues embedded in a partial cartoon representation. Thiamine is given in grey stick representation; in the stick representation all atoms N, O, S are colored in blue, red and yellow, respectively. The representation shows hydrogen bonds stabilizing the binding in green with corresponding distances in Å. A water molecule is shown as a light blue sphere; amino acids are labeled. B: Similar to A, but without labels and in wall eye stereo view. Figure was created with The PyMOL Molecular Graphics System, Version 1.7.4 Schrödinger, LLC.

2.5 Evaluation of potential thiamine analogs - analyzing the activation via *S. aureus*

TPK

Based on the results obtained for the ligand bound TPK, a potential atomic positioning of thiamine analogs formed out of cpd1 or cpd2 and a HMP-moiety were produced. Figure 27 is showing the positioning of these in the active site of TPK (Figure 27 A-D) in comparison to the natural ligand thiamine (Figure 27 E, F). A surface of the active site to show the enclosed area as well as a stick representation is given.

The prepositioning of possible thiamine analogs is feasible. The most expected sterical hindering would occur due to the additional methyl group at the nitrogen atom of the pyrazole ring (consensus nomenclature number 06) from cpd1, which is pointing towards L184. A thiamine analog out of cpd2 will have a slight advanced freedom at the substituted sulfur atom as the van der Waals radius is smaller and would therefore perhaps be less stabilized in the binding site.

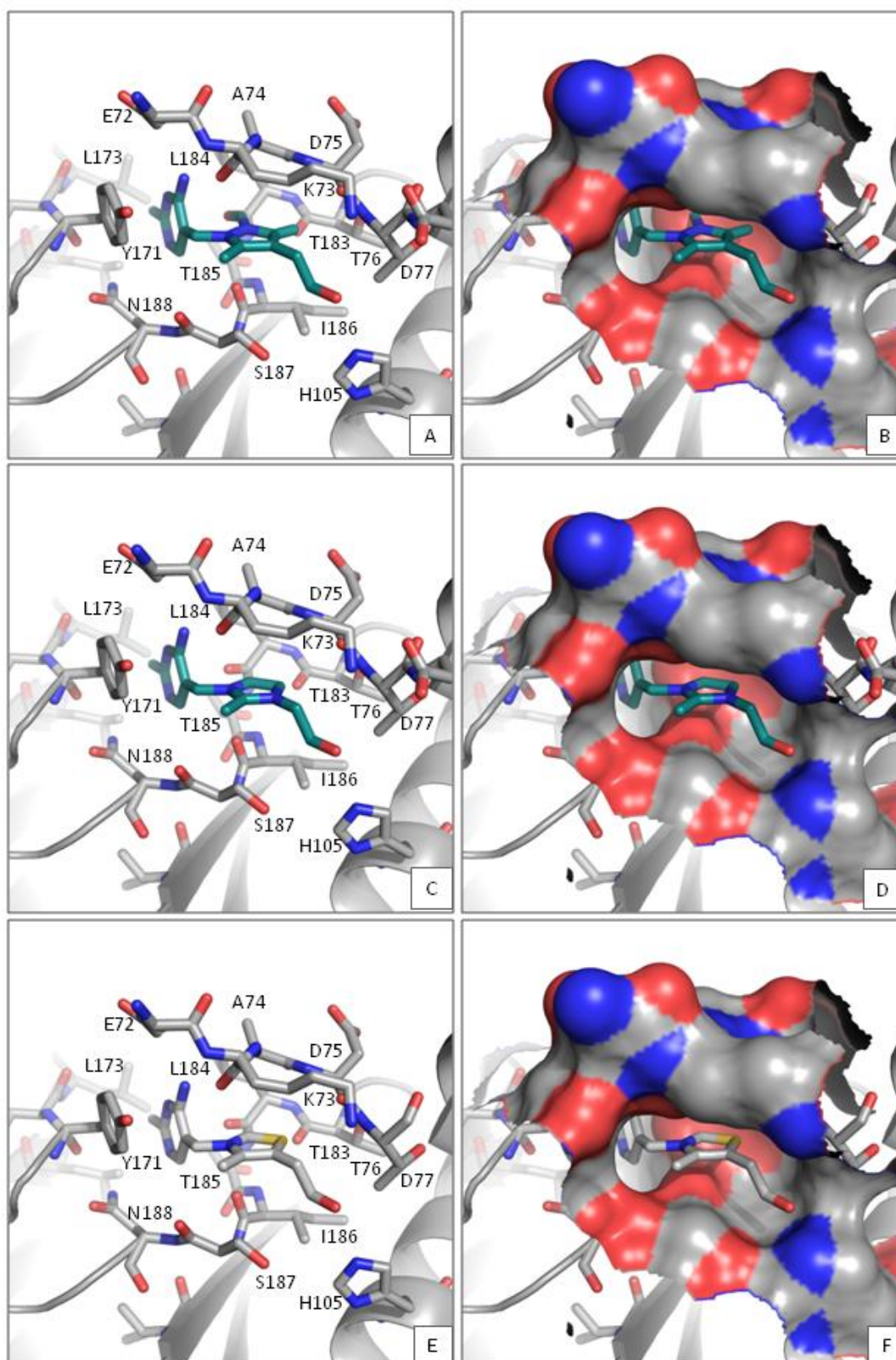


Figure 27: Theoretical thiamine analogs prepositioned in the active site of TPK.

The figure shows the active site of TPK incorporating a hypothetical thiamine-cpd1 in A, a theoretical thiamine-cpd2 in C and in comparison the natural ligand in E. TPK is overall colored in grey, the surface (B, D and F) in the active site is calculated in red for oxygen and blue for nitrogen. In all stick representations carbons of thiamine are colored in grey, carbons of the analogs are colored in teal, atoms N, O and S atoms are colored in blue, red and yellow, respectively. Figure was created with The PyMOL Molecular Graphics System, Version 1.7.4 Schrödinger, LLC.

2.6 Comparison and differentiation of *S. aureus* TPK to eukaryotic TPK

To estimate the evolutionary differentiation of the specificity of *S. aureus* TPK towards thiamine a sequence comparison and binding analysis to murine - (pdb code: 1IG3, RMSD: 1.9 Å), human - (pdb code: 3S4Y, RMSD: 2.1 Å) and yeast - *Saccharomyces cerevisiae* (pdb code: 1IG0, RMSD: 2.0 Å) TPK homologs was performed [306–309]. Figure 28 shows the overall sequence alignment, murine TPK has a sequence identity of 26 % and human and yeast share 25 % identity with *S. aureus* TPK (BLAST). The overall fold is highly conserved; the not resolved part of *S. aureus* TPK could possibly form an additional β -sheet and a short helix on top of the β_3 -strand of the $\alpha\beta$ -domain.

In bacterial species the binding residues of thiamine are extremely conserved, only A74 is exchanged to a D in *B. subtilis* and S555 and D75 and N172 are exchanged to a Q and a P respectively in *B. subtilis* (Figure 22). In contrast, the thiamine stabilizing amino acids in eukaryotic species differ in several positions as can be gathered from Figure 28.

The π -stacking interaction between tyrosine 171 of *S. aureus* TPK is exchanged in all eukaryotic members to a tryptophan. The partial closing residue glutamic acid 72 is exchanged in mouse and human TPK to an aspartic acid and to a threonine in yeast. Also the lysine 73 is substituted by a glutamine in all eukaryotic members to which *S. aureus* TPK was compared and aspartic acid 75 is exchanged by an histidine in mouse and human and a serine in yeast. Furthermore, the histidine 105 is substituted to a glutamine in all other eukaryotic members compared. In addition, isoleucine 186 is exchanged to threonine in mouse and human TPK and to a serine in yeast. A partial conservation could be found in leucine 173 in humans and mouse but not in yeast, where it is exchanged to a valine.

Of the hydrophobic interactions mediated through A74, D75, T76, T183, L184, T185, S187 and N188 only T76, S187 and N188 are conserved. Alanine 74 is exchanged by an aspartic acid in human and mouse and a tyrosine in yeast. Threonine 183 is exchanged by a leucine in mouse and human and an arginine in yeast and threonine 185 is substituted by a serine in all species. Leucine 184 is substituted in all eukaryotic species to a valine. The probable catalytic residue aspartic acid 77 in *S. aureus* TPK is conserved among all considered species. Also the glycine rich motif GATGG, found in *S. aureus* TPK in position 97-101 can be found in variants in the eukaryotic species as GGLGG in murine, GGLAG in human and GGIGG in yeast TPK.

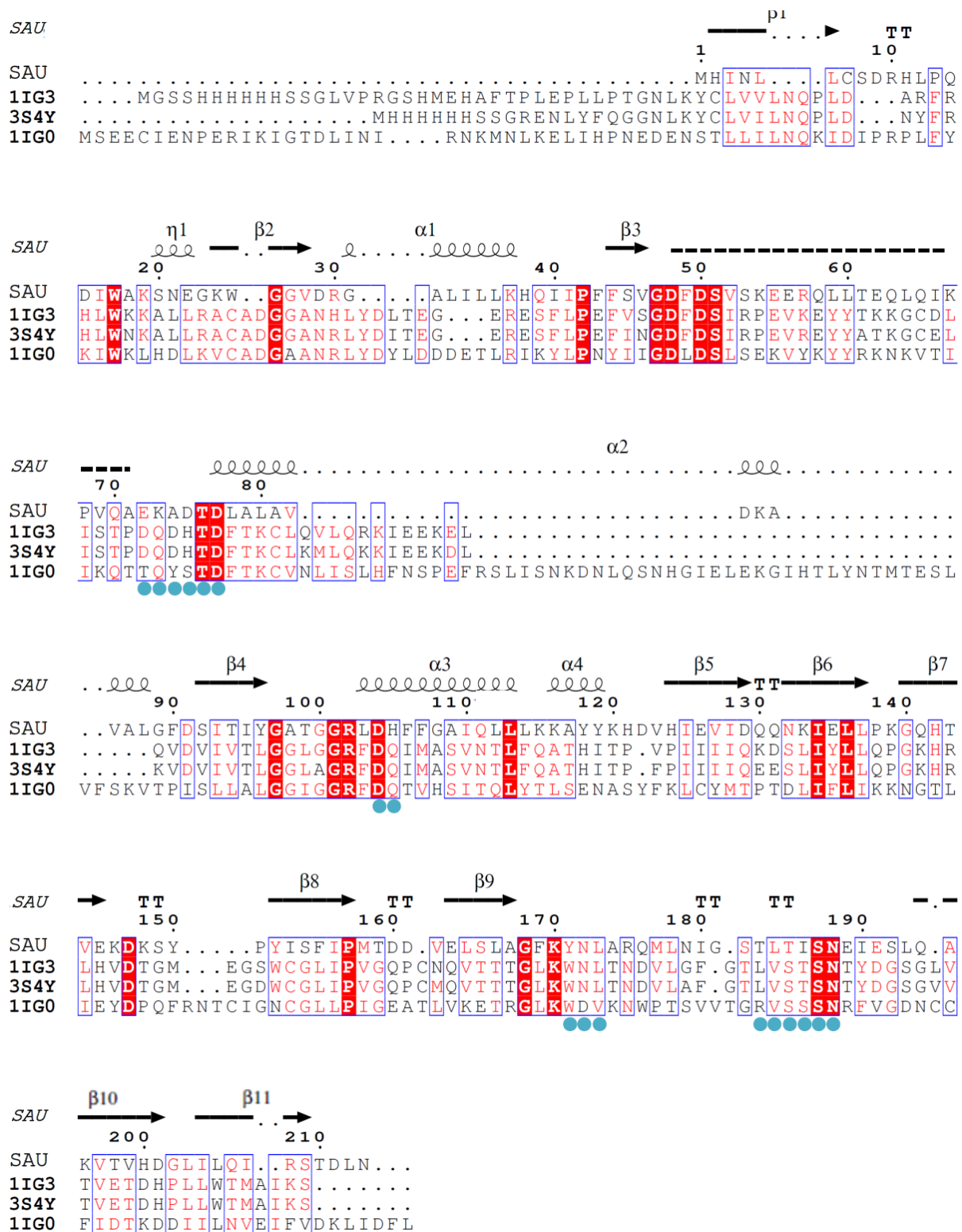


Figure 28: Sequence alignment of *S. aureus* (SAU), murine (1IG3), human (3S4Y) and yeast (1IG0) TPK.

Multiple sequence alignment was performed using ClustalW2, representation was generated with ESPrit. Identical residues are highlighted in red boxes, similar residues in white boxes. The secondary structure of *S. aureus* PdxK is annotated on the top, spirals represent α -helices, arrows represent β -strands, T stands for turns and μ do represent 3_{10} helices. A dashed line indicates a disordered region. The teal circles below the sequence indicate the residues stabilizing the substrate thiamine in *S. aureus* TPK.

2.7 Growth and evaluation of *S. aureus* TPK micro crystals

Due to the tendency of TPK to produce needle shaped crystals under various conditions, an optimization of these needles for further serial X-ray crystallographic approaches was conducted.

In the crystallization condition 2.0 - 2.2 M ammonium sulfate and 0.1 M Bis Tris, pH 5.5, added to 10.0 mg mL⁻¹ *S. aureus* TPK, supplemented with 3 mM thiamine, in vapor diffusion sitting drop as well as batch setup to a total volume of 20 μ L very reproducible micro crystals with dimensions of approx. $<50 \times 5 \mu\text{m}^2$, appearing in 1-5 h at RT, could be produced (Figure 29 A, B). Powder diffracting verified that the sample contained protein crystals (Figure 29 C).

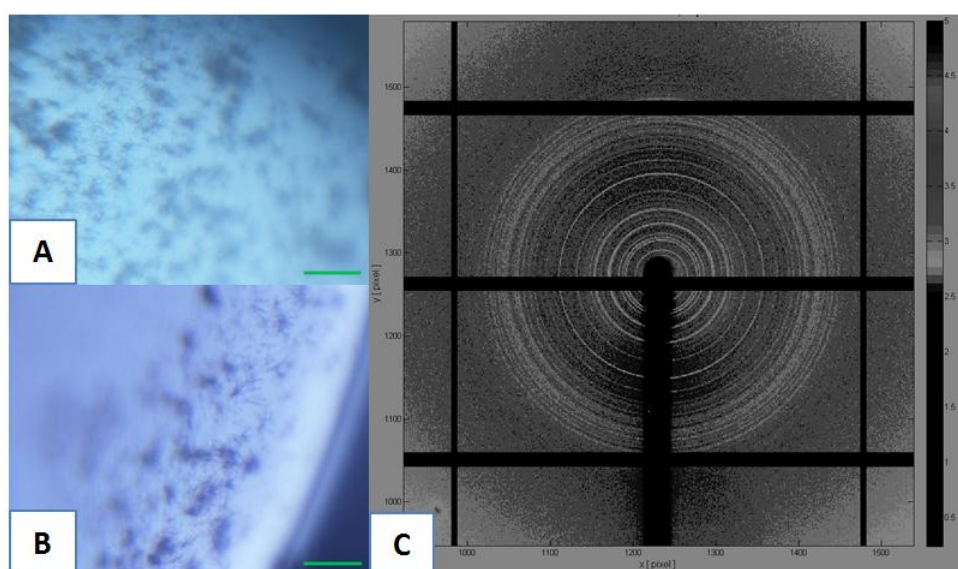


Figure 29: Micro crystals grown from *S. aureus* TPK and corresponding powder diffraction pattern.

A and B: Micro crystals grown at RT in sitting drop format, adding 3 μ L 2.0 M (A) and 2.2 M (B) ammonium sulfate, 0.1 M Bis Tris, pH 5.5 to 3 μ L protein solution (10.0 mg mL⁻¹) supplemented with 3 mM thiamine; scale bar equals to 100 μ m; C: powder diffraction pattern, recorded at P11 (PETRAIII).

3 *Staphylococcus aureus* PdxK

3.1 *S. aureus* PdxK: Recombinant expression, purification and characterization

S. aureus PdxK fused to a TEV protease recognition site and a His₆-tag as well as a Strep-tagged version were recombinantly expressed in *E. coli* BLR pLysS cells. Gene expression was conducted for 4 h at 37 °C starting at an OD₆₀₀ of 0.5-0.6.

The standard buffer system for *S. aureus* PdxK purification was T/N300 buffer (see Table 4). The Strep-tagged protein was purified from the cleared cell lysate, obtained from the standard procedure described in chapter III 4.15.1, via affinity chromatography (chapter III 4.15.2). The His₆-tagged protein was purified from the cleared cell lysate, obtained from the standard procedure described III 4.15.1 via affinity chromatography using a washing step of 40 mM imidazole in buffer T/N300 and was finally eluted in buffer T/N300 supplemented with 300 mM imidazole (Figure 30 A, B). For later optimization of the crystallization condition, which finally yielded in the crystals used for diffraction data collection, the His₆-tagged protein construct was cut with TEV protease to eliminate the tag. Subsequent to the initial affinity purification, the protein was applied to a Sephadex G-25 Fine, XK 50/30 column operated with the ÄKTA prime system and transferred to an imidazole free T/N300 buffer. The TEV digest was performed under standard conditions (chapter III 4.17) and a subsequent second affinity chromatography was performed to eliminate uncut protein and the TEV protease (Figure 30 C).

Subsequently, the Strep-tagged and the digested *S. aureus* PdxK were regularly applied to a superdex 200 column operated with the ÄKTA purifier at 4 °C. Proteins were thereby transferred to a T/N300 buffer. In comparison with a calibration curve the Strep-tagged *S. aureus* PdxK eluted at a calculated molecular size of approx. 61 kDa and digested PdxK eluted at a calculated molecular size of approx. 55 kDa.

The dispersity of the protein solution after the size exclusion chromatography was monitored via DLS. Figure 30 D shows a representative DLS pattern of the protein solution after size exclusion chromatography with a concentration of 3.2 mg mL⁻¹ in T/N300 buffer.

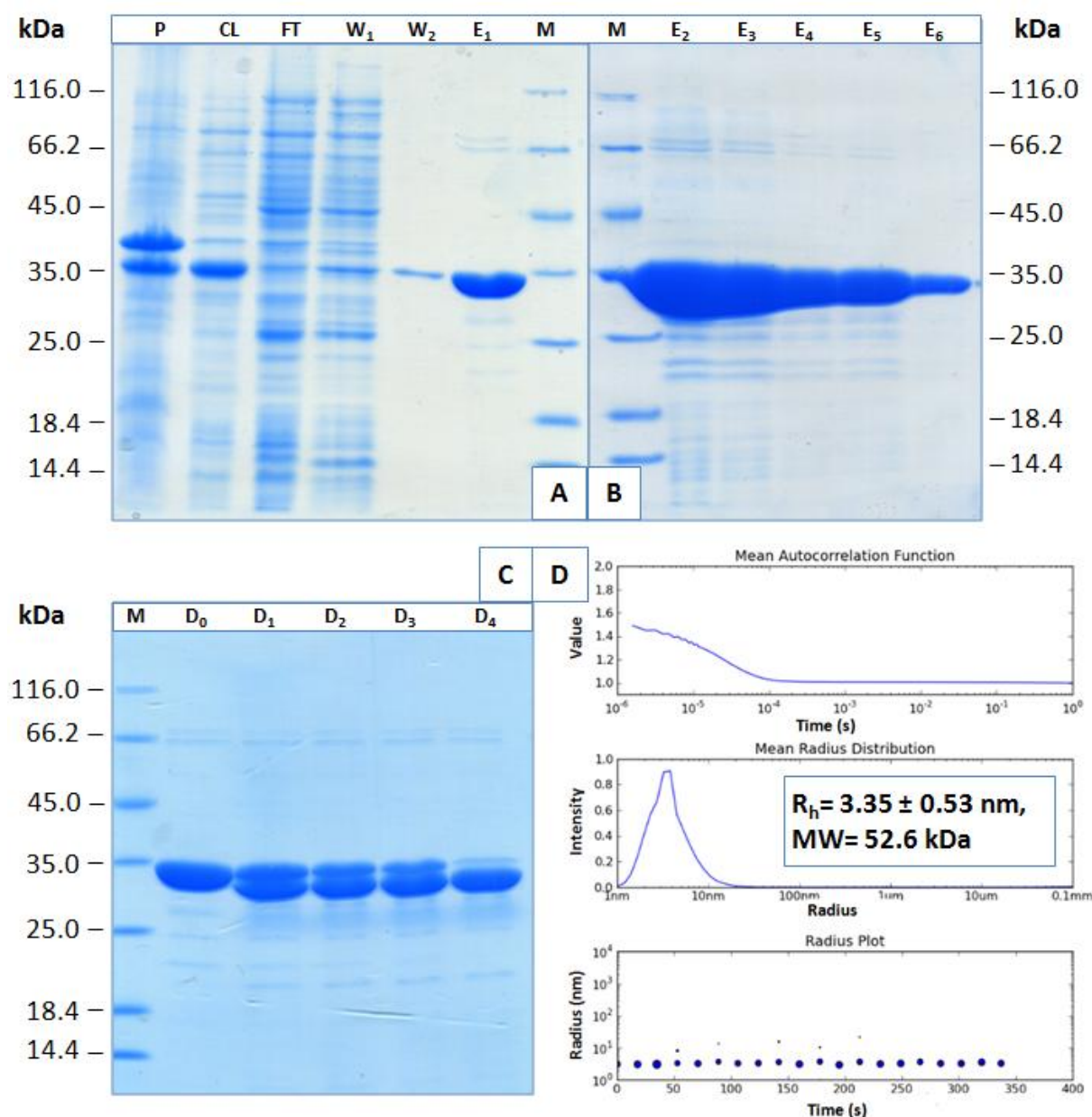


Figure 30: Summary of purification, TEV protease digest and DLS characterization of *S. aureus* PdxK.

A, B: Purification of recombinant His₆-tagged *S. aureus* PdxK; M- protein molecular weight marker [8 μ L], P- pellet [1 μ L], CL- supernatant of cell lysate [2 μ L], FT- flow through [2 μ L], W₁- wash step1 [2 μ L], W₂- wash step2 [5 μ L], E₁- elution step 1 [2 μ L], E_{2,3,4,5}- elution step 2/3/4/5 [3 μ L], E₆- elution step 6 [1 μ L], C: evaluation of TEV digest; M- protein molecular weight marker [8 μ L], D₀- before digest [3 μ L], D₁₋₄ different time points of TEV digest (2 h, 4 h, 6 h, 24 h) D: DLS characterization of His₆-tagged *S. aureus* PdxK top down: Mean autocorrelation function of the DLS signal, mean radius distribution: Plotting radius against intensity, radius plot: Plotting time against radius; the hydrodynamic radius (R_h) is given as well as the calculated molecular weight (MW).

3.2 *S. aureus* PdxK SAXS structure

To validate the oligomeric state of *S. aureus* PdxK in solution SAXS measurements at beamline X33 (Hasylab, EMBL) were performed. The His₆-tag of *S. aureus* PdxK was cut and the protein was prepared as described in chapter III 6. For all reference measurements the buffer (T/N300) from size exclusion chromatography was used. On the basis of the forward scattering a molecular weight of 61.9 kDa [310] could be estimated, which is consistent with the molecular weight of 61.4 kDa for dimeric *S. aureus* PdxK.

In consideration of the D_{\max} of 8.6 nm and the R_g of 3.1 ± 0.24 nm an elongated particle was expected. *Ab initio* modeling was performed with DAMMIF [294], taking a P2 symmetry as a basis. The final model merged from ten single models with DAMAVER [295] fits the experimental data with a χ -value of 1.152. The obtained *ab initio* model is in good agreement with the crystal structure and confirms the dimeric assembly in solution (Figure 31).

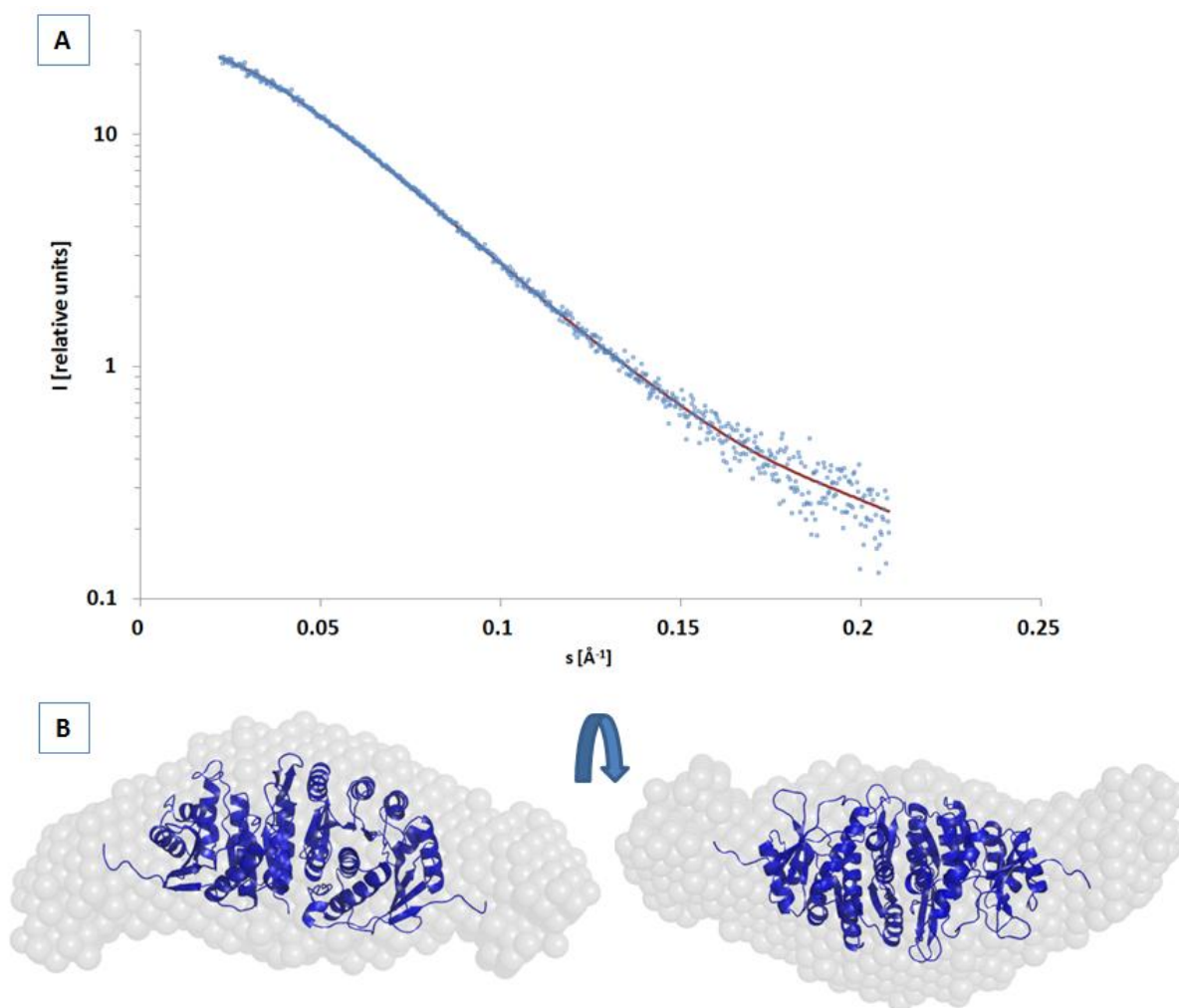


Figure 31: Processed small angle X-ray scattering data of *S. aureus* PdxK.

A: The processed experimental solution scattering pattern (light blue dots) and the fit of the *ab initio* model (red line) is plotted. B: *Ab initio* model (grey dots) in superimposition with dimeric *S. aureus* PdxK (structure I) in blue cartoon representation. Figure was created with The PyMOL Molecular Graphics System, Version 1.7.4 Schrödinger, LLC.

3.3 *S. aureus* PdxK: Crystallization

Initial screening was performed applying the commercially available crystallization screens JCSG-plus, PACT premier, Cryos Suite and Stura FootPrint & MacroSol in sitting drop vapor diffusion in MRC 96-well sitting drop crystallization plate (Molecular Dimensions, UK) at a protein concentration of 8 mg mL^{-1} of His₆-tagged PdxK. Under these conditions no crystals could be obtained. Hereupon the TEV digested variant was produced and successfully crystallized as shown in Figure 32 A and B. The crystals were grown at a protein concentration of 5.2 mg mL^{-1} with the addition of 0.75 mM pyridoxine (molar ratio of protein to ligand = 1 : 4.7) with a precipitant solution containing 0.01 M sodium borate, 1.5 M sodium citrate, pH 8.5 in protein over precipitant ratio of 1 : 1.4 in a MRC 96-well sitting drop crystallization plate (Molecular Dimensions, UK) at 4 °C. After approx. four weeks crystals appeared and reached an approx. size of $0.25 \times 0.25 \times 0.2 \text{ mm}^3$.

In addition, crystals were grown at a protein concentration of 9.0 mg mL^{-1} without vitamin B₆ supplement, by adding 2.4 M sodium malonate pH 7.0 as precipitant (ratio of protein to precipitant 1 : 1) after storing this plate for approx. eight weeks at 4 °C and transferring it to RT for approx. two weeks. These crystals are shown in Figure 32 C and D and could be grown to an approx. size of $0.2 \times 0.15 \times 0.1 \text{ mm}^3$.

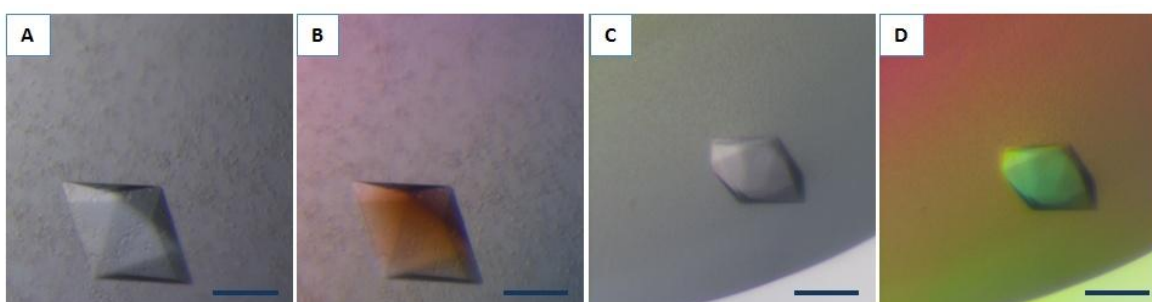


Figure 32: Crystals of *S. aureus* PdxK.

A, B show a crystal grown with a precipitant solution containing 0.01 M sodium borate and 1.5 M sodium citrate, pH 8.5 (5.2 mg mL^{-1} *S. aureus* PdxK supplemented with 0.75 mM pyridoxine). C, D show a crystal grown with 2.4 M sodium malonate pH 7 as precipitant (9.0 mg mL^{-1} *S. aureus* PdxK). Images of *S. aureus* PdxK crystals without (A and C) and with crossed polarizers (B and D), scale bar equals to 100 μm .

Henceforth these two conditions are referred to as condition I and structure I (precipitant: 0.01 M sodium borate, 1.5 M sodium citrate, pH 8.5) and condition II and structure II (precipitant: 2.4 M sodium malonate pH 7.0) in diffraction data collection, analysis and model building.

Trials to reproduce the successful crystallization of the His₆-tagged *S. aureus* PdxK construct after TEV digest in both conditions with the Strep-tagged *S. aureus* PdxK were not successful.

3.1 *S. aureus* PdxK: Diffraction data collection, processing and model building I

Crystals out of condition I used for data collection had a bipyramidal shape and could be cryoprotected by the supplement of 15 % (v/v) glycerol to the precipitant solution containing 0.75 mM pyridoxine as well. The crystals were flash cooled in gaseous nitrogen at 100 K and the diffraction data were collected at P14 EMBL beamline at DESY campus.

Diffraction data were collected to 2.0 Å resolution using 0.1 degree oscillation and subsequently indexed, integrated and scaled with XDS. Data were cut to 2.0 Å monitoring R_{merge} , I/σ and $CC1/2$. The crystal was found to belong into the trigonal space group $P3_121$ with unit cell dimensions of $a = b = 113.4$ Å and $c = 81.4$ Å. The Matthews coefficient was calculated 4.9 Å³ Dalton⁻¹ with one molecule in the asymmetric unit, which corresponds to a solvent content of 75 %.

Molecular replacement applying MOLREP [281] was conducted by using the model of monomeric *B. subtilis* pyridoxal kinase (pdb code: 2I5B) [311]. Search for one monomer resulted in a solution with an R-factor of 58.7 % and a correlation coefficient of 49.6 %. The contrast value for the solution was 1.61 [299]. Subsequently, the model was completed and further modified using Coot [284] and refined using refmac5 [285] restrained refinement with isotropic B factors. Additionally, a TLS group was defined and the TLS contribution is finally included in the pdb file. The final model has an R-factor of 16.80 % and an R_{free} -factor of 18.84 %. The N-terminal methionine was not visible in the electron density and was thus excluded from the final model. The model demonstrates excellent geometry and no Ramachandran outliers. Data collection, processing and refinement statistics are summarized in Table 30.

Table 30: Data collection statistics for *S. aureus* PdxK condition I, structure I.

Data collection statistics^a	
Beamline	P14
Wavelength [Å]	0.976262
Space group	P3 ₁ 21
Unit cell parameters: a = b, c [Å]	113.4, 81.4
Resolution [Å]	30.0 - 2.0
Temperature [K]	100
R _{merge} ^b	6.2 (88.1)
Measured reflections	811623
Unique reflections	41090
Average I/σ(I)	30.0 (3.8)
Mn(I) half-set correlation CC(1/2)	100.0 (92.8)
Completeness [%]	100.0 (100.0)
Redundancy	19.8 (20.2)
Refinement statistics	
Resolution range [Å]	30.0 - 2.0
R/ R _{free} [%]	16.99/18.90
Protein atoms	2143
Water molecules	118
Ligand atoms	-
Rms deviation	
Bond-length [Å]	0.020
Bond angle [°]	1.883
B factor [Å ²]	
Protein	44.7
Water	46.1
Ligand	-
Ramachandran plot analysis:	
Most favored regions [%]	97.8
Allowed regions [%]	2.2
Generously allowed regions [%]	0

^aValues in parentheses are for the highest resolution shell. ^b $R_{merge} = \frac{\sum_{hkl} \sum_i |I_i(hkl) - \langle I(hkl) \rangle|}{\sum_{hkl} \sum_i I_i(hkl)}$, where $I(hkl)$ is the mean intensity of the reflections hkl, \sum_{hkl} is the sum over all reflections and \sum_i is the sum over i measurements of reflection hkl.

3.2 *S. aureus* PdxK: Diffraction data collection, processing and model building II

Due to the blocking of the active site (see later analysis of the structure models in chapter IV 3.3), a second data set of the native *S. aureus* PdxK was collected at 100 K at P14 EMBL beamline at DESY campus with a crystal from condition II. The crystal did not have the same bipyramidal shape when grown with 2.4 M sodium malonate (pH 7.0) and did not need any extra cryo protection. Diffraction data were collected to 1.9 Å resolution using the oscillation method (0.1 degree) and subsequent indexed, integrated and scaled with XDS. Data were cut to 1.9 Å monitoring R_{merge} , I/σ and CC1/2.

The crystal was found to belong to the trigonal space group $P3_121$ with unit cell dimensions of $a = b = 113.0$ Å and $c = 81.7$ Å. The Matthews coefficient was calculated to 4.8 Å³ Dalton⁻¹ which corresponded to a solvent content of 74.1 % with one molecule in the asymmetric unit.

Molecular replacement applying MOLREP [281] was conducted by using the monomeric *S. aureus* PdxK from the final model obtained from condition I. Search for one monomer resulted in a solution with an R-factor of 52.3 % and a correlation coefficient of 78.2 %. The contrast value for the solution was 5.51 [299]. Subsequently, the model was completed and further modified using Coot [284] and refined using re mac5 [285] (Restrained refinement with isotropic B factors).

The final model has an R-factor of 17.94 % and an R_{free} -factor of 20.96 %. Like structure I the N-terminal methionine was not visible in the electron density and was thus excluded from the final model. A patch of positive electron density was found close to W49 and F264 that could be interpreted as a molecule of malonic acid and was included in the model. The model demonstrates excellent geometry and no Ramachandran outliers. Data collection, processing and refinement statistics are summarized in Table 31.

Table 31: Data collection statistics for *S. aureus* PdxK condition II, structure II.

Data collection statistics^a	
Beamline	P14
Wavelength [Å]	0.976300
Space group	P3 ₁ 21
Unit cell parameters: a = b, c [Å]	113.0, 81.7
Resolution [Å]	30 - 1.9
Temperature [K]	100
R _{merge} ^b	5.6 (90.0)
Measured reflections	479306
Unique reflections	47717
Average I/σ(I)	23.4 (2.6)
Mn(I) half-set correlation CC(1/2)	100 (83.3)
Completeness [%]	99.9 (100.0)
Redundancy	10.0 (10.2)
Refinement statistics	
Resolution range [Å]	30 - 1.9
R/ R _{free} [%]	17.64/20.65
Protein atoms	2143
Water molecules	140
Ligand atoms (MAL-malonic acid)	7
Rms deviation	
Bond-length [Å]	0.020
Bond angle [°]	1.856
B factor [Å ²]	
Protein	37.4
Water	43.5
Ligand (MAL-malonic acid)	39.7
Ramachandran plot analysis:	
Most favored regions [%]	98.2
Allowed regions [%]	1.8
Generously allowed regions [%]	0

^a Values in parentheses are for the highest resolution shell. ^b $R_{merge} = \frac{\sum_{hkl} \sum_i |I_i(hkl) - \langle I(hkl) \rangle|}{\sum_{hkl} \sum_i I_i(hkl)}$, where $I(hkl)$ is the mean intensity of the reflections hkl, \sum_{hkl} is the sum over all reflections and \sum_i is the sum over i measurements of reflection hkl.

3.3 *S. aureus* PdxK: Structure analysis and comparison of the two models

Both crystals belong to the same space group and show one monomer in the asymmetric unit. The deviation of both models is small, they can be superimposed with an RMSD of < 0.2 Å.

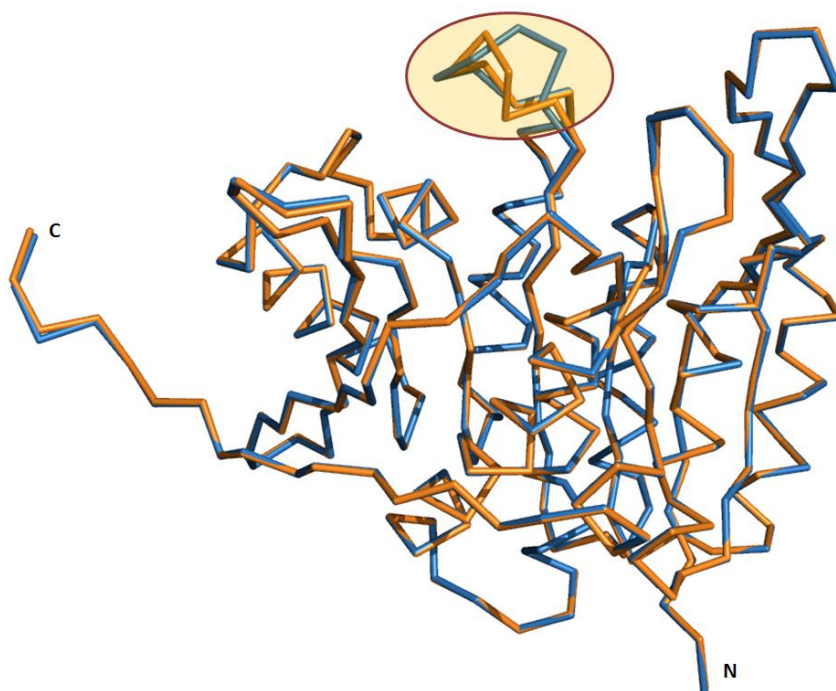


Figure 33: Ribbon representation of both *S. aureus* PdxK structures.

The C α ribbon of *S. aureus* PdxK structure I is colored in blue and the ribbon of *S. aureus* PdxK structure II in orange; N- and C-terminus are labeled and the loop between V109 and E115 is highlighted. Figure was created with The PyMOL Molecular Graphics System, Version 1.7.4 Schrödinger, LLC.

The highest displacement can be found in the loop region V109-E115, highlighted in the ribbon representation in Figure 33 as an orange circle.

Via crystallographic symmetry the biologically active dimer, expected from homology modeling and on the basis of the DLS and size exclusion chromatography results, could be constructed. The tertiary structure of the monomer reveals a highly conserved ribokinase fold [312, 313] and is thus belonging to the ribokinase like kinase of the Rossmann-like fold group (Figure 34). A central nine stranded β -sheet in the arrangement of 2-1-4-5-6-7-8-9-10, where the last three strands are antiparallel, is flanked by five highly conserved α -helices and two 3_{10} -helices on the one and four α -helices on the other side, resulting in an $\alpha\beta$ -sandwich. Additionally, the β_2 -strand forms an antiparallel sheet with strand β_3 at the dimer interface.

The total surface area of one monomer accounts for approx. 13180 Å² whereof 1820 Å² (13.8 %) are buried as a result of dimer formation; analysis was done using PDBePISA [289]. Up to 12 hydrogen bonds in accompany with 2 salt bridges stabilize the dimer formation. Additionally, 179 and

165 hydrophobic interactions in structure I and II respectively do stabilize the interface (PDBsum and CONTACT analysis out of CCP4 software suite [283]).

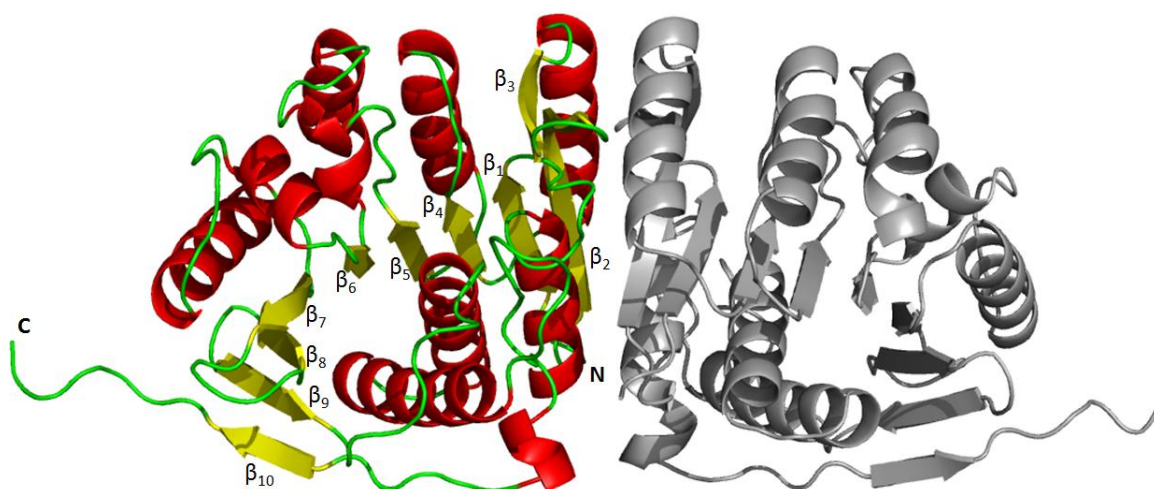


Figure 34: Dimeric assembly of *S. aureus* PdxK.

A *S. aureus* PdxK dimer in secondary structure representing cartoon illustration is shown; yellow is used for β -strands, red for α -helix and green for turns and loops. The dimeric partner created applying crystallographic symmetry is represented in grey cartoon representation. The central β -sheet is sequentially numbered; labels of the N- and C-terminus are shown. Figure was created with The PyMOL Molecular Graphics System, Version 1.7.4 Schrödinger, LLC.

Sequence identity was analyzed using Basic Local Alignment Search Tool applying the BLAST algorithm. Maximum sequence identity (51 %) was identified to pyridoxal kinase from *Bacillus subtilis* (pdb code: 2I5B). Second most identical protein is the phosphomethylpyrimidine kinase from *Clostridium difficile* with a sequence identity of 40 %, saved in pdb database as 4JJP. The human pyridoxal kinase shares 34 % sequence identity with *S. aureus* PdxK and is deposited under pdb code 3KEU. The following Figure 35 shows a sequence alignment of *S. aureus*, *B. subtilis*, *C. difficile* and human PdxK.

The RMSD obtained by superimposing structure II with the slightly higher resolution of 1.9 Å, could be determined as 1.2 Å for *B. subtilis*, 1.4 Å for *C. difficile*, and 2.4 Å for human PdxK; determined by Protein structure comparison service PDBeFold [290].

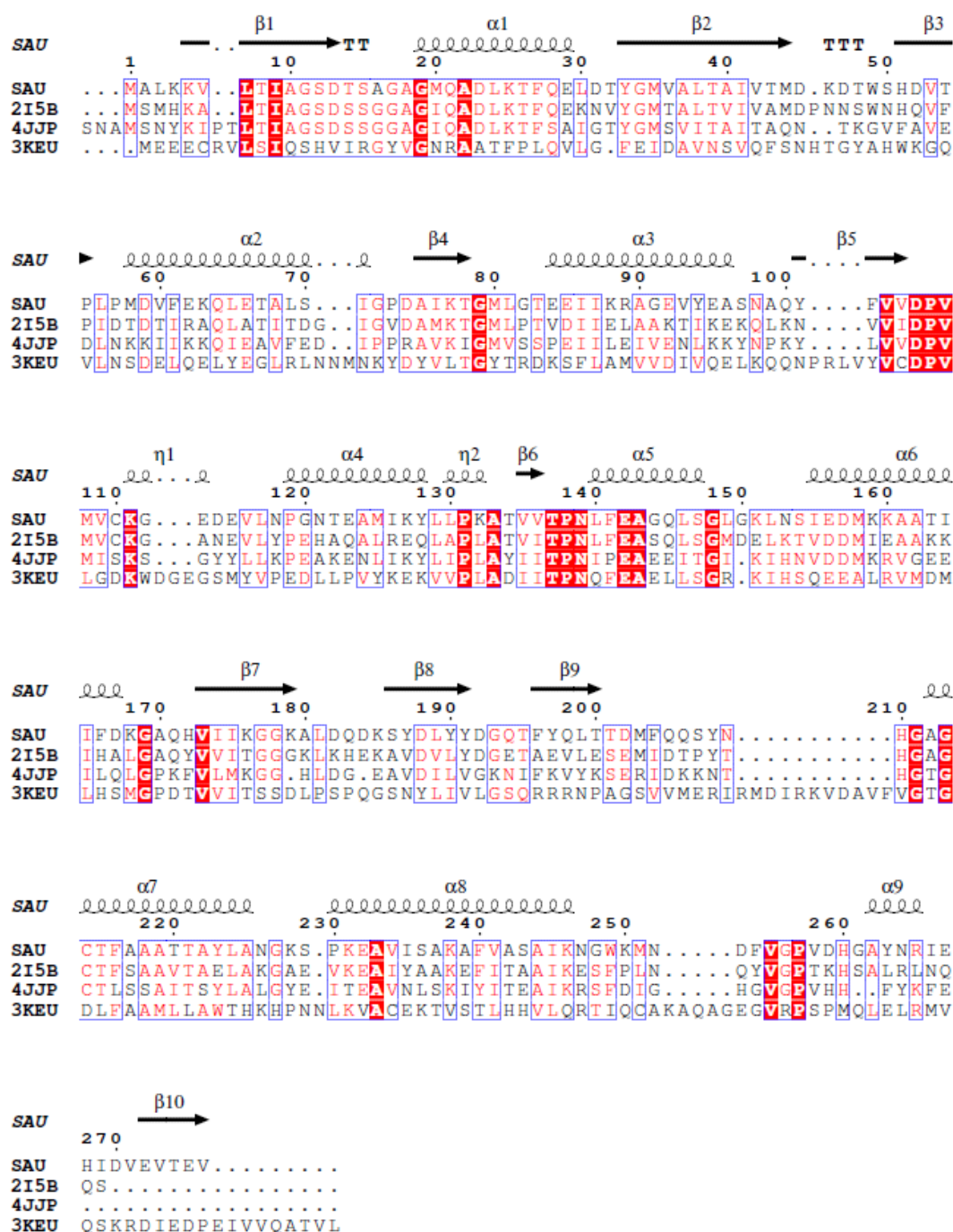


Figure 35: Sequence alignment of *S. aureus* (SAU), *B. subtilis* (2I5B), *C. difficile* (4JJP) and human PdxK (3KEU).

Multiple sequence alignment was performed using ClustalW2, representation was generated with ESPrit. Identical residues are highlighted in red boxes, similar residues in white boxes. The secondary structure of *S. aureus* PdxK is annotated on the top, spirals represent α -helices, arrows represent β -strands, T stands for turns and μ do represent 3_{10} helices.

From the structure of *B. subtilis* pyridoxal kinase ligated with ADP (pdb code: 2I5B), the structure of pyridoxal kinase from *E. coli* in complex with pyridoxal (pdb code: 2DDW, sequence identity 24 %) and the knowledge of conserved nucleotide binding motives it was possible to elucidate the probable binding site of the B_6 vitamer substrate and ATP [216, 301, 307, 311, 313, 314].

On this basis ATP was expected to bind in a groove between β_8 -strand and α -helix 7 and 8, placing the γ -phosphate in close proximity to the anion hole at the beginning of α -helix 7 and pyridoxal could be estimated to bind, like in the pyridoxal kinase of *E. coli*, in a cleft formed by the loop after β_4 -strand, the β_1 -strand and α -helix 1.

In both models the artificial C-terminus of the TEV protease recognition site, hence the remaining five amino acids ENLYFQ, are sticking into this active site of a neighboring molecule. An overview of this is given in Figure 36.

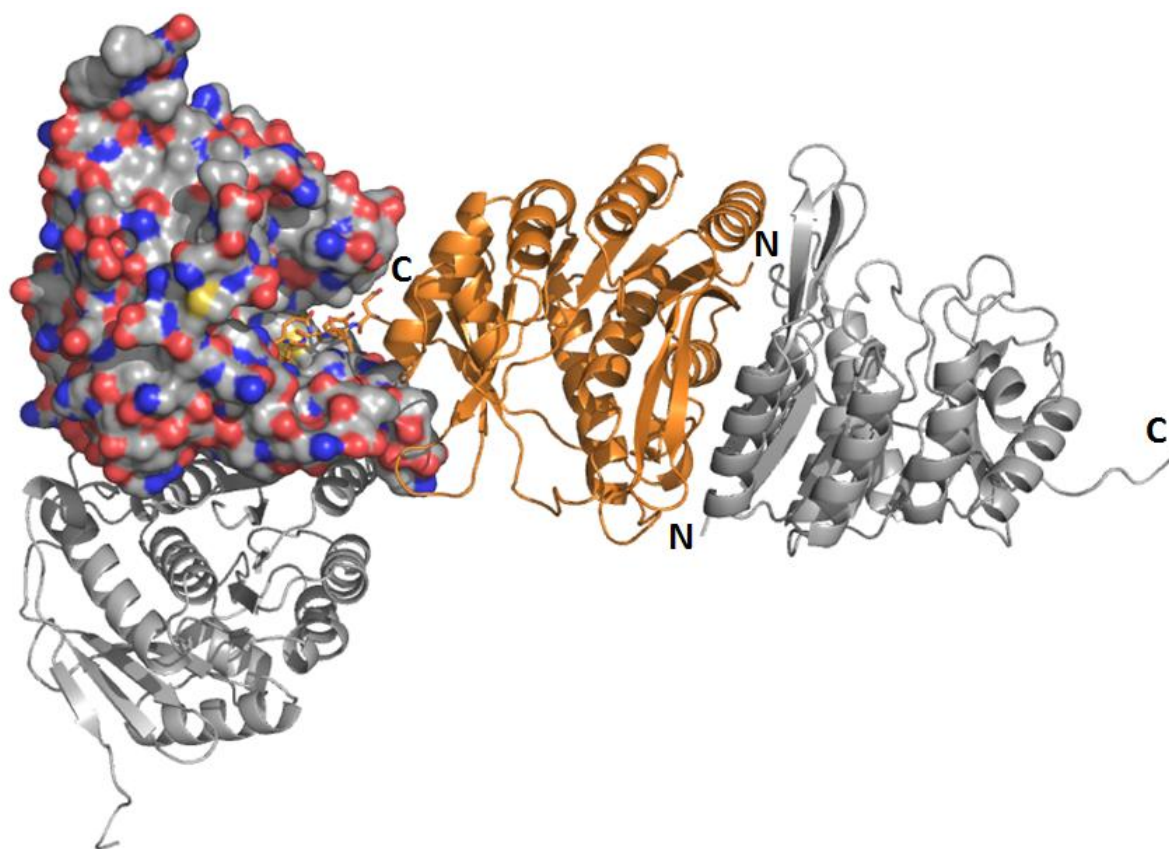


Figure 36: *S. aureus* PdxK (structure II) orientation in the crystal lattice.

A monomer of *S. aureus* PdxK (structure II) in orange cartoon representation, together with two symmetry related monomers in grey cartoon representation and one monomer with surface representation (grey) with atoms N, O, S colored in blue, red and yellow, respectively, resulting in two dimers is shown. The C-terminus of the orange monomer is placed in the cleft of the symmetry related monomer of a second dimer. Figure was created with The PyMOL Molecular Graphics System, Version 1.7.4 Schrödinger, LLC.

In general the C-terminus shows a similar orientation in both solved models, as can be seen from the ribbon representation in Figure 33. However, the side chain orientation of Y280 in the C-terminus of structure I and II differs, as shown in Figure 37.

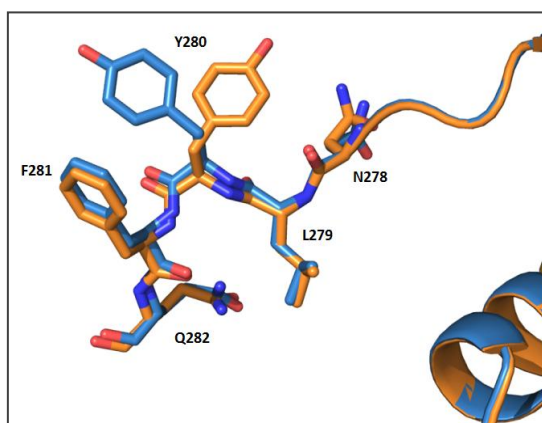


Figure 37: Comparison of the orientation of the C-terminus.

Structure I is shown in blue and structure II in orange stick representation, atoms N, O, S are colored in blue, red and yellow respectively; amino acids are labeled. The orientation of Y280 differs in the structures and is rotated by approximate 90°. Figure was created with The PyMOL Molecular Graphics System, Version 1.7.4 Schrödinger, LLC.

In Figure 38 the binding of the C-terminus in structure I is given; the E282 forms a hydrogen bond to the main chain G211 (2.9 Å) and Y280 main chain nitrogen forms a hydrogen bond to H51 (3.0 Å). Additionally, Y280 is stabilized via hydrophobic interactions with residues V53 and M80. Further, F281 is stabilized via hydrophobic interactions with residues D13, A18 and G19.

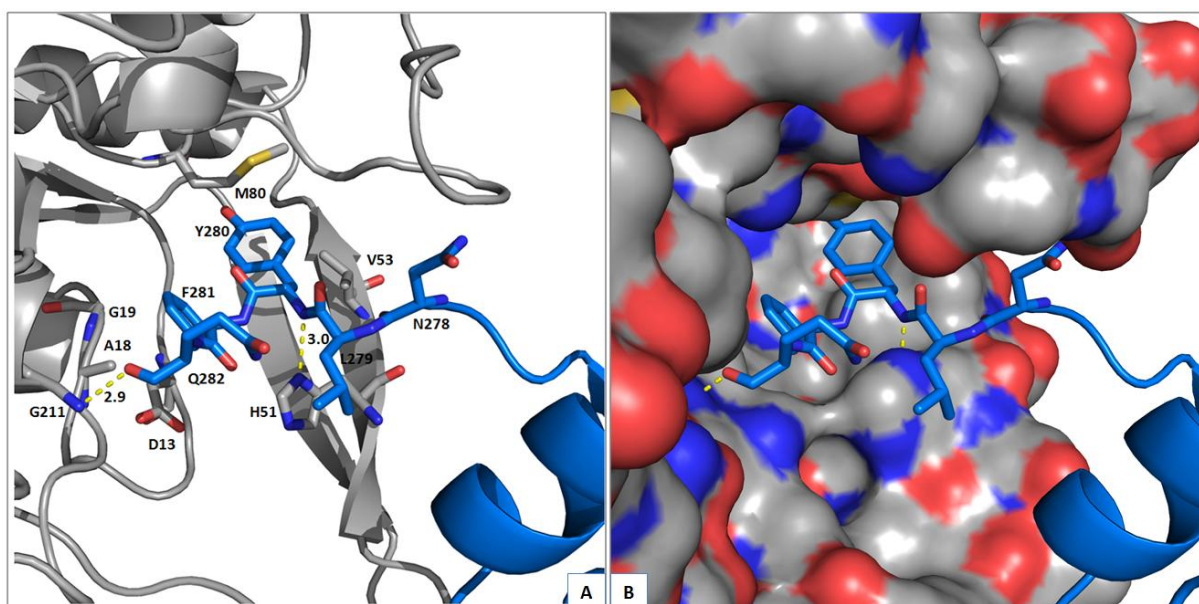


Figure 38: Interaction of the C-terminus with a symmetry equivalent molecule of structure I.

A: A monomer of *S. aureus* PdxK (structure I) in blue cartoon representation, last four residues (N278-Q282) of the TEV protease recognition site in stick representation, together with a symmetry related monomer in grey cartoon representation with interacting residues shown in stick representation as well; atoms N, O, S colored in blue, red and yellow respectively, hydrogen bonds as yellow dashed lines; labels of amino acids and bond length are shown. B: Illustration of the binding in an overall surface representation. Figure was created with The PyMOL Molecular Graphics System, Version 1.7.4 Schrödinger, LLC.

In Figure 39 the binding of the C-terminus in structure II is shown. The orientation of Y280 differs in this structure and is rotated by approximately 90° to the solvent accessible region. Nevertheless, E282 can form a hydrogen bond with the main chain G211 (2.9 Å) and Y280 main chain nitrogen atom forms, just as in structure I, a hydrogen bond with H51 (3.0 Å). Further, Y280 is stabilized via hydrophobic interactions with residues V53 and M80 and further from V109 as Y280 is pointing more

to the loop region V109-E115. F281 is stabilized, like in structure I, via hydrophobic interactions with residues D13, A18 and G19.

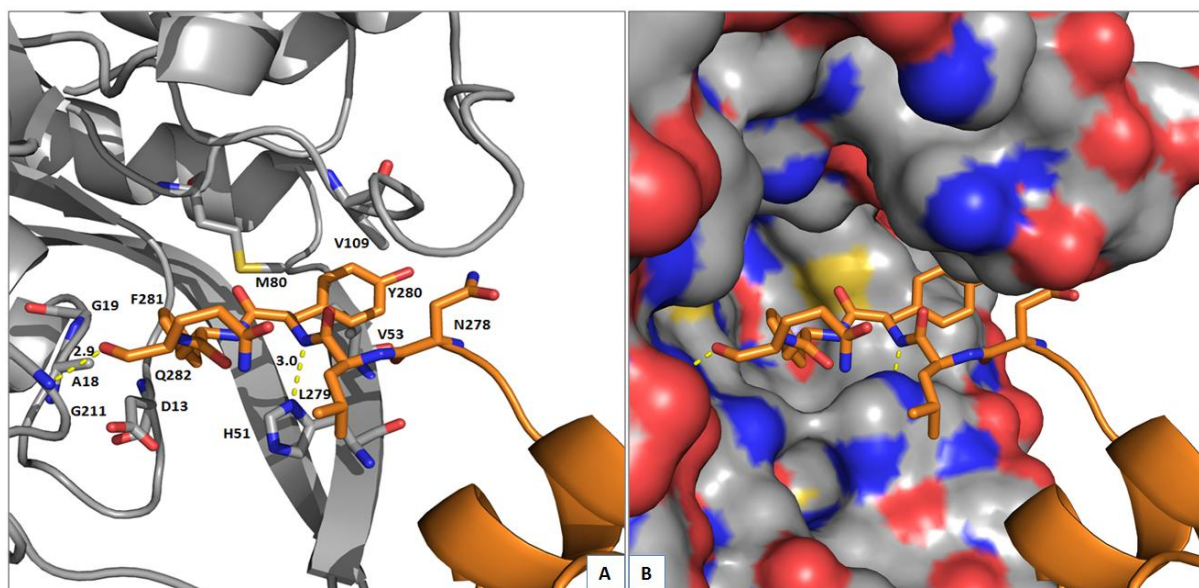


Figure 39: Interaction of the C-terminus with a symmetry equivalent molecule of structure II.

A: A monomer of *S. aureus* PdxK (structure I) in blue cartoon representation, last four residues (N278-Q282) of the TEV protease recognition site in stick representation, together with a symmetry related monomer in grey cartoon representation with interacting residues shown in stick representation as well; atoms N, O, S colored in blue, red and yellow respectively, hydrogen bonds as yellow dashed lines; labels of amino acids and bond length are shown. B: Illustration of the binding in an overall surface representation. Figure was created with The PyMOL Molecular Graphics System, Version 1.7.4 Schrödinger, LLC.

Prompted by this very specific and reproducible binding of the ‘peptide’ into the active site *in silico* docking experiments were performed to study and validate the binding of this kind of auto-inhibitor with structure I (see chapter III 4.22).

Unfortunately, in progress of this work the structure of native, PL and ADP and AMP-PCP ligated *S. aureus* PdxK was solved by Nodwell *et al.* from the University of Munich [222]. But on the other hand these information gave a vital basis for comparing the structure model for artifacts in the active site due to the binding of the artificial C-terminus and thus to further analyze the binding of the ‘peptide’ into the active site.

A comparison of the structure from Nodwell *et al.* (4C5N) revealed that the overall fold is highly comparable and gave for structure I and II in comparison an RMSD of 0.7 Å. The highest deviations are found in loop region 45-50 (~0.7 Å) and 253-254 (~1 Å - 2 Å) due to crystal packing contacts. Additionally, G144 in proximity to the binding site showed a displacement of ~1 Å and region 148-155 of 1-1.3 Å, which might be a consequence of substrate binding. Further, region 177-186 and 200-204 deviate due to the nucleotide binding. An overall comparison of the C α chain is depicted in Figure 40.

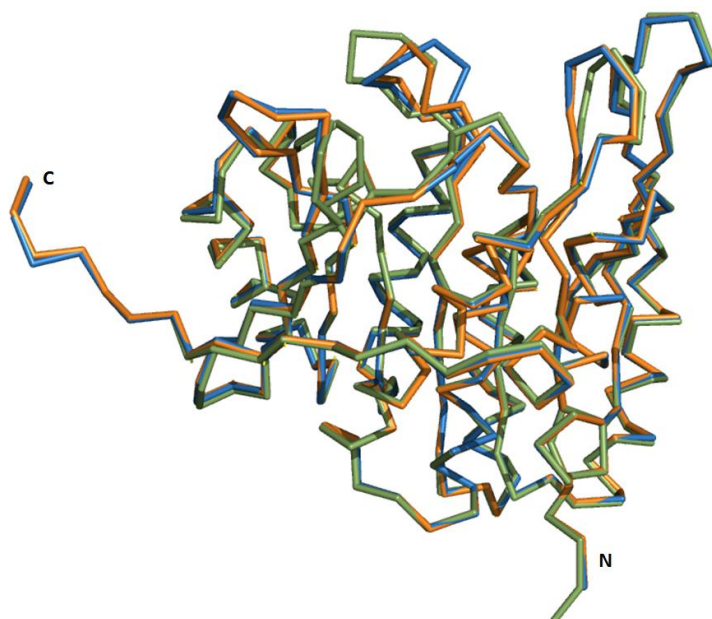


Figure 40: Alignment of the C α chain of *S. aureus* PdxK structure I and II and *S. aureus* PdxK solved by Nodwell *et al.*

In the ribbon overlay *S. aureus* PdxK structure I and II are colored in blue and orange respectively, *S. aureus* PdxK in complex with PL and AMP-PCP from Nodwell *et al.* (pdb code: 4C5N) is colored in green; N- and C-terminus are labeled. Figure was created with The PyMOL Molecular Graphics System, Version 1.7.4 Schrödinger, LLC.

Interestingly, Nodwell and colleagues found that PL could be locked in the active site of PdxK via the formation of a hemithioacetal with C110. The cysteine is positioned in the loop after β_5 -strand and could shield the active site as a flap (Figure 41). Furthermore, the substrate binding is strengthened by the rotation of M80 towards PL.

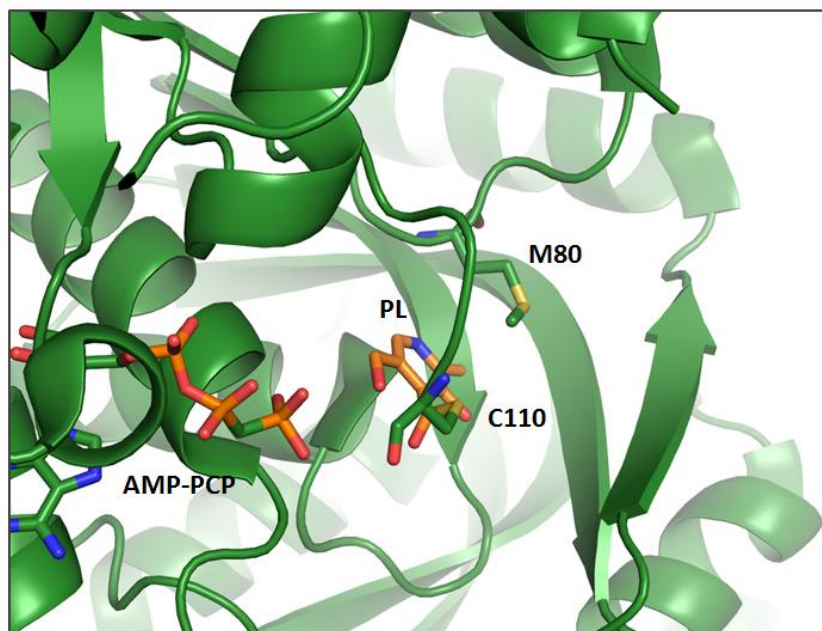


Figure 41: Hemithioacetal formation of PL and C110 in *S. aureus* PdxK.

4C5N is colored in green, the substrates AMP-PCP and PL are colored in green and orange; atoms N, O and S are colored in stick representation in blue, red and yellow, respectively. Substrates AMP-PCP PL and amino acids C110 and M80 are labeled. Figure was created with The PyMOL Molecular Graphics System, Version 1.7.4 Schrödinger, LLC.

Comparing the position of the C-terminal peptide in the active site clearly shows that F281 is positioned in the area of the natural substrate PL and Y280 is interfering with M80 (Figure 42). In the peptide incorporated PdxK structure model of this study (structure I) the loop containing the C110 (in Figure 42 shown in red) is pointing away. The occupation of this space with a peptide would thus inhibit the formation of the hemithioacetal. Furthermore, the position of Y280 would inhibit the improvement of the substrate fit by the rotation of M80.

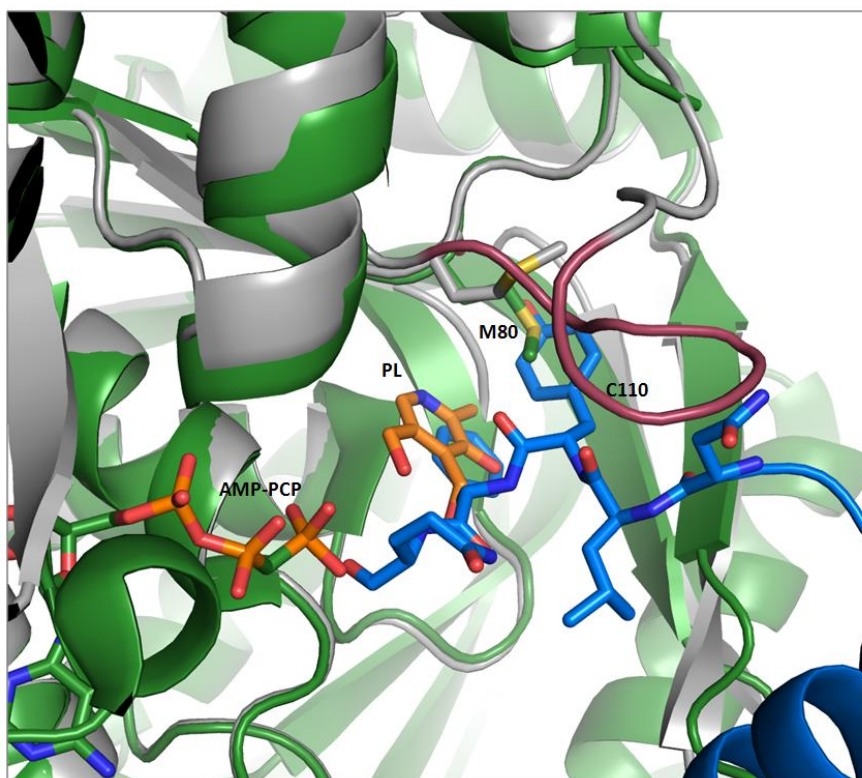


Figure 42: Overlay of *S. aureus* PdxK structure I and 4C5N from Nodwell *et al.*

Structure I is represented in blue and the symmetry mate in grey, 4C5N is colored in green, the substrates AMP-PCP and PL are colored in green and orange; atoms N, O, S are colored in stick representation in blue, red and yellow, respectively. The loop between M108 and D114 containing the C110 of structure I is highlighted in dark red, the corresponding amino acids from 4C5N are hidden. Figure was created with The PyMOL Molecular Graphics System, Version 1.7.4 Schrödinger, LLC.

3.4 Results of docking and analysis of peptidomimetics targeting *S. aureus* PdxK

On basis of the observed, well arranged binding of the artificial amino acids of the TEV protease recognition site into the active site of both *S. aureus* PdxK structures and the results of studies from Ghatge *et al.* [217], which demonstrated that PLP is a slow tight binding inhibitor of *E. coli* PdxK, di- and tri-peptides were analyzed *in silico* using molecular docking with structure I of *S. aureus* PdxK in cooperation with Dr. D. Rehders. As a result three modified peptides (#3-#5) listed in Table 32, as well as a di-peptide that matches the original peptide sequence (#1), were selected.

Table 32: Peptides and their corresponding molecular weight selected in the molecular docking process.

Number #	Sequence	Molecular weight [g mol ⁻¹]
1	YF- NH ₂	327.37
2	YFW- NH ₂	513.59
3	Ac-YF-NH ₂	369.37
4	Y-[F(3-Met)]-NH ₂	341.42
5	Y-[F(3-Cl)] NH ₂	361.84

The tri-peptide (#2) showed an enhanced binding towards A18 and G19 and could be further stabilized, like the native Q282, through a hydrogen bond of its C-terminal carboxy-group to the G211 main chain amide group in the *in silico* modeling.

The di-peptide (#3) showed enhanced hydrophobic interactions with A18 and G19 due to the N-terminal acetylation of the tyrosine as well and could possibly stabilize the H210 in the active site via a hydrogen bond of the acetyl moiety. Comparably, peptide #4 demonstrated an enhanced hydrophobic interaction in the direction of G11 and G19 due to its modification of the original phenylalanine to a 3'-methyl-phenylalanine as well. In peptide #5 the original phenylalanine is substituted to 3'-chloro-phenylalanine and the peptide demonstrated enhanced hydrophilic interactions with G11 and S12 carboxyl groups in the active site.

Successfully docked peptides were purchased in a C-terminal amidated version to mimic the amide bond and for enhanced water solubility the N-terminus is not tailored, except peptide #3, where it possesses an acetylation.

Further binding affinity analysis via Microscale Thermophoresis (MST) in Monolith NT.115 was intended using the Strep-tagged PdxK to exclude any bias from the TEV protease recognition site. These measurements require a fluorophore, thus the protein was non-specifically labeled via its primary amids (22 lysine residues in the protein, 8 % of total amino acids) with the Monolith Protein Labeling Kit NT 647 V012 via NHS-ester chemistry. The unspecific labeling procedure resulted in a labeling efficiency of approx. 90 %, estimated by absorption measurement at 280 nm and 647 nm to determine the concentration of protein and dye respectively.

After the unspecific labeling procedure the protein was not able to bind PL, PN nor ATP or ADP. The complete inhibition of any substrate binding might be attributed to the unspecific labeling of lysines and thus blocking or changing the folding of the active site.

3.5 Activity and analysis of substrate specificity of *S. aureus* PdxK

The activity of the His₆-tagged protein in solution was determined via the absorbance (388 nm) based assay described in III 7.1. The K_m for *S. aureus* PdxK could be determined to be $2333 \pm 371 \mu\text{M}$ towards pyridoxal. In contrast, Nodwell and colleagues determined the K_m of *S. aureus* PdxK towards pyridoxal to be $111 \pm 53 \mu\text{M}$ and towards pyridoxine to be $2072 \pm 332 \mu\text{M}$ [222]. Additionally, they also determined the activity towards HMP and found significant activity yielding in a K_m of $1998 \pm 268 \mu\text{M}$.

Earlier studies of Wrenger and colleagues (Bernhard-Nocht Institute, Hamburg, unpublished data) also revealed a dual substrate acceptance of *S. aureus* PdxK towards the two B₆ vitamers and HMP. In contrast *S. aureus* PdxK is only capable to phosphorylate HMP once and not twice like ThiD.

Furthermore, pyridoxal kinases bifunctionality acting on pyridine (PL, PN, PM) and on the pyrimidine compound HMP could also be shown for *Plasmodium falciparum* PdxK [227], *E. coli* PdxK [228, 229], *Trypanosoma brucei* PdxK [230] and the *thiD* gene product from *B. subtilis* [231].

To further elucidate the specificity of *S. aureus* PdxK and *S. aureus* ThiD towards the vitamin B₆ vitamers and the refusal of HMPP for a second phosphorylation of PdxK, in cooperation with *T. Kronenberger* (University São Paulo), molecular modeling studies were conducted to evaluate possible residues involved in substrate recognition.

The molecular modeling studies could elucidate the residues listed in Table 33 as determining elements for substrate recognition, refusal of HMPP and activity.

Table 33: Residues selected in *S. aureus* PdxK selected for mutagenesis to alter substrate specificity to HMPP.

Amino acid in <i>S. aureus</i> Pdxk	Corresponding amino acid in <i>S. aureus</i> ThiD	Mutagenesis	Anticipated effect
S12	T13	A	} Change of substrate recognition
H51	Q51	V and Q	
M80	M81	A	
A212	T213	T	Activity decrease
C214	C215	A and D	Activity increase
N252	G253	G	Change of substrate recognition and substrate shielding

The sequence similarity of *S. aureus* PdxK to ThiD was determined to be 35 % (BLAST). Figure 43 shows an alignment of both enzymes of *S. aureus* with the residues assumed for bifunctional substrate recognition of HMP and B₆ vitamers, highlighted in green boxes.

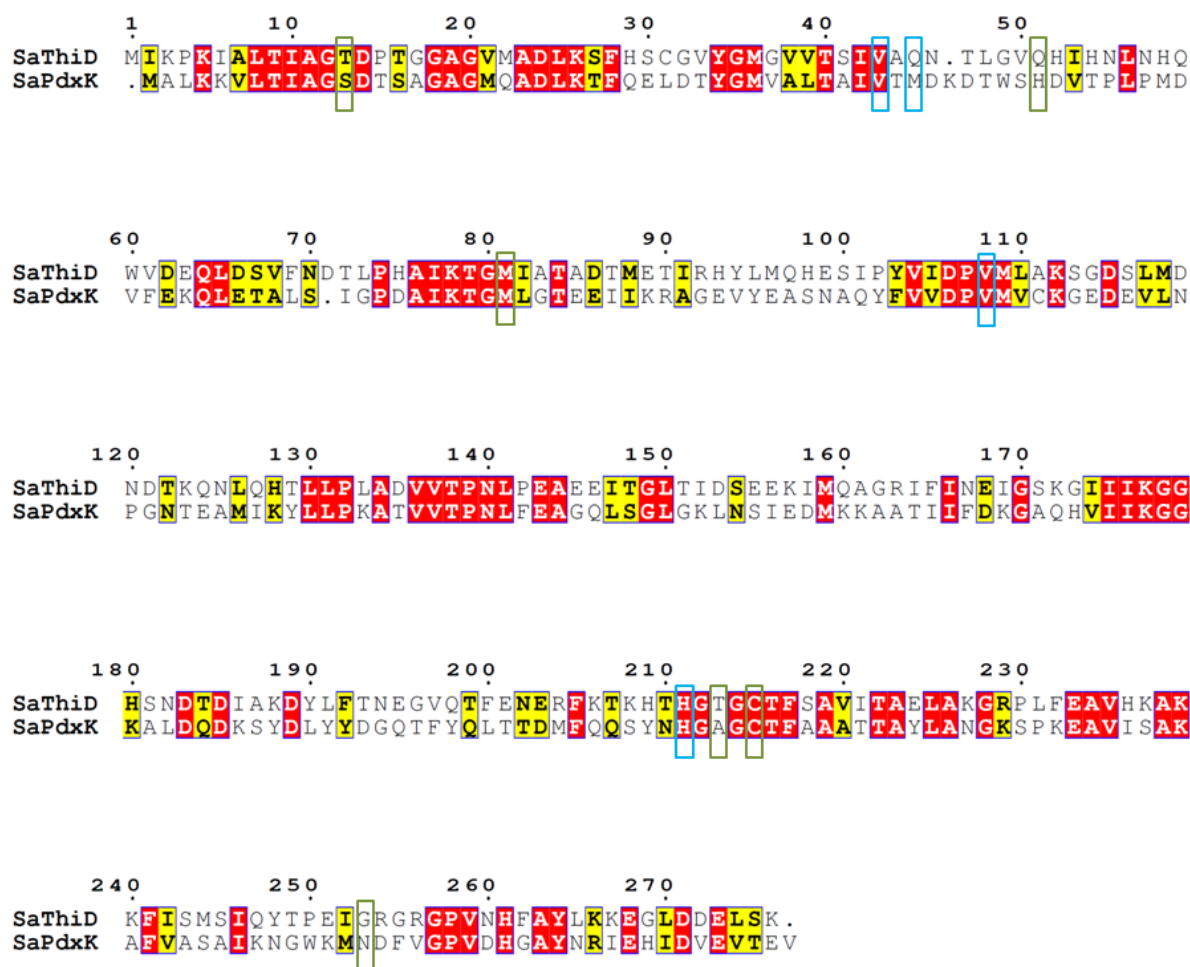


Figure 43: Sequence alignment of *S. aureus* ThiD and PdxK.

Sequence alignment was performed using ClustalW2, representation was generated with ESPrit. Identical residues are highlighted in red, similar residues in yellow boxes. Green boxes indicate residues of *S. aureus* PdxK selected in this study to create an *S. aureus* PdxK with specific activity towards HMPP. Blue boxes indicate key residues reported by Castro-Fernandez and colleagues [230] to be determinative for acceptance of HMP or vitamin B₆.

Furthermore, the results were confirmed by the structure of *S. aureus* PdxK in complex with PL solved by Nodwell and colleagues [222]. Supplementary, a study of Castro-Fernandez and colleagues [230], which aimed to find the general ancestor of pyridoxal kinases, evaluated the same set of residues with the exception of N252 and with the addition of V42, V107 and H210 in *S. aureus* PdxK.

Based on the findings in this study mutants of *S. aureus* PdxK were produced according to the record in Table 33 of the Strep-tagged and the His₆-tagged *S. aureus* PdxK variant (oligonucleotides used as primer listed in chapter III 4.13.1 in Table 12) and tested for expression to make them available for enzymatic activity determination. All mutated *S. aureus* PdxK variants showed comparable expression profiles to the native *S. aureus* PdxK variants and are not shown in detail.

4 *Trypanosoma cruzi* PdxK

4.1 Recombinant expression, purification and characterization

T. cruzi PdxK fused to His₆-tag was recombinantly expressed in *E. coli* BLR cells. Gene expression was conducted for 4 h at 37 °C starting at an OD₆₀₀ of 0.5-0.6. The protein was purified from the cleared cell lysate, obtained from the standard procedure described in chapter III 4.15.1 via affinity chromatography using a washing step of 60 mM imidazole in buffer P/N and was finally eluted in buffer P/N supplemented with 300 mM imidazole. The rate of yield was calculated to approx. 36 mg L⁻¹ bacterial culture.

Subsequently, the eluate was applied to a superdex 200 column operated by an ÄKTA purifier at 4 °C and transferred to an imidazole free P/N buffer. In comparison to a calibration curve *T. cruzi* PdxK eluted at a calculated molecular weight of approx. 62 kDa. The dispersity of the protein solution was monitored via DLS. Figure 44 shows the DLS pattern of the protein solution before and after size exclusion chromatography at a concentration of 6.4 mg mL⁻¹ and 5.2 mg mL⁻¹ in P/N buffer.

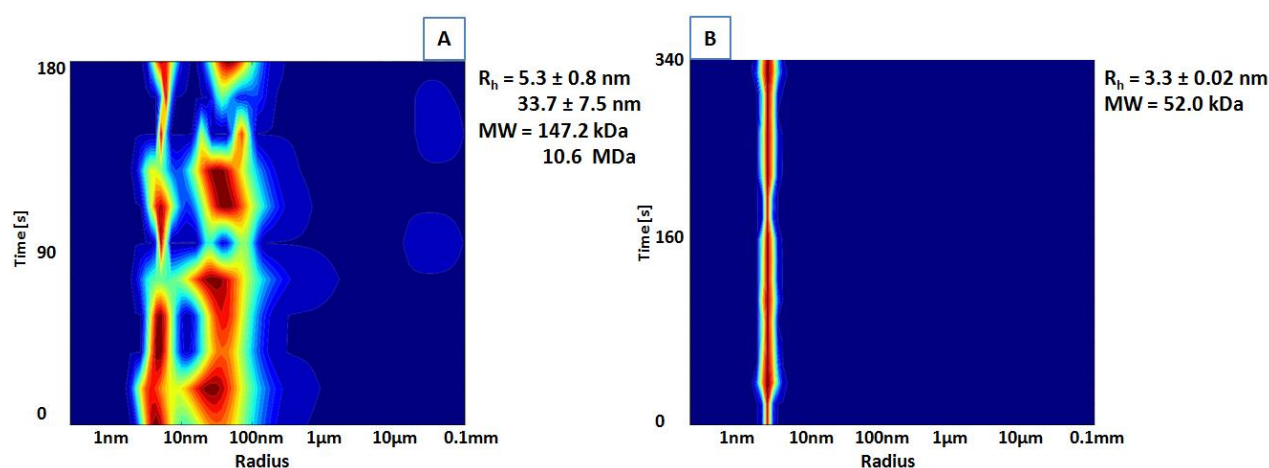


Figure 44: DLS pattern of *T. cruzi* PdxK before (A) and after (B) size exclusion chromatography.

The particle size is plotted against time, the heat map colors indicate the relative occurrence of the size fraction in the solution; dark blue representing zero occurrence and red being the maximum. The hydrodynamic radius (R_h) and the calculated molecular weight (MW) for an ideal sphere are noted.

4.2 Crystallization of *T. cruzi* PdxK

T. cruzi PdxK in a concentration of 7 and 21 mg mL⁻¹ in buffer P/N as well as 6.2 and 21 mg mL⁻¹ in buffer T/N was used for initial crystallization screens at RT by the sitting drop vapor diffusion method. Crystallization screens JCSG-plus, PACT premier, Cryos Suite and Morpheus were tested in sitting drop vapor diffusion in MRC 96-well sitting drop crystallization plate (Molecular Dimensions, UK). All optimizations were performed after a buffer exchange to T/N buffer.

Finally, the condition 425 mM ammonium sulfate, 85 mM tri-sodium citrate, pH 5.6, 85 mM lithium sulfate supplemented with 15 % (v/v) glycerol resulted in the crystals shown in Figure 45 A and B after an incubation of 5 d at RT at a ratio of protein to precipitant of 1 : 1 and 1 : 1.75, respectively. The protein concentration was 21 mg mL⁻¹ in buffer T/N. In Figure 45 C and D a protein concentration of 7.0 mg mL⁻¹ was used in the same setup as A and B. Optimization of this condition allows growing crystals in the size of 0.2 x 0.3 x 0.1 mm³ in MRC MAXI 48-well optimization plate (Molecular Dimensions, UK) by adding 0.5 M ammonium sulfate, 85 mM tri-sodium citrate, pH 5.6, 85 mM lithium sulfate supplemented with 15 % (v/v) glycerol to a protein solution containing 20.0 mg mL⁻¹ in a ratio of 1 : 1 and 1 : 1.75 (Figure 45 E and F, respectively).

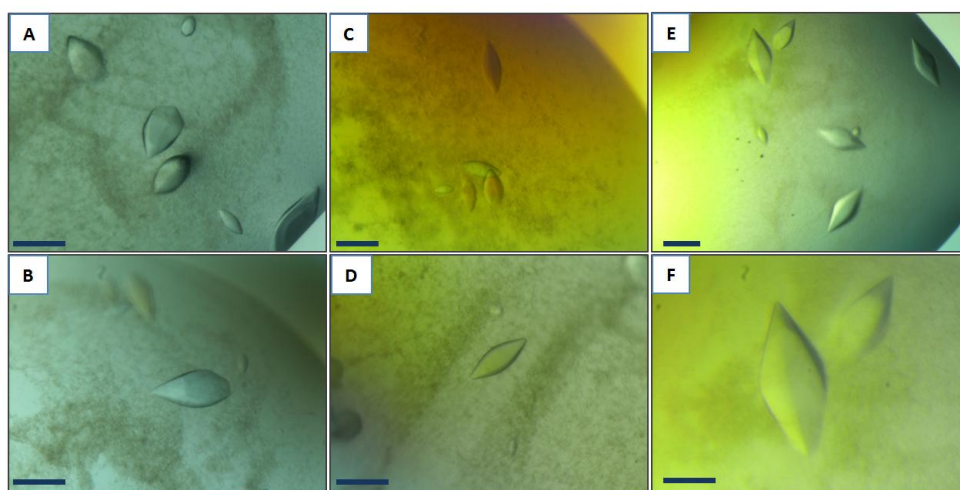


Figure 45: Protein crystals of *T. cruzi* PdxK.

A and B showing the results of the screening (protein concentration: 21.0 mg mL⁻¹; precipitant: 425 mM ammonium sulfate, 85 mM tri-Na citrate, pH 5.6, 85 mM lithium sulfate supplemented with 15 % (v/v) glycerol in ratios of 1 : 1 and 1 : 1.75); Crystals shown in C and D are grown in the same condition as A and B, but at a protein concentration of 7 mg mL⁻¹. E and F showing crystals from the optimized condition (protein concentration: 20 mg mL⁻¹; precipitant: 0.5 M ammonium sulfate, 85 mM tri-Na citrate, pH 5.6, 85 mM lithium sulfate supplemented with 15 % (v/v) glycerol in ratios of 1:1 and 1:1.75). The scale bar equals to 100 µm in all pictures.

4.3 *T. cruzi* PdxK: Diffraction data collection, processing and model building

Crystals used for data collection showed a flattened lens shape and dimensions of approx. 0.2 x 0.25 x 0.1 mm³. As the precipitant solution contained 15 % (v/v) glycerol no addition of cryo protectant was necessary. The crystals were flash cooled in gaseous nitrogen at 100 K and the diffraction data were collected on an in house X-ray radiation source (rotating anode). Diffraction data were collected to 2.5 Å resolution using the oscillation method (0.5 degree) and subsequently indexed, integrated and scaled with XDS. Data were cut to 2.5 Å monitoring R_{merge} , I/σ and CC1/2. The crystal was found to belong to the hexagonal space group P6₁22 with unit cell dimensions of $a = b = 102.4$ Å and $c = 170.1$ Å. The Matthews coefficient was calculated to be 3.8 Å³ Dalton⁻¹ which corresponded to a solvent content of 67.3 % with one molecule in the asymmetric unit.

Molecular replacement using the model of monomeric *T. brucei* PdxK (pdb code: 3ZS7) was performed with MOLREP [281]. Search for one monomer resulted in a solution with an R-factor of 48.6 % and a correlation coefficient of 57.6 %. The contrast for the solution was 22.95 [299]. Subsequently, the model was completed and further modified using Coot and refined using refmac5 (Restrained refinement with isotropic B factors). Two patches of positive electron density were found close to Q285, V284, S283 and additionally close to G228, K185, that have been interpreted as SO_4^{2-} ions and were subsequently included in the model. The final model has an R-factor of 19.30 % and an R_{free} -factor of 23.78 %. The three N-terminal residues M1, S2 and E3, the loops D124-M127 and E266-M275 as well as the His₆-tag were not visible and thus excluded from the final model. The model shows very good geometry and no Ramachandran outliers. Data collection, processing and refinement statistics are summarized in Table 34.

Table 34: Summary of data collection statistics and refinement statistics for *T. cruzi* PdxK.

Data collection statistics^a	
X-Ray source	Rotating Anode
Wavelength [Å]	1.5418
Space group	P6 ₁ 22
Unit cell parameters: a = b, c [Å]	102.4, 170.1
Resolution [Å]	20.0 - 2.5
Temperature [K]	100
R _{merge} ^b	18.3 (70.6)
Measured reflections	174203
Unique reflections	18918
Average I/σ(I)	13.5 (3.6)
Mn(I) half-set correlation CC(1/2)	99.4 (84.1)
Completeness [%]	99.8 (100.0)
Redundancy	9.2 (9.3)
Refinement statistics	
Resolution range [Å]	20.0 - 2.5
R/ R _{free} [%]	19.30/23.78
Protein atoms	2211
Water molecules	69
Ion atoms (2x SO ₄ ²⁻)	10
Rms deviation	
Bond-length [Å]	0.018
Bond angle [°]	1.884
B factor [Å ²]	
Protein	26.31
Water	18.77
Ion (2x SO ₄ ²⁻)	46.9
Ramachandran plot analysis:	
Most favored regions [%]	96.0
Allowed regions [%]	4.0
Generously allowed regions [%]	0

^a Values in parentheses are for the highest resolution shell. ^b $R_{merge} = \frac{\sum_{hkl} \sum_i |I_i(hkl) - \langle I(hkl) \rangle|}{\sum_{hkl} \sum_i I_i(hkl)}$, where $I(hkl)$ is the mean intensity of the reflections hkl, \sum_{hkl} is the sum over all reflections and \sum_i is the sum over i measurements of reflection hkl.

4.4 *T. cruzi* PdxK: Structure analysis

The *T. cruzi* PdxK monomer shows, similar to the *S. aureus* PdxK monomer, the highly conserved ribokinase fold in the tertiary structure [312, 313]. In Figure 46 the inner 8-stranded β -sheet, made up of seven parallel and one antiparallel strand (β_9) in the arrangement of 2-1-5-6-7-8-9-10, is consecutively numbered. This central sheet is flanked by four α -helices on the one side and five α -helices and one 3_{10} -helix on the other side. Additionally, a small 2-stranded anti-parallel β -sheet (strands β_3 and β_4) completes the model at the interface region. The dimeric assembly of *T. cruzi* PdxK, which was already expected from homology modeling, as well as the results of size exclusion chromatography and DLS, can be created applying crystallographic symmetry.

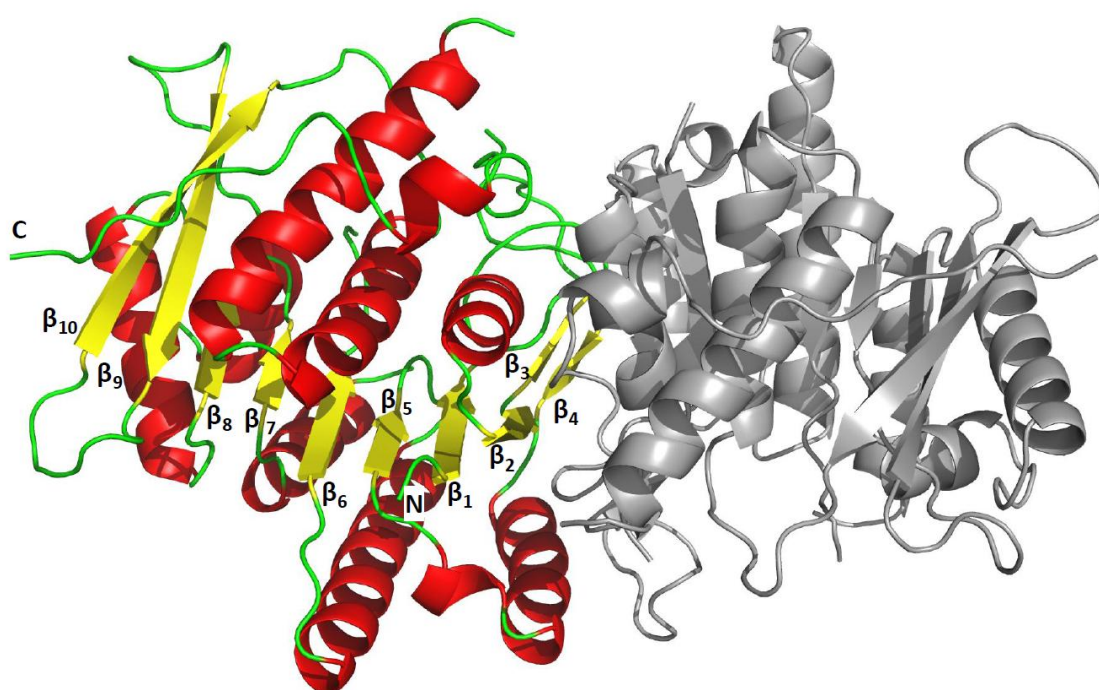


Figure 46: *T. cruzi* PdxK dimeric structure model created via crystallographic symmetry.

A *T. cruzi* PdxK monomer is shown in secondary structure representing cartoon illustration; yellow is used for β -sheets, red for α -helix and green for turns and loops. The central β -sheet is sequentially numbered; labels of the N- and C-terminus are shown. The dimeric assembly created via crystallographic symmetry is represented in grey cartoon representation. The figure was created with The PyMOL Molecular Graphics System, Version 1.7.4 Schrödinger, LLC.

The total surface area of one monomer accounts for 12716 \AA^2 whereof 1582 \AA^2 (12.5 %) are buried as a result of dimer formation; analysis was done using PDBePISA [289]. Up to 12 hydrogen bonds in cooperation with 10 salt bridges can stabilize the dimer formation. Additionally, 156 hydrophobic interactions stabilize the interface (PDBsum and CONTACT analysis out of CCP4 software suite [283]).

Examination of the sequence similarity of *T. cruzi* PdxK with *T. brucei* PdxK (pdb code: 3ZS7) and human PdxK (pdb code: 3KEU) revealed 70 % and 37 % sequence similarity and a structure similarity

of 0.8 Å and 1.6 Å, respectively. Alignment analysis was conducted using ClustalW and RMSD calculation by PDBeFold [290] and graphically arranged with ESPrit [315].

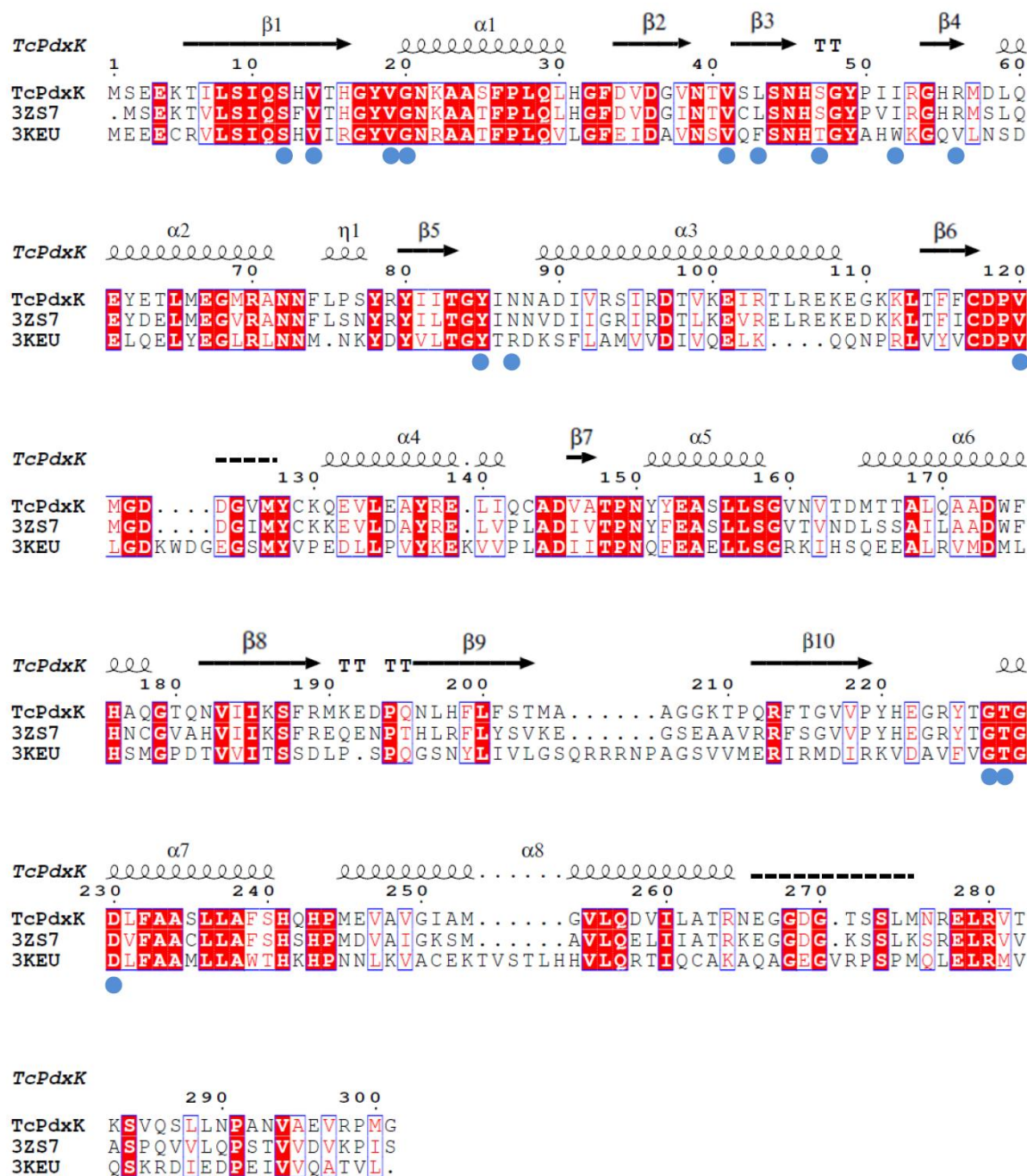


Figure 47: Sequence alignment of *T. cruzi* (Tc), *T. brucei* (3ZS7) and human (3KEU) PdxK.

Multiple sequence alignment was performed using ClustalW2, representation was generated with ESPrit. Identical residues are highlighted in red boxes, similar residues in white boxes. The secondary structure of *T. cruzi* PdxK is annotated on the top, spirals represent α -helices, arrows represent β -strands, T stands for turns, μ do represent 3_{10} helices and the dashed line indicates a disordered region. Blue dots highlight the proposed active site residues.

The two sulfate molecules are stabilized via hydrogen bond formation to G229 main chain nitrogen and K186 side chain NZ on the one hand and Q286 main chain nitrogen, V285 main chain

nitrogen and S284 side chain OG on the other hand. The sulfate ion stabilized via G229 and K186 binds in the conserved ATP binding site.

A comparison of the structures of human PdxK in complex with ATP and PLP with *T. brucei* PdxK in complex with ATP allows differentiating putative PLP binding site residues. It could be evaluated that *T. cruzi* PdxK also shows one active site per monomer. In Figure 48 *T. cruzi* PdxK putative binding site is shown with corresponding PLP binding site residues and overlaid with PLP binding site residues from human and *T. brucei* PdxK.

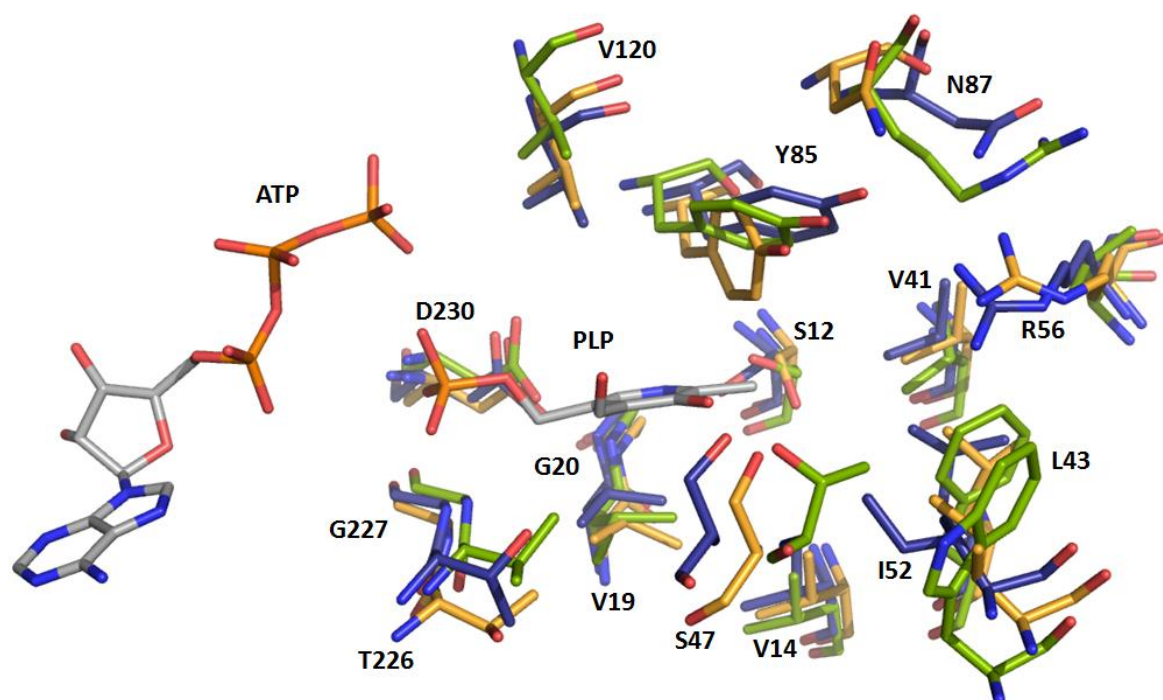


Figure 48: Active site composition in *T. cruzi*, *T. brucei* and human PdxK.

ATP and PLP were taken from 3KEU, (human PdxK) and depicted in grey stick representation. Stick representation of PLP interacting residues is shown for *T. cruzi* PdxK in blue, *T. brucei* PdxK in orange and human PdxK in green. In all stick representations atoms N and O are colored in blue and red, respectively. Amino acids of *T. cruzi* PdxK and substrates ATP and PLP are labeled. Figure was created with The PyMOL Molecular Graphics System, Version 1.7.4 Schrödinger, LLC.

The overall assembly of the pyridoxal binding site seems to be highly conserved with a few modifications: In the assumption that PL/PLP would adopt a similar positioning in the active site of *T. cruzi* PdxK, it could be stabilized by three hydrogen bonds formed by S12 and the pyrimidine N as well as S47 and D230 to the oxygen atoms O3 and O5. Additionally, hydrophobic stabilization is achieved due to the presence of V14, V19, G20, V41, L43, I52, V120, T226 and G227 in the close proximity. The main difference between the human and *T. cruzi* PdxK is the stabilization of PLP at residues R56 and N87. In the human PdxK this stabilization is achieved through the residues V56 and R86 respectively. Additionally, the Y85 (human Y84) could stabilize the pyridine ring of the pyridoxal via π -stacking interactions in all three compared structure models.

In Table 35 the assumed residues interacting with the substrate are compared between *T. cruzi* and human PdxK:

Table 35: Comparison of the active site residues interacting with the ligand vitamin B₆ in *T. cruzi* and human PdxK.

TcPdxK	S12	V14	V19	G20	V41	L43	S47	I52	R56	Y85	N87	V120	T226	G227	D230
Human PdxK	S12	V14	V19	G20	V41	F43	T47	W52	V56	Y84	R86	V115	V230	G231	D234

In addition the GAGT motif, a conserved ribokinase anion hole motif for the phosphate transfer [216, 301], could be identified in *T. cruzi* PdxK in residues 227-230 as GTGD. This motif generally stabilizes the binding of the phosphate moiety of the ATP and helps to neutralize negative charges and the transition state in the active site, as it can be found in *T. brucei* PdxK in amino acids 226-229 and human PdxK in amino acids 231-234.

Interestingly, a further comparison of the bifunctional enzymes PdxK, ThiD of *S. aureus* and *T. cruzi* and the human PdxKs highlighted in Figure 49, reveals that the residues for substrate binding are less conserved between *S. aureus* and eukaryotic species. In Figure 49 also the residues, which were identified by Castro-Fernandez and colleagues [230] as determinates for substrate selectivity are highlighted. This provides evidences for the evolution of the substrate recognition in pyridoxine kinases and HMPP kinases.

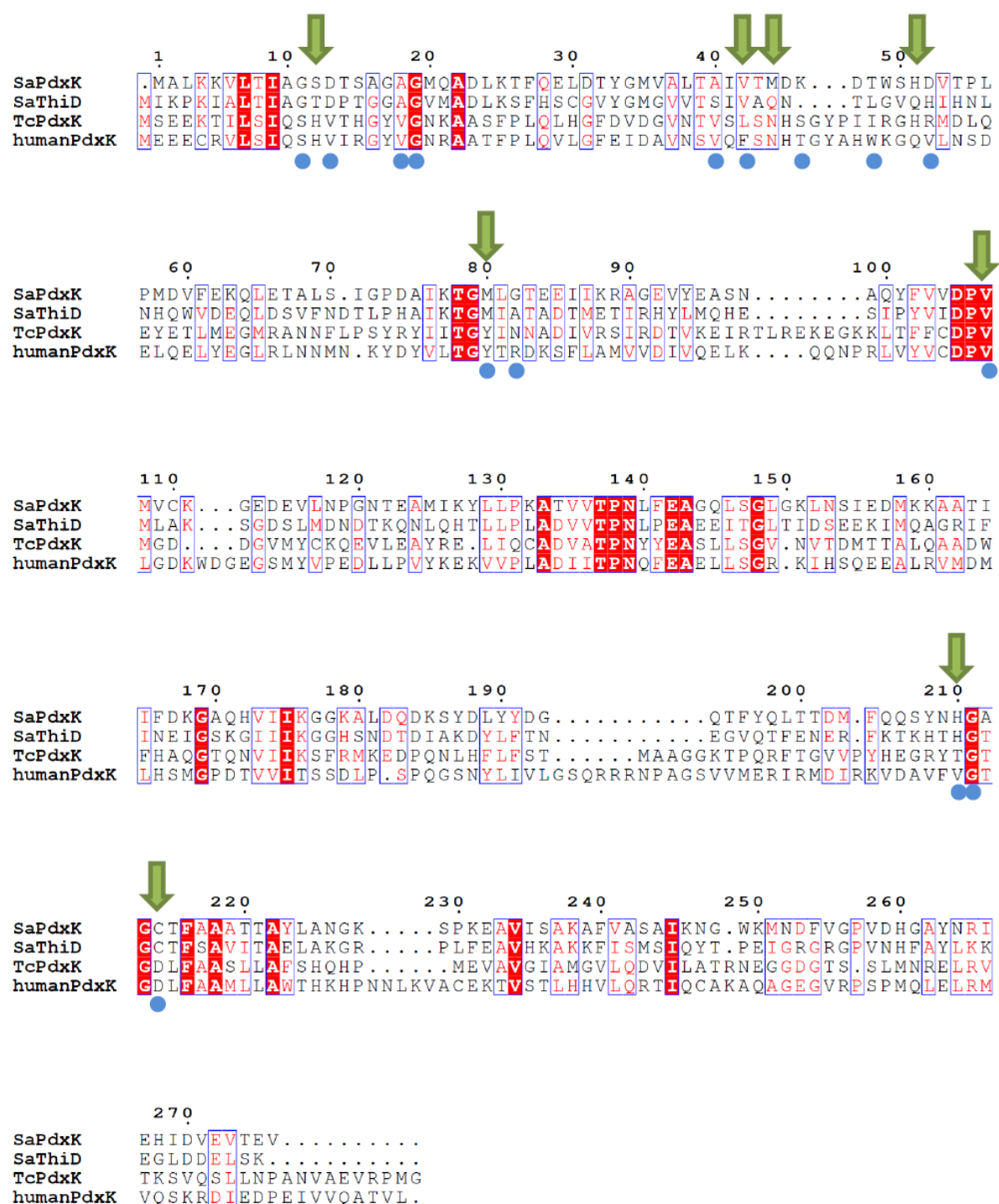


Figure 49: Sequence alignment of *S. aureus* PdxK, ThiD, *T. cruzi* PdxK and human PdxK.

Sequence alignment was performed using ClustalW2, representation was generated with ESPrit. Identical residues are highlighted in red, similar residues in white boxes. Green arrows indicate the determinates for substrate selectivity towards HMP or B₆ vitamers. Blue dots indicate the proposed active site residues of *T. cruzi* PdxK.

5 Insect cell expression and *in vivo* crystallization trials

Besides the work summarized so far, also *S. aureus* ThiD fused to a C-terminal Strep-tag or fused to a N-terminal triple alanine linker and a His₆-tag or fused to a C-terminal His₆-tag with a TEV protease recognition site or to a N-terminal maltose binding protein (MBP) by a TEV protease recognition site and C-terminal to a second TEV protease recognition site and an additional His₆-tag were tested of expression in *E. coli* and purification. Further *S. aureus* ThiE N-terminal fused to a His₆-tag with a EV protease recognition site and the unspecific GTPase out of the vitamin B₁ metabolism of *S. aureus* fused to a C-terminal Strep-tag were tested for expression in *E. coli* and purification.

As either the expression yield was very low or the protein produced in the cytoplasm of *E. coli*, was insoluble, variables like lowering the expression temperature to 18 °C and 25 °C, changing the expression media (2YT, TB), the addition of glucose and betaine as well as for *S. aureus* ThiD the fusion of the protein to a solubility enhancing protein, like the MBP, were tested. None of these methods resulted in sufficient amounts of monodisperse high quality protein for the purpose of protein crystallization. Hence for future experiments elucidating the vitamin B₁ metabolism and the interplay with the B₆ pathways, the genes were tested for expression in insect cells (*Sf9*) and analyzed for their potential to form *in vivo* crystals.

All proteins of the vitamin B₁ metabolism and PdxK of *S. aureus* were cloned in the vectors pFastBac1 and pFastHTb. Additionally, constructs in pFastBac1 with a carboxy-terminal three amino acid long peroxisomal targeting signal (PTS1) SKL [316] were produced.

After bacmid preparation, purification and validation *Sf9* cells were transfected with the bacmid and virus stocks were produced subsequently. Finally, P3 infected cells were monitored for a possible formation of *in vivo* crystals. Since none could be observed cells were harvested after 2.5 d post infection and the gene expression was analyzed in a western blot (Figure 50) after a cell lysate preparation of the His₆-tag containing constructs.

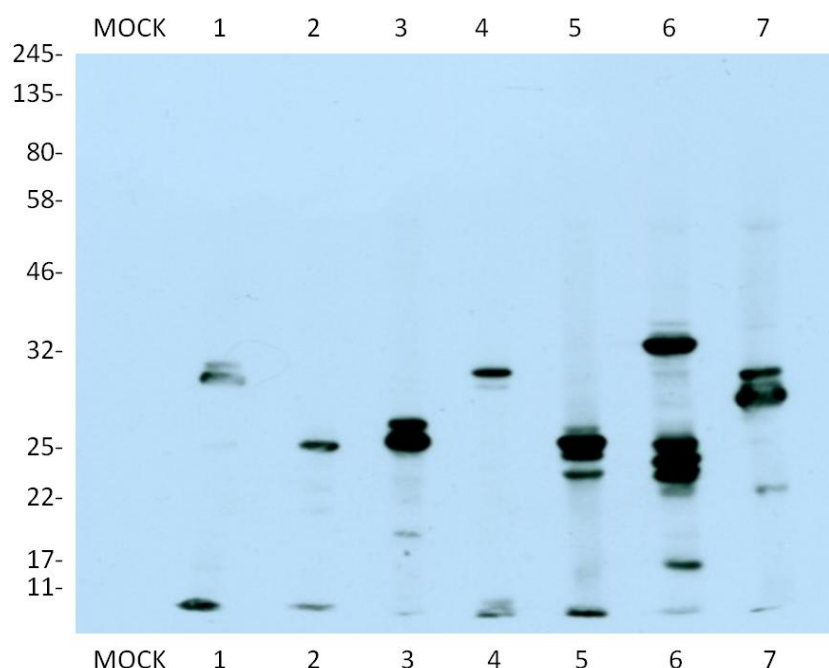


Figure 50: Western Blot of P3 infected insect cell lysates, 2.5 d post infection.

20 µg total cell lysate protein were applied on a 12 % SDS-PAGE; MOCK- control lysate of non infected cells, 1= *S. aureus* PdxK, 2= *S. aureus* ThiE, 3= *S. aureus* TenA, 4= *S. aureus* ThiD, 5= *S. aureus* TPK, 6= *S. aureus* GTPase, 7= *S. aureus* ThiM bacmid transfected and onwards infected cells. Specific detection of His₆-tag was conducted via anti-His mouse IgG1 and visualization with HRP conjugated secondary antibody and ECL detection.

Figure 50 shows the results of the western blot. The very first lane contained MOCK transfected cell lysate and no His₆-specific protein could be detected. Lane number one contained cell lysate from putative *S. aureus* PdxK producing cells; a double band could be detected approx. in the expected size of 32.0 kDa. In lane two a single band in the approx. size of 26 kDa could be detected. Lane three showed a dominant double band at approx. 27-30 kDa. In lane four a single band with a faint second band in the range approx. 32 kDa could be detected. Lanes five and six are showing more than a single band; in lane five three bands in the size of approx. 24-27 kDa and in lane six a dominant band could be detected at the molecular weight of 36 kDa and further at approx. 23-25 kDa and 18 kDa. In the last lane a dominant double band in the approx. size of 30- 32 kDa could be detected. As a control experiment *Trypanosoma brucei* Cathepsin B *in vivo* crystals [317] were produced in parallel (virus kindly provided by Prof. Duszzenko, University of Tübingen). The P3 Cathepsin B infected cells showed *in vivo* formed crystals.

Moreover, as a remote study the influence of 2.5 and 5 mM sodium butyrate as well as the addition of 2 % and 4 % (v/v) DMSO to the cells 1 d before infection were tested to further enhance protein expression via the inhibition of histone deacetylase [318, 319]. In this first study neither an enhancing effect nor a decreasing effect could be detected on *Trypanosoma brucei* Cathepsin B *in vivo* crystal production.

V Discussion

1 First steps to *in vivo* produced thiamine analogs in *S. aureus*

In order to obtain specific THZ analogs in the *in silico* screening the following three restraints were applied: Firstly the sulfur within the thiazole ring should be replaced in order to inhibit the carbanion formation for thiamine-dependent enzymes [320], secondly the hydroxyl group at the thiazole moiety as well as thirdly the nitrogen atom within the heterocycle, have to be retained to keep the phosphorylation site and ensure subsequent HMP-PP addition by thiamine phosphate synthase ThiE. This screening and *in vitro* activity analysis resulted in the pyrazole and imidazole based cpd1 and cpd2, respectively. But still the structural elucidation of the preposition of the compounds in ThiM's active site was missing, because the crystallization condition established by Dr. J. Drebes has only been successful for THZ binding. The absent binding of cpd1 and cpd2, perhaps due to ligand solubility or binding affinity in the first specific precipitant solution [321], led to the use of a second crystallization condition (0.1 M Tris pH 8.0, 20 % (w/v) PEG 6000 with 0.2- 0.26 M MgCl₂). Within this study an optimized crystallization condition could be defined that allowed the structural analysis of the compound binding. The location of the THZ analogs cpd1 and cpd2 in the active site regions of the ThiM trimer is significantly comparable to the preposition of THZ, the natural substrate, and thus permits an adequate pre-positioning for the phosphoryl transfer reaction. The structure models clearly revealed a beneficial preposition of the compounds in the active site and no changes in the binding site architecture are triggered upon compound binding of the *in silico* screened and *in vitro* tested compounds could be observed.

For further optimization especially the methyl group at position 10 in cpd1 should be under revision due to the close contact to the loop between β -strand 3 and α -helix 4 which could reveal a non-favorable interaction within the active site.

Thiamine and particularly its active diphosphorylated variant TDP operates as an electrophilic covalent catalyst in the decarboxylation of 2-oxo acids, in carboligations of aldehydes and lyase-type reactions (cf. chapter I 4.1). By now a set of stable analogs of the reaction intermediates of TDP reactions were produced *in vitro* and used to study the enzymatic mechanistic of vitamin dependent enzymes and the role of the cofactor *per se* [176, 180–182]. None of these were intended to be produced *in vivo* in the bacterial vitamin production. In order to design and evaluate compounds which are dynamically metabolized in the exclusive bacterial vitamin pathway, this study represents the first approach targeting the bacterial thiazole kinase ThiM. By this means it is attempted to infiltrate the bacterial *de novo* vitamin production *in vivo* and block the vitamin dependent enzymes in consequence.

Based on aforementioned studies it is known that modifications of the positively charged thiazole ring of TDP can lead to very potent inhibitors of the cofactor dependent enzymes. This is exemplified by the variants thiamine 2-thiazolone diphosphate, where the hydrogen at the C2 position (compare Figure 25) in the thiazole ring has been replaced by an oxygen atom, or thiamine 2-thiothiazolone diphosphate, on the contrary where the hydrogen was replaced by a sulfur atom inhibiting the E1 component of pyruvate dehydrogenase (PDH) of *E. coli* [322]. The binding of the thiamine 2-thiazolone diphosphate to PDH E1 of *E. coli* (PDB code: 1RP7) is suspected to be tighter due to the formation of additional hydrogen bonds and therefore hinders the functionality of PDH [180]. Interestingly, a further thiamine analog, the 3-deazathiamine diphosphate, where the N3 in the thiazole ring is replaced by a carbon atom resulting in a neutral thiophene ring, demonstrates an irreversible inhibition of *Zymomonas mobilis* pyruvate decarboxylase [182].

In comparison with the natural thiazole moiety in thiamine the compounds used in this study consistently lack the sulfur, which is replaced by a carbon atom. The nitrogen in position 07 is retained and a second nitrogen atom is included in cpd1 and cpd2 at position 06 and 04, respectively. Moreover, in cpd1 two additional methyl groups were added to atom 05 and 06, according to the consensus nomenclature as stated in Figure 14.

In cpd1 this modification leads to a stable aromatic heterocycle, a pyrazole, with more hydrophobic interaction potential due to the addition of two methyl groups. If cpd1 would be fused to the HMP moiety, it can possibly create extra hydrophobic interactions in cofactor dependent enzymes and therefore act as a competitive inhibitor. In both compounds the sulfur was exchanged to a carbon atom which might lead to a higher flexibility in the active site as a consequence of the smaller van der Waals radius. Cpd2 has an additional nitrogen atom in position 04, resulting in an imidazole ring, and could undergo TDP imino tautomerization after HMP-fusion like cpd1. Perhaps the additional nitrogen in position 04 of the heterocycle could also mediate an extra hydrogen bond in cofactor dependent enzymes. Noteworthy, this compound possesses a heterocycle structure analogous to the known antibiotic metronidazole, which has an additional nitrogen group at the heterocycle in position 01. This substance is known to be interchanged in thiamine via thiaminase, TenA in MRSA, which is responsible for thiamine hydrolysis in bacterial metabolism. This substitution results in a thiamine antagonist tested on baker's yeast TPK equally potent to the known antagonist pyrithiamine [323]. Pyrithiamine is an isosteric pyridine analog of thiamine, where the thiazole moiety is exchanged by a pyridine ring.

It has been shown that the selected compounds are effectively phosphorylated by ThiM and the overall positioning in the active site is equivalent to the natural substrate THZ. In future, especially the acceptance of the phosphorylated THZ analogs by ThiE should be addressed to analyze the efficient fusion of HMP and THZ to thiamine-monophosphate. Moreover, metabolizable compound

analogues from the aminopyrimidine moiety, processed by ThiD, could be investigated on structural basis and result in a further starting point to develop *in vivo* generated thiamine analogues. Bacimethrin, an analogue of the HMP, which is a natural product from gram-positive bacteria like *Streptomyces albus* and *Bacillus megaterium* [324], shows an inhibitory effect on thiamine dependent enzymes in *E. coli*. Examples for this are the α -ketoglutarate dehydrogenase, transketolase and deoxy-D-xylulose-5-phosphate synthase [325] after its phosphorylation via ThiD and condensation to the antimetabolite 2'-methoxy-thiamine diphosphate. This clearly demonstrates that the poisoning of the thiamine production in bacteria is a biological strategy already used by bacteria in nature and could serve as a promising approach for inhibition of essential cofactor dependent pathways.

Further structural studies will help to improve compound accuracy to reliably infiltrate cofactor build-up and could lead to an intrinsically produced inactive cofactor, which will preferably block multiple cofactor dependent bacterial enzymes and in addition will perhaps also block the thiamine riboswitch in bacteria [166]. Here the first steps are presented towards a development of a prodrug-like thiamine analogue, specifically produced in bacteria cells *in vivo*, and which could potentially open the route for the development of new antimicrobial substances.

2 Cpd12 - a halogenated compound specifically unfolds *S. aureus* ThiM

In former studies cpd12 showed an inhibitory effect on *S. aureus* ThiM, with a higher affinity for cpd12 ($K_i = 17 \pm 4 \mu\text{M}$) compared to THZ ($K_M = 44 \pm 5 \mu\text{M}$). This unexpected effect of cpd12, which was also *in silico* selected as a potential substrate analogue of THZ, resulted in two supposed binding sites after a second *in silico* docking: One is very close to the possible ATP binding site between β_3 -strand, α -helix 3 and α -helix 5 and the other was predicted in the loop between α -helix 8 and α -helix 9. The first one suggests a possible block of the active site and the second one led to the assumption of a specific conformational change in the folding, which results in an inhibitory mechanism [298].

In this study a concentration as well as time dependent partial unfolding of *S. aureus* ThiM upon cpd12 addition could be elucidated. The loss of folding was observed on basis of the circular dichroism signal and could be further affirmed through the observation of the enhanced aggregation identified in the DLS analysis over time (chapter IV 1.4). These observations and the absence of this effect through the control with the protein BSA suggest a specific effect on the thiazole kinase.

Perhaps the bromine atom fused to the oxazole ring in cpd12 (chemical structure integrated in Table 25) could participate in a very specific halogen bond in a ThiM-cpd12 protein ligand complex. This distinct halogen bonding could be formed if the bromine acts as a Lewis acid and an electron donor, like the oxygen of the side chain of a serine or any main chain carbonyl group from the

peptide bond, could function as a Lewis base. Furthermore, also the sulfur in methionine and cysteine but also nitrogen in histidine and conjugated π systems from tyrosine, phenylalanine or tryptophan can interact with halogens via electrostatically driven halogen bonding [326–328].

In chemical biology, medicinal chemistry and especially compound library design halogens are becoming more and more focused due to their capability to enhance specificity of compound binding, like a brominated anticancer inhibitor targeting the aminopeptidase N [329]. Even though a screen for substrate analogs was performed, this observation of a *S. aureus* ThiM specific inhibitory effect could serve as an additional approach targeting the bacterial enzyme ThiM directly.

The specific nature of the halogen bonding needs to be further elucidated to serve as a new scaffold for an inhibitor design. A crystallographic approach was not applicable so far, due to the loss of the natural fold and consequently the proteins native structure. However, epitop mapping with tryptophan-scanning (introduction of tryptophan in solvent-exposed positions and measurement of their intrinsic fluorescence) [330, 331] or site directed mutagenic studies in combination with CD- and DLS analysis might be feasible approaches to analyze the mode of action of cpd12 in future.

3 Towards dynamics - *S. aureus* ThiM nano crystallization and NPE-caged ATP complex formation

By means of the STD-NMR measurements a simultaneous binding of NPE-caged ATP and THZ within *S. aureus* ThiM's active site could be confirmed, albeit the two crystallization conditions used for THZ and compound crystallization were not suitable for co-crystallization of NPE-caged ATP with ThiM or to soak the caged compound in combination with THZ into ThiM. Based on the results of the STD-NMR measurements parallel binding of THZ and NPE-caged ATP could be confirmed. Perhaps changes in crystal formation are accredited to partial changes in the folding upon nucleotide binding. Furthermore, limited solubility of the caged compounds in the respective precipitant and crystallization solution could interfere with effective soaking into ThiM crystals [321]. The onwards screening for further crystallization conditions revealed a promising condition (0.2 M ammonium sulfate, 0.1 M MES pH 6.5, 30 % (w/v) PEG 5000 MME), which needs some optimization to enhance diffracting capacity and will then serve as a valuable approach in future experiments.

Auxiliary, a vital basis for producing ThiM crystals in a defined nano-scale size necessary for further serial crystallography applications was produced by using the XtalController technology. This initial experimental condition for ThiM nano crystal formation provides the crucial basis for revealing the phosphorylation mechanisms in the major class of ribokinase-like kinases and opens a route to further optimize rational drug development processes.

4 Analysis of *S. aureus* TPK in complex with thiamine

After optimization of the protein purification and stabilization in magnesium salt buffer, a structural model of *S. aureus* TPK was solved to a high resolution of 1.4 Å in complex with its natural ligand thiamine. The data reveal a dimeric assembly, already postulated from SAXS analysis [298]. Upon *S. aureus* TPK dimer formation 15 % of the total solvent accessible area is buried (IV 2.4). This suits well with the examination of the surface accessible area buried upon a general dimer formation, which is generally assumed between 6.5 and 29.4 % [332].

The ligand, thiamine, adopts a low energy F-conformation in TPK, which is known for enzymes activating but not utilizing thiamine as a cofactor [305]. The binding is stabilized via fourteen polar and nonpolar interactions in the interface region of two monomers.

The analysis of the sequence and structure of *S. aureus* TPK reveals a highly conserved ligand binding in bacteria compared to its closest structurally characterized homologues from *E. coli* and *B. subtilis*. In *B. subtilis* only one residue responsible for the thiamine binding is exchanged (D75Q). On the contrary, comparing the sequence and structures of the structural analyzed closest monocellular eukaryote, yeast [309], as well as the eukaryotic representatives, mouse [306] and human [307, 308], reveals a highly conserved overall fold and a comparable composition of a $\alpha\beta$ -domain and a β -domain, but a less rigid conservation of the amino acid composition responsible for thiamine recognition (chapter IV 2.6).

Based on the examination of the natural substrate binding site in *S. aureus* TPK, an estimation of the probable ability to accept and thus activate thiamine substrate analogs, consisting of cpd1 and cpd2, could be presumed. Generally, an activation of the analogs is likely, even if maybe some sterically hindering of the additional methyl group at atom O6 (consensus nomenclature, stated in Figure 14) in cpd1 can arise. Furthermore, taking the results of the overall similar half-open cleft-architecture shown for mouse TPK and the results of Liu and colleagues [306] into consideration, which clearly confirmed the binding of pyrithiamine into mouse TPK, an acceptance of a component with a larger THZ moiety, like in cpd1, can be expected.

Additionally, it was possible to optimize highly uniform needle shaped crystals of *S. aureus* TPK in the presence of the natural substrate and to verify their diffraction capacity with powder diffraction. Onozuka and colleagues [333] postulated an enzymatic ping pong mechanism for human TPK. In terms of this mechanism, firstly ATP binds and donates its pyrophosphoryl group to the enzyme, generating a phosphor-enzyme intermediate and secondly a transfer to the onward bound substrate occurs after release of the nucleotide [334]. However, quite the opposite is demonstrated by the ternary complex of pyrithiamine pyrophosphate, Mg^{2+} , AMP and mouse TPK observed by Liu and colleagues [306].

On the basis of the well-defined micro crystals, an experimental setup for serial X-ray crystallography could be established in future to elucidate the enzymes mechanism in pump-probe experiments with caged nucleotide analogs. Revealing the mechanistics behind the pyrophosphorylation of thiamine and thus the activation of the precious cofactor would be of great interest for analyzing the mode of action of this specific enzyme class.

The structural knowledge about the substrate recognition and delimitation against the eukaryotic representatives gives an excellent basis for encouraging further compound design of the suicide drug approach or might serve as the basis for a species-specific approach of targeting *S. aureus* TPK directly. For *Saccharomyces cerevisiae* [335] and *Saccharomyces pombe* [336] it is known that null mutation of TPK is lethal. Thus, if *S. aureus* ThiE fuses the selected THZ analog compounds *in vivo* and the resulting thiamine analogs would block TPK in *S. aureus* directly, also this altered inhibitory mechanism could be bacteria specific and valuable. Perhaps the bacteria could counteract compounds that directly target vitamin metabolism enzymes by single mutation or by enhancing basal gene expression, but the implicated disadvantage in cost of protein production and possible deficiency in growth will perhaps show an antibiotic effect as well.

The knowledge of the enzyme, specifically activating thiamine in *S. aureus* and thus regulating the homeostasis in the bacteria, presents the structural basis for further rational suicide compound and drug development and provides positive evidence of the concept of infiltrating the B₁ metabolism with THZ analogs.

5 Structure analysis of *S. aureus* PdxK - Peptidomimetics targeting *S. aureus* PdxK

In this study the high resolution structural model of *S. aureus* PdxK could be determined and the dimeric assembly in solution could be verified with SAXS analysis. The *ab initio* model of the biological dimer out of the SAXS analysis fits the experimental data quite well with a χ -value of 1.152 and the high resolution model superimposes very well with the *ab initio* model. Merely the C-terminus, which has a higher degree of freedom in solution in contrary to the crystal, has a larger impact on the *ab initio* model (Figure 31).

S. aureus PdxK shows the classical ribokinase superfamily fold and belongs to the Rossmann-like fold group. On the basis of the homolog bacterial enzymes from *B. subtilis* ligated with ADP and the structure of pyridoxal kinase from *E. coli* in complex with pyridoxal, a binding site analysis has been conducted and revealed a binding of the C-terminal TEV protease recognition site into the proposed active site region. No magnesium ion in the region of the substrate binding could be observed as magnesium was included neither in the protein buffer nor in the precipitant solution.

Although the structure was solved from Nodwell and colleagues [222] in 2014 as well, their results in combination with the observed binding of the C-terminal TEV protease recognition peptide into the active site in the crystallographic studies provide a very interesting starting point to analyze probable competitive binding peptides as possible inhibitors in future. In the study of Nodwell *et al.* *S. aureus* PdxK was solved natively and in complex with PL, AMP-PCP, ADP and PL and AMP-PCP simultaneously. Their work elucidated that a cysteine (C110) in the loop region V109 to E115, adjacent to the catalytic cysteine 214 in the anion hole, is mandatory for the PL phosphorylation due to a charge relay network. They found that the C110 forms a hemithioacetal with the 4'-aldehyde of PL after the loop closure (V109 to E115) upon substrate binding. Further, they could elucidate that this cysteine is conserved in the bacterial dual-function ribokinase subfamily and introduced the term of CC-PL-kinases. Finally, they proposed that this cysteine represents the target amino acid of the natural product antibiotic rugulactone [337].

The comparison of the PdxK structural model from Nodwell *et al.* with the model presented in this work revealed, that the overall fold and especially active site architecture is not biased by the binding of the C-terminal peptide of a neighboring PdxK molecule. The binding of the C-terminus, which was highly conserved in both structures, just varies in the orientation of the tyrosine 280. A peptide that specifically binds to this defined region of the protein would thus either lead to a competitive inhibition of PdxK due to replacement or displacement of the substrate, or would destabilize the reaction towards PL because of the prevention of the hemithioacetal formation. Interestingly, it should be noted that in the preparation of crystal I for structure I (chapter IV 3.3) also 0.75 mM pyridoxine (molar ratio of protein to ligand = 1 : 4.7) was included and in spite of the natural substrate the 'peptide' was bound into the active site.

Moreover, it should be noted that the highly hydrophobic character of the 'peptidic substrate', and thus its stabilization through hydrophobic interactions as well as two hydrogen bonds in the active site, is in good agreement with the strong hydrophobic binding of ginkgotoxin (4'-O-methylpyridoxine), a known competitive inhibitor of human and *T. brucei* PdxK, (pdb code: 4EN4 in human PdxK) [243, 338, 339].

Consequently, the observed very specific binding of the C-terminus into the active site - firstly recognized as a crystallographic artifact - could serve as an approach to design and evaluate possible peptidomimetic compounds. In this study the *in silico* analysis of five peptides is presented and their binding and potential inhibitory effect on *S. aureus* PdxK needs now further emphasis by *in vitro* assaying. A binding analysis with label-dependent MST analysis was not suitable. Perhaps isothermal titration calorimetry (ITC) or competitive phosphorylation assays are suitable to determine binding and activity in presence of the apparent inhibitory peptidic compounds.

The observation made upon the crystallization studies could result in a very new approach in directly targeting PL-kinases like *S. aureus* PdxK. An onwards design of compounds, specifically interfering with the hemithioacetal formation, could be a conceivably follow-up approach for specifically targeting *S. aureus* PdxK.

6 Analyzing substrate promiscuity of *S. aureus* PdxK and ThiD

The K_m of *S. aureus* PdxK towards pyridoxal was determined to be $2333 \pm 371 \mu\text{M}$. This is comparable to the K_m determined by Nodwell *et al.* for pyridoxine ($2072 \pm 332 \mu\text{M}$), but contradictory to the K_m determined by them towards PL, which was $111 \pm 53 \mu\text{M}$ [222]. Additionally, they also determined the activity towards HMP and determined a K_m of $1998 \pm 268 \mu\text{M}$. The significant difference of the K_m evaluation could perhaps be attributed to the different experimental setups. In contrast to Nodwell *et al.*, who used a pyruvate kinase/lactate dehydrogenase coupled assay with N-terminally Strep-tagged *S. aureus* PdxK [222], in this study the formation of pyridoxal 5'-phosphate was monitored by the change in absorbance at 388 nm using C-terminal TEV His₆-tagged *S. aureus* PdxK. Furthermore, results presented here were obtained in a buffer containing 70 mM potassium phosphate (pH 6.5) and 10 mM magnesium chloride at 30 °C, whereas Nodwell *et al.* used a setup at 37 °C in a buffer containing 50 mM Tris (pH 8.0), 50 mM potassium chloride and 10 mM magnesium chloride. Certainly it is known that magnesium is needed by the kinases for catalysis, but also that the monovalent ion K^+ and Na^+ could considerably modify the activity of human and *E. coli* PdxK in enzymatic *in vitro* assays [216, 307, 308]. Perhaps the different ion content, as well as the changed temperature and pH, could explain the different K_m values obtained.

The acceptance of both, the B₆ vitamer substrate and HMP, is also known for *Plasmodium falciparum* PdxK [227], *E. coli* PdxK [228, 229], *Trypanosoma brucei* PdxK [230] and the *thiD* gene product from *B. subtilis* [231]. With the intention of specifically targeting the B₁ metabolism in bacteria and particularly in *S. aureus*, an analysis of PdxK's bifunctionality and the structural setup for the refusal on HMPP is necessary to allow further differentiation of potential interplay and correlation between these two crucial metabolisms. Particularly, if a second substrate infiltration, like the one in ThiM, into the bacterial B₁ metabolism via ThiD is addressed, a deeper understanding of the evolutionary determinants and structural delimitations to border the enzymes participating in the vitamin B₁ and B₆ metabolisms need to be specified. But also targeting a B₆ kinase with inhibitory peptides by the peptidomimetic approach and facing the disparity between PdxK and the HMP-kinase ThiD needs to be known.

Four amino acids responsible for accurate substrate recognition and discrimination towards HMP and especially HMPP in *S. aureus* PdxK (S12, H51, M80 and N252) could be identified after the structure determination and evaluation by *in silico* modeling. Serine 12, histidine 51 and

methionine 80 are assumed to be directly involved in the substrate preference towards HMP or B₆ vitamers and were selected for site directed mutagenesis to alanine, valine or glutamine and alanine, respectively. Residue asparagine 252 was assumed to restrict the enzyme to the first phosphorylation and enhance the refusal of the second phosphorylation regularly performed by ThiD during vitamin B₁ *de novo* synthesis. The selected residues are in accordance to a later published study of Castro-Fernandez and colleagues [230], which revealed by *in silico* analysis and enzymatic characterization how bifunctionality towards HMP and PL emerged in a convergent evolutionary process. The mentioned amino acids were exchanged in *S. aureus* PdxK as noted in chapter IV 3.5 and their recombinant expression capability was successfully analyzed. Additionally, alanine 212 and cysteine 214 were mutated to analyze the influence of the composition of the active site residues on the substrate turnover. In future, activity studies will elucidate the significance assumed for the bifunctional substrate recognition of HMP, HMPP and B₆ vitamers. They will also clarify the promiscuous capability of diphosphorylated substrates and will support future rational drug developments.

7 Structure analysis of *T. cruzi* PdxK - Analyzing the evolution and conservation of Vitamin B₆ activating enzymes

With the structural analysis of the *T. cruzi* PdxK the evolutionary pathway in the ribokinase superfamily and especially within the PdxK subgroup could be studied. *T. cruzi* PdxK also shows the classical ribokinase superfamily fold and could be identified dimeric in solution, based on the results of the size exclusion chromatography and the DLS analysis. The dimeric assembly in the high resolution structure could be constructed applying crystallographic symmetry. The loop between amino acid 124 and 127 could not be resolved; upon substrate binding it might serve as a small flap together with the adjacent residues, like in other vitamin B₆ kinases. It is four amino acids shorter compared to the human loop and thus is not being expected to form a longer two stranded β -sheet covering the active site. The active site composition was compared to the human and *T. brucei* PdxK and even if the differences are small the structural knowledge could be valuable for further drug development.

In a recent study in 2014, Kimura and colleagues elucidated that *T. cruzi* PdxK is a possible target of primaquine, a quinoline used for treatment of trypanosomiasis [244]. Based on the structure, presented in this study, a further analysis of the observed inhibitory effect might also serve as a vital basis for further drug developments targeting trypanosomiasis. Currently the structural data are used for *in silico* selection and docking of possible lead structures to specifically inhibit the crucial vitamin metabolism in *T. cruzi*.

Furthermore, *T. cruzi*, a monocellular parasitic flagellate protozoan, could provide more knowledge about the evolutionary link between eukaryotic PdxKs as well as *S. aureus* PdxK and ThiD structures. A sequence comparison (Figure 49) of *S. aureus* PdxK, ThiD, *T. cruzi* PdxK and human PdxK revealed that the conservation of the substrate determining residues is low, only the valine 107 (*S. aureus* PdxK numbering) is identical. All proteins show a highly conserved fold, but the hemithioacetal forming cysteine, like in *S. aureus* PdxK, is missing in *T. cruzi* and human PdxK. On basis of this fundamental data from *T. cruzi*, a further differentiation of the bacterial salvage pathway will be achievable and a bordering of the evolutionary developments within these specific kinases, producing the very reactive and ubiquitary necessitated cofactor, is possible.

8 Outlook: Mining the bacterial vitamin B₁ metabolism and B₆ salvage for advanced structural based drug developments

The identification of highly conserved residues, the characterization of the general structural setup and the discrimination of residues that are uniquely present in the active site of a target structure is a central task in structure-based drug design. Aiming to target the unique vitamin B₁ metabolism in *S. aureus* to generate *in vivo* produced non-functional thiamine analogs needs the structural knowledge of the participating enzymes as well as the biological closely related enzymes from other species.

Especially the interplay between B₁ metabolism and B₆ salvage pathway are in focus and need detailed investigations to differentiate the metabolization preferences to analyze bacterial possibilities to circumvent the pharmacological strategy and to estimate potential side effects.

In order to validate and generate target specific chemical scaffolds in future, which specifically mask a cofactor and will block the dependent enzymes, like NTZ, information of these dependent enzymes is needed and will then open the route for the design of bacteria specific new antibiotics with a great innovation potential.

This study contributes to these aims by elucidating two substrate analog enzyme complexes of THZ-kinase ThiM, revealing the structure of TPK with its natural substrate thiamine and an estimation of the acceptance of the first selected compounds of this enzyme. Furthermore, a differentiation of the vitamin B₁ metabolism from the related B₆ salvage pathway in *S. aureus* and analysis of the substrate preferences is made and could give first hints about the interplay of both vitamin metabolisms in *S. aureus*. Moreover, the structural analysis of PdxK from the monocellular eukaryotic protozoan *T. cruzi* gives an additional basis to border species specific characteristics, which will help to estimate side effects of onwards developed strategies and small molecules.

Studies on the substrate specificity of PdxK will be the basis to discriminate and estimate possible side effects of targeting either the vitamin B₁ metabolism or B₆ salvage pathway. With the structural information obtained in this study it is feasible to further define and distinguish between bacterial and eukaryotic target structures. Additionally, with the coincidental block of the active site in the crystal structure of *S. aureus* PdxK, a further route of targeting this essential bacterial enzyme by specific inhibitors might arise.

Still the structural information of ThiD, ThiE and the GTPase from the vitamin B₁ metabolism are missing and a recombinant expression of these genes in *E. coli* did not seem feasible. However, all proteins of the vitamin B₁ metabolism seem to express in insect cells and this expression system can be applied henceforth. As some of the proteins show degradation perhaps an optimizing in expression duration and further purification is needed. In this study also the possibility to encourage crystal formation by the channeling of proteins to peroxisomes was tested. Two effects are used by this specific protein channeling: First the local concentration is increased and second the cellular compartment serves as an additional crystallization environment. In the first tests no positive effects could be observed by this directed localization of the recombinant protein in *Sf9* cells. Furthermore, no enhancing effect of adding DMSO or sodium butyrate to the Cathepsin B expression could be observed in this study, but this will need further tests. Cathepsin B production is already at a limit, maybe a positive effect will be observed for other targets with lower basal expression. In future, this needs additional statistical analysis and could serve as a vital basis for further optimization of the *in vivo* production of protein crystals in *Sf9* cells.

Supplementary structural analysis of the enzymes in the B₁ metabolism and also especially of the further player in the B₆ salvage pathway, like PNPOx, will be central for the future developments in specifically targeting the pathways in *S. aureus*.

The aimed specific targeting either of the vitamin B₁ metabolism or the B₆ salvage pathway in *S. aureus* would be an innovative method of filling the innovation gap in the antibiotic development towards MRSA.

VI Summary

Just 72 years after the mass production of the first broad spectrum antibiotic penicillin started *Staphylococcus aureus* represents a daunting global threat again. In the golden era of the antibiotic development the drug pipeline fighting this and other human pathogenic bacteria was filled repeatedly to combat the ongoing bacterial resistant development and spread. However, in the late 1980's an ongoing discovery void in antibiotic development began, missing innovative novel targets, and the risk of entering a post-antibiotic era is evident these days.

In this study a promising new strategy is presented, which uses the bacterial vitamin B₁ *de novo* biosynthesis, that is entirely absent in humans. In the course of this approach substrate analogs, also termed 'suicide drugs' are channeled into the bacterial metabolism and will finally, after a set of metabolization steps, block a specific variety of cofactor dependent enzymes inside the bacterium as an inactive cofactor. This uncouples the site of drug infiltration and target action and entails multiple downstream effects.

The structure of *S. aureus* ThiM in complex with two of these substrate analogs was solved via X-ray crystallography. Furthermore ThiM was successfully evaluated for its binding of NPE-caged ATP via STD-NMR, which could serve, in combination with an initially controlled rational crystallization conducted in the XtalController900, as a serial X-ray crystallographic pump-probe approach in future. Additionally, the mode of action of a former identified inhibitor of ThiM was elucidated. Moreover, the structure of TPK in complex with its natural ligand thiamine was solved. This allowed the analysis of possible thiamine analogs, build up out of the two promising substrate analogs studied for ThiM, incorporation.

Furthermore, the structures of *S. aureus* and the monocellular eukaryotic protozoan *Trypanosoma cruzi* vitamin B₆ kinase – PdxK were solved to high resolution via X-ray crystallography and *S. aureus* PdxK structure was analyzed in solution via small angle X-ray scattering. The structural analysis allowed the differentiation of PdxK, which also shows promiscuous activity towards the first substrate of the kinase ThiD, which is an essential kinase for the HMP feeding into the vitamin B₁ metabolism in *S. aureus*. Based on these results the interplay of the metabolisms and the structural delimitation can now be further studied and will highlight the evolutionary relations.

Beyond that, a pepdimometric approach targeting PdxK could be followed on basis of the crystallization result of *S. aureus* PdxK and could reveal an innovative possibility of inhibiting these kinases. Furthermore, an additional expression system using insect cells was tested and all proteins of the vitamin B₁ and B₆ pathways were successfully produced. In summary this work provides valuable information for the development of innovative antibiotic substances based on proteins' structural data to specifically target MRSA.

VII Zusammenfassung

Nur 72 Jahre nach Beginn der Massenproduktion des ersten Breitbandantibiotikums Penicillin stellt *Staphylococcus aureus* wieder eine kritische globale Bedrohung dar. Im goldenen Zeitalter der Antibiotikaentwicklung wurde die Medikamenten-Pipeline zur Behandlung dieses und anderer humanpathogener Bakterien regelmäßig gefüllt, um der Entwicklung und Verbreitung bakterieller Resistenzen begegnen zu können. Seit Ende der 1980er Jahre hingegen ist die Entwicklung in der Antibiotikaforschung defizitär und innovative Targets fehlen, sodass heute das Risiko einer post-antibiotischen Ära evident ist.

Diese Arbeit präsentiert eine neue, aussichtsreiche Strategie, die auf die bakterielle Vitamin B₁ (Thiamin) *de novo* Biosynthese, welche beim Menschen nicht vorkommt, abzielt. Hierzu werden Substrat-Analoga - „Suicide Drugs“ - in den bakteriellen Metabolismus eingeschleust und führen letztlich, nach mehreren Metabolisierungsschritten als inaktive Co-Faktoren zur Blockade multipler Co-Faktor-abhängiger Enzyme im Bakterium. Auf diese Weise werden der Wirkstoff-Eintrittsort und der Wirkort voneinander entkoppelt.

Die Struktur von *S. aureus* ThiM im Komplex mit zweien dieser Substrat-Analoga konnte via Protein-Kristallographie bestimmt werden. Außerdem konnte ThiM erfolgreich auf sein Potenzial, NPE-caged ATP via STD-NMR zu binden, untersucht werden. Dieses könnte zukünftig - in Kombination mit dem evaluierten, kontrollierten Kristallisierungs-Setup mittels XtalController900 - für serielle röntgenkristallographische Pump-Probe-Experimente genutzt werden. Zusätzlich konnte die Wirkungsweise eines bereits zuvor identifizierten Inhibitors von ThiM näher analysiert werden.

Des Weiteren wurde die Struktur von TPK im Komplex mit seinem natürlichen Liganden mittels Protein-Kristallographie gelöst. Auf dieser Basis konnte die Akzeptanz möglicher Thiamin-Analoga, hergestellt aus den zwei für ThiM untersuchten Substrat-Analoga, strukturell untersucht werden.

Weiterhin wurde die Struktur der Vitamin B₆ Kinase (PdxK) aus *S. aureus* und des eukaryotischen Protozoen *Trypanosoma cruzi* mittels Protein-Kristallographie gelöst und zusätzlich die *S. aureus* PdxK Struktur in Lösung mittels SAXS überprüft.

Die strukturelle Analyse erlaubt nun die Untersuchung der Substratspezifität von PdxK, welche gegenüber dem ersten Substrat (HMP) der Kinase ThiD, das die HMP-Zufuhr im Vitamin B₁ Metabolismus in *S. aureus* sicher stellt, ebenfalls Aktivität zeigt. Auf Basis dieser Ergebnisse kann nun das Zusammenspiel des B₁ und B₆ Metabolismus sowie die strukturelle Differenzierung weiter untersucht und die evolutionären Verbindungen analysiert werden.

Darüber hinaus kann auf Basis der Kristallisationsergebnisse von *S. aureus* PdxK ein auf PdxK zielender peptidometrischer Ansatz verfolgt werden und innovative Möglichkeiten der Blockade

dieser spezifischen Kinasen bieten. Ferner wurde zusätzlich ein Expressionssystem unter Nutzung von Insektenzellen getestet, bei welchem sämtliche *S. aureus* Proteine des Vitamin B₁ Metabolismus und PdxK erfolgreich produziert werden konnten. Zusammenfassend bietet diese Arbeit wertvolle Informationen für die rationale Entwicklung innovativer antibiotischer Substanzen basierend auf strukturellen Daten, um MRSA spezifisch zu targetieren.

VIII References

1. Clifton CE: **Large-Scale Production of Penicillin.** *Science* 1943, **98**:69–70.
2. Fleming A: **The Nobel Prize in Physiology or Medicine 1945.** *nobelprize.org. Nobel Media AB 2014. accessed 19.03.2015.* <http://www.nobelprize.org/nobel_prizes/medicine/laureates/1945/> .
3. D’Costa VM, McGrann KM, Hughes DW, Wright GD: **Sampling the antibiotic resistome.** *Science* 2006, **311**(January):374–377.
4. Barbosa TM, Levy SB: **The impact of antibiotic use on resistance development and persistence.** *Drug Resist Updat* 2000, **3**:303–311.
5. Alekshun MN, Levy SB: **Molecular Mechanisms of Antibacterial Multidrug Resistance.** *Cell* 2007, **128**:1037–1050.
6. Beatson SA, Walker MJ: **Tracking antibiotic resistance.** *Science (80-)* 2014, **345**:1454–1455.
7. Heinemann J a.: **How antibiotics cause antibiotic resistance.** *Drug Discov Today* 1999, **4**:72–79.
8. Levy S: **Antibiotic Resistance: The Antibiotic Paradox: How the Misuse of Antibiotics Destroys Their Curative Powers.** *JAMA* 2002, **288**:2898.
9. Palumbi SR: **Humans as the World ’ s Greatest Evolutionary Force The Pace of Human-Induced Evolution.** *Science (80-)* 2001, **293**(September):1786–1790.
10. Grundmann H, Aires-de-Sousa M, Boyce J, Tiemersma E: **Emergence and resurgence of meticillin-resistant *Staphylococcus aureus* as a public-health threat.** *Lancet* 2006, **368**:874–85.
11. Gonzales R, Steiner JF, Sande M a: **Antibiotic prescribing for adults with colds, upper respiratory tract infections, and bronchitis by ambulatory care physicians.** *JAMA* 1997, **278**:901–904.
12. Colgan R, Powers JH: **Appropriate antimicrobial prescribing: Approaches that limit antibiotic resistance.** *Am Fam Physician* 2001, **64**:999–1004.
13. Spellberg B, Powers JH, Brass EP, Miller LG, Edwards JE: **Trends in antimicrobial drug development: implications for the future.** *Clin Infect Dis* 2004, **38**:1279–1286.
14. Spellberg B, Bartlett J, Wunderink R, Gilbert DN: **Novel Approaches Are Needed to Develop Tomorrow’s Antibacterial Therapies.** *Am J Respir Crit Care Med* 2015, **191**:135–140.
15. Wagstaff B: **Impact of antibiotic restrictions: the patient’s perspective.** *Clin Microbiol Infect* 2006, **12**:10–15.
16. Wegener HC: **Antibiotics in animal feed and their role in resistance development.** *Curr Opin Microbiol* 2003, **6**:439–445.
17. Martinez JL: **Environmental pollution by antibiotics and by antibiotic resistance determinants.** *Environ Pollut* 2009, **157**:2893–902.
18. Silver LL: **Challenges of antibacterial discovery.** *Clin Microbiol Rev* 2011, **24**:71–109.

19. WHO: **ANTIMICROBIAL RESISTANCE Global Report on Surveillance 2014**. *who.int World Health Organization* 2014 accessed 12.03.2015. <<http://www.who.int/drugresistance/documents/surveillance-report/en/>> 2014.
20. Fischbach MA, Walsh CT: **Antibiotics for emerging pathogens**. *Science* 2009, **325**:1089–1093.
21. Falagas ME, Bliziotis IA, Kasiakou SK, Samonis G, Athanassopoulou P, Michalopoulos A: **Outcome of infections due to pandrug-resistant (PDR) Gram-negative bacteria**. *BMC Infect Dis* 2005, **5**:24.
22. O'Neill J: **Review on Antimicrobial Resistance. Antimicrobial Resistance: Tackling a Crisis for the Health and Wealth of Nations**. *amr-review.org* 2014 accessed 05.05.2015 <<http://amr-review.org/>> 2014(December).
23. Smith R, Coast J: **The true cost of antimicrobial resistance**. *BMJ Br Med J* 2013, **346**:1–5.
24. WHO: **Antimicrobial drug resistance - Report by the Secretariat**. *who.int World Health Organization* 2014. accessed 12.03.2015. <http://apps.who.int/gb/ebwha/pdf_files/WHA67/A67_39-en.pdf> 2014:1–5.
25. WHO: **World Health Assembly addresses antimicrobial resistance, immunization gaps and malnutrition**. *who.int* accessed 15.06.2015 <<http://www.who.int/mediacentre/news/releases/2015/wha-25-may-2015/en/>> 2015:who.int.
26. Newsom SWB: **Ogston's coccus**. *J Hosp Infect* 2008, **70**:369–372.
27. Kluytmans JAN, Verbrugh H: **Nasal Carriage of Staphylococcus aureus: Epidemiology, Underlying Mechanisms and Associated Risks**. 1997, **10**:505–520.
28. Peacock SJ, De Silva I, Lowy FD: **What determines nasal carriage of Staphylococcus aureus?** *Trends Microbiol* 2001, **9**:605–610.
29. Gorwitz RJ, Kruszon-Moran D, McAllister SK, McQuillan G, McDougal LK, Fosheim GE, Jensen BJ, Killgore G, Tenover FC, Kuehnert MJ: **Changes in the prevalence of nasal colonization with Staphylococcus aureus in the United States, 2001–2004**. *J Infect Dis* 2008, **197**:1226–1234.
30. Foster TJ: **Immune evasion by staphylococci**. *Nat Rev Microbiol* 2005, **3**:948–958.
31. Miller LG, Perdreau-Remington F, Rieg G, Mehdi S, Perlroth J, Bayer AS, Tang AW, Phung TO, Spellberg B: **Necrotizing fasciitis caused by community-associated methicillin-resistant Staphylococcus aureus in Los Angeles**. *N Engl J Med* 2005, **352**:1445–1453.
32. Bisno AL, Stevens DL: **Streptococcal Infections of Skin and Soft Tissues**. *N Engl J Med* 1996, **334**:240–246.
33. Kluytmans JAJW, Mouton JW, Ijzerman EPF, Vandenbroucke-Grauls CMJE, Maat AWPM, Wagenvoort JHT, Verbrugh HA: **Nasal Carriage Of Staphylococcus aureus As A Major Risk Factor For Wound Infections After Cardiac Surgery**. *J Infect Dis* 1995, **171**:216–219.
34. Von Eiff C, Becker K, Machka K, Stammer H, Peters G: **Nasal carriage as a source of Staphylococcus aureus bacteremia**. *N Engl J Med* 2001, **344**:11–16.
35. Morell E a., Balkin DM: **Methicillin-resistant Staphylococcus aureus: A pervasive pathogen highlights the need for new antimicrobial development**. *Yale J Biol Med* 2010, **83**:223–233.
36. Wenzel RP, Perl TM: **The significance of nasal carriage of Staphylococcus aureus and the incidence of postoperative wound infection**. *J Hosp Infect* 1995, **31**:13–24.

37. Fleming A: **On the antibacterial action of cultures of a penicillium, with special reference to their use in the isolation of B. influenzae.** *Br J Exp Pathol* 1929, **10**:226–236.
38. Houbraeken J, Frisvad JC, Samson RA: **Fleming ' s penicillin producing strain is not Penicillium chrysogenum but P . rubens.** 2011, **2**:87–95.
39. Barber M, Rozwadowska-Dowzenko M: **Infection by penicillin-resistant staphylococci.** *Lancet* 1948, **2**:641–644.
40. Barber M: **Staphylococcal infection due to penicillin-resistant strains.** *Br Med J* 1947, **2**:863–5.
41. Barber M: **Methicillin-resistant staphylococci.** *J Clin Pathol* 1961, **14**:385–393.
42. Parker MT, Hewitt JH: **Methicillin resistance in Staphylococcus aureus.** *Lancet* 1970, **1**:800–804.
43. Hartman BJ, Tomasz a: **Low-affinity penicillin-binding protein associated with beta-lactam resistance in Staphylococcus aureus.** *J Bacteriol* 1984, **158**:513–516.
44. Katayama Y, Ito T, Hiramatsu K: **A new class of genetic element, staphylococcus cassette chromosome mec, encodes methicillin resistance in Staphylococcus aureus.** *Antimicrob Agents Chemother* 2000, **44**:1549–1555.
45. Wielders CLC, Vriens MR, Brisse S, De Graaf-Miltenburg LAM, Troelstra A, Fleer A, Schmitz FJ, Verhoef J, Fluit AC: **Evidence for in-vivo transfer of mecA DNA between strains of Staphylococcus aureus.** *Lancet* 2001, **357**:1674–1675.
46. Peacock JE, Marsik FJ, Wenzel RP: **Methicillin-resistant Staphylococcus aureus: Introduction and spread within a hospital.** *Ann Intern Med* 1980, **93**:526–532.
47. Walsh CT: **What are antibiotics and where do they come from?** *Antibiot Actions, Orig Resist* 2003.
48. Hiramatsu K, Hanaki H, Ino T, Yabuta K, Oguri T, Tenover FC: **Methicillin-resistant Staphylococcus aureus clinical strain with reduced vancomycin susceptibility.** *Journal of Antimicrobial Chemotherapy* 1997:135–136.
49. Shlaes DM, Shlaes JH: **Teicoplanin selects for Staphylococcus aureus that is resistant to vancomycin.** *Clin Infect Dis* 1995, **20**:1071–1073.
50. Sieradzki K, Tomasz A: **Inhibition of Cell Wall Turnover and Autolysis by Vancomycin in a Highly Vancomycin-Resistant Mutant of Staphylococcus aureus.** 1997, **179**:2557–2566.
51. Hanaki H, Labischinski H, Inaba Y, Kondo N, Murakami H, Hiramatsu K: **Increase in glutamine-non-amidated muropeptides in the peptidoglycan of vancomycin-resistant Staphylococcus aureus strain Mu50.** *J Antimicrob Chemother* 1998, **42**:315–320.
52. Hanaki H, Kuwahara-Arai K, Boyle-Vavra S, Daum RS, Labischinski H, Hiramatsu K: **Activated cell-wall synthesis is associated with vancomycin resistance in methicillin-resistant Staphylococcus aureus clinical strains Mu3 and Mu50.** *J Antimicrob Chemother* 1998, **42**:199–209.
53. Walsh TR, Howe RA: **The prevalence and mechanisms of vancomycin resistance in Staphylococcus aureus.** *Annu Rev Microbiol* 2002, **56**:657–675.
54. Blackwell A: **Teicoplanin.** *J Antimicrob Chemother* 1984, **14**:441–445.
55. CDC: **Vancomycin-resistant Staphylococcus aureus-Pennsylvania, 2002.** *MMWR Morb Mortal Wkly Rep* 2002, **51**:902.

56. Tenover FC, Biddle JW, Lancaster M V.: **Increasing resistance to vancomycin and other glycopeptides in *Staphylococcus aureus*.** *Emerg Infect Dis* 2001, **7**:327–332.
57. Tenover FC, Weigel LM, Appelbaum PC, McDougal LK, Chaitram J, McAllister S, Clark N, Killgore G, O'Hara CM, Jevitt L, Patel JB, Bozdogan B: **Vancomycin-Resistant *Staphylococcus aureus* Isolate from a Patient in Pennsylvania.** *Antimicrob Agents Chemother* 2004, **48**:275–280.
58. Smith TL, Pearson ML, Wilcox KR, Cruz C, Lancaster M V, Robinson-Dunn B, Tenover FC, Zervos MJ, Band JD, White E, Jarvis WR: **Emergence of vancomycin resistance in *Staphylococcus aureus*. Glycopeptide-Intermediate *Staphylococcus aureus* Working Group.** *N Engl J Med* 1999, **340**:493–501.
59. Chang S, Sievert DM, Hageman JC, Boulton ML, Tenover FC, Downes FP, Shah S, Rudrik JT, Pupp GR, Brown WJ, Cardo D, Fridkin SK: **Infection with vancomycin-resistant *Staphylococcus aureus* containing the *vanA* resistance gene.** *N Engl J Med* 2003, **348**:1342–1347.
60. Lowy FD: **Antimicrobial resistance: The example of *Staphylococcus aureus*.** *J Clin Invest* 2003, **111**:1265–1273.
61. González-Zorn B, Courvalin P: **VanA-mediated high level glycopeptide resistance in MRSA.** *Lancet Infect Dis* 2003, **3**:67–68.
62. Bortolaia V, Mander M, Jensen LB, Olsen JE, Guardabassi L: **Persistence of vancomycin resistance in multiple clones of *Enterococcus faecium* isolated from Danish broilers 15 years after the ban of avoparcin.** *Antimicrob Agents Chemother* 2015, **59**:AAC.05072–14.
63. Furuya EY, Lowy FD: **Antimicrobial-resistant bacteria in the community setting.** *Nat Rev Microbiol* 2006, **4**(January):36–45.
64. Baba T, Takeuchi F, Kuroda M, Yuzawa H, Aoki K, Oguchi A, Nagai Y, Iwama N, Asano K, Naimi T, Kuroda H, Cui L, Yamamoto K, Hiramatsu K: **Genome and virulence determinants of high virulence community-acquired MRSA.** *Lancet* 2002, **359**:1819–1827.
65. Gonzalez BE, Hulten KG, Dishop MK, Lamberth LB, Hammerman WA, Mason EO, Kaplan SL: **Pulmonary Manifestations in Children with Invasive Community-Acquired *Staphylococcus aureus* Infection.** 2005, **77030**(July):583–590.
66. Lina G, Piémont Y, Godail-Gamot F, Bes M, Peter MO, Gauduchon V, Vandenesch F, Etienne J: **Involvement of Panton-Valentine leukocidin-producing *Staphylococcus aureus* in primary skin infections and pneumonia.** *Clin Infect Dis* 1999, **29**:1128–1132.
67. Vandenesch F, Naimi T, Enright MC, Lina G, Nimmo GR, Heffernan H, Liassine N, Bes M, Reverdy M, Etienne J: **Community-Acquired Methicillin- Resistant *Staphylococcus aureus* Carrying Panton-Valentine Leukocidin Genes : Worldwide Emergence.** 2003, **9**.
68. Otto M: **Basis of virulence in community-associated methicillin-resistant *Staphylococcus aureus*.** *Annu Rev Microbiol* 2010, **64**:143–62.
69. Li M, Diep BA, Villaruz AE, Braughton KR, Jiang X, DeLeo FR, Chambers HF, Lu Y, Otto M: **Evolution of virulence in epidemic community-associated methicillin-resistant *Staphylococcus aureus*.** *Proc Natl Acad Sci U S A* 2009, **106**:5883–5888.
70. Wang R, Braughton KR, Kretschmer D, Bach TL, Queck SY, Li M, Kennedy AD, Dorward DW, Klebanoff SJ, Peschel A, Deleo FR, Otto M: **Identification of novel cytolytic peptides as key virulence determinants for community-associated MRSA.** 2007, **13**:1510–1514.

71. Fey PD, Rupp ME, Hinrichs SH, Davis CC, Kreiswirth BN, Schlievert PM: **Comparative Molecular Analysis of Community- or Hospital-Acquired Methicillin-Resistant Staphylococcus aureus**. *Antimicrob Agents Chemother* 2003, **47**:196–203.
72. Rooijackers SHM, Ruyken M, van Roon J, van Kessel KPM, van Strijp J a G, van Wamel WJB: **Early expression of SCIN and CHIPS drives instant immune evasion by Staphylococcus aureus**. *Cell Microbiol* 2006, **8**:1282–1293.
73. Seybold U, Kourbatova E V, Johnson JG, Halvosa SJ, Wang YF, King MD, Ray SM, Blumberg HM: **Emergence of community-associated methicillin-resistant Staphylococcus aureus USA300 genotype as a major cause of health care-associated blood stream infections**. *Clin Infect Dis* 2006, **42**:647–656.
74. Meyer E, Schröder C, Gastmeier P, Geffers C: **The reduction of nosocomial MRSA infection in Germany: an analysis of data from the Hospital Infection Surveillance System (KISS) between 2007 and 2012**. *Dtsch Arztebl Int* 2014, **111**:331–6.
75. EFSA: **Antimicrobial resistance in zoonotic and indicator bacteria from humans , animals and food in the European Union in 2012**. *EFSA J* 2014, **12**:1–336.
76. Köck R, Becker K, Cookson B, van Gemert-Pijnen JE, Harbarth S, Kluytmans J, Mielke M, Peters G, Skov RL, Struelens MJ, Tacconelli E, Navarro Torné A, Witte W, Friedrich AW: **Methicillin-resistant Staphylococcus aureus (MRSA): burden of disease and control challenges in Europe**. *Euro Surveill* 2010, **15**:19688.
77. Huijsdens XW, van Dijke BJ, Spalburg E, van Santen-Verheuve MG, Heck MEOC, Pluister GN, Voss A, Wannet WJB, de Neeling AJ: **Community-acquired MRSA and pig-farming**. *Ann Clin Microbiol Antimicrob* 2006, **5**:26.
78. Loeffler A, Kearns AM, Ellington MJ, Smith LJ, Unt VE, Lindsay JA, Pfeiffer DU, Lloyd DH: **First isolation of MRSA ST398 from UK animals: a new challenge for infection control teams?** *J Hosp Infect* 2009, **72**:269–271.
79. Wendlandt S, Kadlec K, Feßler AT, Monecke S, Ehrlich R, Van De Giessen AW, Hengeveld PD, Huijsdens X, Schwarz S, Van Duinkerken E: **Resistance phenotypes and genotypes of methicillin-resistant: Staphylococcus aureus isolates from broiler chickens at slaughter: And abattoir workers**. *J Antimicrob Chemother* 2013, **68**:2458–2463.
80. Fluit AC: **Livestock-associated Staphylococcus aureus**. *Clin Microbiol Infect* 2012, **18**:735–744.
81. Cuny C, Köck R, Witte W: **Livestock associated MRSA (LA-MRSA) and its relevance for humans in Germany**. *Int J Med Microbiol* 2013, **303**:331–337.
82. Wulf M, Voss a.: **MRSA in livestock animals - An epidemic waiting to happen?** *Clin Microbiol Infect* 2008, **14**:519–521.
83. ECDC, EMEA: **ECDC/EMEA Joint technical report The bacterial challenge : time to react**. 2009, **6 July 201**(September):54.
84. Uchil RR, Kohli GS, Katekhaye VM, Swami OC: **Strategies to combat antimicrobial resistance**. *J Clin Diagn Res* 2014, **8**:ME01–4.
85. Rupp ME, Holley HP, Lutz J, Dicpinigaitis P V., Woods CW, Levine DP, Veney N, Fowler VG: **Phase II, randomized, multicenter, double-blind, placebo-controlled trial of a polyclonal anti-Staphylococcus aureus capsular polysaccharide immune globulin in treatment of Staphylococcus aureus bacteremia**. *Antimicrob Agents Chemother* 2007, **51**:4249–4254.

86. Zhang BZ, Hua YH, Yu B, Lau CCY, Cai JP, Zheng SY, Yam WC, Kao RYT, Sze KH, Zheng BJ, Yuen KY, Huang JD: **Recombinant ESAT-6-Like Proteins Provoke Protective Immune Responses against Invasive Staphylococcus aureus Disease in a Murine Model.** *Infect Immun* 2015, **83**:339–345.
87. Baker M: **Anti-infective antibodies: finding the path forward.** *Nat Biotechnol* 2006, **24**:1491–1493.
88. Patel M, Kaufman DA: **Anti-lipoteichoic acid monoclonal antibody (pagibaximab) studies for the prevention of staphylococcal bloodstream infections in preterm infants.** *Expert Opin Biol Ther* 2015, **15**:595–600.
89. Lee MC, Rios AM, Aten MF, Mejias A, Cavuoti D, McCracken GH, Hardy RD: **Management and outcome of children with skin and soft tissue abscesses caused by community-acquired methicillin-resistant Staphylococcus aureus.** *Pediatr Infect Dis J* 2004, **23**:123–127.
90. Pankey G a, Sabath LD: **Clinical relevance of bacteriostatic versus bactericidal mechanisms of action in the treatment of Gram-positive bacterial infections.** *Clin Infect Dis* 2004, **38**:864–870.
91. Chambers HF, DeLeo FR: **Waves of resistance: Staphylococcus aureus in the antibiotic era.** *Nat Rev Microbiol* 2009, **7**:629–641.
92. Anstead GM, Cadena J, Javeri H: **Treatment of infections due to resistant Staphylococcus aureus.** *Methods Mol Biol* 2014, **1085**:259–309.
93. Bassetti M, Merelli M, Temperoni C, Astilean A: **New antibiotics for bad bugs: where are we?** *Ann Clin Microbiol Antimicrob* 2013, **12**:22.
94. Drugs.com: **New Drug Approvals.** *Drugs.com Web* 14.03.2015 <<http://www.drugs.com/newdrugs.html>> 2015.
95. Holmes NE, Howden BP: **What's new in the treatment of serious MRSA infection?** *Curr Opin Infect Dis* 2014, **27**:471–478.
96. Holmes N, Tong S, Davis J, Hal S: **Treatment of Methicillin-Resistant Staphylococcus aureus: Vancomycin and Beyond.** *Semin Respir Crit Care Med* 2015, **36**:017–030.
97. Morales G, Picazo JJ, Baos E, Candel FJ, Arribi A, Peláez B, Andrade R, de la Torre M-A, Fereres J, Sánchez-García M: **Resistance to linezolid is mediated by the cfr gene in the first report of an outbreak of linezolid-resistant Staphylococcus aureus.** *Clin Infect Dis* 2010, **50**:821–825.
98. Sahm DF, Deane J, Bien PA, Locke JB, Zuill DE, Shaw KJ, Bartizal KF: **Results of the Surveillance of Tedizolid Activity and Resistance Program : in vitro susceptibility of Gram-positive pathogens collected in 2011 and 2012 from the United States and Europe.** *Diagn Microbiol Infect Dis* 2015, **81**:112–118.
99. Hill CM, Krause KM, Lewis SR, Blais J, Benton BM, Mammen M, Humphrey PP, Kinana A, Janc JW: **Specificity of induction of the vanA and vanB operons in vancomycin-resistant enterococci by telavancin.** *Antimicrob Agents Chemother* 2010, **54**:2814–2818.
100. Yu F, Lu C, Liu Y, Sun H, Shang Y, Ding Y, Li D, Qin Z, Parsons C, Huang X, Li Y, Hu L, Wang L: **Emergence of quinupristin/dalfopristin resistance among livestock-associated Staphylococcus aureus ST9 clinical isolates.** *Int J Antimicrob Agents* 2014, **44**:416–419.
101. Peleg AY, Adams J, Paterson DL: **Tigecycline efflux as a mechanism for nonsusceptibility in Acinetobacter baumannii.** *Antimicrob Agents Chemother* 2007, **51**:2065–2069.
102. Humphries RM, Pollett S, Sakoulas G: **A current perspective on daptomycin for the clinical microbiologist.** *Clin Microbiol Rev* 2013, **26**:759–780.

103. Chan LC, Basuino L, Diep B, Hamilton S, Chatterjee SS, Chambers HF: **Ceftobiprole- and Ceftaroline-resistant Methicillin-Resistant Staphylococcus aureus**. *Antimicrob Agents Chemother* 2015, **59**:AAC.05004–14.
104. Krause KM, Blais J, Lewis SR, Lunde CS, Barriere SL, Friedland HD, Kitt MM, Benton BM: **In vitro activity of telavancin and occurrence of vancomycin heteroresistance in isolates from patients enrolled in phase 3 clinical trials of hospital-acquired pneumonia**. *Diagn Microbiol Infect Dis* 2012, **74**:429–431.
105. Münch D, Engels I, Müller A, Reder-Christ K, Falkenstein-Paul H, Bierbaum G, Grein F, Bendas G, Sahl H-G, Schneider T: **Structural Variations of the Cell Wall Precursor Lipid II and Their Influence on Binding and Activity of the Lipoglycopeptide Antibiotic Oritavancin**. *Antimicrob Agents Chemother* 2015, **59**:772–781.
106. Boucher HW, Wilcox M, Talbot GH, Puttagunta S, Das AF, Dunne MW: **Once-weekly dalbavancin versus daily conventional therapy for skin infection**. *N Engl J Med* 2014, **370**:2169–79.
107. Allen NE, Alborn WE, Hobbs JN: **Inhibition of membrane potential-dependent amino acid transport by daptomycin**. *Antimicrob Agents Chemother* 1991, **35**:2639–2642.
108. Debono M, Barnhart M, Carrell CB, Hoffmann J a, Occolowitz JL, Abbott BJ, Fukuda DS, Hamill RL, Biemann K, Herlihy WC: **A21978C, a complex of new acidic peptide antibiotics: isolation, chemistry, and mass spectral structure elucidation**. *J Antibiot (Tokyo)* 1987, **40**:761–777.
109. Bayer AS, Schneider T, Sahl H-G: **Mechanisms of daptomycin resistance in Staphylococcus aureus: role of the cell membrane and cell wall**. *Ann N Y Acad Sci* 2013, **1277**:139–58.
110. Bertsche U, Yang SJ, Kuehner D, Wanner S, Mishra NN, Roth T, Nega M, Schneider A, Mayer C, Grau T, Bayer AS, Weidenmaier C: **Increased Cell Wall Teichoic Acid Production and D-alanylation Are Common Phenotypes among Daptomycin-Resistant Methicillin-Resistant Staphylococcus aureus (MRSA) Clinical Isolates**. *PLoS One* 2013, **8**:1–11.
111. Nickolaus B: **Schwere MRSA-Infektionen Stellenwert von Linezolid wird klar**. *Dtsch Arztebl* 2012, **109**:2207.
112. Kloss P, Xiong L, Shinabarger DL, Mankin AS: **Resistance mutations in 23 S rRNA identify the site of action of the protein synthesis inhibitor linezolid in the ribosomal peptidyl transferase center**. *J Mol Biol* 1999, **294**:93–101.
113. Meka VG, Gold HS: **Antimicrobial resistance to linezolid**. *Clin Infect Dis* 2004, **39**:1010–1015.
114. Toh SM, Xiong L, Arias CA, Villegas M V., Lolans K, Quinn J, Mankin AS: **Acquisition of a natural resistance gene renders a clinical strain of methicillin-resistant Staphylococcus aureus resistant to the synthetic antibiotic linezolid**. *Mol Microbiol* 2007, **64**:1506–1514.
115. Kehrenberg C, Cuny C, Strommenger B, Schwarz S, Witte W: **Methicillin-resistant and -susceptible Staphylococcus aureus strains of clonal lineages ST398 and ST9 from swine carry the multidrug resistance gene cfr**. *Antimicrob Agents Chemother* 2009, **53**:779–781.
116. Chen H, Yang Q, Zhang R, He W, Ma X, Zhang J, Xia F, Zhao F, Cao J, Liu Y, Wu W, Hu D, Wang Q, Zhao C, Zhang F, Wang X, Wang Z, Li H, Wang H: **In vitro antimicrobial activity of the novel oxazolidinone tedizolid and comparator agents against Staphylococcus aureus and linezolid-resistant Gram-positive pathogens: a multicentre study in China**. *Int J Antimicrob Agents* 2014, **44**:276–277.
117. Locke JB, Zurenko GE, Shaw KJ, Bartizal K: **Tedizolid for the management of human infections: In vitro characteristics**. *Clin Infect Dis* 2014, **58**:35–42.
118. Stryjewski ME, Szczech L a, Benjamin DK, Inrig JK, Kanafani Z a, Engemann JJ, Chu VH, Joyce MJ, Reller LB, Corey GR, Fowler VG: **Use of vancomycin or first-generation cephalosporins for the treatment of**

hemodialysis-dependent patients with methicillin-susceptible *Staphylococcus aureus* bacteremia. *Clin Infect Dis* 2007, **44**:190–196.

119. Awad SS, Rodriguez AH, Chuang YC, Marjanek Z, Pareigis AJ, Reis G, Scheeren TWL, Sánchez AS, Zhou X, Saulay M, Engelhardt M: **A phase 3 randomized double-blind comparison of ceftobiprole medocartil versus ceftazidime plus linezolid for the treatment of hospital-acquired pneumonia.** *Clin Infect Dis* 2014, **59**:51–61.

120. Espedido B a., Jensen SO, van Hal SJ: **Ceftaroline fosamil salvage therapy: an option for reduced-vancomycin-susceptible MRSA bacteraemia.** *J Antimicrob Chemother* 2014, **70**:797–801.

121. Hershberger E, Donabedian S, Konstantinou K, Zervos MJ: **Quinupristin-dalfopristin resistance in gram-positive bacteria: mechanism of resistance and epidemiology.** *Clin Infect Dis* 2004, **38**:92–98.

122. Fuchs PC, Barry a. L, Brown SD: **Bactericidal activity of quinupristin-dalfopristin against *Staphylococcus aureus*: Clindamycin susceptibility as a surrogate indicator.** *Antimicrob Agents Chemother* 2000, **44**:2880–2882.

123. Dancer SJ, Robb a., Crawford a., Morrison D: **Oral streptogramins in the management of patients with methicillin-resistant *Staphylococcus aureus* (MRSA) infections.** *J Antimicrob Chemother* 2003, **51**:731–735.

124. Allington DR, Rivey MP: **Quinupristin/dalfopristin: A therapeutic review.** *Clin Ther* 2001, **23**:24–44.

125. Entenza JM, Moreillon P: **Tigecycline in combination with other antimicrobials: a review of in vitro, animal and case report studies.** *Int J Antimicrob Agents* 2009, **34**:8.e1–8.e9.

126. Yahav D, Lador A, Paul M, Leibovici L: **Efficacy and safety of tigecycline: A systematic review and meta-analysis.** *J Antimicrob Chemother* 2011, **66**:1963–1971.

127. Prasad P, Sun J, Danner RL, Natanson C: **Excess deaths associated with tigecycline after approval based on noninferiority trials.** *Clin Infect Dis* 2012, **54**:1699–1709.

128. Florescu I, Beuran M, Dimov R, Razbadauskas a., Bochan M, Fichev G, Dukart G, Babinchak T, Cooper C a., Ellis-Grosse EJ, Dartois N, Gandjini H: **Efficacy and safety of tigecycline compared with vancomycin or linezolid for treatment of serious infections with methicillin-resistant *Staphylococcus aureus* or vancomycin-resistant enterococci: a Phase 3, multicentre, double-blind, randomized study.** *J Antimicrob Chemother* 2008, **62** Suppl 1.

129. FDA: **Linezolid (marketed as Zyvox) Information.** *fda.gov Web* 02.05.2015 <<http://www.fda.gov/Drugs/DrugSafety/PostmarketDrugSafetyInformationforPatientsandProviders/ucm101503.htm>> .

130. Walsh TR, Weeks J, Livermore DM, Toleman M a.: **Dissemination of NDM-1 positive bacteria in the New Delhi environment and its implications for human health: An environmental point prevalence study.** *Lancet Infect Dis* 2011, **11**:355–362.

131. Stryjewski ME, Corey GR: **Methicillin-resistant *Staphylococcus aureus*: an evolving pathogen.** *Clin Infect Dis* 2014, **58**(Suppl 1):S10–9.

132. Sanfilippo CM, Hesje CK, Haas W, Morris TW: **Topoisomerase mutations that are associated with high-level resistance to earlier fluoroquinolones in *Staphylococcus aureus* have less effect on the antibacterial activity of besifloxacin.** *Chemotherapy* 2012, **57**:363–371.

133. Lim KT, Teh CSJ, Yusof MYM, Thong KL: **Mutations in *rpoB* and *fusA* cause resistance to rifampicin and fusidic acid in methicillin-resistant *Staphylococcus aureus* strains from a tertiary hospital in Malaysia.** *Trans R Soc Trop Med Hyg* 2014, **108**:112–118.

134. Dale GE, Broger C, D'Arcy a, Hartman PG, DeHoogt R, Jolidon S, Kompis I, Labhardt a M, Langen H, Locher H, Page MG, Stüber D, Then RL, Wipf B, Oefner C: **A single amino acid substitution in Staphylococcus aureus dihydrofolate reductase determines trimethoprim resistance.** *J Mol Biol* 1997, **266**:23–30.
135. Vimberg V, Lenart J, Janata J, Novotna GB: **ClpP-independent function of ClpX interferes with telithromycin resistance conferred by Msr(A) in Staphylococcus aureus.** *Antimicrob Agents Chemother* 2015(March):AAC.04367–14.
136. Maple P, Hamilton-Miller J, Brumfitt W: **Ciprofloxacin resistance in methicillin- and gentamicin-resistant Staphylococcus aureus.** *Eur J Clin Microbiol Infect Dis* 1989, **8**:622–624.
137. Moellering RC: **Linezolid: The first oxazolidinone antimicrobial.** *Annals of Internal Medicine* 2003:135–142.
138. Centers for Disease Control and Prevention: **Antibiotic Resistance Threats in the United States, 2013.** *cdc.gov 2013 accessed 21.10.2014* <<http://www.cdc.gov/drugresistance/threat-report-2013/index.html>> 2013.
139. ECDC: **Summary of the latest data on antibiotic resistance in the European Union.** *ecdc.europa.eu accessed 08.05.2014* <http://ecdc.europa.eu/en/eaad/Documents/EARS-Net-summary.pdf> 2014.
140. European Surveillance System - TESSy: **European Senter for Disease Prevention and Control, Antimicrobial resistance interactive database (EARS-Net).** *ecdc.europa.eu accessed 22.04.2015* <http://ecdc.europa.eu/en/healthtopics/antimicrobial_resistance/database/Pages/map_reports.aspx> 2015.
141. Pérez-Cobas AE, Gosalbes MJ, Friedrichs A, Knecht H, Artacho A, Eismann K, Otto W, Rojo D, Bargiela R, von Bergen M, Neulinger SC, Däumer C, Heinsen F-A, Latorre A, Barbas C, Seifert J, dos Santos VM, Ott SJ, Ferrer M, Moya A: **Gut microbiota disturbance during antibiotic therapy: a multi-omic approach.** *Gut* 2013, **62**:1591–601.
142. Rice LB: **The Complex Dynamics of Antimicrobial Activity in the Human Gastrointestinal Tract.** *Trans Am Clin Climatol Assoc* 2013, **124**:123–132.
143. Fernebro J: **Fighting bacterial infections-future treatment options.** *Drug Resist Updat* 2011, **14**:125–139.
144. Levy SB, Marshall B: **Antibacterial resistance worldwide: causes, challenges and responses.** *Nat Med* 2004, **10**(12 Suppl):S122–9.
145. Kohanski MA, Dwyer DJ, Hayete B, Lawrence CA, Collins JJ: **A common mechanism of cellular death induced by bactericidal antibiotics.** *Cell* 2007, **130**:797–810.
146. Kohanski MA, DePristo MA, Collins JJ: **Sublethal antibiotic treatment leads to multidrug resistance via radical-induced mutagenesis.** *Mol Cell* 2010, **37**:311–20.
147. Rattray AJ, Strathern JN: **Error-prone DNA polymerases: when making a mistake is the only way to get ahead.** *Annu Rev Genet* 2003, **37**:31–66.
148. European Commission: **Communication from the Commission to the European Parliament and the Council - Action plan against the rising threats from Antimicrobial Resistance.** *ec.europa.eu accessed 20.08.2014* <http://ec.europa.eu/dgs/health_food-safety/docs/communication_amr_2011_748_en.pdf> 2011:1–17.
149. Cars O: **Securing access to effective antibiotics for current and future generations. Whose responsibility?** 2014(April):209–214.
150. Rex JH: **ND4BB: addressing the antimicrobial resistance crisis.** *Nat Rev Microbiol* 2014, **12**:231–232.

151. Centers for Disease Control and Prevention: **National Strategy for Combating Antibiotic Resistant Bacteria**. *cdc.gov* accessed 05.02.2015 <http://www.cdc.gov/drugresistance/pdf/carb_national_strategy.pdf> 2014.
152. FDA: **New FDA task force will support innovation in antibacterial drug development**. *fda.org* accessed 20.04.2014 <<http://www.fda.gov/NewsEvents/Newsroom/PressAnnouncements/ucm320643.htm>> 2012.
153. Policy IP: **The 10 x '20 Initiative: pursuing a global commitment to develop 10 new antibacterial drugs by 2020**. *Clin Infect Dis* 2010, **50**:1081–1083.
154. WHO: **Draft global action plan on antimicrobial resistance - Report by the Secretariat**. *who.int* accessed 18.08.2014 <http://apps.who.int/gb/ebwha/pdf_files/WHA67/A67_39Add1-en.pdf> 2014:1–3.
155. FDA: **FDA approves Orbactiv to treat skin infections**. *fda.org* accessed 2015-04-23 <<http://www.fda.gov/NewsEvents/Newsroom/PressAnnouncements/ucm408475.htm>> 2014.
156. Mensa B, Howell GL, Scott R, DeGrado WF: **Comparative mechanistic studies of brilacidin, daptomycin, and the antimicrobial peptide LL16**. *Antimicrob Agents Chemother* 2014, **58**:5136–5145.
157. Ling LL, Schneider T, Peoples AJ, Spoering AL, Engels I, Conlon BP, Mueller A, Schäberle TF, Hughes DE, Epstein S, Jones M, Lazarides L, Steadman V a, Cohen DR, Felix CR, Fetterman KA, Millett WP, Nitti AG, Zullo AM, Chen C, Lewis K: **A new antibiotic kills pathogens without detectable resistance**. *Nature* 2015, **517**:455–459.
158. Walsh F, Duffy B: **The culturable soil antibiotic resistome: a community of multi-drug resistant bacteria**. *PLoS One* 2013, **8**:e65567.
159. Jurgenson CT, Begley TP, Ealick SE: **The structural and biochemical foundations of thiamin biosynthesis**. *Annu Rev Biochem* 2009, **78**:569–603.
160. Lu'o'ng KVQ, Nguyễn LTH: **Thiamine and Parkinson's disease**. *J Neurol Sci* 2012, **316**:1–8.
161. Gibson GE, Zhang H: **Interactions of oxidative stress with thiamine homeostasis promote neurodegeneration**. *Neurochem Int* 2002, **40**:493–504.
162. Müller S, Kappes B: **Vitamin and cofactor biosynthesis pathways in Plasmodium and other apicomplexan parasites**. *Trends Parasitol* 2007, **23**:112–121.
163. Zhang G, Ding H, Chen H, Ye X, Li H, Lin X, Ke Z: **Thiamine nutritional status and depressive symptoms are inversely associated among older Chinese adults**. *J Nutr* 2013, **143**:53–8.
164. Müller IB, Bergmann B, Groves MR, Couto I, Amaral L, Begley TP, Walter RD, Wrenger C: **The vitamin B1 metabolism of Staphylococcus aureus is controlled at enzymatic and transcriptional levels**. *PLoS One* 2009, **4**:e7656.
165. Bettendorff L, Wins P: **Thiamin diphosphate in biological chemistry: New aspects of thiamin metabolism, especially triphosphate derivatives acting other than as cofactors**. *FEBS J* 2009, **276**:2917–2925.
166. Sudarsan N, Cohen-Chalamish S, Nakamura S, Emilsson GM, Breaker RR: **Thiamine pyrophosphate riboswitches are targets for the antimicrobial compound pyrithiamine**. *Chem Biol* 2005, **12**:1325–1335.
167. Webb E, Claas K, Downs D: **thiBPQ encodes an ABC transporter required for transport of thiamine and thiamine pyrophosphate in Salmonella typhimurium**. *J Biol Chem* 1998, **273**:8946–8950.

168. Hollenbach AD, Dickson K a., Washabaugh MW: **Overexpression, purification, and characterization of the periplasmic space thiamin-binding protein of the thiamin traffic ATPase in Escherichia coli.** *Protein Expr Purif* 2002, **25**:508–518.
169. Rodionov DA, Vitreschak AG, Mironov AA, Gelfand MS: **Comparative genomics of thiamin biosynthesis in procaryotes. New genes and regulatory mechanisms.** *J Biol Chem* 2002, **277**:48949–48959.
170. Dorrestein PC, Zhai H, McLafferty FW, Begley TP: **The biosynthesis of the thiazole phosphate moiety of thiamin: the sulfur transfer mediated by the sulfur carrier protein ThiS.** *Chem Biol* 2004, **11**:1373–81.
171. Jordan F: **Current mechanistic understanding of thiamin diphosphate-dependent enzymatic reactions.** *Nat Prod Rep* 2003, **20**:184–201.
172. Wikner C, Meshalkina L, Nilsson U, Nikkola M, Lindqvist Y, Sundström M, Schneider G: **Analysis of an Invariant Cofactor-Protein Interaction in Thiamin Diphosphate-dependent Enzymes by Site-directed Mutagenesis: Glutamic acid 418 in transketolase is essential for catalysis.** *J Biol Chem* 1994, **269**:32144–32150.
173. Pohl M, Sprenger G a, Müller M: **A new perspective on thiamine catalysis.** *Curr Opin Biotechnol* 2004, **15**:335–42.
174. Breslow R: **On the Mechanism of Thiamine Action. IV. 1 Evidence from Studies on Model Systems.** *J Am Chem Soc* 1958, **80**:3719–3726.
175. Leeper FJ, Hawksley D, Mann S, Perez Melero C, Wood MDH: **Studies on thiamine diphosphate-dependent enzymes.** *Biochem Soc Trans* 2005, **33**:772–775.
176. Agyei-Owusu K, Leeper FJ: **Thiamin diphosphate in biological chemistry: analogues of thiamin diphosphate in studies of enzymes and riboswitches.** *FEBS J* 2009, **276**:2905–16.
177. Hafferl W, Lundin R, Ingraham LL: **Activated Hydrogens in Compounds Related to Thiamine.** *Biochemistry* 1963, **2**:1298–1305.
178. Haake P, Miller WB: **A Comparison of Thiazoles and Oxazoles.** *J Am Chem Soc* 1963, **85**:4044–4045.
179. Schellenberger A: **Structure and Mechanism of Action of the Active Center of Yeast Pyruvate Decarboxylase.** *Angew Chemie Int Ed English* 1967, **6**:1024–1035.
180. Arjunan P, Chandrasekhar K, Sax M, Brunskill A, Nemeria N, Jordan F, Furey W: **Structural Determinants of Enzyme Binding Affinity: The E1 Component of Pyruvate Dehydrogenase from Escherichia coli in Complex with the Inhibitor Thiamin Thiazolone Diphosphate.** *Biochemistry* 2004, **43**:2405–2411.
181. Heinrich PC, Steffen H, Janser P, Wiss O: **Studies on the reconstitution of apotransketolase with thiamine pyrophosphate and analogs of the coenzyme.** *Eur J Biochem* 1972, **30**:533–541.
182. Mann S, Perez Melero C, Hawksley D, Leeper FJ: **Inhibition of thiamin diphosphate dependent enzymes by 3-deazathiamin diphosphate.** *Org Biomol Chem* 2004, **2**:1732–41.
183. Lakaye B, Wirtzfeld B, Wins P, Grisar T, Bettendorff L: **Thiamine Triphosphate , a New Signal Required for Optimal Growth of Escherichia coli during Amino Acid Starvation.** 2004, **279**:17142–17147.
184. Gigliobianco T, Lakaye B, Wins P, El Moulaj B, Zorzi W, Bettendorff L: **Adenosine thiamine triphosphate accumulates in Escherichia coli cells in response to specific conditions of metabolic stress.** *BMC Microbiol* 2010, **10**:148.
185. Bettendorff L: **Thiamine homeostasis in neuroblastoma cells.** *Neurochem Int* 1995, **26**:295–302.

186. Bettendorff L, Wirtzfeld B, Makarchikov AF, Mazzucchelli G, Frédérich M, Gigliobianco T, Gangolf M, De Pauw E, Angenot L, Wins P: **Discovery of a natural thiamine adenine nucleotide.** *Nat Chem Biol* 2007, **3**:211–2.
187. Gangolf M, Czerniecki J, Radermecker M, Detry O, Nisolle M, Jouan C, Martin D, Chantraine F, Lakaye B, Wins P, Grisar T, Bettendorff L: **Thiamine status in humans and content of phosphorylated thiamine derivatives in biopsies and cultured cells.** *PLoS One* 2010, **5**:1–13.
188. Eliot AC, Kirsch JF: **Pyridoxal phosphate enzymes: mechanistic, structural, and evolutionary considerations.** *Annu Rev Biochem* 2004, **73**:383–415.
189. Percudani R, Peracchi A: **The B6 database: a tool for the description and classification of vitamin B6-dependent enzymatic activities and of the corresponding protein families.** *BMC Bioinformatics* 2009, **10**:273.
190. Percudani R, Peracchi A: **A genomic overview of pyridoxal-phosphate-dependent enzymes.** *EMBO Rep* 2003, **4**:850–854.
191. Schneider G, Käck H, Lindqvist Y: **The manifold of vitamin B6 dependent enzymes.** *Structure* 2000, **8**:1–6.
192. Phillips RS: **Chemistry and diversity of pyridoxal-5'-phosphate dependent enzymes.** *Biochim Biophys Acta - Proteins Proteomics* 2015:6–13.
193. Toney MD: **Reaction specificity in pyridoxal phosphate enzymes.** *Arch Biochem Biophys* 2005, **433**:279–287.
194. Caulkins BG, Bastin B, Yang C, Neubauer TJ, Young RP, Hilario E, Huang YM, Chang CA, Fan L, Dunn MF, Marsella MJ, Mueller LJ: **Protonation States of the Tryptophan Synthase Internal Aldimine Active Site from Solid-State NMR Spectroscopy: Direct Observation of the Protonated Schiff Base Linkage to Pyridoxal-5'-Phosphate.** *J Am Chem Soc* 2014, **136**:12824–12827.
195. Ferreira GC, Vajapey U, Hafez O, Hunter G a, Barber MJ: **Aminolevulinate synthase: lysine 313 is not essential for binding the pyridoxal phosphate cofactor but is essential for catalysis.** *Protein Sci* 1995, **4**:1001–1006.
196. Begley TP, Kinsland C, Mehl RA, Osterman A, Dorrestein P: **The biosynthesis of nicotinamide adenine dinucleotides in bacteria.** *Vitam Horm* 2001, **61**:103–119.
197. Pearl PL, Hartka TR, Taylor J: **Diagnosis and treatment of neurotransmitter disorders.** *Curr Treat Options Neurol* 2006, **8**:441–450.
198. Lambrecht G, Braun K, Damer M, Ganso M, Hildebrandt C, Ullmann H, Kassack MU, Nickel P: **Structure-activity relationships of suramin and pyridoxal-5'-phosphate derivatives as P2 receptor antagonists.** *Curr Pharm Des* 2002, **8**:2371–2399.
199. Huq MDM, Tsai N, Lin Y, Higgins L, Wei L: **Vitamin B6 conjugation to nuclear corepressor RIP140 and its role in gene regulation.** *Nat Chem Biol* 2007, **3**:161–165.
200. Oka T: **Modulation of gene expression by vitamin B6.** *Nutr Res Rev* 2001, **14**:257–266.
201. Komatsu S, Yanaka N, Matsubara K, Kato N: **Antitumor effect of vitamin B6 and its mechanisms.** *Biochim Biophys Acta* 2003, **1647**:127–130.
202. Galluzzi L, Vacchelli E, Michels J, Garcia P, Kepp O, Senovilla L, Vitale I, Kroemer G: **Effects of vitamin B6 metabolism on oncogenesis, tumor progression and therapeutic responses.** *Oncogene* 2013, **32**:4995–5004.

203. Chetyrkin S V, Mathis ME, Ham AJL, Hachey DL, Hudson BG, Voziyan PA: **Propagation of protein glycation damage involves modification of tryptophan residues via reactive oxygen species: inhibition by pyridoxamine.** *Free Radic Biol Med* 2008, **44**:1276–1285.
204. Kannan K, Jain SK: **Effect of vitamin B6 on oxygen radicals, mitochondrial membrane potential, and lipid peroxidation in H2O2-treated U937 monocytes.** *Free Radic Biol Med* 2004, **36**:423–428.
205. Bhatt AN, Bhakuni V: **Characterization of pyridoxal 5'-phosphate-binding domain and folding intermediate of Bacillus subtilis serine hydroxymethyltransferase: An autonomous folding domain.** *J Biochem* 2008, **144**:295–303.
206. Groha C, Bartholmes P, Jaenicke R: **Refolding and reactivation of Escherichia coli tryptophan synthase beta2 subunit after inactivation and dissociation in guanidine hydrochloride at acidic pH.** *Eur J Biochem* 1978, **92**:437–441.
207. Deu E, Kirsch JF: **Cofactor-directed reversible denaturation pathways: The cofactor-stabilized Escherichia coli aspartate aminotransferase homodimer unfolds through a pathway that differs from that of the apoenzyme.** *Biochemistry* 2007, **46**:5819–5829.
208. Cellini B, Bertoldi M, Montioli R, Laurents D V., Paiardini A, Voltattorni CB: **Dimerization and folding processes of Treponema denticola cystalysin: The role of pyridoxal 5'-phosphate.** *Biochemistry* 2006, **45**:14140–14154.
209. Tambasco-Studart M, Titiz O, Raschle T, Forster G, Amrhein N, Fitzpatrick TB: **Vitamin B6 biosynthesis in higher plants.** *Proc Natl Acad Sci U S A* 2005, **102**:13687–13692.
210. Tanaka T, Tateno Y, Gojobori T: **Evolution of vitamin B6 (pyridoxine) metabolism by gain and loss of genes.** *Mol Biol Evol* 2005, **22**:243–250.
211. Mittenhuber G: **Phylogenetic analyses and comparative genomics of vitamin B6 (pyridoxine) and pyridoxal phosphate biosynthesis pathways.** *J Mol Microbiol Biotechnol* 2001, **3**:1–20.
212. Belitsky BR: **Physical and Enzymological Interaction of Bacillus subtilis Proteins Required for de Novo Pyridoxal 5'-Phosphate Biosynthesis.** In *Journal of Bacteriology. Volume 186*; 2004:1191–1196.
213. Fitzpatrick TB, Amrhein N, Kappes B, Macheroux P, Tews I, Raschle T: **Two independent routes of de novo vitamin B6 biosynthesis: not that different after all.** *Biochem J* 2007, **407**:1–13.
214. Mukherjee T, Hanes J, Tews I, Ealick SE, Begley TP: **Pyridoxal phosphate: Biosynthesis and catabolism.** *Biochimica et Biophysica Acta - Proteins and Proteomics* 2011:1585–1596.
215. Zhao G, Winkler ME: **Kinetic limitation and cellular amount of pyridoxine (pyridoxamine) 5'- phosphate oxidase of Escherichia coli K-12.** *J Bacteriol* 1995, **177**:883–891.
216. Safo MK, Musayev FN, Di Salvo ML, Hunt S, Claude JB, Schirch V: **Crystal structure of pyridoxal kinase from the Escherichia coli pdxK gene: Implications for the classification of pyridoxal kinases.** *J Bacteriol* 2006, **188**:4542–4552.
217. Ghatge MS, Contestabile R, di Salvo ML, Desai J V, Gandhi AK, Camara CM, Florio R, González IN, Parroni A, Schirch V, Safo MK: **Pyridoxal 5'-phosphate is a slow tight binding inhibitor of E. coli pyridoxal kinase.** *PLoS One* 2012, **7**:e41680.
218. Lainé-Cessac P, Cailleux A, Allain P: **Mechanisms of the inhibition of human erythrocyte pyridoxal kinase by drugs.** *Biochem Pharmacol* 1997, **54**:863–870.

219. Hvas A-M, Juul S, Bech P, Nexø E: **Vitamin B6 level is associated with symptoms of depression.** *Psychother Psychosom* 2004, **73**:340–343.
220. Merrill AH, Henderson JM: **Diseases associated with defects in vitamin B6 metabolism or utilization.** *Annu Rev Nutr* 1987, **7**:137–156.
221. Burns KE, Xiang Y, Kinsland CL, McLafferty FW, Begley TP: **Reconstitution and biochemical characterization of a new pyridoxal-5'-phosphate biosynthetic pathway.** *J Am Chem Soc* 2005, **127**:3682–3683.
222. Nodwell MB, Koch MF, Alte F, Schneider S, Sieber SA: **A subfamily of bacterial ribokinases utilizes a hemithioacetal for pyridoxal phosphate salvage.** *J Am Chem Soc* 2014, **136**:4992–4999.
223. Zeidler J, Sayer BG, Spenser ID: **Biosynthesis of Vitamin B 1 in Yeast. Derivation of the Pyrimidine Unit from Pyridoxine and Histidine. Intermediacy of Urocanic Acid.** *J Am Chem Soc* 2003, **125**:13094–13105.
224. Zeidler J, Ullah N, Gupta RN, Pauloski RM, Sayer BG, Spenser ID: **2'-hydroxypyridoxol, a biosynthetic precursor of vitamins B6 and B1 in yeast.** *J Am Chem Soc* 2002, **124**:4542–4543.
225. Lai RY, Huang S, Fenwick MK, Hazra A, Zhang Y, Rajashankar K, Philmus B, Kinsland C, Sanders JM, Ealick SE, Begley TP: **Thiamin pyrimidine biosynthesis in candida albicans: A remarkable reaction between histidine and pyridoxal phosphate.** *J Am Chem Soc* 2012, **134**:9157–9159.
226. Schultz A, Atkin L, Frey CN: **The Biochemical Classification of Yeast Strains.** *J Bacteriol* 1940, **40**:339–346.
227. Wrenger C, Eschbach M-L, Müller IB, Laun NP, Begley TP, Walter RD: **Vitamin B1 de novo synthesis in the human malaria parasite Plasmodium falciparum depends on external provision of 4-amino-5-hydroxymethyl-2-methylpyrimidine.** *Biol Chem* 2006, **387**:41–51.
228. Mizote T, Nakayama H: **Purification and properties of hydroxymethylpyrimidine kinase from Escherichia coli.** *Biochim Biophys Acta - Gen Subj* 1989, **991**:109–113.
229. Yang Y, Tsui HCT, Man TK, Winkler ME: **Identification and function of the pdxY gene, which encodes a novel pyridoxal kinase involved in the salvage pathway of pyridoxal 5'-phosphate biosynthesis in Escherichia coli K-12.** *J Bacteriol* 1998, **180**:1814–1821.
230. Castro-Fernandez V, Bravo-Moraga F, Ramirez-Sarmiento C a., Guixe V: **Emergence of pyridoxal phosphorylation through a promiscuous ancestor during the evolution of hydroxymethyl pyrimidine kinases.** *FEBS Lett* 2014, **588**:3068–3073.
231. Park JH, Burns K, Kinsland C, Begley TP: **Characterization of Two Kinases Involved in Thiamine Pyrophosphate and Pyridoxal Phosphate Biosynthesis in Bacillus subtilis: 4-Amino-5-Hydroxymethyl-2-Methylpyrimidine Kinase and Pyridoxal Kinase.** *J Bacteriol* 2004, **186**:1571–1573.
232. FDA (Hlavsa): **YellowBook Chapter 3 Infectious Diseases Related To Travel - Cryptosporidiosis.** *cdc.gov* accessed 05.02.2015 <<http://wwwnc.cdc.gov/travel/yellowbook/2014/chapter-3-infectious-diseases-related-to-travel/cryptosporidiosis>> 2013.
233. Yamamoto Y, Hakki A, Friedman H, Okubo S, Shimamura T, Hoffman PS, Rossignol JF: **Nitazoxanide, a nitrothiazolide antiparasitic drug, is an anti-helicobacter pylori agent with anti-vacuolating toxin activity.** *Chemotherapy* 1999, **45**:303–312.
234. Sisson G, Goodwin A, Raudonikiene A, Hughes NJ, Mukhopadhyay AK, Berg DE, Hoffman PS: **Enzymes Associated with Reductive Activation and Action of Nitazoxanide , Nitrofurans , and Metronidazole in Helicobacter pylori.** 2002, **46**:2116–2123.

235. De Carvalho LPS, Lin G, Jiang X, Nathan C: **Nitazoxanide kills replicating and nonreplicating *Mycobacterium tuberculosis* and evades resistance.** *J Med Chem* 2009, **52**:5789–5792.
236. Hoffman PS, Sisson G, Croxen M a., Welch K, Harman WD, Cremades N, Morash MG: **Antiparasitic drug nitazoxanide inhibits the pyruvate oxidoreductases of *Helicobacter pylori*, selected anaerobic bacteria and parasites, and *Campylobacter jejuni*.** *Antimicrob Agents Chemother* 2007, **51**:868–876.
237. Hemphill A, Mueller J, Esposito M: **Nitazoxanide, a broad-spectrum thiazolide anti-infective agent for the treatment of gastrointestinal infections.** *Expert Opin Pharmacother* 2006, **7**:953–964.
238. Devasahayam G, Scheld WM, Hoffman PS: **Newer Antibacterial Drugs for a New Century.** *Expert Opin Investig Drugs* 2011, **19**:215–234.
239. Müller IB, Wu F, Bergmann B, Knöckel J, Walter RD, Gehring H, Wrenger C: **Poisoning pyridoxal 5-phosphate-dependent enzymes: A new strategy to target the malaria parasite *Plasmodium falciparum*.** *PLoS One* 2009, **4**.
240. Wrenger C, Knöckel J, Walter RD, Müller IB: **Vitamin B1 and B6 in the malaria parasite: Requisite or dispensable?** *Brazilian Journal of Medical and Biological Research* 2008:82–88.
241. Kappes B, Tews I, Binter A, MacHeroux P: **PLP-dependent enzymes as potential drug targets for protozoan diseases.** *Biochim Biophys Acta - Proteins Proteomics* 2011, **1814**:1567–1576.
242. Kronenberger T, Lindner J, Meissner K a., Zimbres FM, Coronado M a., Sauer FM, Schetttert I, Wrenger C: **Vitamin B6-dependent enzymes in the human malaria parasite *plasmodium falciparum*: A druggable target?** *Biomed Res Int* 2014, **2014**.
243. Jones DC, Alphey MS, Wyllie S, Fairlamb AH: **Chemical, genetic and structural assessment of pyridoxal kinase as a drug target in the African trypanosome.** *Mol Microbiol* 2012, **86**:51–64.
244. Kimura T, Shirakawa R, Yaoita N, Hayashi T, Nagano K, Horiuchi H: **The antimalarial drugs chloroquine and primaquine inhibit pyridoxal kinase , an essential enzyme for vitamin B6 production.** *FEBS Lett* 2014, **588**:3673–3676.
245. Drebes J, Künz M, Pereira CA, Betzel C, Wrenger C: **MRSA infections: from classical treatment to suicide drugs.** *Curr Med Chem* 2014, **21**:1809–19.
246. Nathan C: **Fresh Approaches to Anti-Infective Therapies.** *Sci Transl Med* 2012, **4**:140sr2–140sr2.
247. Mullis KB, Faloona FA: **Specific synthesis of DNA in vitro via a polymerase-catalyzed chain reaction.** *Methods Enzymol* 1987, **155**:335–50.
248. Chien A, Edgar DB, Trela JM: **Deoxyribonucleic acid polymerase from the extreme thermophile *Deoxyribonucleic Acid Polymerase from the Extreme Thermophile Thermus aquaticus*.** 1976, **127**:1550–1557.
249. Lundberg KS, Shoemaker DD, Adams MWW, Short JM, Sorge JA, Mathur EJ: **High-fidelity amplification using a thermostable DNA polymerase isolated from *Pyrococcus furiosus*.** *Gene* 1991, **108**:1–6.
250. Breslauer KJ, Frank R, Blöcker H, Marky LA: **Predicting DNA duplex stability from the base sequence.** *Proc Natl Acad Sci U S A* 1986, **83**:3746–3750.
251. Sugimoto N, Nakano SI, Yoneyama M, Honda KI: **Improved thermodynamic parameters and helix initiation factor to predict stability of DNA duplexes.** *Nucleic Acids Res* 1996, **24**:4501–4505.
252. Heckman KL, Pease LR: **Gene splicing and mutagenesis by PCR-driven overlap extension.** *Nat Protoc* 2007, **2**:924–932.

253. Ho SN, Ho SN, Hunt HD, Hunt HD, Horton RM, Horton RM, Pullen JK, Pullen JK, Pease LR, Pease LR: **Site-directed mutagenesis by overlap extension using the polymerase chain reaction.** *Gene* 1989, **77**:51–9.
254. Costa GL, Bauer JC, McGowan B, Angert M, Weiner MP: **Site-directed mutagenesis using a rapid PCR-based method.** *Methods Mol Biol* 1996, **57**:239–248.
255. Havaei SA, Azimian A, Fazeli H, Naderi M, Ghazvini K, Samiee SM, Masoumi Z, Akbari M: **Genetic Characterization of Methicillin Resistant and Sensitive, Vancomycin Intermediate Staphylococcus aureus Strains Isolated from Different Iranian Hospitals.** *ISRN Microbiol* 2012, **2012**:215275.
256. Inoue H, Nojima H, Okayama H: **High efficiency transformation of Escherichia coli with plasmids.** *Gene* 1990, **96**:23–28.
257. Hanahan D, Jessee J, Bloom FR: **Plasmid transformation of Escherichia coli and other bacteria.** *Methods Enzymol* 1991, **204**:63–114.
258. Laemmli UK: **Cleavage of structural proteins during the assembly of the head of bacteriophage T4.** *Nature* 1970, **227**:680–685.
259. Skerra A: **Use of the tetracycline promoter for the tightly regulated production of a murine antibody fragment in Escherichia coli.** *Gene* 1994, **151**:131–135.
260. Maina C V, Riggs PD, Grandea AG, Slatko BE, Moran LS, Tagliamonte JA, McReynolds LA, Guan CD: **An Escherichia coli vector to express and purify foreign proteins by fusion to and separation from maltose-binding protein.** *Gene* 1988, **74**:365–373.
261. Di Guan C, Li P, Riggs PD, Inouye H: **Vectors that facilitate the expression and purification of foreign peptides in Escherichia coli by fusion to maltose-binding protein.** *Gene* 1988, **67**:21–30.
262. Kapust RB, Tözsér J, Copeland TD, Waugh DS: **The P1' specificity of tobacco etch virus protease.** *Biochem Biophys Res Commun* 2002, **294**:949–955.
263. Kapust RB, Tözsér J, Fox JD, Anderson DE, Cherry S, Copeland TD, Waugh DS: **Tobacco etch virus protease: mechanism of autolysis and rational design of stable mutants with wild-type catalytic proficiency.** *Protein Eng* 2001, **14**:993–1000.
264. Bertani G: **Studies on lysogenesis. I. The mode of phage liberation by lysogenic Escherichia coli.** *J Bacteriol* 1951, **62**:293–300.
265. Ciccarone VC, Polayes DA, Luckow VA: **Generation of Recombinant Baculovirus DNA in E.coli Using a Baculovirus Shuttle Vector.** *Methods Mol Med* 1998, **13**:213–235.
266. Bradford MM: **A rapid and sensitive method for the quantitation of microgram quantities of protein utilizing the principle of protein-dye binding.** *Anal Biochem* 1976, **72**:248–254.
267. Artimo P, Jonnalagedda M, Arnold K, Baratin D, Csardi G, De Castro E, Duvaud S, Flegel V, Fortier A, Gasteiger E, Grosdidier A, Hernandez C, Ioannidis V, Kuznetsov D, Liechti R, Moretti S, Mostaguir K, Redaschi N, Rossier G, Xenarios I, Stockinger H: **ExPASy: SIB bioinformatics resource portal.** *Nucleic Acids Res* 2012, **40**:597–603.
268. Kapust RB, Waugh DS: **Escherichia coli maltose-binding protein is uncommonly effective at promoting the solubility of polypeptides to which it is fused.** *Protein Sci* 1999, **8**:1668–1674.
269. Phan J, Zdanov A, Evdokimov AG, Tropea JE, Peters HK, Kapust RB, Li M, Wlodawer A, Waugh DS: **Structural basis for the substrate specificity of tobacco etch virus protease.** *J Biol Chem* 2002, **277**:50564–50572.

270. Yang JT, Wu CS, Martinez HM: **Calculation of protein conformation from circular dichroism.** *Methods Enzymol* 1986, **130**:208–269.
271. Kelly SM, Jess TJ, Price NC: **How to study proteins by circular dichroism.** *Biochimica et Biophysica Acta - Proteins and Proteomics* 2005:119–139.
272. Chayen NE: **The role of oil in macromolecular crystallization.** *Structure* 1997, **5**:1269–1274.
273. Ng JD, Gavira JA, García-Ruiz JM: **Protein crystallization by capillary counterdiffusion for applied crystallographic structure determination.** *J Struct Biol* 2003, **142**:218–231.
274. Shaw Stewart PD, Kolek S a., Briggs R a., Chayen NE, Baldock PFM: **Random microseeding: A theoretical and practical exploration of seed stability and seeding techniques for successful protein crystallization.** *Cryst Growth Des* 2011, **11**:3432–3441.
275. Bergfors T: **Seeds to crystals.** *J Struct Biol* 2003, **142**:66–76.
276. D'Arcy A, Sweeney A Mac, Haber A: **Modified microbatch and seeding in protein crystallization experiments.** *J Synchrotron Radiat* 2004, **11**:24–26.
277. Meyer A, Dierks K, Hilterhaus D, Klupsch T, Mühlig P, Kleesiek J, Schöpflin R, Einspahr H, Hilgenfeld R, Betzel C: **Single-drop optimization of protein crystallization.** *Acta Crystallogr Sect F Struct Biol Cryst Commun* 2012, **68**:994–998.
278. Kabsch W: **XDS.** *Acta Crystallogr D Biol Crystallogr* 2010, **66**(Pt 2):125–32.
279. Evans P: **Scaling and assessment of data quality.** In *Acta Crystallographica Section D: Biological Crystallography. Volume 62.* International Union of Crystallography; 2006:72–82.
280. Battye TGG, Kontogiannis L, Johnson O, Powell HR, Leslie AGW: **iMOSFLM: A new graphical interface for diffraction-image processing with MOSFLM.** *Acta Crystallogr Sect D Biol Crystallogr* 2011, **67**:271–281.
281. Vagin a., Teplyakov A: **MOLREP : an Automated Program for Molecular Replacement.** *J Appl Crystallogr* 1997, **30**:1022–1025.
282. McCoy AJ, Grosse-Kunstleve RW, Adams PD, Winn MD, Storoni LC, Read RJ: **Phaser crystallographic software.** *J Appl Crystallogr* 2007, **40**(Pt 4):658–674.
283. Winn MD, Ballard CC, Cowtan KD, Dodson EJ, Emsley P, Evans PR, Keegan RM, Krissinel EB, Leslie AGW, McCoy A, McNicholas SJ, Murshudov GN, Pannu NS, Potterton EA, Powell HR, Read RJ, Vagin A, Wilson KS: **Overview of the CCP4 suite and current developments.** *Acta Crystallographica Section D: Biological Crystallography* 2011:235–242.
284. Emsley P, Cowtan K: **Coot: model-building tools for molecular graphics.** *Acta Crystallogr D Biol Crystallogr* 2004, **60**(Pt 12 Pt 1):2126–32.
285. Murshudov GN, Skubák P, Lebedev AA, Pannu NS, Steiner RA, Nicholls R a, Winn MD, Long F, Vagin AA: **REFMAC5 for the refinement of macromolecular crystal structures.** *Acta Crystallogr D Biol Crystallogr* 2011, **67**(Pt 4):355–67.
286. Adams PD, Afonine P V, Bunkóczi G, Chen VB, Davis IW, Echols N, Headd JJ, Hung L-W, Kapral GJ, Grosse-Kunstleve RW, McCoy AJ, Moriarty NW, Oeffner R, Read RJ, Richardson DC, Richardson JS, Terwilliger TC, Zwart PH: **PHENIX: a comprehensive Python-based system for macromolecular structure solution.** *Acta Crystallogr D Biol Crystallogr* 2010, **66**(Pt 2):213–21.

287. Larkin MA, Blackshields G, Brown NP, Chenna R, McGettigan PA, McWilliam H, Valentin F, Wallace IM, Wilm A, Lopez R, Thompson JD, Gibson TJ, Higgins DG: **Clustal W and Clustal X version 2.0.** *Bioinformatics* 2007, **23**:2947–8.
288. Altschul SF, Madden TL, Schäffer AA, Zhang J, Zhang Z, Miller W, Lipman DJ: **Gapped BLAST and PSI-BLAST: A new generation of protein database search programs.** *Nucleic Acids Res* 1997, **25**:3389–3402.
289. Krissinel E, Henrick K: **Inference of Macromolecular Assemblies from Crystalline State.** *J Mol Biol* 2007, **372**:774–797.
290. Krissinel E, Henrick K: **Secondary-structure matching (SSM), a new tool for fast protein structure alignment in three dimensions.** *Acta Crystallogr D Biol Crystallogr* 2004, **60**(Pt 12 Pt 1):2256–68.
291. Laskowski RA, Hutchinson EG, Michie AD, Wallace AC, Jones ML, Thornton JM: **PDBsum: a Web-based database of summaries and analyses of all PDB structures.** *Trends Biochem Sci* 1997, **22**:488–90.
292. Konarev P V, Volkov V V, Sokolova A V, Koch MHJ, Svergun DI: **PRIMUS : a Windows PC-based system for small-angle scattering data analysis.** *J Appl Crystallogr* 2003, **36**:1277–1282.
293. Svergun DI: **Determination of the regularization parameter in indirect-transform methods using perceptual criteria.** *J Appl Crystallogr* 1992, **25**(pt 4):495–503.
294. Franke D, Svergun DI: **DAMMIF, a program for rapid ab-initio shape determination in small-angle scattering.** *J Appl Crystallogr* 2009, **42**:342–346.
295. Volkov V V, Svergun DI: **Uniqueness of ab initio shape determination in small-angle scattering.** *J Appl Crystallogr* 2003, **36**:860–864.
296. Svergun DI: **Restoring low resolution structure of biological macromolecules from solution scattering using simulated annealing.** *Biophys J* 1999, **76**:2879–2886.
297. Kwok F, Churchich JE: **Brain pyridoxal kinase. Purification, substrate specificities, and sensitized photodestruction of an essential histidine.** *J Biol Chem* 1979, **254**:6489–6495.
298. Drebes J: **Exploiting the Thiamin Biosynthesis of Staphylococcus aureus Towards Pro - Drug Discovery.** University of Hamburg; 2012.
299. Wisedchaisri G, Gonen T: **Phasing electron diffraction data by molecular replacement: strategy for structure determination and refinement.** *Methods Mol Biol* 2013, **955**:243–272.
300. Cheek S, Zhang H, Grishin N V: **Sequence and structure classification of kinases.** *J Mol Biol* 2002, **320**:855–881.
301. Sigrell JA, Cameron AD, Jones TA, Mowbray SL: **Structure of Escherichia coli ribokinase in complex with ribose and dinucleotide determined to 1.8 Å resolution: insights into a new family of kinase structures.** *Structure* 1998, **6**:183–193.
302. Kenyon CP, Roth RL, van der Westhuyzen CW, Parkinson CJ: **Conserved phosphoryl transfer mechanisms within kinase families and the role of the C8 proton of ATP in the activation of phosphoryl transfer.** *BMC Research Notes* 2012:131.
303. Campobasso N, Mathews II, Begley TP, Ealick SE: **Crystal Structure of 4-Methyl-5-β-hydroxyethylthiazole Kinase from Bacillus subtilis at 1.5 Å Resolution † , ‡.** *Biochemistry* 2000, **39**:7868–7877.
304. Rossmann MG, Moras D, Olsen KW: **Chemical and biological evolution of nucleotide-binding protein.** *Nature* 1974, **250**:194–199.

305. Shin W, Oh DG, Chae CH, Yoon TS: **Conformational analyses of thiamin-related compounds. A stereochemical model for thiamin catalysis.** *J Am Chem Soc* 1993, **115**:12238–12250.
306. Timm DE, Liu J, Baker LJ, Harris RA: **Crystal structure of thiamin pyrophosphokinase.** *J Mol Biol* 2001, **310**:195–204.
307. Gandhi AK, Ghatge MS, Musayev FN, Sease A, Aboagye SO, di Salvo ML, Schirch V, Safo MK: **Kinetic and structural studies of the role of the active site residue Asp235 of human pyridoxal kinase.** *Biochem Biophys Res Commun* 2009, **381**:12–5.
308. Musayev FN, di Salvo ML, Ko T, Gandhi AK, Goswami A, Schirch V, Safo MK: **Crystal Structure of human pyridoxal kinase: structural basis of M(+) and M(2+) activation.** *Protein Sci* 2007, **16**:2184–2194.
309. Baker L-J, Dorocke JA, Harris RA, Timm DE: **The Crystal Structure of Yeast Thiamin Pyrophosphokinase.** *Structure* 2001, **9**:539–546.
310. Rambo RP, Tainer J a: **Accurate assessment of mass, models and resolution by small-angle scattering.** *Nature* 2013, **496**:477–81.
311. Newman JA, Das SK, Sedelnikova SE, Rice DW: **The crystal structure of an ADP complex of Bacillus subtilis pyridoxal kinase provides evidence for the parallel emergence of enzyme activity during evolution.** *J Mol Biol* 2006, **363**:520–30.
312. Newman JA, Das SK, Sedelnikova SE, Rice DW: **Cloning, purification and preliminary crystallographic analysis of a putative pyridoxal kinase from Bacillus subtilis.** *Acta Crystallogr Sect F Struct Biol Cryst Commun* 2006, **62**(Pt 10):1006–9.
313. Zhang Y, Dougherty M, Downs DM, Ealick SE: **Crystal structure of an aminoimidazole riboside kinase from Salmonella enterica: implications for the evolution of the ribokinase superfamily.** *Structure* 2004, **12**:1809–21.
314. Cheng G, Bennett EM, Begley TP, Ealick SE: **Crystal Structure of 4-Amino-5-Hydroxymethyl-2-Methylpyrimidine Phosphate Kinase from Salmonella typhimurium at 2.3 Å Resolution.** *Structure* 2002, **10**:225–235.
315. Robert X, Gouet P: **Deciphering key features in protein structures with the new ENDscript server.** *Nucleic Acids Res* 2014, **42**(Web Server issue):W320–4.
316. Titorenko VI, Rachubinski RA: **The life cycle of the peroxisome.** *Nat Rev Mol Cell Biol* 2001, **2**:357–368.
317. Redecke L, Nass K, DePonte DP, White T a, Rehders D, Barty A, Stellato F, Liang M, Barends TRM, Boutet S, Williams GJ, Messerschmidt M, Seibert MM, Aquila A, Arnlund D, Bajt S, Barth T, Bogan MJ, Caleman C, Chao T-C, Doak RB, Fleckenstein H, Frank M, Fromme R, Galli L, Grotjohann I, Hunter MS, Johansson LC, Kassemeyer S, Katona G, et al.: **Natively inhibited Trypanosoma brucei cathepsin B structure determined by using an X-ray laser.** *Science* 2013, **339**:227–30.
318. Peng Y, Song J, Lu J, Chen X: **The histone deacetylase inhibitor sodium butyrate inhibits baculovirus-mediated transgene expression in Sf9 cells.** *J Biotechnol* 2007, **131**:180–187.
319. Hwa Chang K, Hwa Park J, Hyung Lee Y, Ho Kim J, Ok Chun H, Hak Kim J, Sik Chung I: **Dimethylsulfoxide and sodium butyrate enhance the production of recombinant cyclooxygenase 2 in stably transformed Drosophila melanogaster S2 cells.** *Biotechnol Lett* 2002, **24**:1353–1359.
320. Settembre E, Begley TP, Ealick SE: **Structural biology of enzymes of the thiamin biosynthesis pathway.** *Curr Opin Struct Biol* 2003, **13**:739–747.

321. Rondeau, J-M, Klebe G, Podjarny A: **Chapter 3. Ligand Binding: The Crystallographic Approach.** :56–135.
322. Nemeria N, Yan Y, Zhang Z, Brown AM, Arjunan P, Furey W, Guest JR, Jordan F: **Inhibition of the Escherichia coli pyruvate dehydrogenase complex E1 subunit and its tyrosine 177 variants by thiamin 2-thiazolone and thiamin 2-thiothiazolone diphosphates: Evidence for reversible tight-binding inhibition.** *J Biol Chem* 2001, **276**:45969–45978.
323. Alston TA, Abeles RH: **Enzymatic conversion of the antibiotic metronidazole to an analog of thiamine.** *Arch Biochem Biophys* 1987, **257**:357–62.
324. Zilles JL, Croal LR, Downs DM: **Action of the Thiamine Antagonist Bacimethrin on Thiamine Biosynthesis.** *J Bacteriol* 2000, **182**:5606–5610.
325. Reddick JJ, Saha S, Lee J, Melnick JS, Perkins J, Begley TP: **The mechanism of action of bacimethrin, a naturally occurring thiamin antimetabolite.** *Bioorg Med Chem Lett* 2001, **11**:2245–2248.
326. Wilcken R, Liu X, Zimmermann MO, Rutherford TJ, Fersht AR, Joerger AC, Boeckler FM: **Halogen-enriched fragment libraries as leads for drug rescue of mutant p53.** *J Am Chem Soc* 2012, **134**:6810–6818.
327. Wilcken R, Zimmermann MO, Lange A, Joerger AC, Boeckler FM: **Principles and applications of halogen bonding in medicinal chemistry and chemical biology.** *Journal of Medicinal Chemistry* 2013:1363–1388.
328. Lu Y, Liu Y, Xu Z, Li H, Liu H, Zhu W: **Halogen bonding for rational drug design and new drug discovery.** *Expert Opin Drug Discov* 2012, **7**:375–383.
329. Scholfield MR, Vander Zanden CM, Carter M, Ho PS: **Halogen bonding (X-bonding): A biological perspective.** *Protein Sci* 2013, **22**:139–152.
330. Vallée-Bélisle A, Michnick SW: **Visualizing transient protein-folding intermediates by tryptophan-scanning mutagenesis.** *Nat Struct Mol Biol* 2012, **19**:731–736.
331. Eftink MR: **The use of fluorescence methods to monitor unfolding transitions in proteins.** *Biochemistry (Mosc)* 1998, **63**:276–284.
332. Jones S, Thornton JM: **Protein-protein interactions: A review of protein dimer structures.** *Prog Biophys Mol Biol* 1995, **63**:31–65.
333. Onozuka M, Nosaka K: **Steady-state kinetics and mutational studies of recombinant human thiamin pyrophosphokinase.** *J Nutr Sci Vitaminol (Tokyo)* 2003, **49**:156–162.
334. Matte A, Tari LW, Delbaere LT: **How do kinases transfer phosphoryl groups?** *Structure* 1998, **6**:413–419.
335. Nosaka K, Kaneko Y, Nishimura H, Iwashima A: **Isolation and characterization of a thiamin pyrophosphokinase gene, THI80, from Saccharomyces cerevisiae.** *J Biol Chem* 1993, **268**:17440–17447.
336. Fankhauser H, Zurlinden A, Schweingruber AM, Edenharter E, Schweingruber ME: **Schizosaccharomyces pombe thiamine pyrophosphokinase is encoded by gene tnr3 and is a regulator of thiamine metabolism, phosphate metabolism, mating, and growth.** *J Biol Chem* 1995, **270**:28457–28462.
337. Nodwell MB, Menz H, Kirsch SF, Sieber SA: **Rugulactone and its Analogues Exert Antibacterial Effects through Multiple Mechanisms Including Inhibition of Thiamine Biosynthesis.** *ChemBioChem* 2012, **13**:1439–1446.
338. Kästner U, Hallmen C, Wiese M, Leistner E, Drewke C: **The human pyridoxal kinase, a plausible target for ginkgotoxin from Ginkgo biloba.** *FEBS J* 2007, **274**:1036–1045.

339. Gandhi AK, Desai J V., Ghatge MS, di Salvo ML, Di Biase S, Danso-Danquah R, Musayev FN, Contestabile R, Schirch V, Safo MK: **Crystal structures of human pyridoxal kinase in complex with the neurotoxins, ginkgotxin and theophylline: Insights into pyridoxal kinase inhibition.** *PLoS One* 2012, **7**:1–11.

IX Acknowledgements

Zunächst möchte ich mich bei meinem Doktorvater Prof. Ch. Betzel für die Überlassung des interessanten Themas, die Möglichkeiten selbstständig wissenschaftlich in seinem Arbeitskreis zu arbeiten, mich fortzubilden und seine Betreuung herzlich bedanken. Meinem Co-Betreuer Prof. Carsten Wrenger und seinem Team in Sao Paulo möchte ich für die Themenstellung und die Unterstützung in Brasilien danken - muito obrigado! Meinem zweiten Co-Betreuer PD Dr. Markus Perbandt möchte ich für sein offenes Ohr für Fragen und Diskussion, sowie Anleitung in der Proteinkristallographie danken.

Mein herzlicher Dank gilt auch JProf. Henning Tidow für die Übernahme des Zweitgutachtens der hier vorliegenden Arbeit. Furthermore, I like to thank Prof. Andrew Torda and Dr. Thomas Hackl for being the Co-referees.

An dieser Stelle möchte ich mich bei allen meinen Laborkollegen des Arbeitskreises bedanken, es war eine spannende Zeit. Vor allem möchte ich hierbei Dr. Dirk Rehders, Dr. Raphael Eberle, Dr. Julia Drebes, Dr. Dominik Oberthür, Marco Klinge, Robin Schubert und Svetlana Kapis, Theresa Nuguid sowie Aline Melro Murad und Petra Belda erwähnen. Ihr alle habt meinen Laboralltag immer bereichert und in jeglicher Situation mit Selbstverständlichkeit eine helfende Hand gereicht. Keinen Tanz der Moleküle, unvorhergesehene und doch absehbare Manöver „Please fasten your seatbelt“, Truckexkursionen oder auch special moves möchte ich missen.

Überdies möchte ich mich für die Monate der Zusammenarbeit mit meinen Bachelor- und Masterstudenten Benjamin Dose, Nora Kleen und Boris Krichel bedanken, ihr habt durch eure Projekte einen wertvollen Beitrag geleistet; ich danke euch für die super Zeit!

Für fleißiges Korrekturlesen bedanke ich mich bei Robin Schubert, Manja Czech-Sioli und Felix Müller - Etwaige verbliebene Fehler habe ich zu verantworten.

Erwähnen möchte ich auch unsere Labornachbarn der AK Hahn, Bredehorst und Rentmeister, danke für eure spontane Hilfe im Alltag und lohnenden Diskussionen.

In unserer Kooperationsarbeit mit dem UKE dient mein Dank Prof. Nicole Fischer, ihrem Team, und im Besonderen hierbei Manja Czech-Sioli für Unterstützung, Telefonzentralentätigkeit und Kaffee. Des Weiteren möchte ich mich auch für die Zusammenarbeit mit Thales Kronenberger, Dr. Björn Windshügel, Dr. Dirk Rehders, Juliane Klare und Dr. Thomas Hackl bedanken, mit euch zusammen konnte ich einen Blick auch aus anderen wissenschaftlichen Richtungen auf mein Projekt werfen.

Ich danke vor allem auch meinen Freunden und meiner Familie, welche mich immer unterstützt, aufgefangen, bei „Sturm und Niedrigwasser“ ertragen und mir keine Absage oder nächtliche Ruhestörung übelgenommen haben. Ein besonderer Dank gilt vor allem Felix Müller, danke für einfach alles und kein Stück weniger. Meinen Eltern und meiner Familie (Künz-Müller-Bubeck-Vogel) danke ich sehr, denn Sie haben mich in freiem Denken stets bestärkt und unterstützt.

X Curriculum vitae

- entfällt aus datenschutzrechtlichen Gründen –

XI Appendix

Table 36: References for the illustration of the time course of antibacterial resistance development (Figure 1) first documented resistance of any bacteria - clinical isolates and *in vitro* studies - against specific compounds.

Antibiotic compound	Discovery (not ultimately on market, adapted from Silver [18])	First reported resistance	PubMed ID
Salvarsan	1908	1949	15400370
Penicillin	1928	1945	21005048
Sulfonamide	1932	1946	17754356
Streptomycin	1943	1946	20995215
Bacitracin	1945	1949	18132374
Nitrofusan	1946	1952	14912065
Chloramphenicol	1947	1950	14796661
			14785226
			14774530
Polymyxin	1947	1953	13031655
Chlortetracycline	1948	1950	15402506
Cephalosporin	1948	1965	14342258
Pleuromutilin	1950	1982	7050084
Erythromycin	1952	1953	13047352
			24542681
			13090461
			13109350
Vancomycin	1953	1988	3376618
Streptogramin	1953	1956	13379520
Cycloserine	1955	1957	13470425
Novobiocin	1956	1957	13444794
Rifampicin	1957	1968	4179219
Metronidazole	1959	1963	14047071
Methicillin	1960	1961	13686776
Ampicillin	1962	1964	14287955
Nalidixic acid	1961	1968	4898540
Trimethoprim	1961	1972	4110643
Licomycin	1961	1967	5596212
Fusidic acid	1961	1966	5928604
Fosfomycin	1969	1974	4604487
Mupirocin	1971	1987	2886836
Carbapenem	1976	1983	6578701
Oxazolidinone	1978	1996	15472854
Daptomycin	1987	1987	2824427

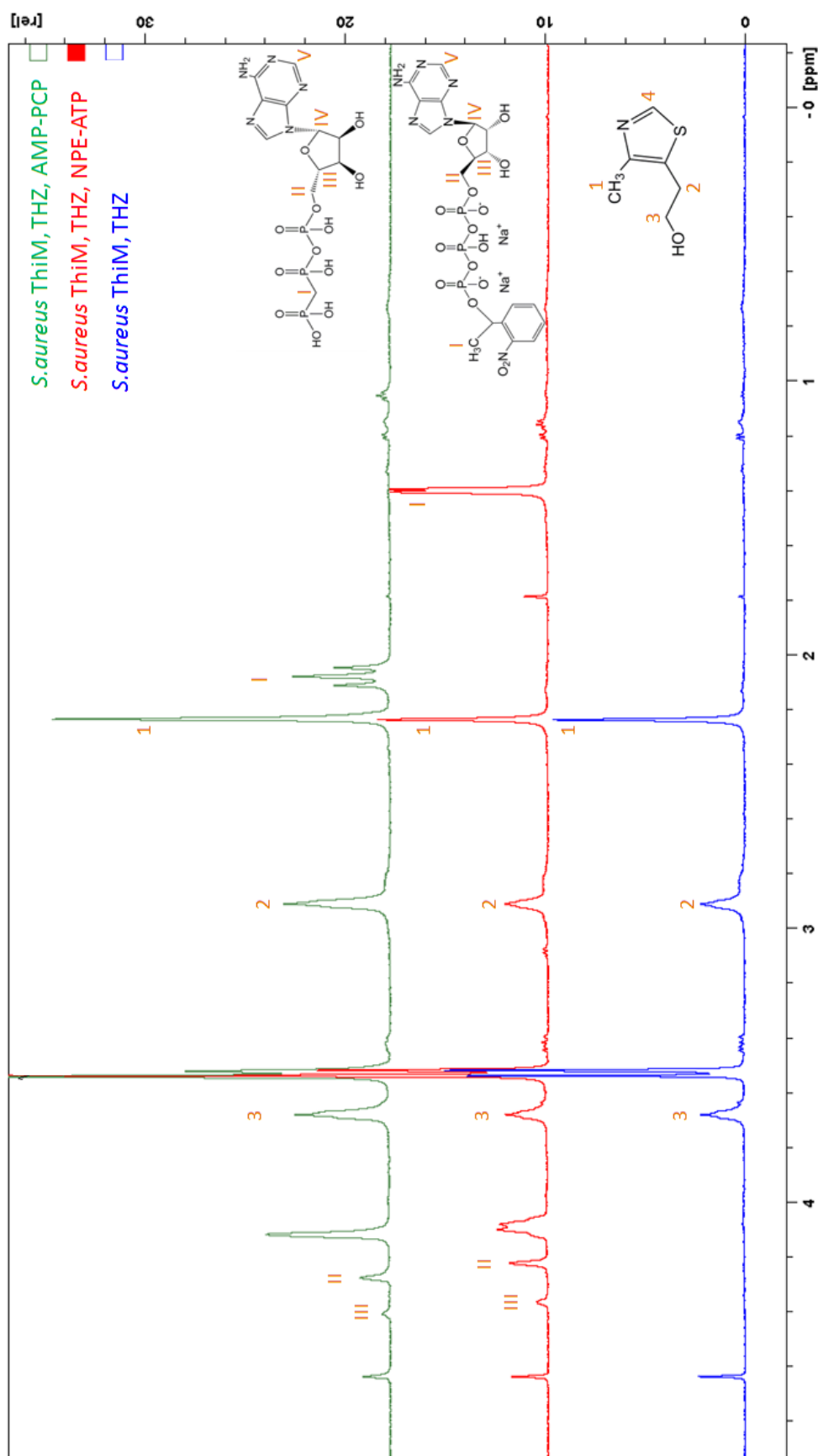


Figure 51: Comparative overview of the ^1H spectra of *S. aureus* ThiM with AMP-PCP, NPE-caged ATP and THZ I.

Section 0-5 ppm of the ^1H spectra of *S. aureus* ThiM with AMP-PCP (green), NPE-caged ATP (red) and THZ (blue) is plotted and the corresponding peak assignment is given to the chemical structure (ChemDraw; PerkinElmer Inc.).

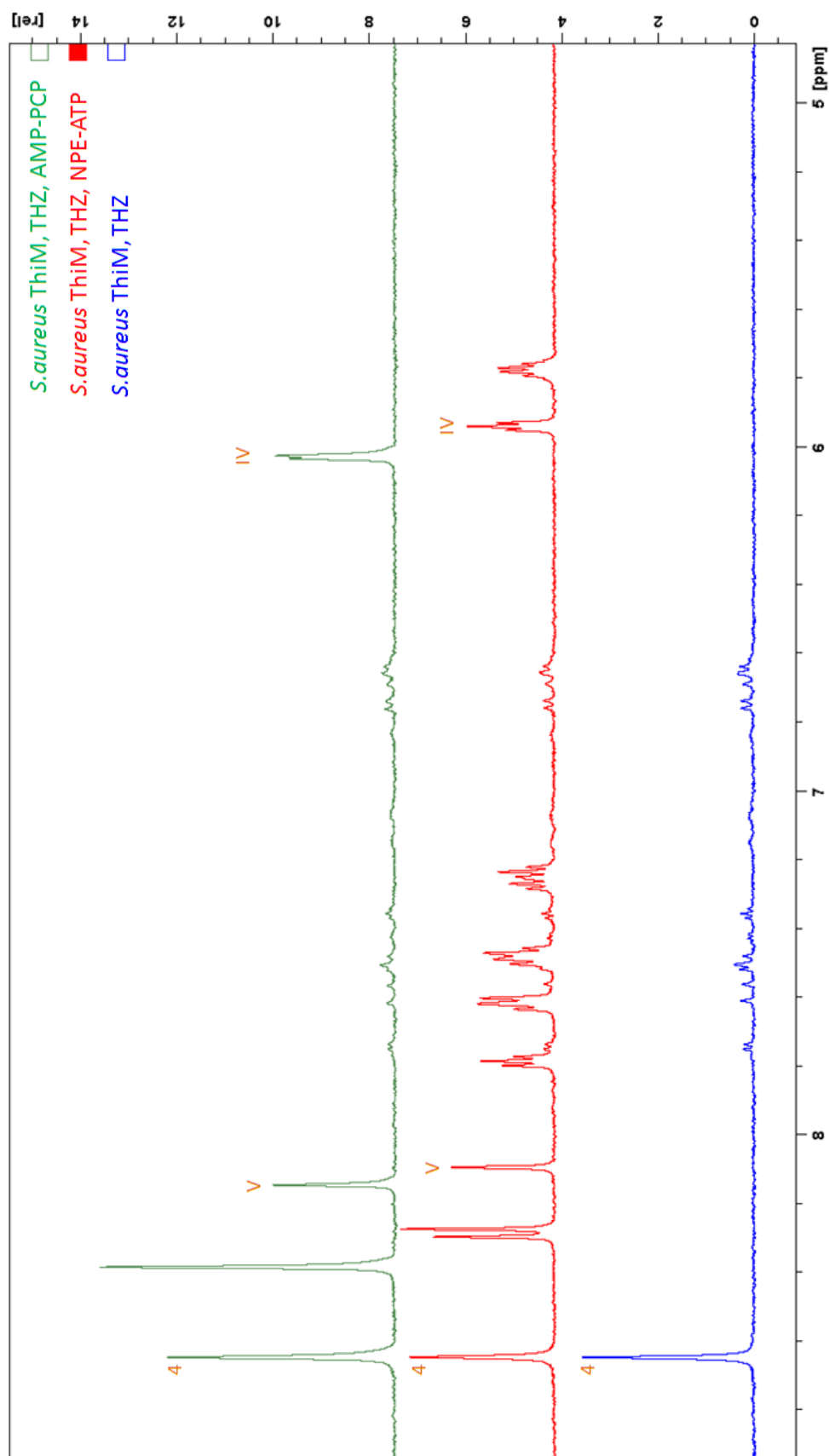


Figure 52: Comparative overview of the ^1H spectra of *S. aureus* ThiM with AMP-PCP, NPE-caged ATP and THZ II.

Section 5-9 ppm of the ^1H spectra of *S. aureus* ThiM with AMP-PCP (green), NPE-caged ATP (red) and THZ (blue) is plotted and the corresponding peak assignment is given to the chemical structure (ChemDraw; PerkinElmer Inc.).

Table 37: STD effects and peak assignment of *S. aureus* ThiM supplemented with 50 μ M THZ.

Assignment, corresponding to the annotation of Figure 51 and Figure 52 respectively, chemical shift, absolute (abs) and relative STD effects are given.

THZ assignment	$\nu(\text{F1})$ [ppm]	STD % (abs) off resonance	STD % (abs) on resonance	Absolute STD [%]	Relative STD [%]
1	2.226	227930808.2800	105344701.0500	53.8	100.0
2	2.903	179812768.9700	94620538.7300	47.4	88.1
3	3.674	125962382.0900	77897741.1900	38.2	70.9
4	8.645	76248872.7200	48881058.4400	35.9	66.7

Table 38: STD effects and peak assignment of *S. aureus* ThiM supplemented with 100 μ M THZ.

Assignment, corresponding to the annotation of Figure 51 and Figure 52 respectively, chemical shift, absolute (abs) and relative STD effects are given.

THZ assignment	$\nu(\text{F1})$ [ppm]	STD % (abs) off resonance	STD % (abs) on resonance	Absolute STD [%]	Relative STD [%]
1	2.226	453113944.0000	268405199.8800	40.8	100.0
2	2.903	344912803.4700	215941074.4200	37.4	91.7
3	3.674	264792669.6200	194098560.8000	26.7	65.5
4	8.645	137757923.6200	93782166.9700	31.9	78.3

Table 39: STD effects and peak assignment of *S. aureus* ThiM supplemented with 50 μ M THZ and 200 μ M ATP-NPE

Assignment, corresponding to the annotation of Figure 51 and Figure 52 respectively, chemical shift, absolute (abs) and relative STD effects are given.

THZ / ATP-NPE assignment	ν (F1) [ppm]	STD % (abs) off resonance	STD % (abs) on resonance	Absolute STD [%]	Relative STD [%]
1	2.233	213388104.0900	100455880.5000	52.9	100.0
2	2.892	172721666.0600	92587763.7800	46.4	87.7
3	3.676	134931620.9100	89919423.4400	33.4	63.0
4	8.644	68690952.9400	40071347.9400	41.7	78.7
I	1.783	24126561.1600	21294704.8400	11.7	22.2
II	4.224	69213618.0000	58424968.6600	15.6	29.5
III	4.363	26542788.1600	22615722.3100	14.8	28.0
IV	5.938	57341771.1900	48589946.6600	15.3	28.8
V	8.089	37807723.2800	29413221.8100	22.2	42.0

Table 40: STD effects and peak assignment of *S. aureus* ThiM supplemented with 100 μ M THZ and 150 μ M ATP-PCP.

Assignment, corresponding to the annotation of Figure 51 and Figure 52 respectively, chemical shift, absolute (abs) and relative STD effects are given.

THZ / ATP-NPE assignment	ν (F1) [ppm]	STD % (abs) off resonance	STD % (abs) on resonance	Absolute STD [%]	Relative STD [%]
1	2.226	441045352.3800	266083873.4100	39.7	100.0
2	2.903	334177654.1600	211778964.0900	36.6	92.3
3	3.674	268709332.3100	200249515.3900	25.5	64.2
4	8.645	122366747.5000	78524929.2000	35.8	90.3
I	2.075	282767452.6400	263677412.6900	6.8	17.0
II	4.273	65420088.8100	58287289.3300	10.9	27.5
III	4.409	22707198.1600	18399371.5200	19.0	47.8
IV	6.023	80087746.9800	72741967.0300	9.2	23.1
V	8.143	51127060.5900	44039171.6700	13.9	34.9

XII Risk and Safety Statements

1 Chemicals used (GHS classification)

Compound	CAS-No.	Supplier	GHS hazard	Hazard Statements	Precautionary Statements
Acetic acid	64-19-7	Chem-solute	GHS02 GHS05	H226, H314	P280, P305+351+338, P310
Acrylamide 37%	79-06-1	Carl Roth	GHS06 GHS08	H301, H312, H315, H317, H319, H332, H340, H350, H361f, H372	P201, P280, P301+310, P305+351+338, P308+313
ATP	34369-07-8	Sigma	-	-	-
Agarose	9012-36-6	Serva	-	-	-
(NH ₄) ₂ SO ₄	7283-20-2	Carl Roth	-	-	-
NH ₄ NO ₃	6484-52-2	Applichem	GHS03	H272	P210
Ampicillin	69-52-3	Carl Roth	GHS08	H334, H317	P280, P261, P302+352, P342+311
AMP-PCP	7414-56-4	Sigma	GHS06	H301, H311, H315, H319, H331, H335	P261, P280, P301+310, P305+351+338, P311
AMP-PNP	25612-73-1	Sigma	-	-	-
APS	7727-54-0	Carl Roth	GHS03 GHS07 GHS08	H272, H302, H315, H317, H319, H334, H335	P280, P305+351+338, P302+352, P304+341, P342+311
Bromphenol blue	115-39-9	Applichem	-	-	-
CaCl ₂	10043-52-4	Merck	GHS07	H319	P305+351+338
Ca(H ₃ CCOO) ₂	114460-21-8	Sigma	-	H315, H319, H335	P261, P305+351+338
Caged ATP	171800-68-3	Sigma	-	-	-
Citric acid	77-92-9	Sigma	GHS05	H318	P305+351+338, P311
Coomassie Brilliant Blue R250	6104-59-2	Serva	-	-	-
CHES	9005-64-5	Sigma	-	H319	P305+351+338
Desthiobiotin	533-48-2	Sigma	-	-	-
DTT	578517	Applichem	GHS07	H302, H315, H319, H335	P302+352, P305+351+338
EDTA	60-00-4	Sigma	GHS07	H319	P305+351+338
Ethanol	64-17-5	Carl Roth	GHS02	H225	P210
Ethidium bromide	1239-45-8	Sigma	GHS06 GHS08	H302, H331, H341	P260, P281, P284, P310
Gentamicin sulfate	1405-41-0	Sigma	GHS08	H317, H334	P261, P280, P342+311
Glycerol	56-81-5	Sigma	-	-	-
Guanidinhydrochlorid	50-01-1	Applichem	GHS07	H302, H315, H319	P305+351+338, P302+352
HABA	1634-82-8	Fluka	GHS07	H315, H319, H335	P261, P305+351+338
Hepes	7365-45-9	Sigma Aldrich	-	-	-
Hydrochloric acid >25 %	7647-01-0	Merck	GHS05 GHS07	H314, H335	P261, P280, P310, P305+351+338
(5-(2-hydroxyethyl)-	137-00-8	Sigma		H315, H319, H335	P261, P280, P304+340,

Compound	CAS-No.	Supplier	GHS hazard	Hazard Statements	Precautionary Statements
4-methylthiazole (THZ)					P305+351+338, P405, P501
Imidazole	288-32-4	Carl Roth	GHS05 GHS06 GHS08	H301, H314, H361	P260, P281, P303+361+353, P301+330+3 31, P305+351+3 38, P308+313
Isopropanol	67-63-0	Carl Roth	GHS02 GHS07	H225, H319, H336.	P210, P233, P305+351+338
KCl	7447-40-7	Carl Roth	-	-	-
LiCl	7447-41-8	Merck	GHS07	H302, H315, H319, H335	P302+352, P305+351+338
Li ₂ SO ₄	10102-25-7	Merck	GHS07	H302	-
Malonic acid	141-82-2	Sigma	GHS05 GHS07	H318, H302, H335, H315	P261, P280, P304+340, P305+351+338, P405, P501
Mg(HCOO) ₂	6150-82-9	Fluka	-	-	-
MgCl ₂	7786-30-3	Carl Roth	-	-	-
MgOAc	16674-78-5	Merck	-	-	-
MgSO ₄	7487-88-9	Merck	-	-	-
MPD	107-41-5	Carl Roth	GHS07	H315, H319	-
2-Mercaptoethanol	60-24-2	Fisher Scientific	GHS06 GHS09	H302, H411, H315, H335, H311, H319	P280, P312, P302+350, P261, P273, P301+312, P305+351+338
NaOAc	127-09-3	Applichem	-	-	-
NaBr	7647-15-6	Merck	-	-	-
(CH ₃) ₂ AsO ₂ (Na)	124-65-2	Sigma	GHS06 GHS09	H301, H331, H410	P261, P273, P301+310, P311, P501
NaCl	7647-14-5	Carl Roth	-	-	-
NaH ₂ PO ₄	10049-21-5	Applichem	-	-	-
NaOH	1310-73-2	Merck	GHS05	H314	P280, P310, P305+351+338
Na ₃ citrate	6132-04-3	Sigma	-	-	-
Ni(II)SO ₄	10101-97-0	Applichem	GHS07 GHS08 GHS09	H302+332, H315, H317, H334, H341, H350i, H360D, H372 H410	P201, P261, P273, P280, P284, P304+340+312
Paraffin	8002-74-2	Applichem	-	-	-
PEG 10000	25322-68-3	Merck	-	-	-
PEG 1500	25322-68-3	Fluka	-	-	-
PEG 2000 MME	25322-68-3	Fluka	-	-	-
PEG 300	25322-68-3	Applichem	-	-	-
PEG 3350	25322-68-3	Sigma	-	-	-
PEG 400	25322-68-3	Sigma	-	-	-
PEG 4000	25322-68-3	Merck	-	-	-
PEG 6000	25322-68-3	Merck	-	-	-
PEG 8000	25322-68-3	Sigma	-	-	-
PMSF	329-98-6	Applichem	GHS06 GHS05	H301, H314	P280, P305+351+3 38, P310
Pyridoxal-HCl	65-22-5	AppliChem	GHS07	H302	P264, P301+312, P330, P501

Compound	CAS-No.	Supplier	GHS hazard	Hazard Statements	Precautionary Statements
Pyridoxine-HCl	58-56-0	Roth	GHS07	H335, H315, H319	P261, P280, P302+352, P305+351+338
SDS	151-21-3	Sigma	GHS02 GHS06	H228, H302, H311, H315, H319, H335	P210, P261, P280, P312, P305+351+338
Sodium borate	1303-96-4	Sigma	GHS08	H360FD	P201, P308 +313
Sodium citrate	1545832	Sigma	-	-	-
Sodium tartrate	868-18-8	Applichem	-	-	-
TEMED	110-18-9	Merck	GHS02 GHS05 GHS07	H225, H302, H314, H332	P261, P280, P305+351+338
Thiamine	67-03-8	Fluka	-	-	-
Tris	1185-53-1	Fluka	GHS07	H315, H319, H335	P261, P305+351+338
Tween 20	9005-64-5	Carl Roth	-	-	-
Yeast Extract	8013-01-2	Serva	-	-	-

2 Commercial Protein Screens and Kits

Name	Supplier	GHS hazard	Hazard Statements	Precautionary Statements
Morpheus	Molecular Dimensions	GHS02 GHS06 GHS07 GHS08 GHS09	H225, H301, H302, H315, H319, H331, H332, H335, H340, H350, H360Fd, H361d, H373, H411	P101, P201, P270, P273, P280, P305+351+338, P309+311, P313
PACT premier	Molecular Dimensions	GHS06	H301, H331, H412	P101, P270, P273, P280, P309+311
Stura FootPrint & MacroSol	Molecular Dimensions	GHS02 GHS06 GHS07 GHS08 GHS09	H225, H301, H302, H315, H319, H332, H335, H340, H350, H360FD, H373, H411	P101, P201, P270, P273, P280, P305+351+338, P309+311, P313
AmSO₄ Suite	Qiagen	GHS02 GHS06 GHS08 GHS09	H225, H301, H330, H350, H340, H360FD, H372, H411	P101, P201, P273, P280, P309+311
Classics Suite	Qiagen	GHS02 GHS06 GHS07 GHS08 GHS09	H225, H301, H302, H315, H319, H331, H332, H335, H340, H350, H360FD, H373, H411	P101, P201, P270, P280, P305+351+338, P309+311, P313
Cryos Suite	Qiagen	GHS02 GHS06 GHS07 GHS08 GHS09	H225, H301, H302, H315, H319, H331, H332, H335, H340, H350, H360FD, H373, H411	P101, P201, P270, P273, P280, P305+351+338, P309+311, P313
JCSG-plus	Molecular Dimensions	GHS02 GHS05 GHS06 GHS07 GHS08	H225, H301, H312, H315, H318, H331, H335, H350, H411	P101, P201, P270, P280, P305+351+338, P309+311, P313

Name	Supplier	GHS hazard	Hazard Statements	Precautionary Statements
		GHS09		
GeneJET Plasmid Miniprep Kit	Thermo Fisher Scientific	GHS05 GHS07	H314	P260, P303+361+353, P305+351+338, P310, P405, P501
GeneJET Gel Extraction Kit	Thermo Fisher Scientific	GHS07	H302, H412	P264, P270, P273, P301+312, P330, P501

3 GHS pictograms



Figure 53: GHS pictograms (source: <https://www.osha.gov/dsg/hazcom/pictograms/index.html>).

4 GHS Hazard Statements

H225	Highly flammable liquid and vapor
H226	Flammable liquid and vapor
H228	Flammable solid
H272	May intensify fire; oxidizer
H301	Toxic if swallowed
H302	Harmful if swallowed
H311	Toxic in contact with skin
H312	Harmful in contact with skin
H314	Causes severe skin burns and eye damage
H315	Causes skin irritation
H317	May cause an allergic skin reaction
H318	Causes serious eye damage
H319	Causes serious eye irritation
H330	Fatal if inhaled
H331	Toxic if inhaled
H332	Harmful if inhaled
H334	May cause allergy or asthma symptoms or breathing difficulties if inhaled
H335	May cause respiratory irritation
H336	May cause drowsiness or dizziness
H340	May cause genetic defects
H341	Suspected of causing genetic defects
H350	May cause cancer
H350i	May cause cancer by inhalation
H360	May damage fertility or the unborn child
H360D	May damage the unborn child
H360Fd	May damage fertility. Suspected of damaging the unborn child

H360FD	May damage fertility. May damage the unborn child
H361	Suspected of damaging fertility or the unborn child
H361d	Suspected of damaging the unborn child.
H361f	Suspected of damaging fertility
H370	Cause damage to organs
H372	Causes damage to organs through prolonged or repeated exposure
H373	May cause damage to organs through prolonged or repeated exposure.
H410	Very toxic to aquatic life with long lasting effects
H411	Toxic to aquatic life with long lasting effects
H412	Harmful to aquatic life with long lasting effects.

5 GHS Precautionary Statements

P101	If medical advice is needed, have product container or label at hand
P201	Obtain special instructions before use
P210	Keep away from heat/sparks/open flames/hot surfaces – No smoking
P233	Keep container tightly closed
P260	Do not breathe dust/fume/gas/mist/vapors/spray
P261	Avoid breathing dust/fume/gas/mist/vapors/spray
P264	Wash thoroughly after handling
P270	Do not eat, drink or smoke when using this product
P273	Avoid release to the environment
P281	Use personal protective equipment as required
P280	Wear protective gloves/protective clothing/eye protection/face protection
P284	Wear respiratory protection
P309	IF exposed or you feel unwell
P310	Immediately call a POISON CENTER or doctor/physician
P311	Call a POISON CENTER or doctor/physician
P312	Call a POISON CENTER or doctor/physician if you feel unwell
P321	Specific treatment (see respective MSDS)
P330	Rinse mouth
P362	Take off contaminated clothing and wash before reuse
P405	Store locked up
P501	Dispose of contents/container in accordance with local/regional/national/international regulations
P301+310	IF SWALLOWED: Immediately call a POISON CENTER or doctor/physician
P301+312	IF SWALLOWED: Call a POISON CENTER or doctor/physician if you feel unwell
P301+330+ 331	IF SWALLOWED: Rinse mouth. Do NOT induce vomiting
P302+352	IF ON SKIN: Wash with soap and water
P303+361+ 353	IF ON SKIN (or hair): Remove/Take off immediately all contaminated clothing. Rinse skin with water/shower
P304+341	IF INHALED: If breathing is difficult, remove victim to fresh air and keep at rest in a position comfortable for breathing
P305+351+338	IF IN EYES: Rinse cautiously with water for several minutes. Remove contact lenses if present and easy to do - continue rinsing
P308+313	IF exposed or concerned: Get medical advice/attention
P309+311	IF exposed or you feel unwell: Call a POISON CENTER or doctor/physician
P332+313	If skin irritation occurs: Get medical advice/attention
P342+311	Call a POISON CENTER or doctor/physician
P403+233	Store in a well-ventilated place. Keep container tightly closed

XIII Eidesstattliche Erklärung

Hiermit versichere ich an Eides statt, die vorliegende Dissertation selbst verfasst und keine anderen als die angegebenen Hilfsmittel benutzt zu haben. Ich versichere, dass diese Dissertation nicht in einem früheren Promotionsverfahren eingereicht wurde.

Ferner versichere ich, dass ich noch keine Promotionsversuche an anderen Universitäten unternommen habe.

Hamburg, 22.06.2015

(Madeleine Künz)

